# ELECTRICAL PROPERTIES OF GALLIUM ARSENIDE IMPLANTED WITH SULPHUR

Thesis submitted for the degree of Doctor of Philosophy at the University of Surrey

by

B. Kearton

January 1977

## ABSTRACT

The electrical properties of sulphur 32 implanted gallium arsenide were investigated using the capacitance-voltage, Copeland and Hall measurement techniques. N-type epitaxial gallium arsenide was implanted with a range of sulphur ion doses from $10^{12}$ions/cm$^2$ to $10^{15}$ions/cm$^2$, with energies from 100 keV to 400 keV and afterwards annealed at temperatures up to 800°C. The implantations were carried out with the specimens held at temperatures up to 180°C. Deep concentration profiles were observed, with super-tails extending three or four microns into the material. These deep profiles were considered to be due to diffusion during subsequent annealing. A saturation in the peak concentration was also observed, with a maximum electrically active peak concentration of $1.7 \times 10^{16}$atoms/cm$^3$. A range of percentage electrical activities, from zero to 86%, was obtained. The resultant concentration profiles were dominated by the effects of the structural damage produced by the implantation process. In order to study the effects of damage further, gallium arsenide was implanted with doses of both protons and argon.

CONTENTS

ACKNOWLEDGEMENTS

I would like to thank my supervisor, Dr. G. Brown, for his assistance with this project. I would like to also acknowledge help from Dr. K.G. Stephens, Head of the Research Group, and thank the Departmental Technicians, Mr. J. Smith, Mr. R. Haining and Mrs. V. Hinton, for their assistance. My thanks too to Miss J. Jones for typing this thesis.

# 1.0 INTRODUCTION

## 1.1 Introduction to Project

Group III-V compound semiconductors have become increasingly important in recent years, because they exhibit a wide range of band-gaps and mobilities. At the time of the commencement of this work, by far the most important of this group of semiconductors was gallium arsenide, due to its applications in high frequency devices. Doping of the III-V semiconductors is made difficult by conventional diffusion processes because of the decomposition of the material at the high temperature involved. Ion implantation of the dopant species would appear to offer controlled doping of the semiconductor at room temperature.

The aim of the work contained in this report was to investigate the electrical properties of gallium arsenide after bombardment with energetic heavy ions, and to assess the effects of:-

(a) the implant ion energy,

(b) the implant ion dose,

(c) the implant rate,

(d) the implant angle with respect to the crystal orientation,

(e) the target temperature,

(f) the anneal temperature and length of anneal.

## 1.2 Measurement Techniques

The main semiconductor parameters, of interest for device applications, are as follows:-

(i) The depth-concentration distribution of electrically active carriers in the semiconductor crystal.

(ii) The depth-mobility distribution of the electrically active carriers in the semiconductor crystal.

(iii) The energy levels, of the donors, acceptors and crystal defects in the band-gap of the doped semiconductor.

(iv) The carrier lifetime.

(v) The diffusion coefficient.

(vi) The semiconductor band-gap.

There is no single measurement technique which can provide all of this information. The measurement techniques available are of two types, called destructive and non-destructive techniques.

### 1.2.1 Destructive Techniques

#### 1.2.1.1 Radio-active Tracer Measurements

In this method, the specimen target is bombarded with radio-active ions of a chosen energy. A radio-active count of the implanted specimen is taken, followed by the removal of a thin layer from the surface of the specimen. Another radio-active count is taken of the implanted specimen. The process is repeated and successive layers are removed, followed by radio-active counts. Using the radio-active count and the thickness of the stripped layers of the specimen, a concentration-depth profile of the implanted radio-active isotope can be obtained.

This technique has been used widely to determine impurity atom profiles by workers such as Carter et al.[1], McCargo et al.[2], Davies et al.[3] and Dearnaley et al.[4]. It will yield the variation of the implanted atom concentration with depth from the implanted surface.

The layer stripping can be achieved by the following three methods.

(i) Chemical Stripping[5]. The layer stripping can be achieved in most semiconductors by the oxidation of the surface of the specimen by anodizing, and subsequently removing this layer by chemical dissolution. In the case of silicon[3] the oxidised layer can be dissolved in hydrofluoric acid. Electrochemical techniques are available for the accurate sectioning of aluminium[6], tungsten[2], silicon[3] and gold[7]. A chemical stripping technique which has been applied to gallium arsenide is described later in this report (see Section 3.3.5.3).

(ii) Mechanical Stripping. Controlled layers of material can be removed by means of mechanical polishing of the surface of the specimen. Mechanical layer removal has been successfully achieved by Whitton[8,9] using a vibratory polisher.

(iii) Sputtering. When a specimen is bombarded with energetic heavy ions, atoms are ejected from the surface of the specimen. The process is known as sputtering and has been successfully used to remove thin layers from the surface of specimens[10,11,12].

### 1.2.1.2 P-n Junction Technique

A series of specimens, each with a different initial resistivity, are implanted with a heavy ion under the same conditions of dose, temperature and energy. The heavy ion is chosen to give a doping action opposite to the doping of the original material. After implantation a p-n junction will exist at the depth at which the implanted, electrically active impurity concentration equals the background carrier concentration[13,14]. By measuring the depth of the p-n junction in each specimen, an electrically active profile can be built up. The p-n junction depth can be found by a drilling (bevelling) and staining technique[15,16]. The surface of the specimen is drilled to form a bevelled edge. By then using a suitable stain on this bevelled edge, the depth of the p-n junction can be determined.

### 1.2.1.3 Resistivity Measurements

The active carrier concentration in a semiconductor can be found from resistivity measurements. The most common method of measuring resistivity is the four-point probe method[17,18]. A small current from a constant current source is passed through the outer two probes and the voltage is measured between the inner two probes. For a thin slice, with its thickness, W, much smaller than its diameter and the probe spacing $S >> W$, the resistivity is given by:-

$$\rho = \left(\frac{\pi}{\ln 2}\right) \frac{V}{I.W}$$

From the resistivity, the active impurity concentration of a semiconductor can be found, from the relation

$$\rho = \frac{1}{e\,\mu_n\,n} \qquad \text{for an n-type semiconductor}$$

By successive surface layer strips and resistivity measurements an active carrier concentration versus depth profile can be obtained[5,19,20,21].

1.2.1.4 Hall Measurements

Hall measurements used in conjunction with surface layer stripping will yield depth information about the concentration and mobility of the electrically active carriers in the semiconductor. Performing Hall measurements at low variable temperatures gives information about the conduction processes in the semiconductor. When making Hall measurements, an electric field is applied along the x-axis of the specimen, a magnetic field applied along the z-axis and the resultant Hall voltage measured on the y-axis of the specimen. The theory of Hall measurements is given in Section 2.6, and the experimental techniques employed in this project are given in Section 3.3.5.

1.2.1.5 Rutherford Backscatter Technique

Using the Rutherford backscatter technique[22,23,24], information can be obtained about crystal damage, location and type of impurity atom. The location and type of impurity atom can be found only when the atomic weight of the impurity atom is greater than the specimen background atomic weight.

The specimen is mounted on a goniometer with two directions of rotation. The specimen is bombarded with a beam of high energy, light ions, such as hydrogen ions (protons) or helium ions. By means of a suitably positioned detector, the resultant backscattered ions can be analysed. Backscattered results can be obtained from a randomly orientated crystal and from a specimen orientated such that the incident beam is in one of the crystal channeling directions. Analysis of the energy of the backscattered yield will give information on the

crystal damage and the location and type of impurity atom.

This technique might be considered non-destructive, however the method produces radiation damage in the material.

### 1.2.2 Non-Destructive Techniques

#### 1.2.2.1 Surface Barrier Diode Techniques

The following measurement techniques all utilise the properties of metal-semiconductor junctions. A surface barrier diode is manufactured by depositing a metal, with a suitable work function, onto the surface of the semiconductor[25]. This deposition of metal can be achieved by chemical deposition, electrochemical deposition or vacuum deposition. The most commonly used method is vacuum deposition; whereby the metal is heated to vaporisation temperature under a vacuum, and the vaporised metal allowed to condense onto the surface of the semiconductor. For measurement purposes, ohmic contact has to be made to the semiconductor. This can be achieved by the deposition of a suitable metal onto the semiconductor. The surface barrier diode approximates to an abrupt junction, the theory of which is given in Section 2.4.1.

As well as the surface barrier diode it is possible to use a shallow p-n junction. However, problems arise in knowing the depth of the p-n junction and its abruptness.

Although these techniques are in principle non-destructive, in practice the removal of the metal from the semiconductor is difficult to achieve without contamination of the surface of the material. However the process of carrying out the measurements does not damage the material.

#### 1.2.2.1.1 Current-Voltage Measurements

Measurement of the forward voltage-current characteristics of the diode can yield information about the diode barrier height and give an indication of electron lifetime and mobility[29].

#### 1.2.2.1.2 Capacitance-Voltage Measurements

Capacitance-voltage measurements on a surface barrier diode will yield the concentration of electrically active impurities with depth from the surface of the specimen. The measurement method is based on the fact that for an abrupt junction[30] the slope of the reciprocal of the square of junction capacitance versus applied reverse bias voltage, is a simple function of the electrically active doping concentration at the edge of the depletion region (see Section 2.4.1). The most common method of carrying out the capacitance measurements is to use a transformer ratio arm bridge. Variations with frequency have been found by workers[31,36], such that the selection of the measuring frequency is important (see Section 2.4.2). If a high enough frequency is chosen, then only shallow levels will respond. The capacitance and hence the concentration will reflect this fact.

Several methods have been developed for carrying out automatic capacitance-voltage measurements[26,27,28,32]. Most of these plot concentration with depth directly. Probably the best known is the Copeland technique[33]. This technique is an automatic one, giving a direct active impurity concentration profile with depth using an a.c. method suggested by Meyer[34] and later developed by Copeland[33] and Spiwack[35]. The automatic methods have the advantage of speed with a minimum of analysis, but suffer from the disadvantage that

measurements are carried out at a fixed frequency. It is possible to carry out manual measurements at different frequencies. From such measurements, it may be possible to determine the concentration of deep energy levels[36,37].

## 1.3 The Properties and Applications of Gallium Arsenide

Early semiconductor technology was based on the two group IV elemental semiconductors, germanium and silicon, with the technology of silicon superceding that of germanium. Of all the semiconductor materials silicon has the most highly developed technology and is the most widely used. Considerable research has directed attention away from silicon now, towards the newer compound semiconductors. Generally the technology of compound semiconductors has been more difficult than that of silicon, hence the preference to use silicon wherever possible. Of the compound semiconductors the III-V compounds have proved to be the most important and those with the most applications.

Gallium arsenide is a direct-gap semiconductor with a zinc blende crystal structure, whereas the elemental semiconductors, germanium and silicon, both have a diamond crystal structure and indirect band-gap. Table I shows the main properties of gallium arsenide, germanium and silicon.

In the group IV elemental semiconductors doping is by the introduction of small quantities of group III or group V impurities. Donor action is brought about by the replacement of a group IV atom in the crystal structure by a group V impurity atom. The group IV atom has four valence electrons, the group V atom has five valence electrons and the group III atom has three valence electrons. Replacement of a group IV atom with a group V atom will leave one excess electron, not used in the covalent bonding within the material, bound to the atom.

If sufficient energy is given to this electron it becomes free of the atom it is bound to and is able to move around in the crystal structure. This free electron is known as a donor electron. Similarly if a group IV atom is replaced by a group III atom a deficiency of one electron is left in the structure. This deficiency, or hole, is not able to move in the structure, but is bound to the atom. The hole effectively moves by being filled by an electron from another atom. The mechanism for the production of donor electrons and holes in compound semiconductors is not quite so straightforward.

In gallium arsenide the common donor atoms come from the groups IVB and VIB of the periodic table. The donor action being brought about by the replacement of a group III or group V atom in the crystal structure by a group IV or a group VI impurity atom respectively. The replacement of a gallium or arsenic atom in the crystal structure by a group IV or group VI atom respectively will leave an excess electron loosely bound to the impurity atom. Doping with group IV or group VI impurity atoms can produce two other possible effects:-

(a) The replacement of an arsenic atom by a group IV atom will leave a deficiency of one electron, i.e. the group IV atom in this case is acting as an acceptor. Examples of this are the group IVB impurity atoms, silicon and germanium, which produce acceptor levels at 0.026 eV and 0.08 eV respectively from the valence band.

(b) The replacement of a gallium atom by a group VI atom will leave three excess electrons bound to the impurity atom i.e. three donor electrons. An example of this is selenium as an impurity atom. Selenium in gallium arsenide produces two energy levels, one at 0.005 eV from the conduction band and the other 0.53 eV from the

valence band. The shallow level can be attributed to the replacement of arsenic by selenium and the deep level by the replacement of gallium by selenium.

The situation is much more complicated when considering acceptor impurities in gallium arsenide. Groups I, II, IV, VIA, VIIB and VIII are found to be acceptors. Table II lists some common donors and acceptors in gallium arsenide. The replacement of arsenic by groups I, II and IV can be seen to give a deficiency of electrons. Similarly with the replacement of gallium by groups I and II. Difficulty arises with the groups VIA, VIIB and VIII which exhibit the properties of acceptors, but from the simple explanation outlined above, should be donors. These three groups form part of a series of elements known as the transition elements. One of the more significant properties of transition elements is that of variable valency. Iron exhibits valencies of two, three and six; valencies two and three form the most stable compounds. Manganese can have valencies from two to seven; valancies two and four being the most stable. The variable valencies of the transition elements can be explained as being due to the small differences in energy between the orbitals of the outer and penultimate electron shells (in the case of the first long period, the 4p and 3d orbitals). Copper has a more usual valency of two, chromium three, cobalt three also and nickel of two. These valencies explain, in terms of the theory already outlined, why these impurity atoms act as acceptors and not donors.

Gallium arsenide has important applications in bulk and junction devices.

### 1.3.1 Bulk Devices

The most important and best known application of gallium arsenide as a bulk device is its use in microwave devices. It is widely used as a source of microwaves in the form of the Gunn Oscillator. Gunn[38,39] discovered that when an applied d.c. electric field, across a randomly orientated short n-type sample of gallium arsenide or indium phosphide, exceeded a critical threshold value of several thousand Volts per centimetre, coherent microwave output was generated. The frequency of oscillation was approximately equal to the carrier transit time across the length of the specimen. Hutson et al.[40] and Allen et al.[41] demonstrated that differential negative resistance was responsible for the microwave oscillation. Ridley and Watkins[42] and Hilsum[43] proposed that the mechanism causing the differential negative resistance is a field-induced transfer of conduction-band electrons from a low energy, high mobility valley to higher energy, low mobility satellite valleys.

### 1.3.2 Junction Devices

#### 1.3.2.1 Infra-red Devices

Gallium arsenide diodes are used widely as a source of infra-red radiation. This property has important applications in areas where decoupling between the input signal, or control signal, and the output is required. Gallium arsenide diodes are used therefore as the sources in such devices (e.g. photo-coupled isolators).

Gallium arsenide diodes can be made to emit radiation in the visible region of the spectrum (in the red region). These light emitting diodes (LED) are used widely in solid state displays and are finding applications as replacements for small tungsten filament

bulbs. Their advantages being a long lifetime, low current drain, low operating voltage and small physical size.

### 1.3.2.2 Semiconductor Lasers

Another major application of the gallium arsenide diode is as a junction laser. Gallium arsenide was the first semiconductor material to lase. This laser action was achieved by three groups of workers simultaneously; Hall[44], Nathan[45] and Quist[46] in 1962. To achieve laser action there are three basic requirements:-

(i) A method of excitation, or pumping of electrons from a lower level to a higher level.

(ii) A large number of electrons, which are inverted to give sufficient stimulated emission to overcome the losses.

(iii) A resonant cavity to provide positive feedback and quantum amplification. The most common pumping method in the gallium arsenide laser is electron-hole injection in a p-n junction. The pumping is achieved by simply passing a current through the diode. The most widely used resonant cavity is the Fabry-Perot cavity[47,48], with two opposite sides cleaved or polished and the other two sawn or roughened. The gallium arsenide can be pumped by other techniques e.g. electron beam pumping, avalanche breakdown pumping and optical pumping.

### 1.3.2.3 Metal-Semiconductor Diodes

The earliest work on the metal-semiconductor barrier is attributed to Braun in 1874[49], who noted the dependence of the resistance on the polarity of the applied voltage and on the surface condition. In 1931 Wilson[50] formulated the transport theory of

semiconductors based on the band theory of solids. This theory was applied to the metal-semiconductor contacts. In 1938 Schottky[51] proposed that the potential barrier between a metal and a semiconductor could arise from stable space charges in the semiconductor alone, without the presence of a chemical layer, this being known as the Schottky barrier. Mott in 1938[52] proposed a theoretical model for swept out metal-semiconductor contacts and known as the Mott barrier. Metal-semiconductor contacts have important applications in direct current and microwave work and as tools for physical analysis. Table III lists the metals commonly used as metal contacts on gallium arsenide and the measured Schottky barrier heights[53].

1.3.2.4 Junction Transistors

Of all semiconductor devices the junction transistor is the most important. The invention of the transistor (a contraction of transfer resistor) by a research team at the Bell Laboratories in 1948 has had an unprecedented impact on the electronics industry in general and on solid-state research in particular. Prior to 1948, semiconductors had found application only as thermistors, photo-diodes and rectifiers. 1948 saw the development of the point-contact transistor by Bardeen and Brattain[67]. In the following year Shockley's classic paper on junction diodes and transistors was published[54].

Transistor technology has enjoyed many breakthroughs, particularly in the alloy junction[55] and grown-junction techniques[56] and in zone refining[57], diffusion[58,59,60], epitaxial[61], planar[62], beam lead[63] and ion implantation[64,65] technologies. These technologies have helped to increase the power and frequency capabilities and the reliability of transistors.

Among the three main semiconductors, silicon, germanium and gallium arsenide; the gallium arsenide n-p-n junction transistor can theoretically give the highest cut-off frequency, and germanium transistors have some margin over silicon transistors. In practice however, the silicon transistor with its more advanced device and material technology, gives a performance comparable, or superior, to that of the germanium transistor. Gallium arsenide transistors suffer from many technological problems, which include poor starting material, difficulty in control of the impurity doping profile, difficulty in the insulator masking process, thermal conversion (e.g. it converts from p-type to n-type under high temperature treatment) and from copper contamination[66]. The gallium arsenide transistor also suffers from other fundamental physical limitations such as low hole mobility, low thermal conductivity and low minority carrier lifetime (as a result of its direct band-gap). When the technological problems of gallium arsenide have been solved, it will be possible to take advantage of its properties, in order to extend the performance of transistors to:-

(a) higher frequencies, because of the high electron mobility and electron velocity.

(b) higher powers, because of its high breakdown field and wide band-gap,

(c) cryogenic operation, because of the shallow impurity ionization energies.

## 1.4 The Role of Ion Implantation

Ion implantation offers the promise of highly controlled doping of semiconductors at room temperature. In practice however, all is not as convenient as might have been supposed at first. The bombardment of a crystal with energetic ions causes disruption of the crystal structure. Bonds are broken and atoms are misplaced in the structure. This damage in elemental semiconductors can almost wholly be removed by annealing[68]. However, in compound semiconductors reduction is possible, but annealing will not totally realign the crystal. Complexes are produced by annealing in compound semiconductors and no amount of annealing will completely remove them. Due to the low melting points of Group III-V compound semiconductors, doping with impurity atoms in these materials is made difficult by conventional diffusion techniques. Ion implantation offers the possibility of doping such materials at temperatures much lower than those required for diffusion techniques. Using ion implantation, impurity atoms can be introduced at room temperature into semiconductor crystals. The number of impurity atoms introduced (the ion dose) can be controlled accurately and their depth distribution controlled by means of the incident energy[65]. The greatest problem in the field of the ion implantation of compound semiconductors is the introduction of damage into the crystal during implantation and its subsequent reduction by annealing.

Ion implantation, perhaps, offers its greatest promise in the specialised device market. Devices are being manufactured commercially using ion implantation, these being mainly silicon devices. However, for economic reasons these are of a specialised nature where the advantages of ion implantation can be exploited to produce a superior device. The problems of annealing and encapsulation

have, to date, made the ion implantation manufacture of compound semiconductor devices less practical.

The main experimental technique chosen in this research project to investigate the electrical properties of gallium arsenide, after bombardment with energetic heavy ions, was the differential capacitance-voltage technique.

This measurement technique is a non-destructive technique which can yield considerable information about the concentration of electrically active impurity atoms in the semiconductor as a function of depth. Current-voltage measurements were also carried out on the surface barrier diodes, prepared for differential capacitance measurements. To verify the results obtained by these techniques, a series of Hall measurements was carried out.

When carrying out differential capacitance-voltage measurements the choice of starting material, doping and impurity atom is important. Table IV shows the predicted projected range, calculated from the Lindhard Range Theory[70] of some atoms in gallium arsenide. For early measurements phosphorus was chosen as the impurity atom, but the majority of measurements were carried out using sulphur atoms. Sulphur was chosen because of its long range in gallium arsenide and because it forms a shallow level at 0.007 eV from the conduction band[71]. It was thought that if the capacitance-voltage measurements were employed with an impurity atom with a long range in the target, then the best results would be obtained, enabling the whole of the profile to be measured. Theoretical calculations were used to determine the optimum impurity atom, dose, energy and starting material concentration. A computer program was used to facilitate these calculations. The impurity atoms were assumed to have a Gaussian

distribution and the percentage becoming electrically active assumed. The results of these calculations provided a reasonable starting point for the experimental work. Some implantations were carried out using the inert element argon for damage studies.

Sulphur atoms have a long theoretical range in gallium arsenide. Sansbury and Gibbons[72] and Zelevinskaya and Kachurin[73] have both observed that the impurity atom range of sulphur in gallium arsenide is much greater than that predicted by the Lindhard range theory. They also observed that the profile has a super-tail extending several microns into the material. This they considered to be due to the diffusion of the impurity atoms during annealing.

PROPERTIES OF GALLIUM ARSENIDE, GERMANIUM AND SILICON AT 300K [29]

| PROPERTY | GALLIUM ARSENIDE | GERMANIUM | SILICON |
|---|---|---|---|
| Atoms/$cm^3$ | $2.21 \times 10^{22}$ | $4.42 \times 10^{22}$ | $5.0 \times 10^{22}$ |
| Atomic Weight | 144.63 | 72.6 | 28.08 |
| Crystal Structure | Zinc Blende | Diamond | Diamond |
| Lattice Constant (Å) | 5.6534 | 5.65748 | 5.43086 |
| Density ($g\text{-}cm^{-3}$) | 5.32 | 5.3267 | 2.328 |
| Melting Point (°C) | 1238 | 937 | 1420 |
| Specific Heat ($Jg^{-1}{}^{o}C$) | 0.35 | 0.31 | 0.7 |
| Thermal Conductivity (Watt $cm^{-1}{}^{o}C$) at 300K | 0.46 | 0.64 | 1.45 |
| Thermal Diffusivity ($cm^2sec^{-1}$) | 0.44 | 0.36 | 0.9 |
| Vapour Pressure (Torr) | 1 at 1050°C<br>100 at 1220°C | $10^{-3}$ at 1270°C<br>$10^{-8}$ at 800°C | $10^{-3}$ at 1600°C<br>$10^{-8}$ at 930°C |
| Electron Mobility ($cm^2$/V-sec) | 8500 | 3900 | 1500 |
| Hole Mobility ($cm^2$/V-sec) | 400 | 1900 | 600 |
| $u_{sl}$ (Electrons)(cm $sec^{-1}$) | $10^7$ | $6 \times 10^6$ | $10^7$ |
| $u_{sl}$ (Holes)(cm $sec^{-1}$) | $10^7$ | $6 \times 10^6$ | $6 \times 10^6$ |
| Dielectric Constant | 12 | 12 | 16 |
| Breakdown Field ($V\ cm^{-1}$) for $N_c = 3 \times 10^{15} cm^{-3}$ | $3.8 \times 10^5$ | $2 \times 10^5$ | $3.4 \times 10^5$ |
| Energy Gap at 300K (eV) | 1.43 | 0.803 | 1.12 |
| Intrinsic Carrier Concentration ($cm^{-3}$) | $1.1 \times 10^7$ | $2.5 \times 10^{12}$ | $1.6 \times 10^{10}$ |
| Electron Affinity (Volt) | 4.07 | 4.0 | 4.05 |
| Minority Carrier Lifetime (sec) | $\sim 10^{-8}$ | $10^{-3}$ | $2.5 \times 10^{-3}$ |
| Work Function (Volt) | 4.7 | 4.4 | 4.8 |
| Effective Density of States in conduction band $N_c$ ($cm^{-3}$) | $4.7 \times 10^{17}$ | $1.04 \times 10^{19}$ | $2.8 \times 10^{19}$ |
| Effective Density of States in valence band $N_v$ ($cm^{-3}$) | $7.0 \times 10^{18}$ | $6.1 \times 10^{18}$ | $1.02 \times 10^{19}$ |

TABLE I cont.

| PROPERTY | GALLIUM ARSENIDE | GERMANIUM | SILICON |
|---|---|---|---|
| Effective Mass $m^*$ electrons | 0.068 | $ml^* = 1.6$<br>$mt^* = 0.082$ | $ml^* = 0.97$<br>$mt^* = 0.19$ |
| Effective Mass $m_o$ holes | 0.5 | $mlh^* = 0.04$<br>$mhh^* = 0.3$ | $mlh^* = 0.16$<br>$mhh^* = 0.5$ |

where:-

$ml^*$ = longitudinal effective mass

$mt^*$ = transverse effective mass

$mlh^*$ = light hole effective mass

$mhh^*$ = heavy hole effective mass

TABLE II

ACTIVE DOPANT IMPURITIES IN GALLIUM ARSENIDE[37]

DONORS

| ATOM | ENERGY (electron Volts) |
|---|---|
| Te | 0.003 from conduction band |
| Si | 0.002 from conduction band |
| S | 0.007 from conduction band |
| Ge | Shallow level from conduction band |
| Sn | Shallow level from conduction band |
| O | 0.63 from valence band |
| Se | 0.005 from conduction band<br>0.53 from valence band |

ACCEPTORS

| ATOM | ENERGY (electron Volts) |
|---|---|
| Mg | 0.012 from valence band |
| C | 0.019 from valence band |
| Cd | 0.021 from valence band |
| Zn | 0.024 from valence band |
| Mn | 0.096 from valence band |
| Co | 0.16 from valence band |
| Ni | 0.21 from valence band |
| Si | 0.026 from valence band |
| Ge | 0.08 from valence band |
| Fe | 0.37<br>0.52 from valence band |
| Cr | 0.70 from valence band |
| Li | 0.023<br>0.143 from valence band |
| Cu | 0.023<br>0.15<br>0.24 from valence band<br>0.51 |

TABLE III

MEASURED SCHOTTKY BARRIER HEIGHTS AT 300K[53]

| SEMICONDUCTOR | METAL | BARRIER HEIGHT (VOLTS) | | |
|---|---|---|---|---|
| | | I-V | C-V | Photo |
| n-GaAs (Vacuum cleaved) | Au | | 0.95 | 0.90 |
| | Pt | | 0.94 | 0.86 |
| | Be | | 0.82 | 0.81 |
| | Ag | | 0.93 | 0.88 |
| | Cu | | 0.87 | 0.82 |
| | Al | | 0.80 | 0.80 |
| | Al (77K) | | 0.88 | |
| p-GaAs (Vacuum cleaved) | Au | | 0.48 | 0.42 |
| | Au (77K) | | 0.46 | |
| | Pt (77K) | | 0.48 | |
| | Ag (77K) | | 0.44 | |
| | Cu (77K) | | 0.52 | |
| | Al | | 0.63 | 0.50 |
| | Al (77K) | | 0.61 | |
| n-GaAs | W | 0.71 | 0.77 | 0.80 |

TABLE IV

RANGES (LSS) IN GaAs

| | Energy (keV) | Proj. Range (Å) | Proj. Standard Deviation (Å) |
|---|---|---|---|
| Sulphur 32 | 100 | 766 | 343 |
| | 200 | 1539 | 592 |
| | 300 | 2323 | 802 |
| | 400 | 3097 | 974 |
| Argon 40 | 100 | 678 | 293 |
| | 200 | 1357 | 519 |
| | 300 | 2052 | 711 |
| | 400 | 2755 | 882 |
| Hydrogen - Protons | 100 | 8409 | 1440 |
| | 200 | 13693 | 1578 |
| | 300 | 17863 | 1636 |
| | 400 | 21421 | 1667 |
| | 500 | 24576 | 1687 |
| Tellurium | 200 max. Double charged | 508 | 145 |
| Oxygen | 200 | 3120 | 1061 |
| | 400 | 5984 | 1507 |
| Neon | 200 | 2550 | 901 |
| | 400 | 4932 | 1352 |
| Selenium | 200 | 710 | 244 |
| | 400 | 1378 | 433 |
| Phosphorus | 100 | 819 | 366 |
| | 200 | 1651 | 630 |
| | 300 | 2493 | 850 |
| | 400 | 3322 | 1028 |

Ranges determined using Lindhard Range Theory[70]

# 2.0 THEORY

## 2.1 Symbols used in the Text

| | |
|---|---|
| $A$ | Surface area of diode |
| $A_R^{**}$ | Effective Richardson's constant |
| $\beta$ | Recombination factor |
| $C$ | Capacitance |
| $\chi_s$ | Electron affinity of the semiconductor |
| $d_n$ | Depletion width in n-type material |
| $d_p$ | Depletion width in p-type material |
| $D_n$ | Electron diffusion coefficient |
| $e$ | Electronic charge |
| $E$ | Electric field |
| $E_c$ | Energy level of the bottom of the conduction band |
| $E_f$ | Fermi energy level |
| $E_g$ | Band-gap of the semiconductor |
| $E_s$ | Surface field in the barrier |
| $E_v$ | Energy level of the top of the valence band |
| $\epsilon$ | Permittivity of the semiconductor |
| $\epsilon_o$ | Permittivity of free space |
| $\epsilon_r$ | Relative permittivity of the semiconductor |
| $I$ | Current |
| $J_n$ | Current density |
| $J_o$ | Saturation current density |
| $J_R$ | Recombination current density |
| $k$ | Boltzman's constant |
| $\Gamma_H$ | Hall scattering factor |
| $\mu_H$ | Hall mobility |
| $\mu_n$ | Mobility of electrons |

| | |
|---|---|
| $m_*$ | Effective mass |
| $n$ | Diode quality factor |
| $N$ | Number of particles per unit area |
| $N_A$ | Acceptor concentration |
| $N_c$ | Effective density of states in the conduction band |
| $N_D$ | Donor concentration |
| $\omega$ | Angular frequency |
| $\phi_{Bn}$ | Barrier height of metal-semiconductor barrier |
| $\phi_m$ | Work function of the metal |
| $Q$ | Charge per unit area |
| $R_H$ | Hall coefficient |
| $\rho$ | Space charge density |
| $\sigma$ | Conductivity |
| $\tau$ | Electron lifetime |
| $\tau'$ | Ionization time constant |
| $u$ | Carrier velocity |
| $u_{sl}$ | Scattering-limited velocity |
| $V$ | Applied voltage |
| $V_d$ | In-built potential |

Subscripts:

| | |
|---|---|
| x | in x-direction |
| y | in y-direction |
| z | in z-direction |

## 2.2 Physics of Schottky Barriers

A metal and an n-type semiconductor, whose electron affinity is less than that of the metal, are both electrically neutral and separated from each other. The energy band diagram is shown in Figure 1(a), the zero of energy being the energy of an electron at rest outside either solid. If the metal and semiconductor are connected electrically, electrons flow from the semiconductor to the metal and the Fermi levels move into coincidence due to the laws of thermodynamics. The energy of an electron at rest outside the surfaces of the two solids is no longer the same, and there is an electric field in the gap from right to left as in Figures 1(b) and (c). There must be a negative charge on the surface of the metal balanced by a positive charge on the semiconductor. This positive charge is provided by conduction electrons receding from the surface, leaving uncompensated donor ions. The concentration of these donors is many orders of magnitude less than the concentration of electrons in the metal, the balancing positive charges occupy a layer of appreciable thickness, and the bands in the semiconductor are bent upwards as shown. If the gap between metal and semiconductor disappears then we are left with a potential barrier arising from the band bending. The work function of the metal ($\phi_m$) and the electron affinity of the semiconductor ($\chi_s$) remain unaltered. For a perfect contact,

$$\phi_{Bn} = \phi_m - \chi_s$$

the well-known Schottky relationship[30].

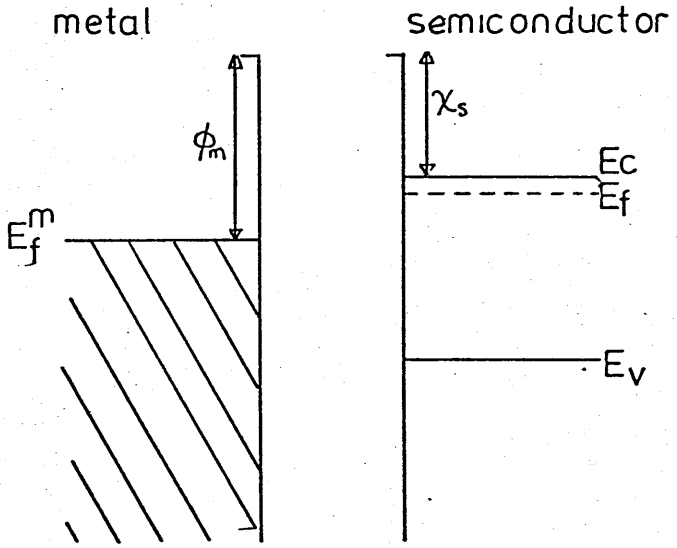


Fig.1a.

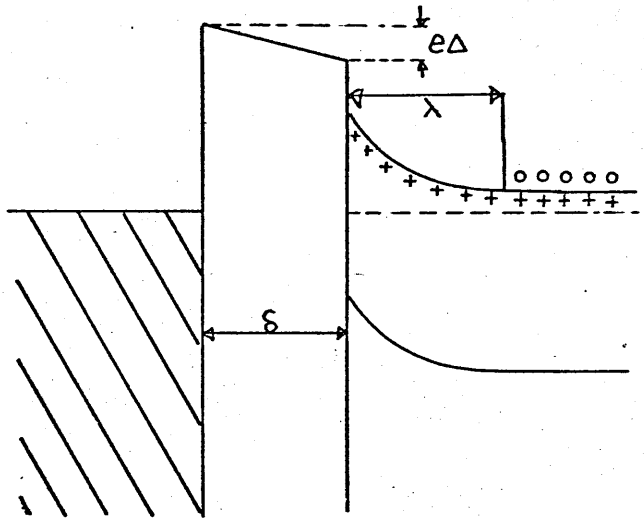


Fig.1b.

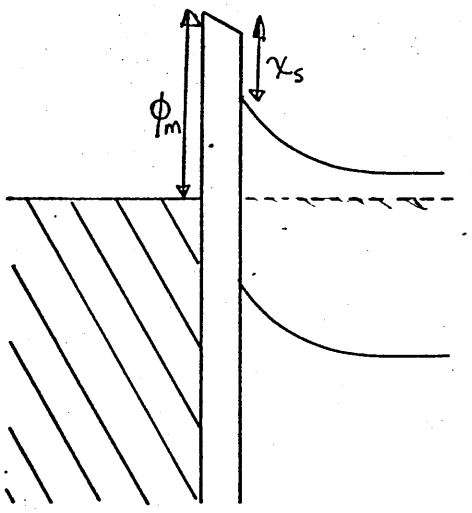


Fig.1c.

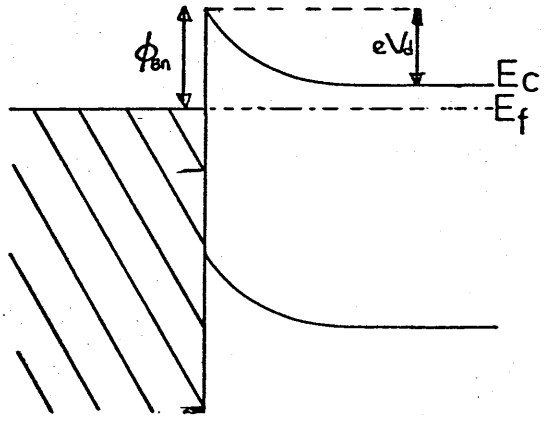


Fig.1d.

Fig. 1. BAND ENERGY DIAGRAMS OF A METAL-SEMICONDUCTOR CONTACT (N-TYPE)

## 2.3 Current-Voltage Characteristics

Consider a metal-semiconductor barrier with impurity or defect levels present in the band-gap. Those levels present can affect the forward bias current if the barrier height is greater than Eg/2, where Eg is the band-gap of the semiconductor. In such a barrier at zero bias, as shown in Figure 1(d), there is a region where the Fermi level is closer to the valence band than the conduction band and the centres can act as hole electron recombination centres. Under the application of forward bias three mechanisms contribute to the total current.

(a) Diffusion

motion of semiconductor electrons over the top of the barrier,

(b) Injection of holes

injection of holes from metal into the semiconductor (minority carrier injection),

(c) Recombination

recombination and generation of hole-electron pairs in the depletion region.

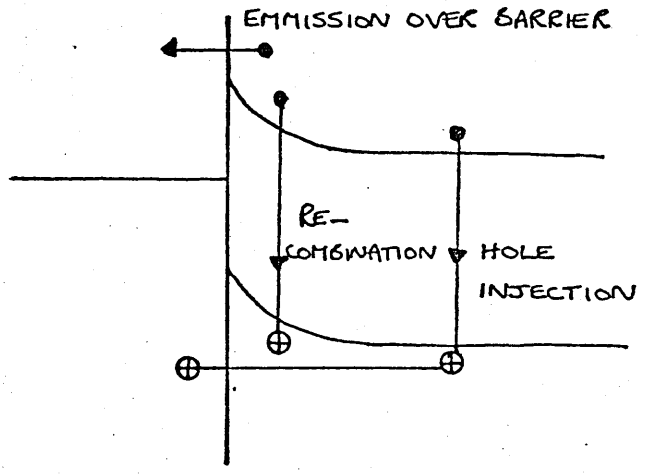


Conduction mechanisms in a Schottky barrier

Figure 2

The term diffusion current is a misnomer since it consists of drift and diffusion terms.

At high currents, limiting of the current will occur due to the series resistance of the diode.

### 2.3.1 Diffusion[76]

A metal semiconductor barrier has donor concentration, $N_D$. The diffusion current is calculated from the solution of the equation:

$$J_n = e\mu_n N(x)E(x) + eD_n \frac{dN(x)}{dx} \quad \text{..... (1)}$$

(drift term) (diffusion term)

For high forward bias the diffusion current predominates and we obtain the diffusion current density:

$$J_n = A_R \left[\exp\left(\frac{eV}{kT}\right) - 1\right] \quad \text{..... (2)}$$

where

$$A_R = \frac{e^2 D_n N_c}{kT} \left[\frac{e\left(V_d - V\right) 2N_D}{\varepsilon}\right]^{\frac{1}{2}} \exp\left(\frac{\phi_{Bn}}{kT}\right) \quad \text{..... (3)}$$

and

$$D_n = \frac{kT}{e} \mu_n \quad \text{..... (4)}$$

hence

$$A_R = eN_c\mu_n \left[\frac{e(V_d - V)\, 2N_D}{\varepsilon}\right]^{\frac{1}{2}} \exp\left(\frac{-\phi_{Bn}}{kT}\right) \quad \text{..... (5)}$$

From ( 2 ) taking logs:

$$\text{In } J_n = \ln A_R + \frac{eV}{kT}$$

for an ideal diode. By plotting ln $J_n$ versus voltage, the intercept with the ln $J_n$ axis gives the value of ln $A_R$. From equation (5), if either $\mu_n$, the mobility of electrons, or the barrier height, $V_d$, is known the other can be obtained. It is therefore possible to calculate the electron mobility, $\mu_n$, for the material knowing the barrier height from C-V measurements.

Usually in practice, the I-V characteristic is of the form:

$$J_n \propto \exp \frac{eV}{nkT} \qquad \ldots\ldots\ldots\ldots\ldots\ldots\ldots \quad (6)$$

where n is known as the quality factor and usually lies between 1 and 2 and gives an indication of the quality of the diode. For an ideal case n would be 1.

The barrier height can be calculated knowing the effective Richardson's constant from:

$$J = A_R^{**}T^2 \exp \frac{\left(-e\phi_{Bn}\right)}{kT} \text{ EXP } \frac{e(\Delta\phi + V)}{kT}$$

where

$$\phi_{Bn} = \frac{kT}{e} \ln \frac{\left(A_R^{**} T^2\right)}{J_o}$$

and $\phi_{Bn}$ is not sensitive to the value of $A_R$.

### 2.3.2 Injection of Holes[75]

For large area evaporated film Schottky contacts on n-type semiconductors, the injection ratio (ratio of electron density at the interface to the hole density in the bulk of the semiconductor) for holes is exceedingly small at low current densities. The injection of holes into the neutral region of the semiconductor plays only a minor part in the total current flowing.

### 2.3.3 Recombination

The current density takes the general form:-

$$J_R = J_o \left| \exp \frac{(eV)}{\beta kT} - 1 \right| \qquad \ldots\ldots\ldots\ldots\ldots\ldots\ldots \quad (7)$$

The factor can take values between 1 and 2 and is given by,

$$\beta = \frac{2V_d\, e}{E_g}$$

For recombination to occur $\beta > 1$.

By suitable analysis[105]:

$$J_R = \frac{1}{\tau}\left[\beta \frac{(kT)}{E_s}\right] N_c \lesssim \exp\left[-\frac{(1)}{\beta kT}(\phi_{Bn} - eV)\right] - 1 \lesssim \qquad \ldots\ldots \quad (8)$$

Hence

$$\tau = \frac{\beta}{J_o} kTN_c \left|\frac{2eN_D V_d}{k}\right|^{-\frac{1}{2}} \exp -\frac{(\phi_{Bn})}{\beta kT} \qquad \ldots\ldots\ldots\ldots\ldots\ldots \quad (9)$$

where

$$E_s = \left|\frac{(2e)}{k} N_D\, V_d\right|^{\frac{1}{2}} \quad \text{and} \quad \beta = \frac{2\phi_{Bn}}{E_g}$$

where $E_s$ is the surface field in the barrier, $\phi_{Bn}$ is the barrier height, $\tau$ is the electron lifetime.

Hence from the graph of ln $J_R$ versus voltage, the barrier height can be obtained and from the extrapolated intercept with the $J_R$ axis an indication of $\tau$, the electron lifetime, can be found.

## 2.4 Capacitance-Voltage Characteristics[77-82]

### 2.4.1 Capacitance of an abrupt junction depletion layer

When considering the Schottky barrier capacitance, the problem is tackled in the same way as an abrupt p-n junction.

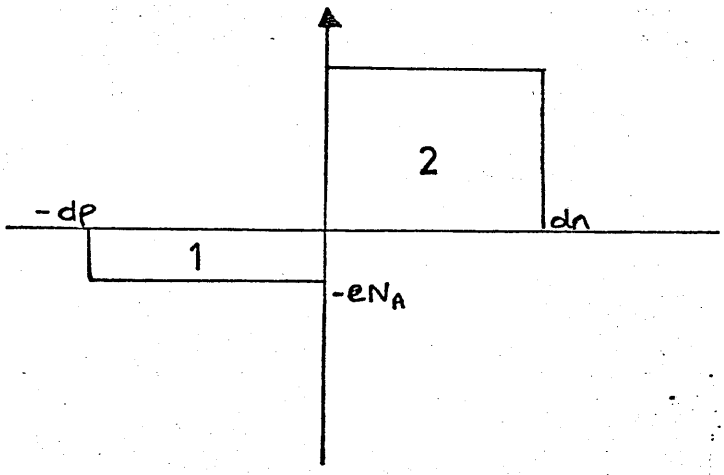


Charge distribution at an abrupt junction

Figure 3

$\rho$ = space charge density

$\rho = e(N_D - N_A)$

Consider a p-n junction formed from p-type material, containing an acceptor concentration, $N_A$, and n-type material containing a donor concentration, $N_D$, then the space charge density, $\rho = e(N_D - N_A)$, is shown in the diagram (Figure 3); such a junction is called an abrupt junction.

Let the depletion layer so formed be the region $-d_p < x < d_n$.

To calculate the distances $d_p$ and $d_n$ we solve Poisson's equation for the two regions:-

Region 1. $\quad -d_p < x < 0$

Region 2. $\quad 0 < x < d_n$

applying the following boundary conditions to the two regions:-

$\psi = 0$, $X = d_n$

$\psi = -(V + V_d)$ at $X = -d_p$

$E = 0$ at $X = d_n$

$E = 0$ at $X = -d_p$

Poisson's Equation:

$$\frac{d^2V}{dx^2} = \frac{eN}{\varepsilon}$$

The result that we obtain is:

$$d_p = \left[\frac{2\varepsilon_o\varepsilon_r}{eN_D\left(1 + \frac{N_A}{N_D}\right)}\right]^{\frac{1}{2}} (V + V_d)^{\frac{1}{2}} \qquad \ldots\ldots\ldots\ldots\ldots\ldots\ldots \quad (10)$$

and

$$d_n = \left[\frac{2\varepsilon_o\varepsilon_r}{eN_D\left(1 + \frac{N_D}{N_A}\right)}\right]^{\frac{1}{2}} (V + V_d)^{\frac{1}{2}} \qquad \ldots\ldots\ldots\ldots\ldots\ldots\ldots \quad (11)$$

The Schottky barrier diode can be considered an asymmetrical junction i.e. metal n-type semiconductor junction, such that $N_A >> N_D$ and $d_p << d_n$ so that $(d_n + d_p) \rightarrow d_n$

$$d_p \rightarrow 0$$

and

$$d_n = \left[\frac{2\varepsilon_o\varepsilon_r(V + V_d)}{eN_D}\right]^{\frac{1}{2}} \quad \ldots\ldots\ldots\ldots\ldots\ldots\ldots \quad (12)$$

Consider the depletion region as a parallel capacitor then:-

$$d_n = \frac{\varepsilon_o\varepsilon_r A}{C} \quad \ldots\ldots\ldots\ldots\ldots\ldots\ldots \quad (13)$$

Substituting (13) into (12)

$$C^2 = \frac{e\varepsilon_o\varepsilon_r A^2 N_D}{2(V + V_d)}$$

then

$$N_D = \frac{2C^2(V + V_d)}{e\varepsilon_o\varepsilon_r A^2} \quad \ldots\ldots\ldots\ldots\ldots\ldots\ldots \quad (14)$$

In practice, we measure the capacitance of the junction by modulating the d.c. bias with a small a.c. voltage, causing a small modulation of the depletion depth. This will result in an incremental change in capacitance. Consider a reverse biased junction, increasing the reverse bias voltage by an increment, $\Delta V$, causes an increase in depletion depth, $\Delta d_n$.

Number of carriers in increment $\Delta d_n = N_D(d_n)\Delta d_n.A$

Total charge in increment $\Delta d_n = e.N_D(d_n).\Delta d_n.A$

Overall charge increase $\Delta Q = e.N_D(d_n).\Delta d_n.A$

But $$C = \frac{dQ}{dV} = eN_D(d_n).A\,\frac{d(d_n)}{dv} \quad \ldots\ldots\ldots\ldots\ldots\ldots\ldots \quad (15)$$

$$dv = \left(\frac{eN_D\,(d_n).A}{C}\right).d(d_n) \qquad \ldots\ldots\ldots\ldots\ldots\ldots\ldots \quad (16)$$

But

$$d_n = \frac{\varepsilon A}{C}\ ,\ \frac{d(d_n)}{dC} = \frac{-\varepsilon A}{C^2}$$

$$dV = \frac{-e.N_D(d_n).A.\varepsilon.A}{C^3}\ .dC \qquad \ldots\ldots\ldots\ldots\ldots\ldots\ldots \quad (17)$$

$$\frac{dv}{d\left(\frac{1}{c^2}\right)} = \frac{eN_D(dn)A^2\varepsilon}{2} \qquad \ldots\ldots\ldots\ldots\ldots\ldots\ldots \quad (18)$$

Hence from the slope of the graph of $(1/C^2)$ versus V we can obtain the net ionised impurity concentration at a depth, $d_n$. For a uniformly doped semiconductor the graph of $(1/C^2)$ versus voltage will be straight and will cut the voltage axis at the diode barrier height, $V_d$, for $1/C^2 = 0$.

For non-uniformly doped semiconductors, by taking the slope of the $(1/C^2)$ versus voltage graph at each point along it, the concentration of ionised impurities can be found and from the corresponding capacitance at each point, the depth from the surface of the semiconductor can be calculated. Hence a concentration-depth profile of the semiconductor can be built up.

### 2.4.2 Capacitance-Voltage against Frequency

If deep or trapping levels are present in the band-gap of the semiconductor the capacitance of the depletion region will be a function of frequency. Due to band bending, even if these levels are below the Fermi level, they can emerge above it near the surface of the

semiconductor. At low frequencies all the levels may respond and come to an equilibrium thermal ionization state in a time short compared with the applied frequency. However, at higher frequencies they may not all respond.

An evaluation of the capacitance at different frequencies can yield energy levels and trapping rates.

The time constant of the centres in the depletion region can be found from the Schockley-Read theory[83,84], and is given by,

$$\tau' = \frac{1}{C_p(p_o + p_1) + C_n(n_o + n_1)} \quad \ldots\ldots\ldots\ldots\ldots\ldots\ldots \quad (19)$$

where $p_1 C_p$ = emission rate of holes

$p_o$ = steady state hole concentration

$C_n n_1$ = emission rate of electrons

$n_o$ = steady state electron concentration

$p_1 = n^2{}_1/n = n_1 \exp (E_i - E_t)/kT$

and

$C_p$ = emission rate for holes.

$C_n$ = emission rate for electrons

$n_1$, $p_1$ $\varepsilon$ = concentration of deep level

$n_o$, $p_o$ $\varepsilon$ = concentration of shallow ionised level

In the depletion region $p_o = n_o = 0$, the time constant is at its largest and the ionisation rate at its most sensitive to frequency.

Figure 4(a) shows the energy diagram of a Schottky barrier with two levels, one shallow and one deep. Due to band bending the deep

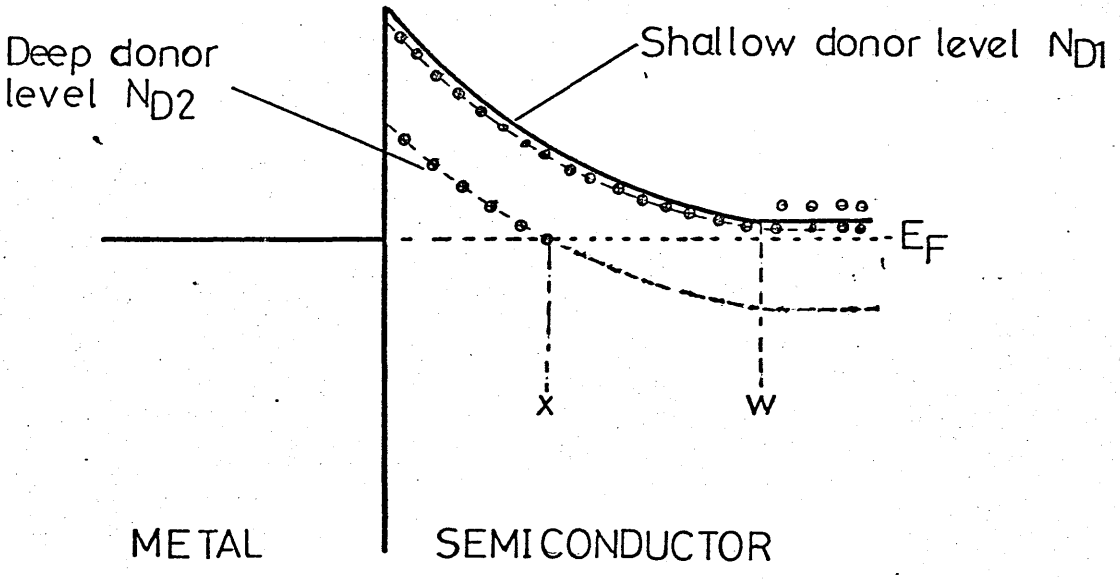


Fig. 4a.

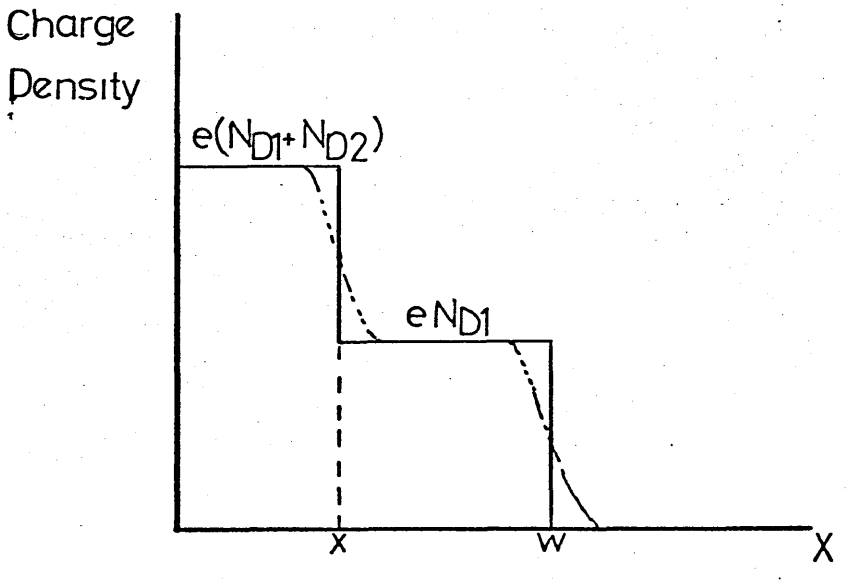


Fig. 4b.

Fig. 4. ENERGY LEVEL DIAGRAM AND CHARGE DENSITY PROFILE WITH TWO LEVELS

level emerges above the Fermi level, near to the surface.

Assuming the Fermi function to be a step function the charge distribution will be as shown in Figure 4(b).

Solving Poisson's equation for this distribution the diffusion voltage, V, is:-

$$V = \frac{e}{2\varepsilon}\left[N_{D_1} W^2 + N_{D_2} X^2\right] \qquad \ldots\ldots\ldots\ldots\ldots\ldots\ldots\ldots \quad (20)$$

Rearranging,

$$\text{Depletion width, } W = \left[\frac{2\varepsilon(V + V_d)}{eN_{D_1}} - \frac{N_{D_2} X^2}{N_{D_1}}\right]^{\frac{1}{2}} \qquad \ldots\ldots\ldots\ldots\ldots\ldots \quad (21)$$

$$W = W_o - \frac{N_{D_2} X^2}{N_{D_1}} \qquad \ldots\ldots\ldots\ldots\ldots\ldots\ldots\ldots \quad (22)$$

and the junction capacitance is:-

$$C = \left[\frac{\varepsilon^2 A^2}{\dfrac{2\varepsilon(V + V_d)}{eN_{D_1}} - \dfrac{N_{D_2} X^2}{\varepsilon^2 A^2 N_{D_1}}}\right]^{\frac{1}{2}} \qquad \ldots\ldots\ldots\ldots\ldots\ldots\ldots\ldots \quad (23)$$

Hence if a deep donor level responds to the applied modulating frequency the depletion width will decrease and the capacitance will increase. Measurements can be used to calculate, $\tau'$, $N_{D_1}$ and $N_{D_2}$ and X. From this the deep energy level can be calculated.

## 2.5 Copeland Technique

The Copeland technique is based upon the following theory[33]:

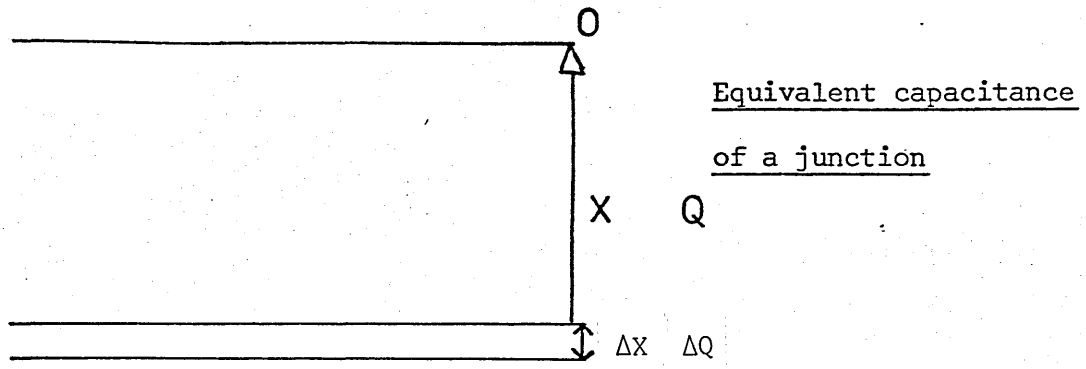


Figure 5

Consider a junction with depletion width, X, with some associated charge, Q, per unit area and potential, V, due to this charge:

$$Q = eNX \qquad \ldots\ldots\ldots\ldots\ldots\ldots \quad (24)$$

$$E = \frac{Q}{\varepsilon} \qquad \ldots\ldots\ldots\ldots\ldots\ldots \quad (25)$$

An incremental change in voltage, $\Delta V$, will cause an incremental change in charge, $\Delta Q$. Hence from (24),

$$\Delta Q = eN(X)\Delta X \qquad \ldots\ldots\ldots\ldots\ldots\ldots \quad (26)$$

For X less than X(Q) the electrical field from (25) and (26) is:-

$$E(X,Q) = \frac{Q}{\varepsilon} - \frac{e}{\varepsilon}\int_0^X N(X)dX \qquad \ldots\ldots\ldots\ldots\ldots\ldots \quad (27)$$

For the depletion layer of a junction, the contact voltage, V, as a function of charge per unit area, Q, is given by,

$$V(Q) = \int E(X,Q)\, dX \qquad \ldots\ldots\ldots\ldots\ldots\ldots \quad (28)$$

If charge per unit area, Q, is increased by $\Delta Q$ then the voltage changes by an increment, $\Delta V$. From (27) and (28) we obtain:-

$$\Delta V = \frac{QX(Q)}{\varepsilon} + \frac{e}{\varepsilon} \int_{X(Q)}^{X(Q+\Delta Q)} \left[N(X')X'\right]_{x}^{X(Q+\Delta Q)} dx \quad \ldots\ldots\ldots\ldots \quad (29)$$

If $\Delta Q$ is small enough so that $N(X)$ may be considered equal to $N(X')$ between $X(Q)$ and $X(Q + \Delta Q)$ then (6) can be written, after taking the difference of two squares:-

$$\Delta V = \frac{\Delta Q X(Q)}{\varepsilon} + \frac{N(X)e}{2\varepsilon} \left\{ X(Q + \Delta Q) - X(Q) \right\}^2 \quad \ldots\ldots\ldots\ldots\ldots \quad (30)$$

From (26)

$$\Delta Q = e \int_{X(Q)}^{X(Q+\Delta Q)} N(x)dx \quad \ldots\ldots\ldots\ldots\ldots\ldots\ldots \quad (31)$$

$$\Delta Q = N(X)e\,[X(Q + \Delta Q) - X(Q)] \quad \ldots\ldots\ldots\ldots\ldots\ldots\ldots \quad (32)$$

Hence substituting in (32) and (30),

$$\Delta V = \frac{\Delta Q}{\varepsilon} X + \frac{\Delta Q^2}{2e\varepsilon N(X)} \quad \ldots\ldots\ldots\ldots\ldots\ldots\ldots \quad (33)$$

If an a.c. current, $I \sin\omega t$, is applied to the diode, an incremental change in charge results:-

$$\Delta Q = \frac{I \cos\omega t}{A\omega}$$

where A is the diode surface area and $\omega$ is the applied frequency $\times 2\pi$. Substitution for $\Delta Q$ in (33),

$$\Delta V = \frac{I \cos\omega t}{\omega\varepsilon A} \cdot X + \frac{I^2[\cos 2\omega t + 1]}{4\omega^2 e\varepsilon A^2} \cdot \frac{1}{N(X)} \quad \ldots\ldots\ldots\ldots\ldots \quad (34)$$

Hence, if an a.c. current is injected into a diode, the fundamental voltage produced is proportional to the depletion layer width and the second harmonic term is proportional to the reciprocal of the net donor density 1/N(X) at depth X. The d.c. term is so small it can be neglected.

The current injection and voltage measurements were carried out using the circuit in Figure 11. The simplified circuit that the diode sees consists of three elements in parallel, a capacitance $C_1$, an inductance $L_1$, and a capacitance, $C_2$, in series with an inductance, $L_2$. The impedance of this idealised circuit is given by:

$$Z(\omega) = \frac{i(\omega L_2 - 1/\omega C_2)}{1 - (\omega C_1 - 1/\omega L_1)(\omega L_2 - 1/\omega C_2)}$$

the condition for $\omega_2 = 2\omega_1$, is given by

$$4(C_2L_1 + C_2L_2 + C_1L_1)^2 = 25\ C_1C_2L_1L_2$$

The solution used for the practical circuit was $L_1C_1 = L_2C_2$ leading to $C_1 = 2C_2$ and $\omega_1 = (2L_1C_1)^{-0.5}$

Due to the finite Q values of the coils, the maximum impedance that can actually be attained is limited to:

$$Z_{max}\ (\omega_1) = Q_1\omega_1L_1$$

$$Z_{max}(\omega_2) = Q_2/\omega_2C_1$$

where $Q_1$ and $Q_2$ are the overall Q values at $\omega_1$ and $\omega_2$:

## 2.6 Hall Effect

The conductivity of a material can be determined by the product of the density and mobility of charge carriers. Evaluation of the charge carrier concentration is not possible from measurements of conductivity alone. Where only one type of charge carrier is present the density of charge carriers can be determined from the Hall coefficient ($R_H$) of the material. Both the carrier density and mobility can be obtained from measurements of conductivity ($\sigma$) and Hall coefficient ($R_H$). The Hall coefficient is defined as:-

$$R_H = \frac{E_Y}{B_Z J_X} \qquad \text{..... (35)}$$

Since the carriers are assumed to be negative, they will drift with an average velocity $\langle u_x \rangle$ in the negative x-direction. When a magnetic field of flux density $B_z$ (Tesla) is applied along the z-direction, the carriers will experience a Lorentz force F, perpendicular to $\langle u_x \rangle$ and to $B_z$; for the configuration of Figure 6(a), the force will be directed along the negative y-axis. The magnitude of this force is given by:-

$$-e\langle u_x \rangle B_z$$

The electronic charge, e, is taken as a positive quantity, so that a minus sign is associated with it for electrons; a positive sign for holes. Thus the negative carriers are driven toward the front face in the sample in Figure 6(a), resulting in an excess of electrons near the front face and a deficiency of electrons near the back face. These charges in turn create an electric field along the negative y-direction. An equilibrium situation is established in which the Lorentz force is just compensated by the force produced by the electric

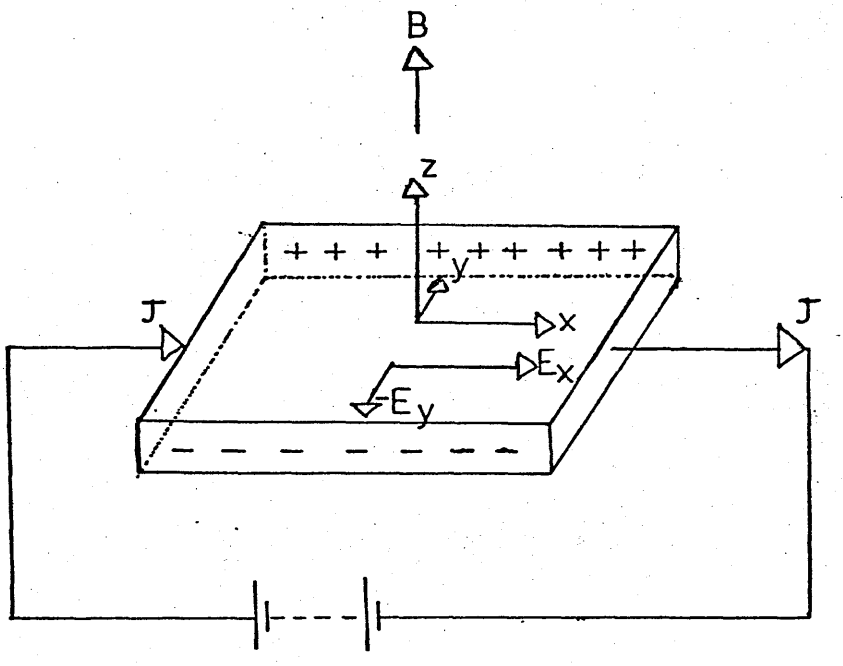


Fig 6a

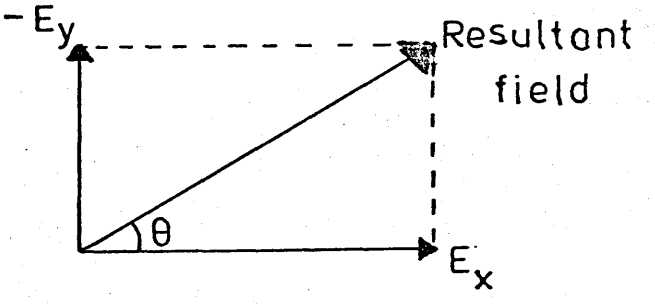


Fig 6b

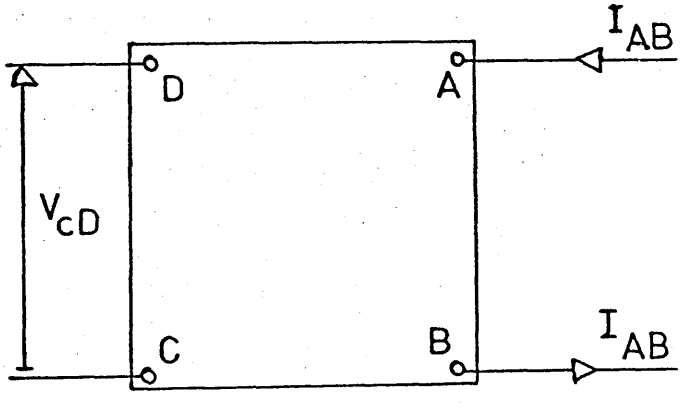


Fig 6c

Fig 6 HALL EFFECT

field along the y-axis. Therefore:-

$$-eE_y = e(B_x u) = -e\langle u_x \rangle B_z \qquad \ldots\ldots\ldots\ldots\ldots\ldots\ldots \quad (36)$$

The current density in the sample is given by:-

$$J_x = -Ne\langle u_x \rangle \qquad \ldots\ldots\ldots\ldots\ldots\ldots\ldots \quad (37)$$

where N is the density of electrons.

From (36) and (37):-

$$E_y = -\frac{1}{Ne} B_Z J_X \qquad \ldots\ldots\ldots\ldots\ldots\ldots\ldots \quad (38)$$

From equations (35) and (38):-

$$R_H = -\frac{1}{eN} \qquad \ldots\ldots\ldots\ldots\ldots\ldots\ldots \quad (39)$$

This is the much quoted Hall expression and can be used to calculate the Hall coefficient, $R_H$, if N and the mobility of carriers, $\mu$, is constant. The current density, $J_x$, is calculated from the expression:-

$$J_x = \frac{I_x}{A}$$

where $I_x$ is the current in the x-direction and A is the cross-sectional area.

Conductivity, $\sigma$, is given by the expression:-

$$\sigma = Ne\mu_H \qquad \ldots\ldots\ldots\ldots\ldots\ldots\ldots \quad (40)$$

Substituting in equation (39) for uniform doping,

$$\mu_H = R_H \sigma \qquad \ldots\ldots\ldots\ldots\ldots\ldots\ldots \quad (41)$$

This will only be true if all the carriers have the same velocity and is not true for the relatively low carrier concentrations obtained in semiconductors. The drift mobility, $\mu_n$, is given by:-

$$\mu_n \simeq \frac{\sigma}{eN}$$

It should be noted that a proper averaging over the velocity distribution of the carriers gives,

$$R_H = -\frac{\Gamma_H}{eN} \text{ where } \Gamma_H \text{ is a constant order of unity.}$$

The factor $\Gamma_H$ is known as the Hall Scattering Factor. The factor $\Gamma_H$ is a function of the processes that influence the velocity of carriers and hence their scattering, e.g. temperature, magnetic field and degeneracy. It can be concluded that the density of charge carriers and their mobility can be obtained from Hall measurements, from the simple expression for $R_H$, providing $\Gamma_H$ is near unity.

### 2.6.1 Profile Measurement

With the use of Hall measurements and layer stripping, the depth distribution of carrier concentration and mobility can be determined. For a non-uniformly doped semiconductor both N and $\mu_H$ are functions of depth (X). Equations (40) and (41) become:-

$$= e\int N(X)\cdot\mu(X)dx \text{ and } R_H = \frac{e\int N(X)\mu^2(X)\cdot dx}{[\sigma^2]} \quad \ldots\ldots\ldots\ldots\ldots \quad (42)$$

Differentiating these two equations for $\sigma$ and $R_H$ we obtain:-

$$d(R_H.\sigma^2) = eN(x)\mu^2(x)\, dx \quad \ldots\ldots\ldots\ldots\ldots\ldots\ldots \quad (43)$$

$$d\sigma = e.N(x).\mu_H(x)\, dx \quad \ldots\ldots\ldots\ldots\ldots\ldots\ldots \quad (44)$$

From (43) and (44),

$$\mu_x = \frac{\frac{d}{dx}(R_H.\sigma^2)}{e.N(x).\mu(x)} \qquad \ldots\ldots\ldots\ldots\ldots\ldots\ldots \quad (45)$$

If thin layers are removed the derivatives can be approximated to:-

$$\frac{d\sigma}{dx} = \frac{\Delta\sigma}{\Delta x}$$

and

$$\frac{d}{dx}(R_H.\sigma^2) = \frac{\Delta(R_H.\sigma^2)}{\Delta x}$$

The mobility in the i'th layer becomes:-

$$\mu_i = \frac{\Delta(R_H\sigma^2)i}{\Delta\sigma_i} \qquad \ldots\ldots\ldots\ldots\ldots\ldots\ldots \quad (46)$$

and the concentration at a depth, x, from equation (44) is:

$$N(x) = \frac{d\sigma/dx}{e\mu(x)}$$

This becomes in the i'th layer

$$N_i = \frac{\Delta\sigma_i}{e\mu_i\Delta x_i} \qquad \ldots\ldots\ldots\ldots\ldots\ldots\ldots \quad (47)$$

where $x_i$ is the thickness of the i'th layer. Using these equations the carrier concentration and mobility versus depth can be calculated.

### 2.6.2 Measurement Geometry

Van der Pauw[85] showed that the specific resistivity and the Hall effect of a flat sample of arbitrary shape can be measured without knowing the current pattern if the following conditions are fulfilled:-

(a) The contacts are at the circumference of the sample.

(b) The contacts are sufficiently small.

(c) The sample is homogeneous in thickness.

(d) The surface of the sample is singly connected, i.e. the sample does not have isolated holes.

Consider a square specimen with a point contact at each corner. See Figure 6(c).

If a current $I_{AB}$ passes between contacts A and B and a voltage $V_{CD}$ is measured between C and D, then:-

$$\text{Resistance } R_{AB} = \frac{V_{CD}}{I_{AB}} \quad \text{and} \quad R_{BC} = \frac{V_{DA}}{I_{BC}}$$

Then the resistivity is given by:-

$$\rho = \frac{\pi d}{2\ln 2} (R_{AB} + R_{BC}).f(R) \qquad \ldots\ldots\ldots\ldots\ldots\ldots \quad (48)$$

where d is the specimen thickness and f(R) is a function of the ratio $R_{AB}/R_{AD}$ and satisfies the relation:

$$\frac{R_{AB} - R_{BC}}{R_{AB} + R_{BC}} = f(R) \text{ arc cosh } \left[\frac{\exp(\ln 2/f(R))}{2}\right] \qquad \ldots\ldots\ldots\ldots\ldots \quad (49)$$

If $R_{AB}$ and $R_{BC}$ are almost equal f(R) can be approximated to

$$f(R) \simeq \left[\frac{R_{AB} - R_{BC}}{R_{AB} + R_{BC}}\right]^2 \frac{\ln 2}{2} - \left[\frac{R_{AB} - R_{BC}}{R_{AB} + R_{BC}}\right]^4 \left[\frac{(\ln 2)^2}{2} - \frac{(\ln 2)^3}{12}\right] \quad .. \quad (50)$$

The Hall mobility can be determined by measuring the change of resistance $R_{BD}$ when a magnetic field B is applied perpendicular to the specimen. The Hall mobility is given by:-

$$\mu_H = \frac{d}{B} \frac{\Delta R_{BD}}{\rho}$$

where $\rho$ is specific resistivity and $\Delta R_{BD}$ is the change of resistance $R_{BD}$ due to the magnetic field, and

$$R_H = \frac{d}{B} \frac{V_{BD}}{I_{AC}}$$

Sheet resistivity and surface carrier concentration can be calculated from:-

$$\text{Sheet resistivity, } \rho_s = \frac{\rho}{d}$$

and

$$\text{Surface carrier concentration } N_s = \frac{R_H}{d}$$

# 3.0 EXPERIMENTAL TECHNIQUE

## 3.1 General

Two types of n-type gallium arsenide material were used in the experiments. The types being a bulk single crystal material, grown by the Czochralski method, and an epitaxial material, grown by the vapour phase epitaxy method. The latter method is used in Gunn devices and consists of an n-type layer, typically of 10 microns thickness, on a $n^+$ background. Early work was on the bulk n-type material only and implantations were carried out using the 160 keV linear heavy ion accelerator. The later work was confined to epitaxial material and all implants were carried out using the 400 keV linear heavy ion accelerator. After implantation the specimens were usually encapsulated in silicon dioxide, annealed and the encapsulant removed. Contacts were put down onto the specimens for both Capacitance-Voltage and Hall measurements. For the Capacitance-Voltage measurements gold Schottky barriers were evaporated onto the specimens. In both cases the specimens were mounted for ease of measurement. Using the Capacitance-Voltage, Current-Voltage and Hall techniques, measurements were then carried out. Some early measurements were taken using the Thermal Probe technique. However, the technique was discontinued because it yielded little useful information, i.e. it would only discern between n-type and p-type surface layers, because with no depth information, results would only give an indication of semiconductor type.

## 3.2 Specimen Preparation

### 3.2.1 Preparation of the Gallium Arsenide

#### 3.2.1.1 Single Crystal Bulk Material

Bulk single crystal n-type gallium arsenide was supplied in ingot form. The ingots were supplied with differing degrees of doping and with various different crystal orientations. The doping concentration of the samples varied from $1.5 \times 10^{15}$ atoms/cm$^3$ to $2 \times 10^{17}$ atoms/cm$^3$.

The ingot of the material was first mounted onto the base plate of a diamond circular saw with white wax, and then sliced into pieces of 0.020 ins. thickness. The slices were then diced into 5 × 5 mm specimens, again by means of the diamond saw. Any traces of wax were removed from the specimen by washing in hot trichloroethylene and analar methanol. The specimens were mounted onto a polishing disc with black wax and polished by hand, using a Hydrocel Pellon Pan W pad, with a polishing fluid of 2% bromine-methanol solution. In early work white wax was used to mount the specimens, but smearing of the specimens was found to occur and thus black wax was used. After polishing, the specimens were given a light etch in a rotating beaker containing 1% bromine-methanol solution. Immediately the specimens were washed thoroughly in methanol solution to remove any traces of the bromine-methanol solution. The specimens were removed from the polishing disc by heat, followed by a wash in an ultrasonic bath containing trichloroethylene (initially toluene was used for washing but was found to effect the results[86]), then isopropyl alcohol vapour and washed in methanol and then dried. The specimens were then ready for implantation.

3.2.1.2 Epitaxial Material

Epitaxial gallium arsenide, consisting of an n-type layer on an $n^+$ substrate was used, with the n layer having a range of doping concentrations from $1 \times 10^{15}$atoms/cm$^3$ to $6 \times 10^{15}$atoms/cm$^3$ and layer thicknesses from 5 microns to 11 microns. In all cases the orientation was within a few degrees of the <100>.

The epitaxial material was diced into specimens 3 mm × 3 mm by one of two methods:-

(1) Cleaving, after scribing the surface with a diamond scribe,

(2) Dicing with a wire saw.

In both cases before implantation, the specimens were washed in trichloroethylene followed by an isopropyl alcohol bath. No further treatment was carried out prior to implantation.

3.2.2 Implantation

Early work was carried out by implanting bulk n-type gallium arsenide with a range of doses, energies and different ions. The ions used were argon, phosphorous and sulphur. Later work using the n-type epitaxial material concentrated on implanting sulphur 32 with a range of doses, from $10^{12}$ions/cm$^2$ to $10^{15}$ions/cm$^2$, energies from 100 keV to 400 keV and with the target at room temperature, 100°C and 180°C. The early implantations of argon and phosphorous were carried out at room temperature on the 160 keV heavy ion accelerator.

For nearly all the specimens shown in the Results Section, 4.0, the ion species used was sulphur 32. During the implantation of these specimens great care was taken to minimise the oxygen content of

the ion beam. When carrying out a mass analysis of the ion beam to be implanted, double charged oxygen will be bent through the same angle as sulphur 32. With the mass analyser available it was not possible to separate molecular oxygen from sulphur 32. To minimise the oxygen content of the ion beam alternative action becomes necessary.

The accelerator source was evacuated to a high vacuum and left for at least 24 hours, to minimise the amount of oxygen in the source. The accelerator beam line was kept almost permanently at high vacuum. To produce the ion beam a gas source was employed with sulphur hexafluoride. To obtain some indication of the oxygen content of the ion beam, a mass analysis was carried out on the beam, with the gas on and off to the ion source. With the gas on, a sulphur 32 peak of 200 nanoamps, was obtained; 20 minutes after turning the gas off, this had fallen to 3 nanoamps, and reduced to 1 nanoamp before the beam was lost. This experiment was carried out shortly after the ion source had been at atmospheric pressure.

From the mass analysis of the beam the sulphur 34 peaks obtained were an order of magnitude less than the sulphur 32 peak. The size of the sulphur 34 peak made it difficult to obtain a stable beam of the ion. Graph 36 shows the results of implanting two specimens under identical conditions with sulphur 32 and 34. The profile tails are very similar for the two ion species. The maximum concentration is greater and at a shallower depth for the specimen implanted with sulphur 34 than sulphur 32. With only such a small difference between the two profiles, the experiment would indicate that the sulphur 32 ion beam is predominantly sulphur 32. The difference being due mainly to the difference in atomic weight. If the ion beam had contained a

large proportion of oxygen it would have been significantly different. Table IV shows that the range of oxygen is double that for sulphur.

For the implantations on the 400 keV accelerator, the specimens were held in a spring loaded specimen holder. A mask was placed in front of the specimen with an aperture in it. For the 5 mm specimens a 4 mm diameter aperture was used and for the 3 mm specimens a 2.5 mm diameter aperture was used. This was done to avoid any edge effects during the subsequent measurements. The Hall specimens were totally flooded with ions, but the outside edges were masked. Electrical connection was made to the specimen through the holder and the spring loaded clip. The holders, three at a time, were mounted onto a plate and into the registerable implantation holder in the machine. The plate had facilities for heating and monitoring the temperature of the specimens to above 180°C. The standard plate was flat and held the specimens normal to the incident beam. Another plate was used which held the specimens 7° off the normal to the incident beam.

### 3.2.3 Passivation and Annealing

Prior to annealing the surface of the specimen was passivated with a layer of silicon dioxide to a thickness of approximately 0.5 μm. The specimens were heated on a hot plate to 300°C in the silane rig chamber. Controlled quantities of the gases, silane, oxygen and nitrogen, were mixed in the chamber above the specimens and silicon dioxides were deposited, from the gas reaction, upon the surface of the specimens. The thickness of the deposited layer could be determined from the fringe colours produced on the deposited surface layer.

After passivation the specimens were placed, passivated surface downwards, on a gallium arsenide boat. This boat was then introduced

into the quartz tube of the annealing furnace, which had been preheated to the required annealing temperature and flushed out with nitrogen. The specimens were annealed for a period of 20 minutes in an atmosphere of nitrogen (i.e. with a flow of 2 to 3 cu.ft./hr.). After annealing, the boat with the specimens was pushed to the edge of the tube, outside the hot zone of the furnace, and allowed to cool, still within a nitrogen atmosphere.

The silicon dioxide layer was dissolved from the surface of the specimens, after annealing, with 40% hydrofluoric acid. The specimens were then washed thoroughly in distilled water, trichloroethylene and isopropyl alcohol vapour.

### 3.2.4 Contacts

Ohmic contact to n-type gallium arsenide can be made by alloying tin dots onto the surface of the gallium arsenide. The contacting was carried out in the apparatus shown in Figure 7. A slice of gallium arsenide was placed on the hot plate and the specimen was placed, implanted surface downward onto this slice. A small piece of tin was placed on top of the specimen. Hydrogen was passed through concentrated hydrochloric acid to produce an atmosphere of hydrogen chloride in the chamber during contacting. The hydrogen chloride acts as a flux to aid the formation of the contact. The system was flushed out thoroughly with hydrogen chloride before starting to heat the specimen. Heat was applied until the tin had melted, globulated and formed onto the surface of the specimen. The heat was removed then and the specimens allowed to cool in a hydrogen atmosphere.

On high concentration n-type material, this technique produced good, low resistance ohmic contacts. Poor results were obtained with low concentration n-type material. The tin melted and globulated, but

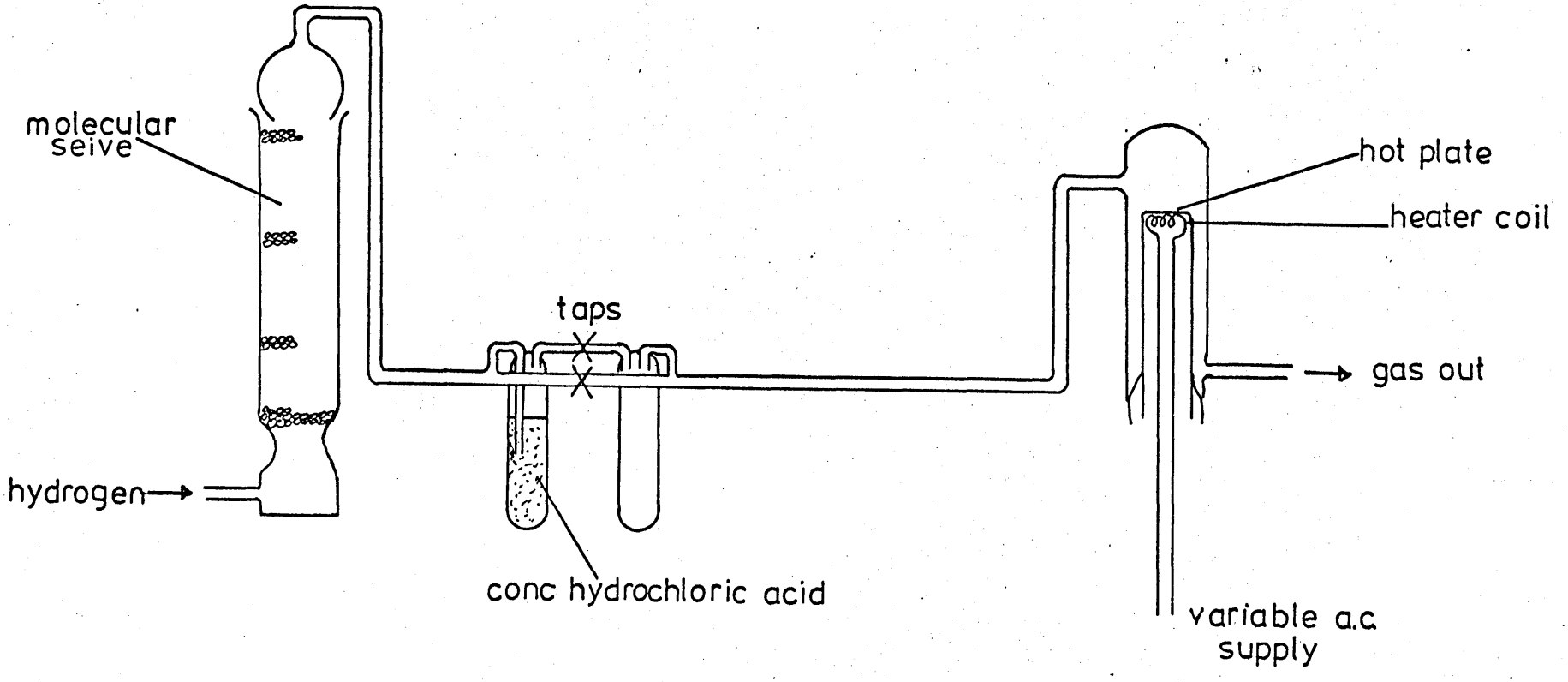


Fig. 7. CONTACTING APPARATUS

tended not to form onto the surface of the specimen.

### 3.2.5 Preparation of Schottky Barriers

Gold Schottky barriers of 1.5 mm diameter were evaporated onto the implanted area of the specimens, using an Edwards vacuum evaporator. The specimens were mounted with their backs against a hot plate and the area to be evaporated onto defined by a mask, with a hole of 1.5 mm diameter in it. Prior to evaporation the vacuum system was pumped down to a pressure of approximately $3 \times 10^{-6}$Torr and the specimens heated to between 100°C and 120°C. The gold was evaporated using a tungsten filament with a quartz chimney around it to direct the gold towards the specimens. After evaporation the specimens were allowed to cool before opening to the atmosphere.

The specimens were mounted onto pieces of aluminium with silver conducting paint to make electrical contact with the rear tin contact.

## 3.3 Measurement Techniques

### 3.3.1 Current-Voltage Measurements

Current-voltage characteristics were measured in the forward and reverse directions for all of the Schottky diodes, using a Tektronic curve tracer. This provided a quick check on the quality of the diode and the range of measuring voltages. Electrical contact to the rear of the specimen was made through the aluminium mounting. Top contact to the specimen was made to the gold probe mounted in a micro-manipulator. The micro-manipulator and specimen were placed in a light-proof box.

Low current current-voltage measurements were carried out using the circuit shown in Figure 8. These measurements were carried out at room temperature in a screened room. Currents were measurable down

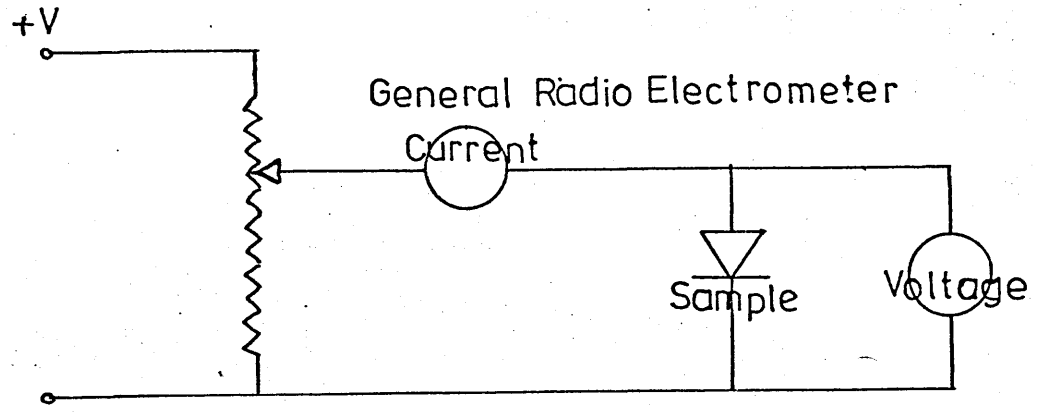


Fig 8 CURRENT-VOLTAGE MEASUREMENT EQUIPMENT

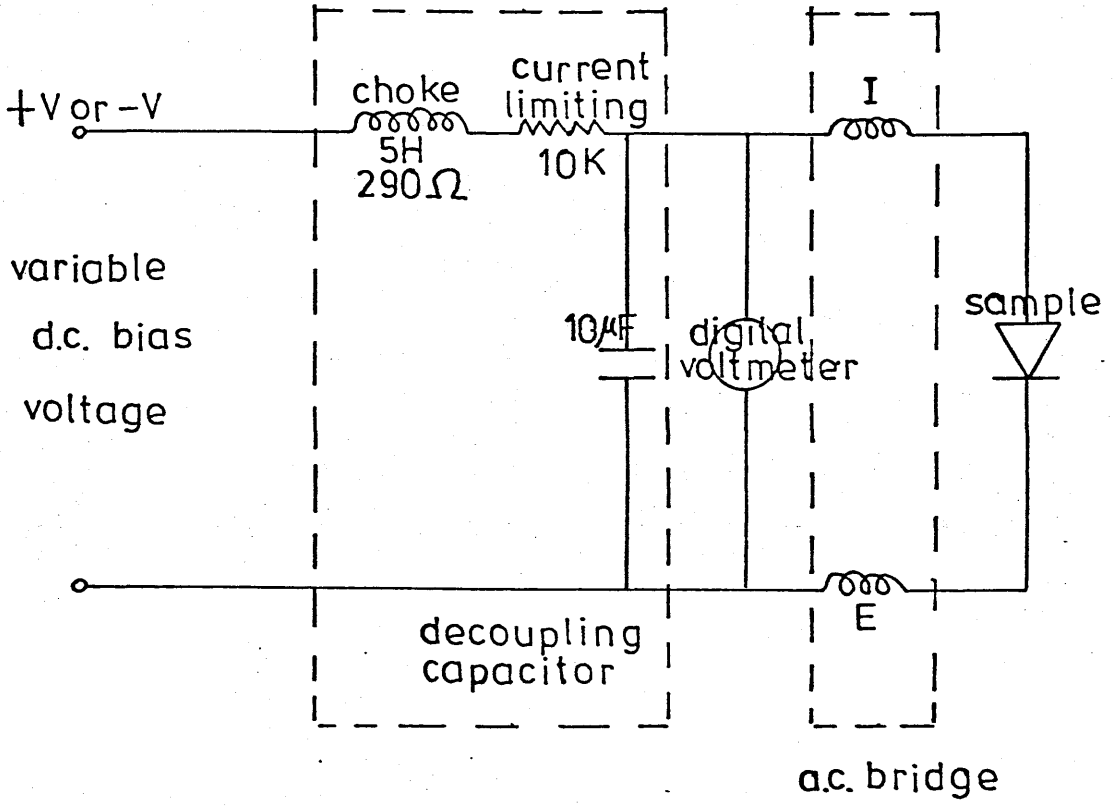


Fig 9 CAPACITANCE-VOLTAGE MEASUREMENT EQUIPMENT

to $10^{-12}$amps on the General Radio Electrometer, using this circuit. The Keithley Instruments 602 Solid State Electrometer was chosen to measure the voltage across the specimen, because of its high input impedance.

### 3.3.2 Capacitance-Voltage Measurements

Differential capacitance measurements versus applied reverse bias voltage were made using the circuit in Figure 9 on the gold Schottky barrier diodes. Contact to the diodes was made as previously described in Section 3.3.1. A series of readings of capacitance versus applied reverse bias were made at 1 KHz and at 50 KHz, these being the lower and upper limits of the measurement system. The capacitance measurements were made using a Wayne Kerr Universal Bridge Type B221 with a Wayne Kerr A.F. Signal Generator, 10 Hz to 120 Hz, and an external detector S.T.C. 96016 Selective Null Detector. The applied bias voltage was measured using a Solartron digital voltmeter.

### 3.3.3 Capacitance-Frequency Measurements

Measurements of capacitance were made over a range of frequencies from 1 KHz to 50 KHz for fixed values of reverse bias.

### 3.3.4 Copeland Measurements

#### 3.3.4.1 Description of Technique

The method to be described is an automatic measuring technique developed by Copeland[33] from an a.c. method suggested by Meyer[34]. The technique is an automatic capacitance-voltage method giving a direct impurity concentration profile plot against depth. Its major advantage over manual capacitance-voltage measurements being one of speed of measurement.

A small radio frequency current is injected into a Schottky barrier diode or shallow p-n junction, which is normally reverse biassed. It is well known[33] (see Section 2.5) that if a radio frequency current is injected into a diode, then the fundamental voltage produced across the diode is proportional to the junction depletion layer width, and the second harmonic voltage produced across the diode is proportional to the reciprocal of the electrically active impurity concentration. By varying the reverse bias on the junction, the depletion layer can be increased (see Section 2.5) and by measuring the fundamental and second harmonic voltages, an impurity concentration profile versus depth can be built up.

Such a measuring system was developed and constructed within the Department of Electronic and Electrical Engineering at the University of Surrey. It was based on a system built at the Mullard Research Laboratories.

3.3.4.2 Design of the Copeland System

The basic requirements that the system has to fulfil are as follows:

(1) The p-n junction formed for measurement purposes has to be abrupt and assymetrical. The minimum depths for measurement will be limited by the junction depth. Therefore a metal surface barrier or Schottky diode was used.

(2) The injected radio frequency current should remain constant. A variation in the radio frequency current will cause a change in the depletion capacitance, which will, in turn, cause an error in the measured impurity profile.

(3) The radio frequency current injected should contain a minimum of second harmonic frequency. The voltage produced by any second harmonic current must be small in comparison with the measured second harmonic voltage to give the minimum of error.

(4) The frequency of the injected radio frequency current should remain constant. A variation in the frequency of the injected current will produce a variation in the capacitance of the depletion layer, leading to measurement error.

(5) Voltage measuring circuits should appear as high impedances to the diode being measured, so that the currents drawn by these circuits are kept to a minimum.

(6) The ambient temperature should remain constant during measurements.

The system was designed to measure impurity concentrations in the range $5 \times 10^{14}$ to $1 \times 10^{17}$ atoms/cm$^3$. Figure 10 shows in block diagram form the Copeland system. A fundamental frequency was chosen to be similar to that selected by Copeland[33]. The chosen frequency being 5.7 MHz because suitable crystals were available at this frequency and twice this frequency. A radio frequency was chosen for the measurements, because only shallow levels will respond to the applied signal.

The 5.7 MHz signal was generated by a crystal controlled oscillator and was designed to drive up to 3 Watts into 75 Ohms. This signal was then passed through a low pass filter to remove any unwanted harmonic frequencies, especially second harmonics. An attenuation of approximately 50 dB being obtained at the second harmonic frequency.

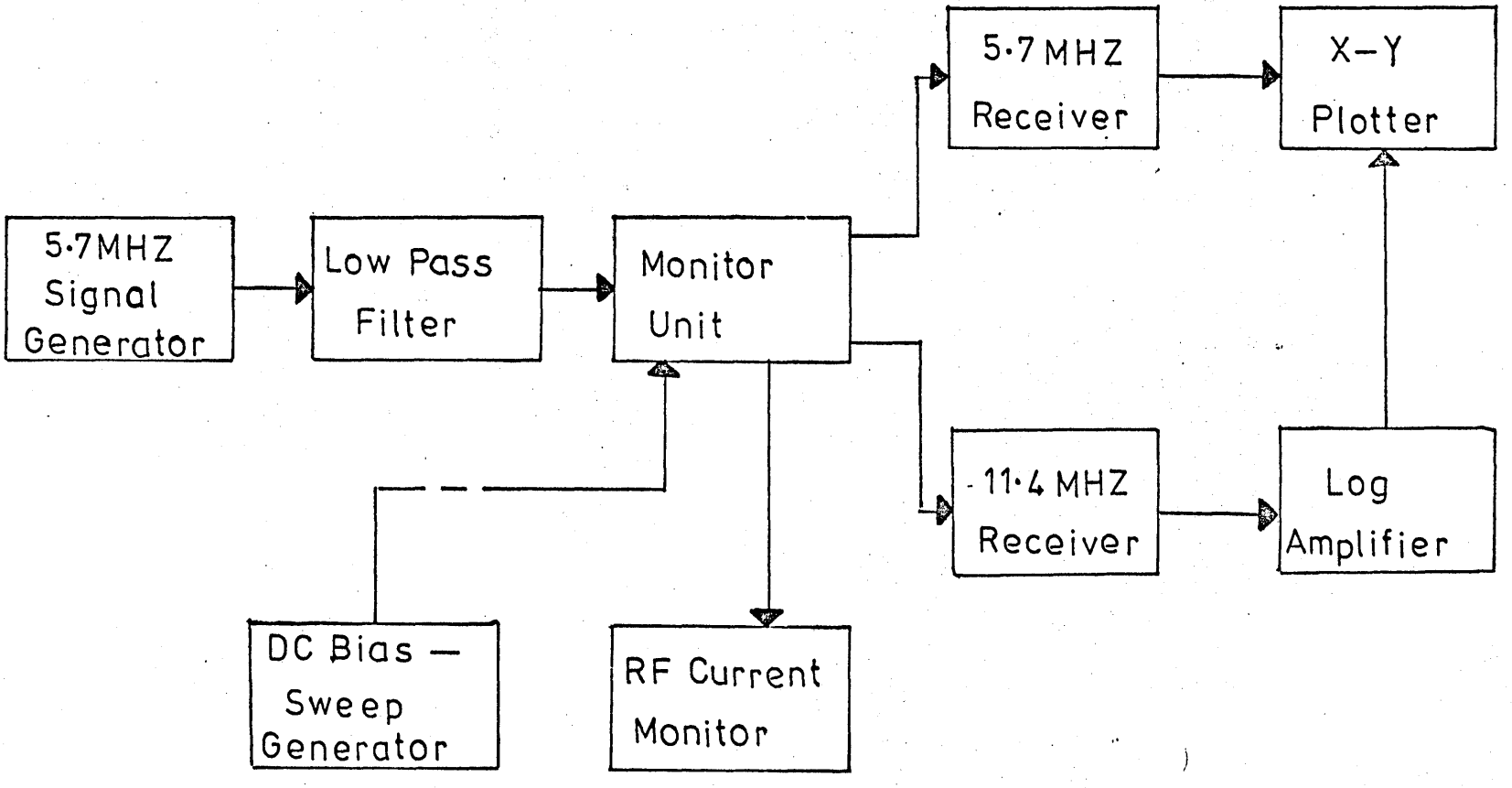


Fig 10 BLOCK DIAGRAM OF COPELAND EQUIPMENT

The heart of the system is the Monitor Unit. The circuit for this is shown in Figure 11. This consists of an input network to provide the constant current drive to the diode and two output networks to monitor the fundamental and second harmonic voltages developed across the diode. The capacitor $C_1$ at the test frequency is a high impedance, such that the drive to the diode will be constant current. The 75 Ohm resistor acts as matching to the low pass filter and the oscillator amplifier. The resonant circuits $C_1$ $L_1$ $C_2$ $L_2$ appear to the diode under test, to be high impedances and connect up to the 5.7 MHz and 11.4 MHz measurement circuits. The values for $C_1$ $L_1$ $C_2$ $L_2$ were calculated from the equations given in Section 2.5. The values shown for $L_1$ and $L_2$ are only approximate and in practice were adjusted to suit the performance of the circuit. The unit was aligned by means of a Polyskop.

The current through the diode was monitored using a series resistance and a voltage measuring circuit. The fundamental and second harmonic voltages were measured by means of two superheterodyne receivers, tuned to the required frequency, and converted into a d.c. signal. In each receiver the voltage signal was amplified by up to 40 dB, this being adjustable by means of a switched gain control. Two crystal controlled local oscillators provided signals at 5.706 MHz and 11.412 MHz. The 5.7 MHz and 5.706 MHz were then passed into a mixer and the difference of the two frequencies extracted by means of filters. Similarly the 11.4 MHz and 11.412 MHz signals were mixed giving the two intermediate frequencies of 6 KHz and 12 KHz. Further amplification followed, the signal then passing into a detector stage, followed by d.c. amplification. The 11.4 MHz channel was followed by a logarithmic amplifier to convert the reciprocal concentration signal to log.

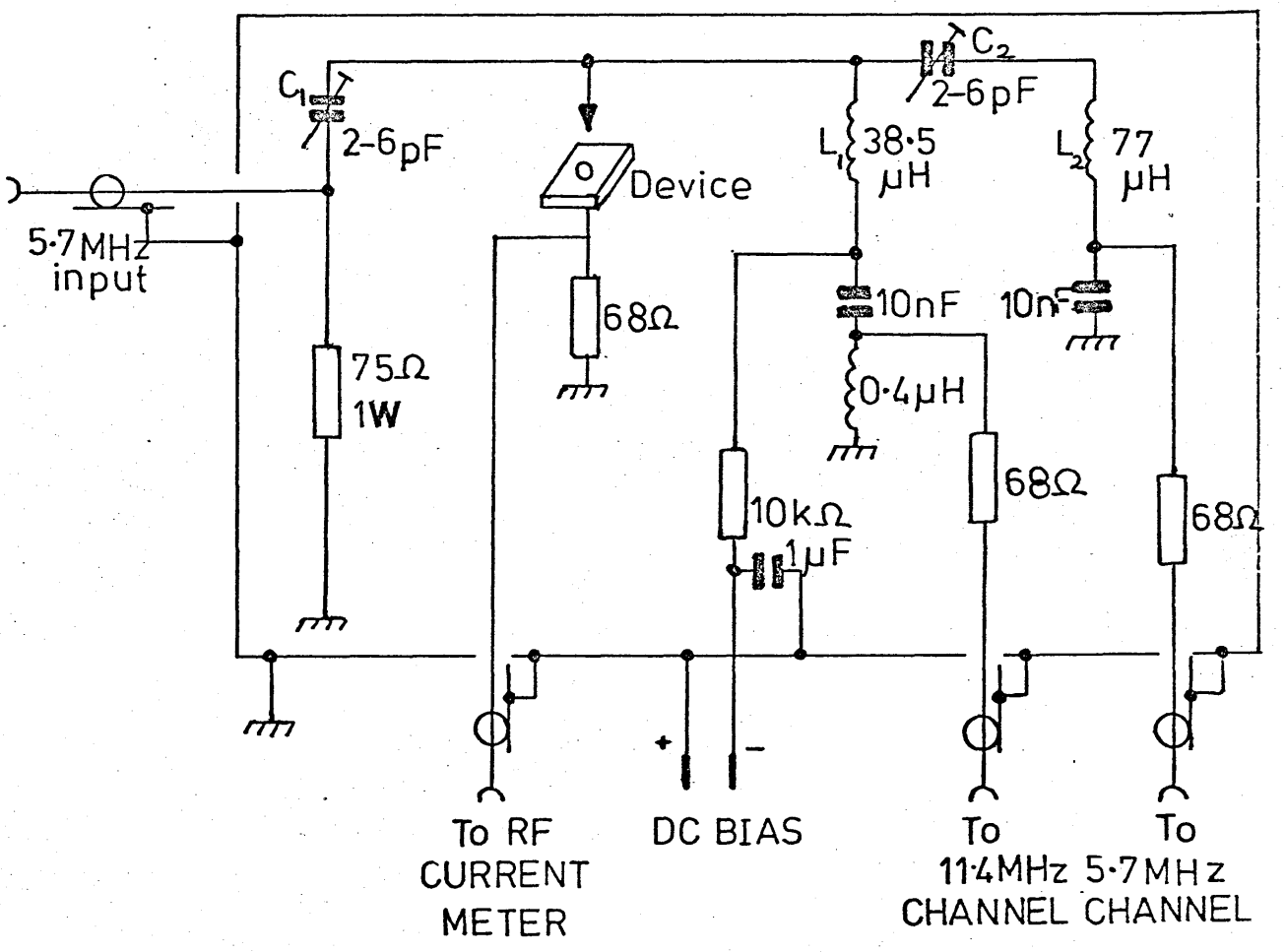


Fig11 THE MONITOR UNIT

concentration. Any further adjustments in gain were achieved by means of the pen recorder amplifiers. The d.c. reverse bias can be applied manually or automatically by means of a ramp generator, the maximum voltage being adjustable from +1 Volt to -40 Volts.

3.3.4.3 Calibration of Copeland System

Two methods can be used to calibrate Copeland, one is absolute, the other is by comparison with a diode of known profile.

A direct calibration of the depth scale (i.e. the fundamental frequency channel) can be obtained by using standard capacitors in place of the diode, and relating the channel output voltage to the depth scale since $C = \varepsilon A/X$ for a parallel plate capacitor and for Copeland the fundamental voltage is proportional to $1/\omega\varepsilon A.X$.

Hence we get the fundamental voltage proportional to I/C and by adjusting the R.F. current it is possible to calibrate the depth scale.

To calibrate the second harmonic channel, a known voltage of second harmonic frequency is injected onto the probe and the channel output measured. This will give the gain of the channel. It is still necessary to know accurately the R.F. current to put into the Copeland formula. This can be found accurately by measuring the standard resistor in the measuring unit on a bridge at fundamental frequency, then shorting the probe to the top of the standard resistor, varying the current and measuring the voltage developed across the standard resistor. Having done this the second harmonic channel can be calibrated. A similar technique can be used on the fundamental channel.

From Copeland[33]:-

$$\text{Fundamental voltage} \propto \frac{I}{\omega \epsilon A} \cdot X$$

$$\text{Second Harmonic voltage} \propto \frac{I^2}{4\omega^2 e \epsilon A^2} \cdot \frac{1}{N(X)}$$

The calibration curves are given in the Results Section 4.1.

3.3.4.4 Measurement Technique

In practice a standard diode was used to calibrate the concentration channel and capacitors used to calibrate the depth scale. The diode radio frequency current was set to several hundred micro-amps and the probe shorted to the pad on the instrument to zero the depth scale. Using a capacitor, the gain switches were adjusted on the 5.7 MHz receiver channel, with final adjustments being made on the X-Y plotter amplifier. This calibrated the depth scale. Then using a standard diode, the 11.4 MHz receiver channel was adjusted for the order of magnitude on the logarithmic scale.

The equipment was then ready for use. The specimens prepared for capacitance-voltage measurements were placed under the probe, the current set, the d.c. bias voltage sweep set and a profile of concentration versus depth taken.

3.3.5 Hall Measurements

Hall measurements and Hall measurements versus temperature were carried out on sulphur implanted epitaxial n-type gallium arsenide. The measurement contacts were positioned at each corner of the specimen (see Section 2.6) and electrical connections made to these contacts through the holder. The specimen and holder were arranged such that they could be positioned between the pole pieces of

an electromagnet so that the magnetic field was normal to the surface of the specimen. For the low temperature measurements, the enclosure between the magnet pole pieces onto which the holder was positioned, was capable of being evacuated to minimise any heat changes of the specimen.

As outlined in the Theory Section, 2.6, a current is passed from a constant current source between a pair of contacts and the voltage is measured across the other pair of contacts. This is repeated, injecting the current into a different pair of contacts and again measuring the voltage. The resistivity is given then by Van der Pauw's equation:

$$\rho = \frac{\pi d}{2\ell n 2} (R_{AB} + R_{BC}).f(R) \qquad \ldots\ldots\ldots\ldots\ldots\ldots\ldots \quad (48)$$

If measurements are carried out now with an applied magnetic field normal to the surface of the specimen, the carrier concentration and mobility can be obtained. This requires four positions for measurements, to eliminate effects due to non-linear contacts and misalignment of the magnetic field. Errors due to the Ettingshausen and Nernst effect are reduced by repeating each measurement in each position with the current and then the magnetic field reversed. Using the contact configuration shown and lettered as in Theory Section, 2.6, the following voltages were measured:-

(1) With a constant current between contacts D and A, the voltage was measured across B and C.

(2) With a constant current between contacts A and B, the voltage was measured across C and D.

(3) With a constant current between D and B, the voltage was measured across A and C.

(4) With an applied magnetic field the measurements of (3) above were repeated.

(5) The measurements of (3) above were repeated.

(6) With a reversed magnetic field the measurements of (3) above were repeated.

(7) Measurements (1) to (6) inclusive were repeated with the current in the reverse direction.

The above measurements yield the Hall resistance, the Hall mobility and resistivity. When combined with layer stripping the measurements yield the surface concentration, mobility and sheet resistivity.

The apparatus that these measurements were made on was designed to be semi-automatic, with the use of relays and a sequence control system. The correct connections to the specimen were made for each of these conditions and changed to the next at the press of a push button. All voltages were measured with a high input impedance voltmeter (Solartron LM1604 digital voltmeter) to minimise current leakage through the meter. This meter was also used to measure the specimen current and magnet current with suitable series resistances. For the specimen current a 100 kohm resistance was used and for the magnet current a resistance. The constant current source for the specimen made use of a high voltage battery (120 V - 720 V) with a high impedance network of resistors to give (1 - 50 Mohm) in series with the battery. The impedance of the specimen under test was several orders of magnitude less than this series resistance, such that

the specimen current effectively remained constant. By varying the series resistance the specimen constant current could be varied. The magnet constant current was supplied from a commercial constant current source manufactured by Kingshill.

On all specimen contacts prior to Hall measurements contact resistance and linearity were measured using a Tektronix transistor curve tracer. This determined whether or not the contacts were ohmic or rectifying. Linearity could be measured directly and contact resistance estimated after eliminating specimen resistance.

3.3.5.1 Preparation of Hall Specimens

The epitaxial gallium arsenide material used for the Hall measurements was nominally an n-type layer of $5 \times 10^{15}$atoms/cm$^3$ on a semi-insulating material with 100 orientation. The material was diced into 5 mm square specimens ready for ion implantation. 300 KeV sulphur ions were implanted into the specimens with doses of $10^{12}$, $10^{13}$ and $10^{14}$ions/cm$^2$. Implants were carried out at room temperature, 100°C and 180°C. After implanting all the specimens were annealed at 650°C for 20 minutes in an atmosphere of nitrogen (see Section 3.2.3).

Four tin contacts were formed onto the implanted surface of each specimen (see Section 3.2.4), positioned in the four corners of the specimen. The contact resistance of each contact was checked with a diode curve tracer. No further treatment was required for the temperature measurements, however, for the depth measurements the following was carried out. The specimen was mounted with its back onto a slide with black wax. Contact was made to each contact with silver dag solution and contact strips made with silver dag to one end of the

slide. These silver dag contact strips and tin contacts were protected with a layer of black wax. The slide was then mounted in a holder which could be positioned to give the correct orientation of the specimen in the magnetic field.

3.3.5.2 Hall-Temperature Measurements

The unmounted specimen was mounted on a holder, designed to mount into the cold finger of a liquid nitrogen cooled cryostat and contact made to the four tin contacts on the specimens by silver dag onto wires. To minimise the heat loss by radiation a cover was screwed onto the cold finger so that the specimen was in a region of constant temperature. The cold finger was then positioned in a vacuum system to minimise condensation and heat loss. Measurements were made at a pressure of typically $5 \times 10^{-5}$Torr, using a current of 85 micro-amps and a magnetic field strength of 5000 gauss. A series of readings were taken at room temperature and then the specimen was cooled to liquid nitrogen temperature, 77°K. A series of measurements were taken as the specimen warmed to room temperature again. The temperature of the cold finger was measured using a constantin chromal thermocouple, mounted near the specimen. The reference junctions were kept at 0°C in crushed ice and water. During warm-up of the specimen, because the thermocouple is not in contact with the specimen, some thermal lag will occur between the cold finger and the specimen. This was felt not to be too serious, because of the slow warm-up rate of the cryostat.

3.3.5.3 Hall-Depth Measurements

With the specimen mounted as previously described in Section 3.3.5.1, a series of measurements were taken after removing successive layers from the surface of the specimen. The layers of gallium arsenide

were removed by means of a solution of hydrogen peroxide and sulphuric acid in water. The solution was mixed in the proportions - 200 ml distilled water: 2 ml hydrogen peroxide: 2 ml sulphuric acid, followed by 300 ml distilled water. After stirring thoroughly, the solution was left for approximately 45 minutes before being used for etching. The specimen was placed in the beaker containing the etching solution for two minutes and then washed twice in distilled water and then in acetone. The use of acetone was discontinued, because the surface of the specimen was found to smear. The etch solution was measured to have an etch rate of approximately 150 Å per minute. Variations occurred from one solution to another, so after each solution was finished, before the next series of etches, a small blob of black wax was placed on the surface of the specimen. Later after the wax had been removed, the etched step height was measured using a Talystep.

### 3.3.6 Thermal Probe Measurements

With some of the early phosphorous and argon room temperature implants in gallium arsenide, thermal probe measurements were made to determine if the surface of the specimen remained n-type or p-type. A room temperature probe was placed on the surface of the implanted specimen. Another probe, held at a constant temperature of 90°C, was also placed on the surface of the specimen. The current developed between the two probes was measured by means of a digital voltmeter and a standard resistor, see Figure 12. The direction of the current flow indicated whether the surface was n-type or p-type.

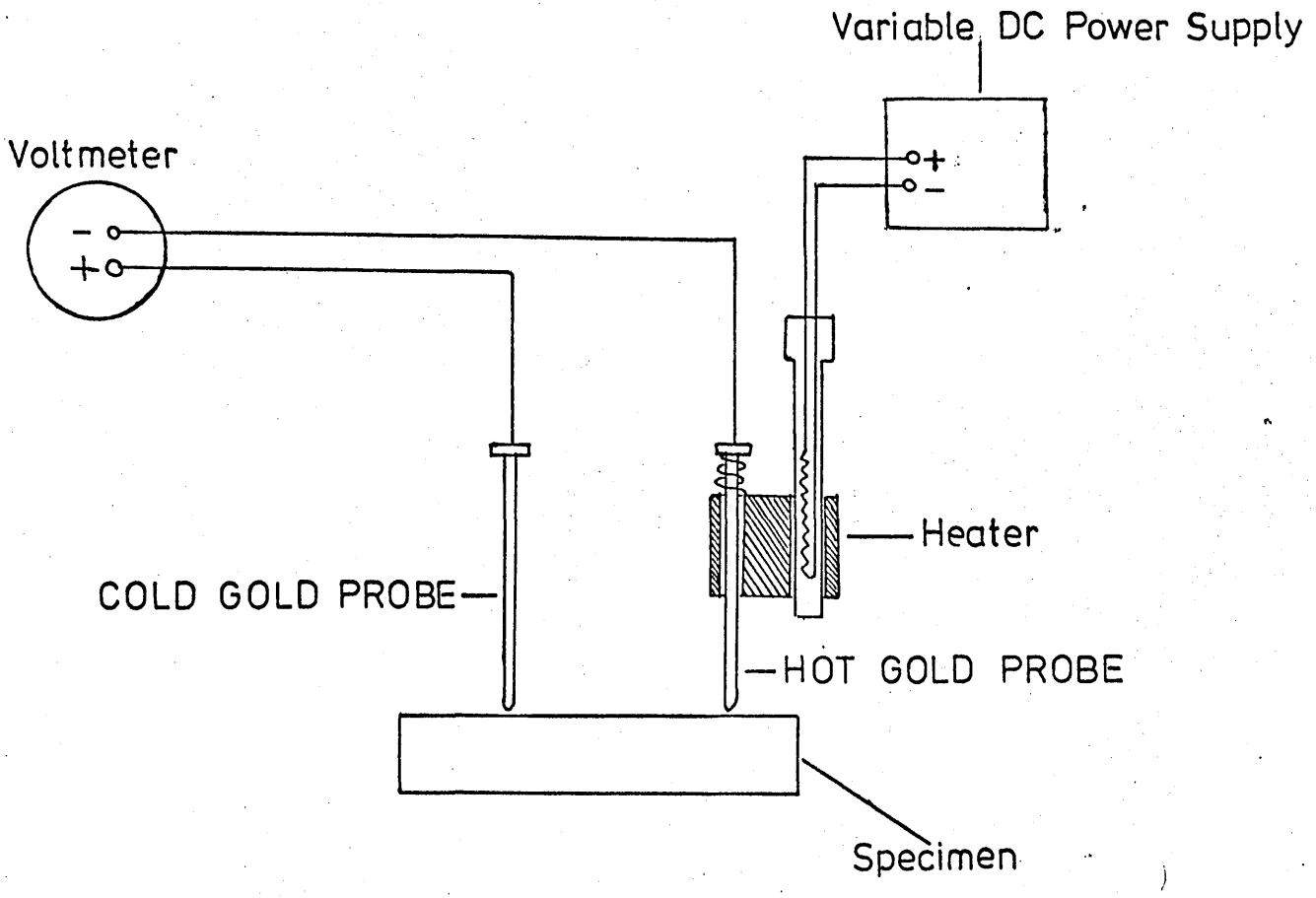


Fig 12 THERMAL PROBE MEASUREMENTS

## 4.0 RESULTS

In the results described later in this Chapter employing current-voltage, capacitance-voltage, capacitance-frequency and Copeland measurements, the semiconductor material used in all cases was n on $n^+$ epitaxial gallium arsenide. The material was as follows:-

### Material D94/6B

Require to fill in average mobility of n layer

| | |
|---|---|
| Nominal n layer thickness | 6 microns |
| Average concentration of n layer | $2 \times 10^{15}$ atoms/cm$^3$ |
| Orientation | <100> |
| Average mobility of n layer | |
| Supplier | MRL |

### Material SS133/D12

| | |
|---|---|
| Nominal n layer thickness | 5.2 microns |
| Average donor concentration of n layer | $2.2 \times 10^{15}$ atoms/cm$^3$ |
| Orientation | 2° off <100> |
| Average mobility of n layer | 8000 cm$^2$/Volt-sec. |
| Dopant species | Silicon |

### Material A237

| | |
|---|---|
| Nominal n layer thickness | 11 microns |
| Average donor concentration of n layer | $2 \times 10^{15}$ atoms/cm$^3$ |
| Orientation | <100> |
| Average mobility of n layer | 7230 cm$^2$/Volt-sec. |
| Dopant species | Silicon |
| Supplier | RRE |

Material MO/9/88

| | |
|---|---|
| Average donor concentration of n layer | $3 \times 10^{15}$ atoms/cm$^3$ |
| Supplier | RRE |

Material $S_{15}R_{26}C$

| | |
|---|---|
| Average donor concentration of n layer | $5 \times 10^{15}$ atoms/cm$^3$ |
| Orientation | <100> |
| Supplier | RRE |

## 4.1 Calibration of the Copeland Equipment

### 4.1.1 R.F. Current Meter

The R.F. current meter on the Copeland system was measured by shorting the gold probe to the base pad of the equipment and measuring the voltage developed across the measurement resistance in the equipment. The current measurement circuit consisted of a resistance with a voltmeter circuit to measure the voltage developed across the resistance. Using an R.F. bridge type B601 with a source-detector type SR628, the impedance of the resistance at 5.7 MHz was found to be 74 Ohms ± 2%. The current measurement circuit impedance was measured initially by injecting a 5.7 MHz signal from an R.F. signal generator, Marconi type TF144H/4, onto the base pad and measuring the voltage from the pad to the earth and the open circuit voltage of the signal generator, with an R.F. Electronic voltmeter, type TF2603. Using this method the current measurement circuit impedance at 5.7 MHz was found to be 40.7 Ohms.

With the gold probe shorted to the base pad the voltage to earth developed across the measurement resistance was measured using the R.F. electronic voltmeter and the current calculated for different

input readings. Graph 1 shows the actual current versus the R.F. meter reading on the 1 mA scale.

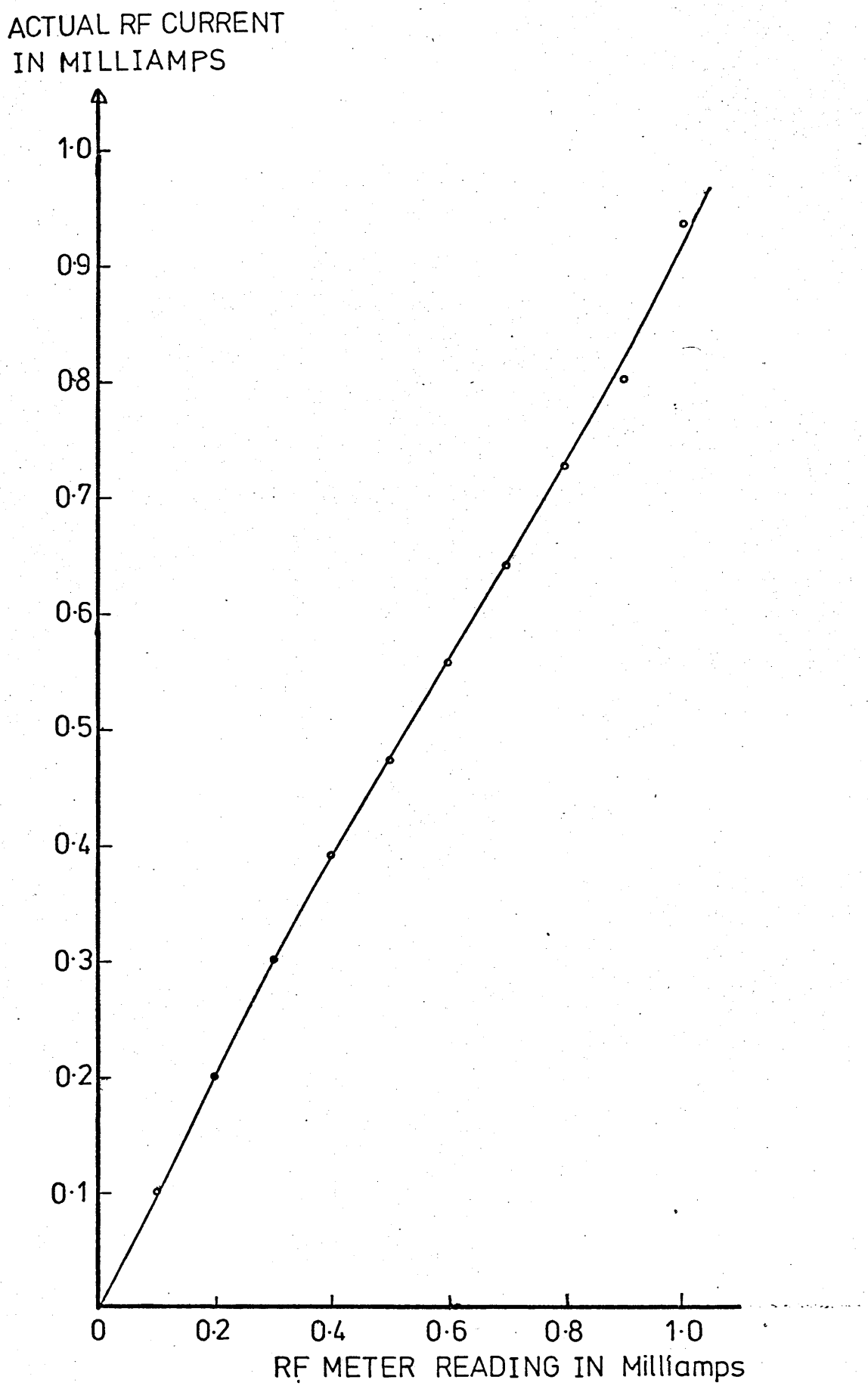


GRAPH 1 CALIBRATION CURVE FOR THE COPELAND RF METER

### 4.1.2 Second Harmonic Channel

The second harmonic voltage developed across the specimens is normally at 11.4 MHz. In order to calibrate the gain of the channel a known input signal is injected and the output measured from the channel for a given gain setting on the amplifier. The amplifier stage contains high Q tuned circuits so it is important to set the frequency of the injected signal from the signal generator accurately. This was achieved by beating the signal generator with the 5.7 MHz internal frequency source until the output was at a minimum. The internal frequency source was found to be at 5.695 MHz and the second harmonic frequency will be at 11.39 MHz.

The measurements were carried out using a Marconi type TF144H/4 signal generator and an Advance R.F. digital voltmeter. A typical calibration curve of input to output is shown in Graph 2, the output is plotted on a logarithmic scale to show the amplifier linearity.

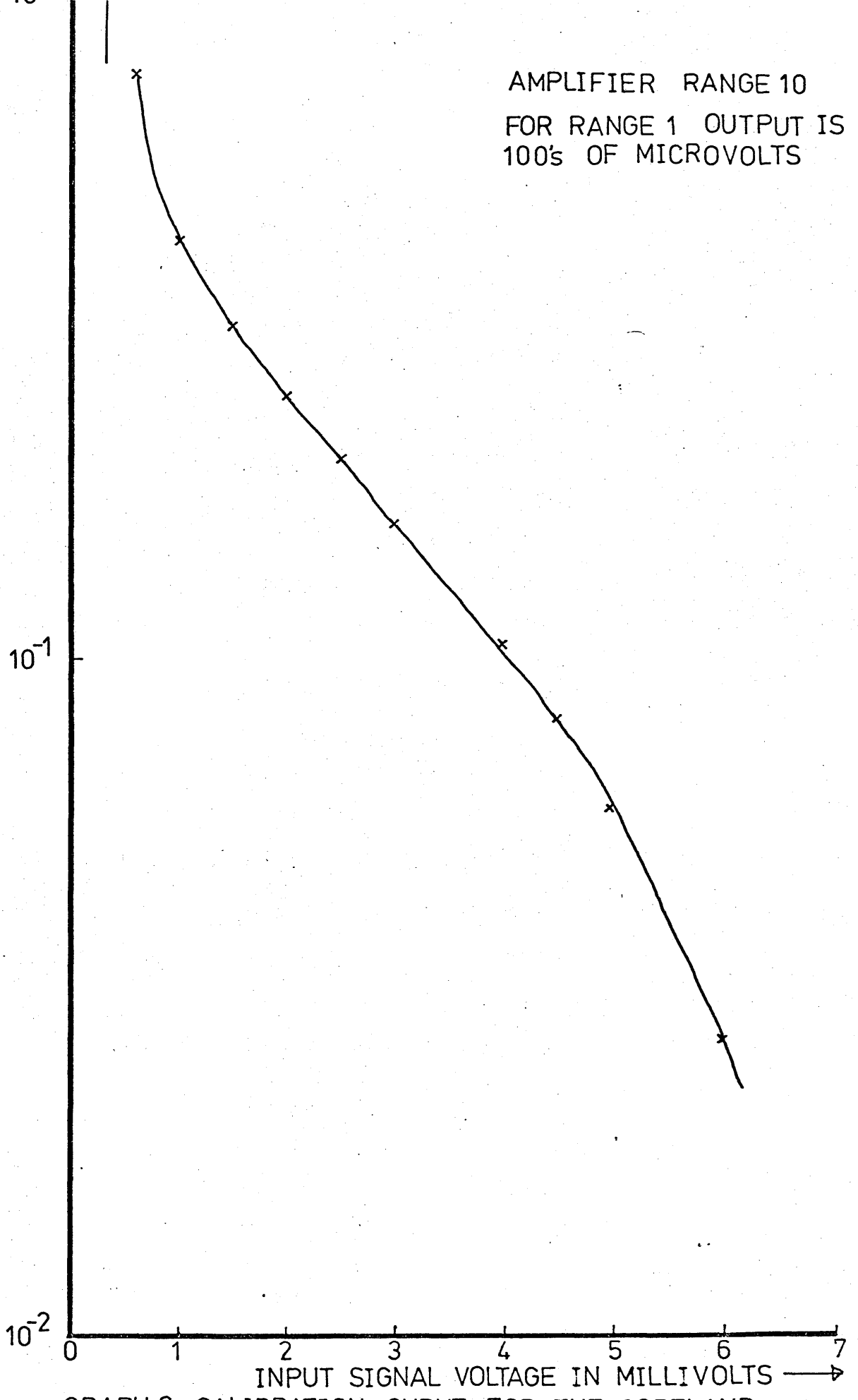


GRAPH 2 CALIBRATION CURVE FOR THE COPELAND 11·4MHZ AMPLIFIER CHANNEL

### 4.1.3 Fundamental Frequency Channel

A similar method of calibration was adopted to that used for the second harmonic channel, described in the previous section. A sine wave signal with a frequency of 5.69 MHz was injected onto the gold probe i.e. onto the input circuit of the amplifier and the output from the channel measured with an Advance R.F. digital voltmeter for a particular gain setting on the channel. A typical calibration curve of input to output is shown in Graph 3.

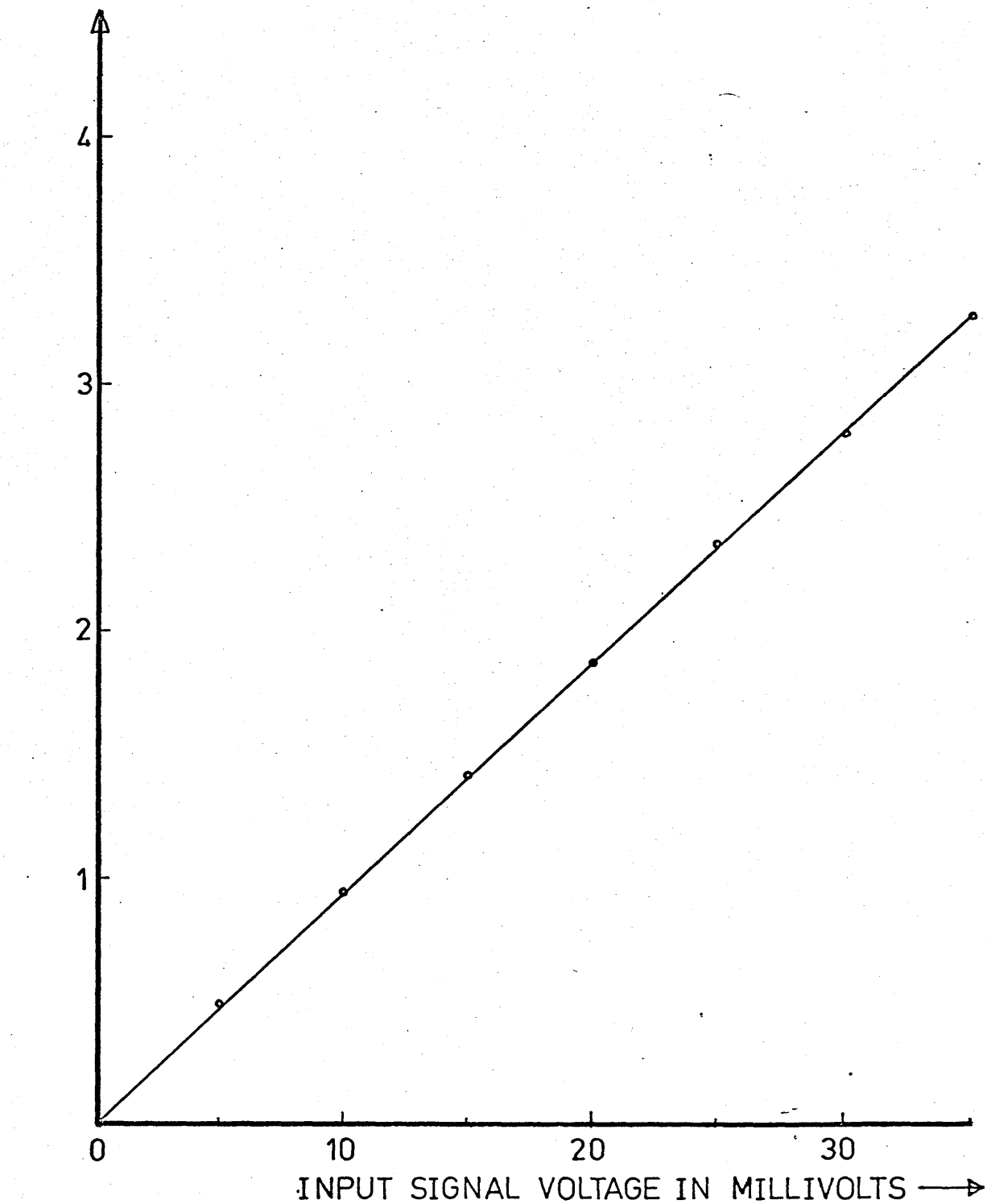


GRAPH 3 CALIBRATION CURVE FOR THE COPELAND 5·7MHZ AMPLIFIER CHANNEL RANGE 3

## 4.2 Current-Voltage Measurements

Low current-forward voltage measurements were carried out on a series of implanted specimens prepared with gold Schottky barriers on the implanted surface. These specimens had been prepared for capacitance-voltage measurements. Graph 4 shows two typical current-forward voltage characteristics for an implanted specimen and an unimplanted specimen. A series of measurements were carried out on 1.5 mm diameter gold Schottky diodes deposited onto sulphur 32 implanted n on $n^+$ epitaxial gallium arsenide, with the n layer nominally $2 \times 10^{15}$atoms/cm$^3$. The specimens were implanted at room temperature, with energies of 200 keV, 300 keV and 400 keV with a dose of $5 \times 10^{12}$ions/cm$^2$ at 300 keV, and afterwards annealed at 650°C. Further specimens were implanted at room temperature with energies of 300 keV and doses of $10^{12}$ions/cm$^2$ and $10^{13}$ions/cm$^2$ and then annealed at 650°C. Two other specimens of the same material were implanted at room temperature with sulphur 32 with an energy of 300 keV and a dose of $5 \times 10^{12}$ions/cm$^2$. These specimens were annealed at 500°C and 600°C. Graphs 5, 6 and 7 show the effects of dose, energy and anneal upon the current-forward voltage characteristics. These graphs have been plotted as $\text{Log}_e$ current density against forward bias voltage. Table V shows the variation of the factor 'n' for varying dose, energy and anneal.

A specimen of n on $n^+$ epitaxial gallium arsenide, with an n concentration of nominally $5.5 \times 10^{15}$atoms/cm$^3$, was implanted at room temperature with a dose of $3 \times 10^{12}$ions/cm$^2$ at an energy of 300 keV. Graph 8 shows the current-forward bias voltage characteristic for the implanted specimen and for an unimplanted specimen of the same material. The measurements used a 1.5 mm diameter gold Schottky barrier diode on the surface of the material.

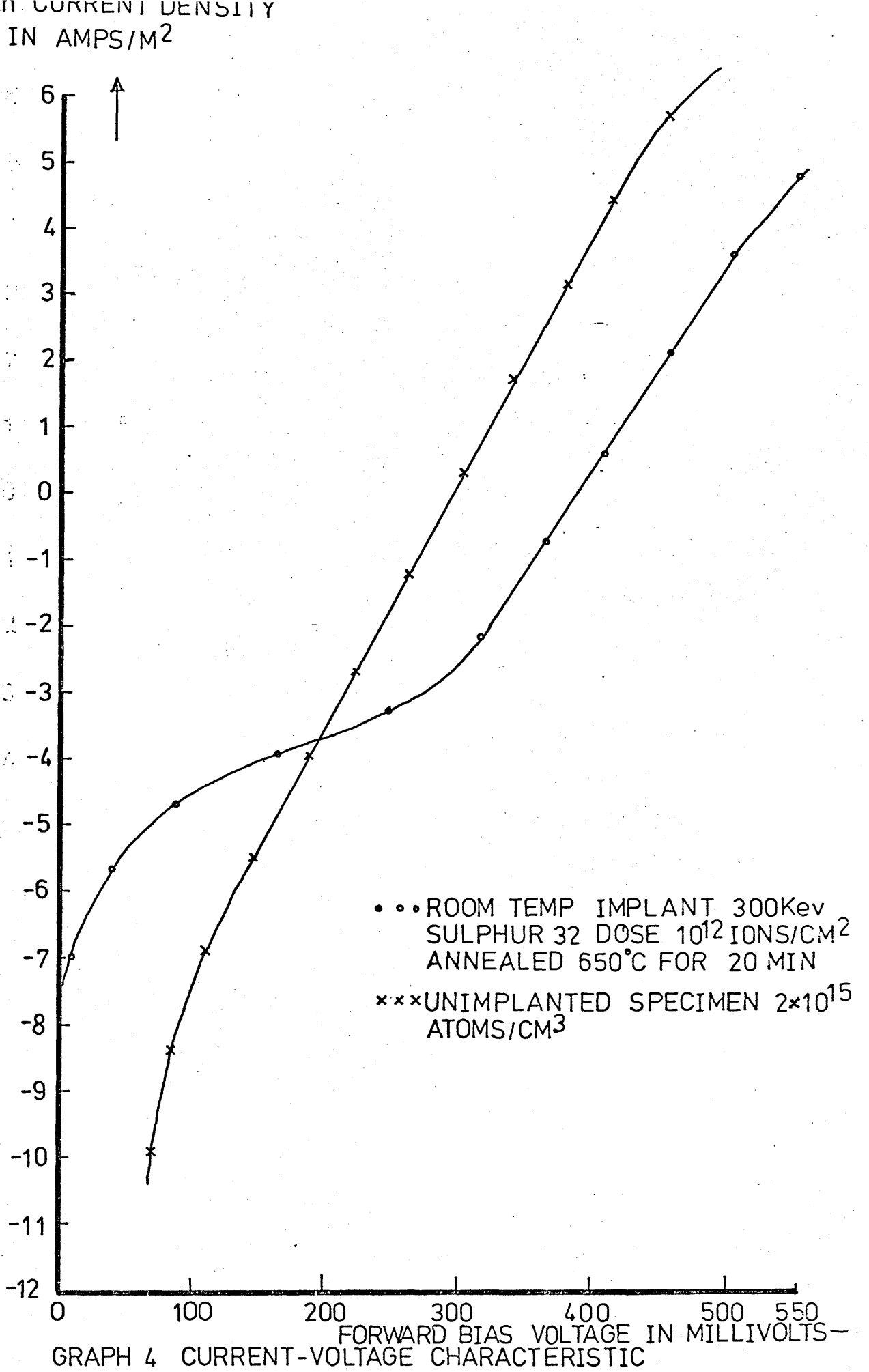


GRAPH 4 CURRENT-VOLTAGE CHARACTERISTIC

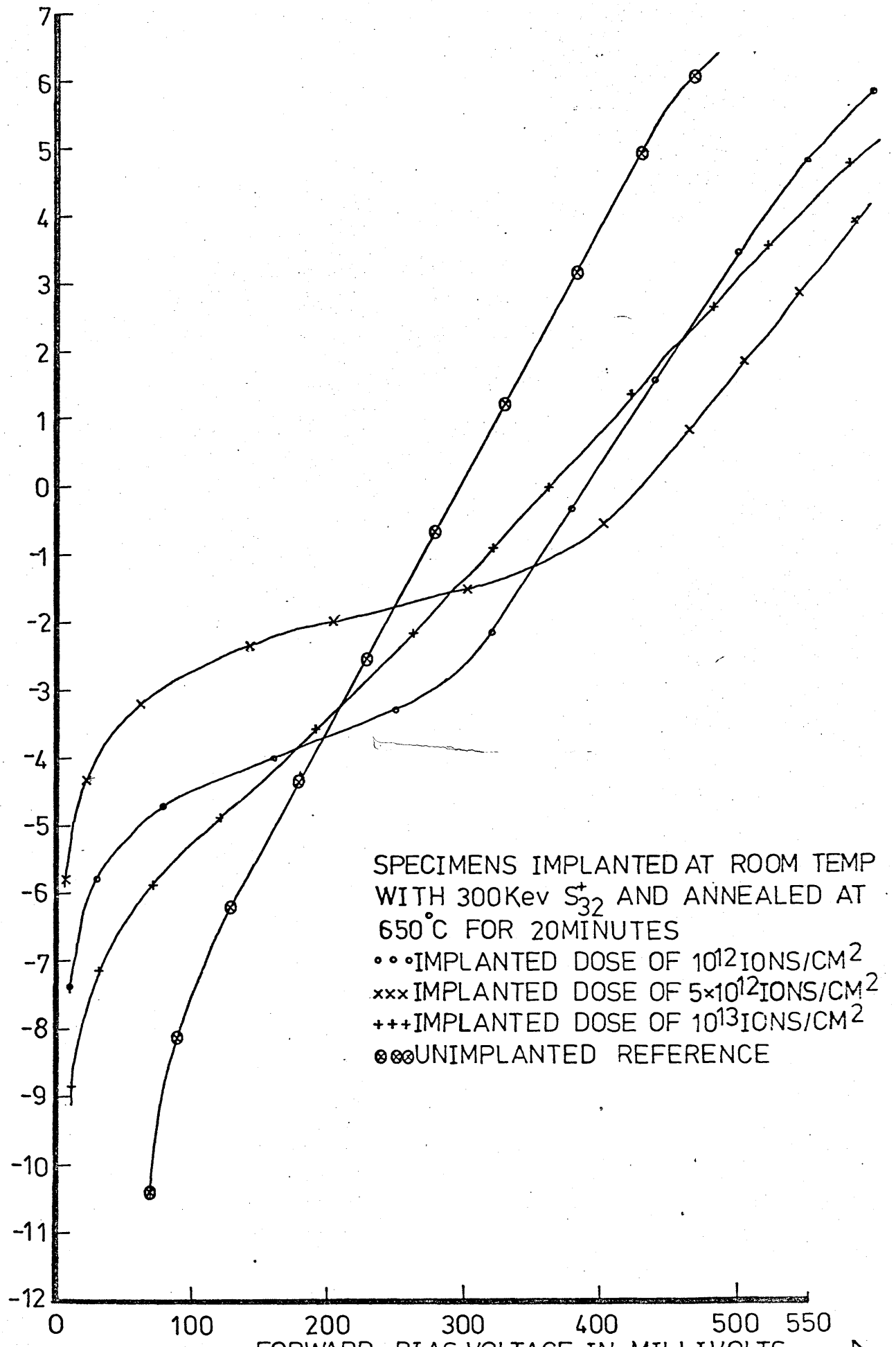


GRAPH 5 CURRENT-VOLTAGE CHARACTERISTICS VARIATION WITH DOSE

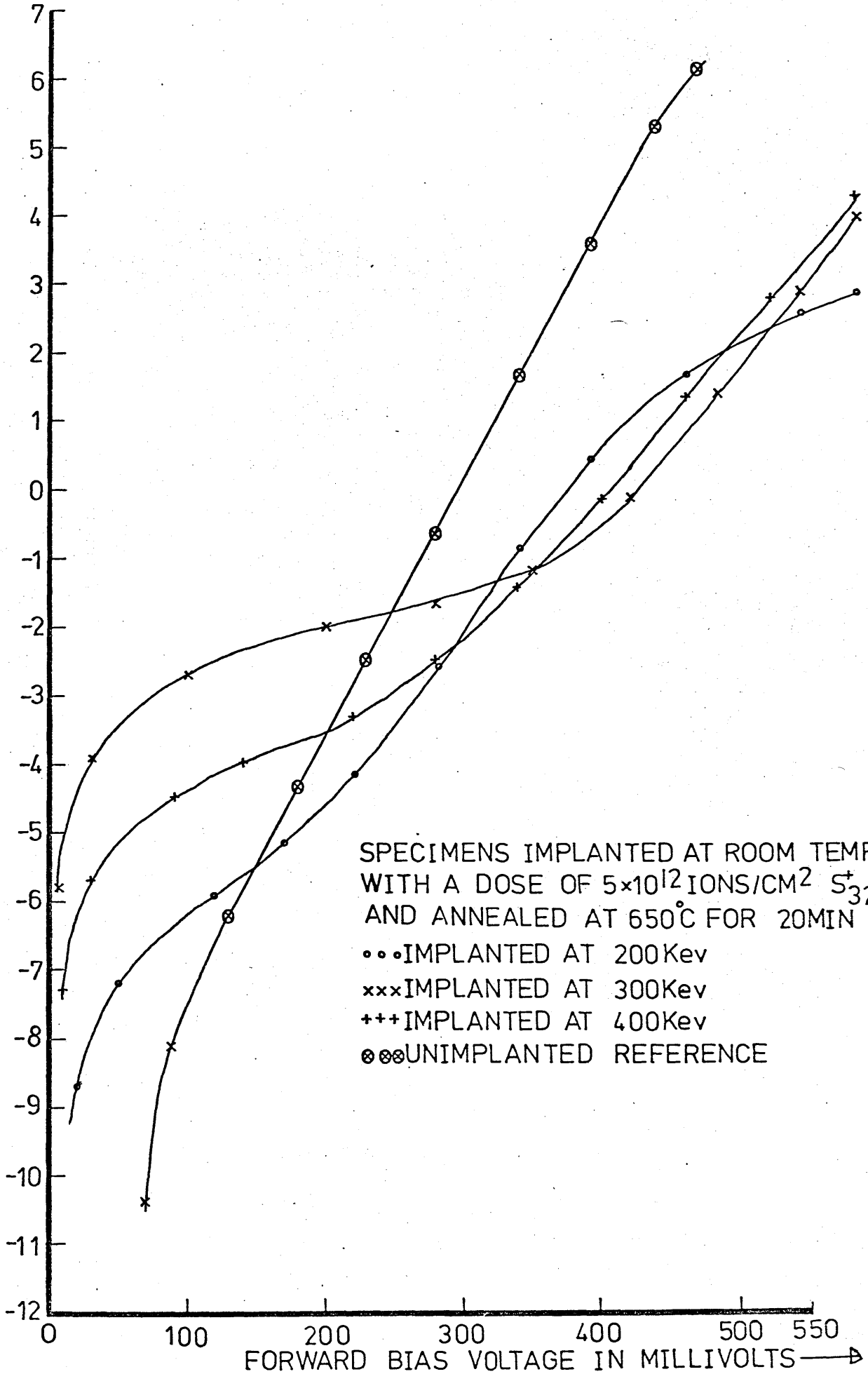


GRAPH 6 CURRENT-VOLTAGE CHARACTERISTICS VARIATION WITH ENERGY

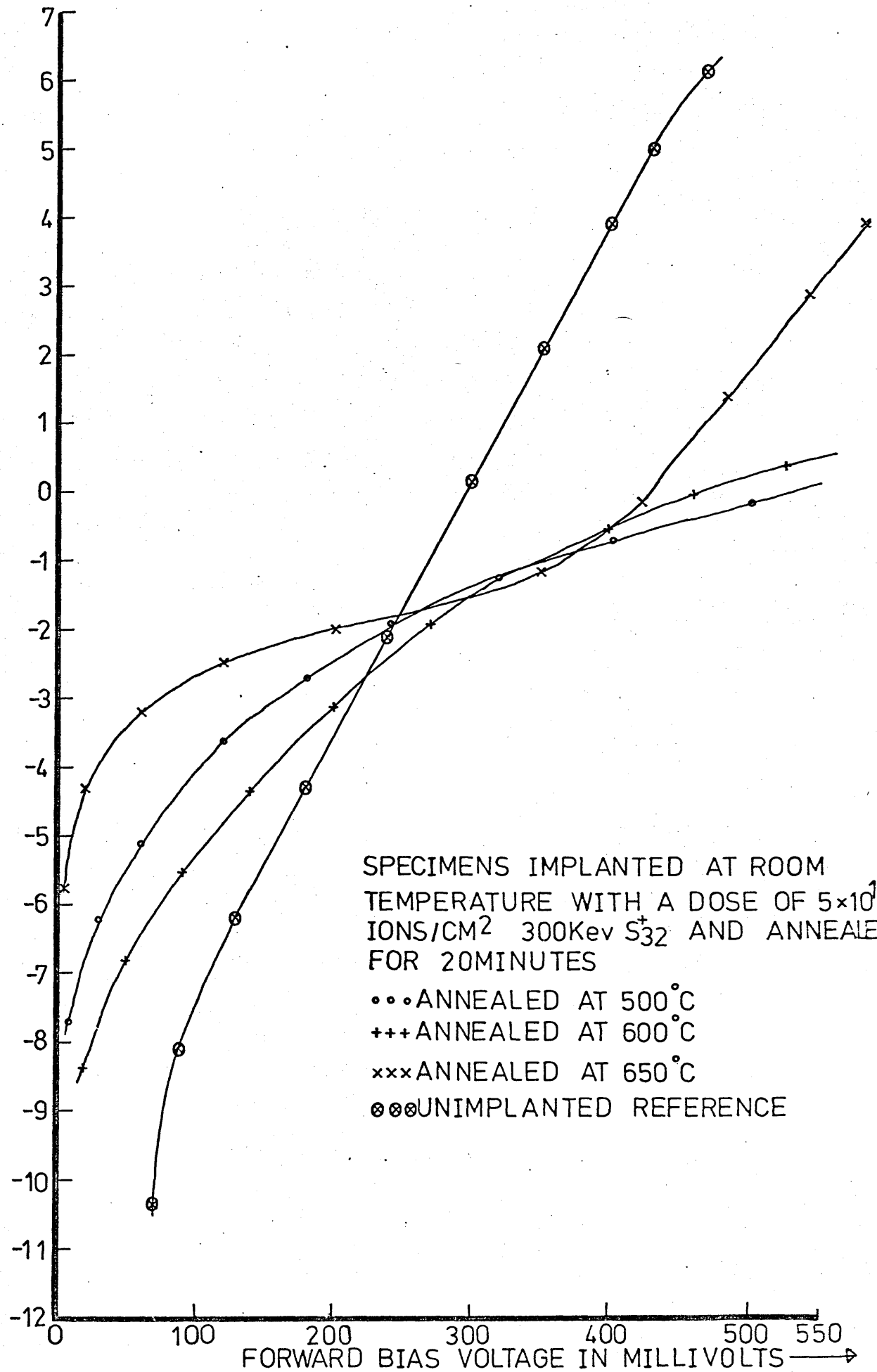


GRAPH 7 CURRENT-VOLTAGE CHARACTERISTICS VARIATION WITH ANNEAL TEMPERATURE

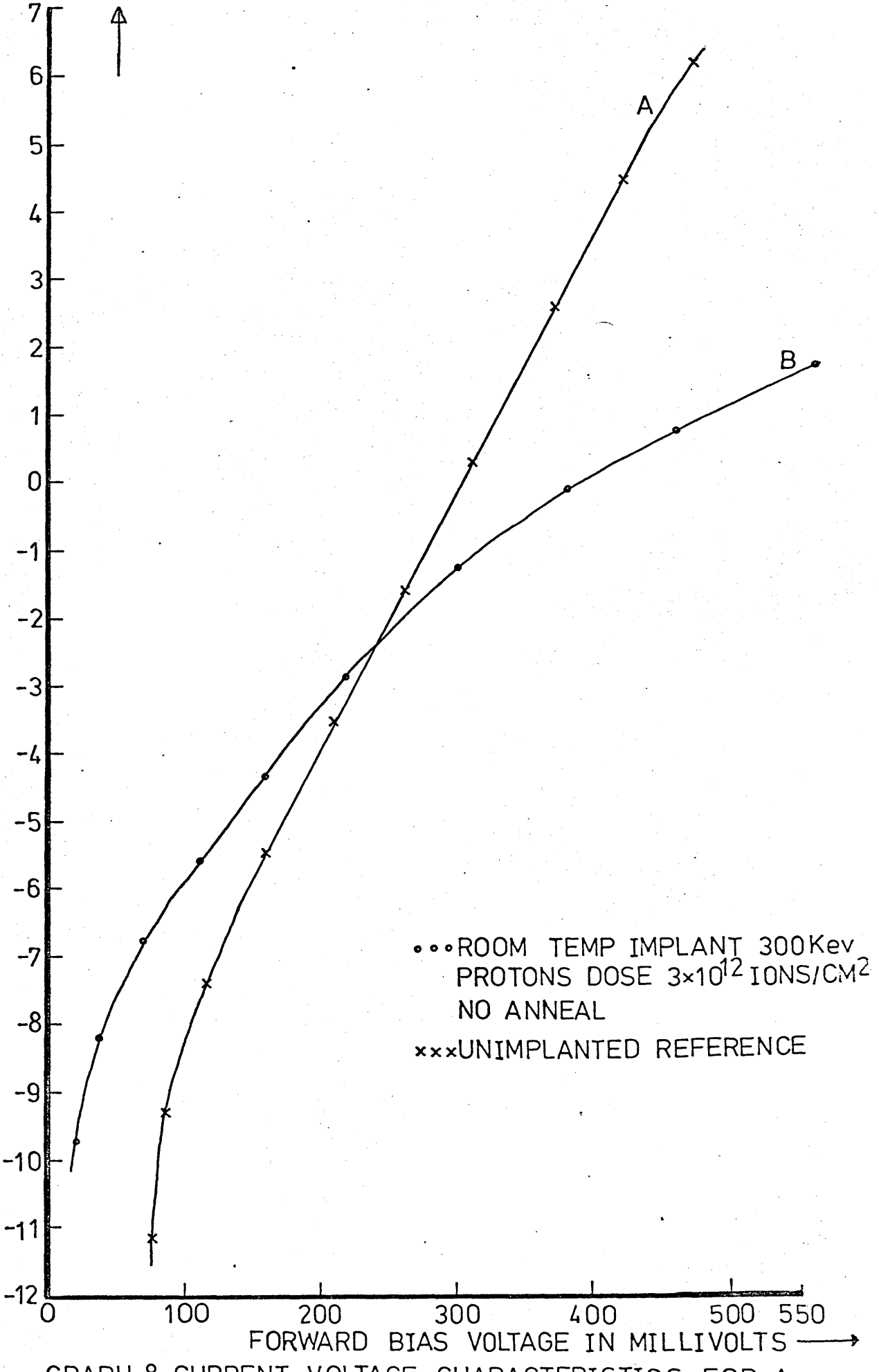


GRAPH 8 CURRENT-VOLTAGE CHARACTERISTICS FOR A PROTON IMPLANTED SPECIMEN

TABLE V

n VALUES FOR I-V CHARACTERISTICS

a) Implant Dose

Specimens implanted at room temperature with 300 keV $S_{32}$ ions and annealed at 650°C for 20 minutes.

| Dose | n Values |
|---|---|
| $10^{12}$ions/cm$^2$ | 1.28 |
| $5 \times 10^{12}$ions/cm$^2$ | 1.55 |
| $10^{13}$ions/cm$^2$ | 1.76 |
| $10^{14}$ions/cm$^2$ | not meaningful |
| $10^{15}$ions/cm$^2$ | not meaningful |

b) Implant Energy

Specimens implanted at room temperature with a dose of $5 \times 10^{12}$ions/cm$^2$ $S_{32}$ ions and annealed at 650°C for 20 minutes.

| Energy | n Values |
|---|---|
| 200 keV | 1.38 |
| 300 keV | 1.55 |
| 400 keV | 1.61 |

Table V cont./...

c) Anneal Temperature

Specimens implanted at room temperature with a dose of $5 \times 10^{12}$ ions/cm$^2$ 300 keV $S_{32}$ ions and annealed for 20 minutes.

| Temperature | n values |
|---|---|
| 500°C | not meaningful |
| 600°C | not meaningful |
| 650°C | 1.55 |
| 700°C | not meaningful |
| 800°C | not meaningful |

N.B. Unimplanted specimen n = 1.03

## 4.3 Capacitance-Frequency Measurements

Capacitance-voltage measurements were carried out mainly at the two fixed frequencies of 1 kHz and 50 kHz and the results of these measurements are described in Section 4.5. However if more than one energy level is present in the band gap, especially deep levels, variation of the diode capacitance will occur with measurement frequency. This variation has been observed by many workers and has been studied by such workers as Schibli and Milnes[68], Schibli[31], Glover[69], Hesse and Strack[74] and Bleicher and Lange[87].

Graphs 9, 10 and 11 show the variation of diode capacitance with measurement frequency for constant reverse bias. Graph 12 shows two typical concentration profiles of an implanted specimen measured at the two different frequencies, 1 kHz and 50 kHz. The concentration and depth being calculated by the method described in Section 2.4.1.

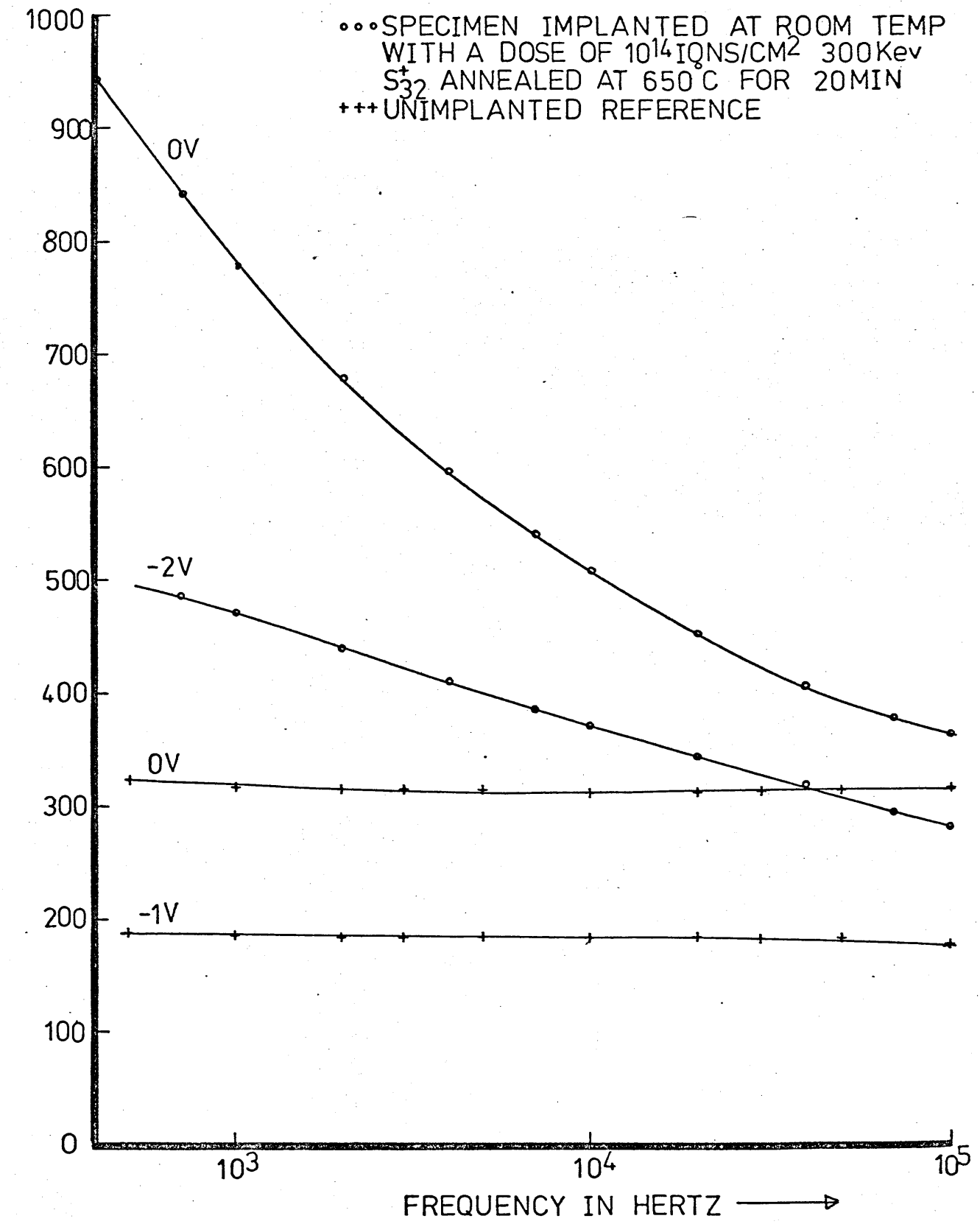


GRAPH 9 CAPACITANCE - FREQUENCY CURVES

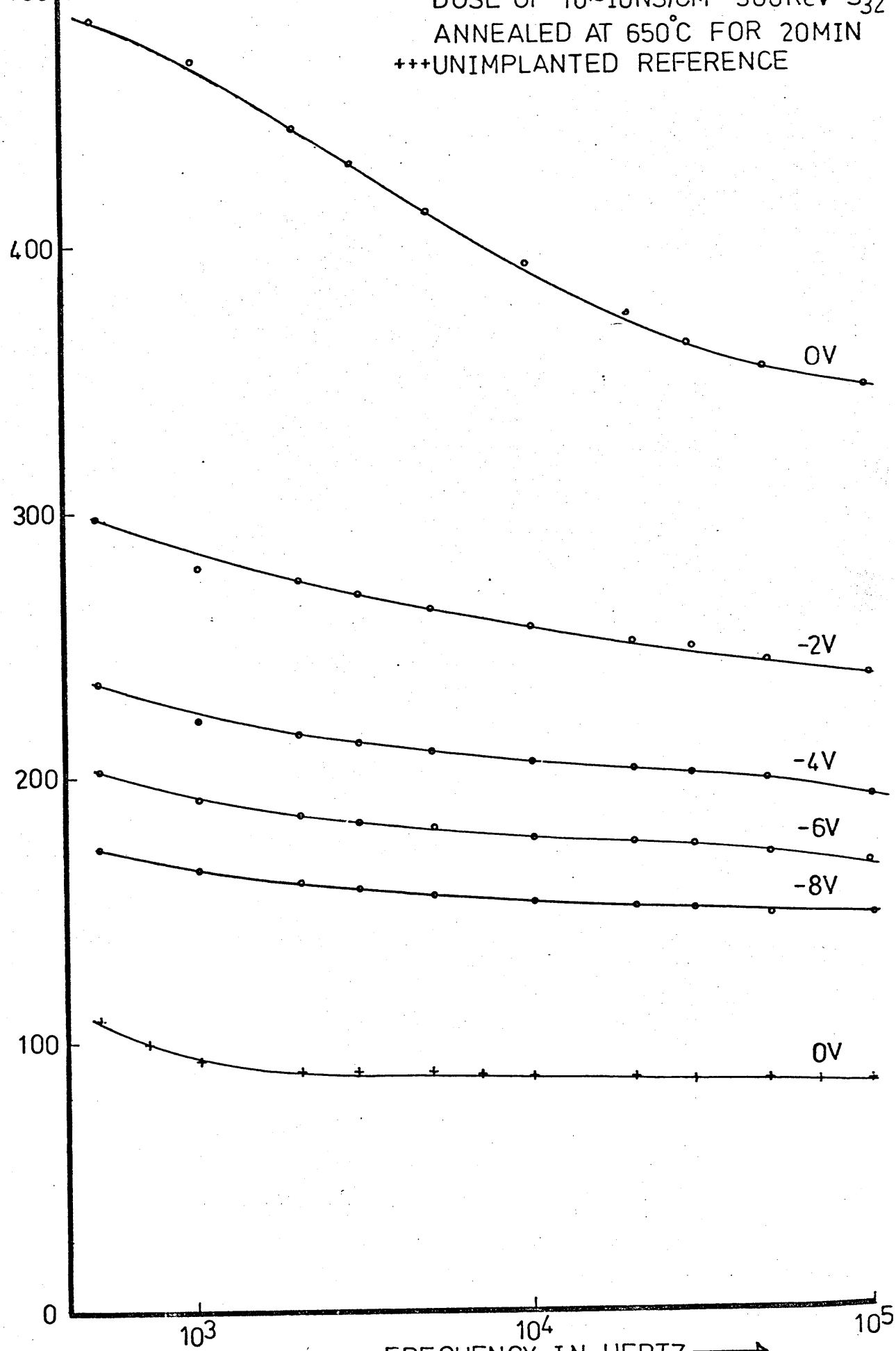


GRAPH 10 CAPACITANCE-FREQUENCY CURVES FOR CONSTANT REVERSE BIAS

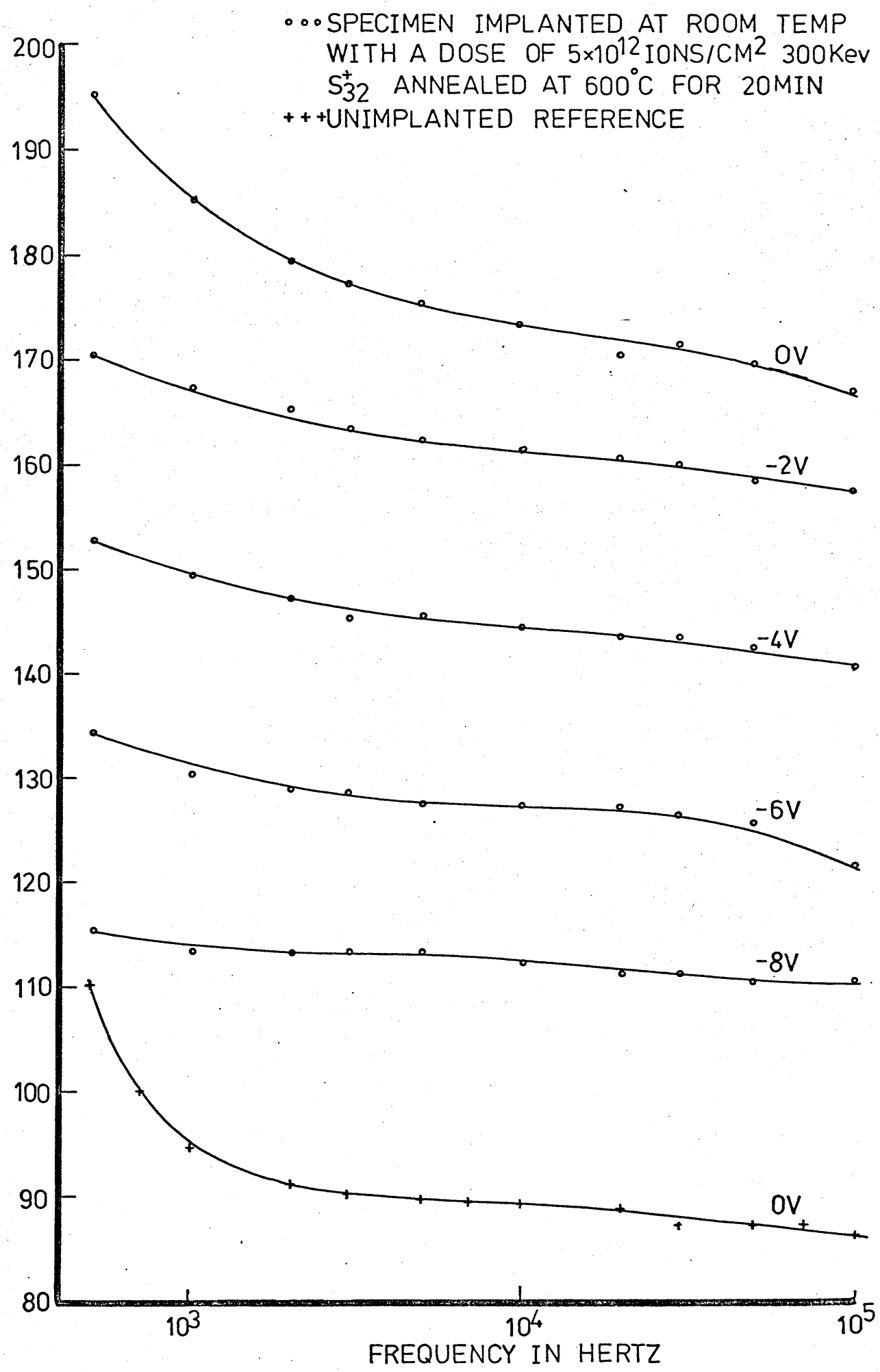


GRAPH 11 CAPACITANCE-FREQUENCY CURVE FOR CONSTANT REVERSE BIAS

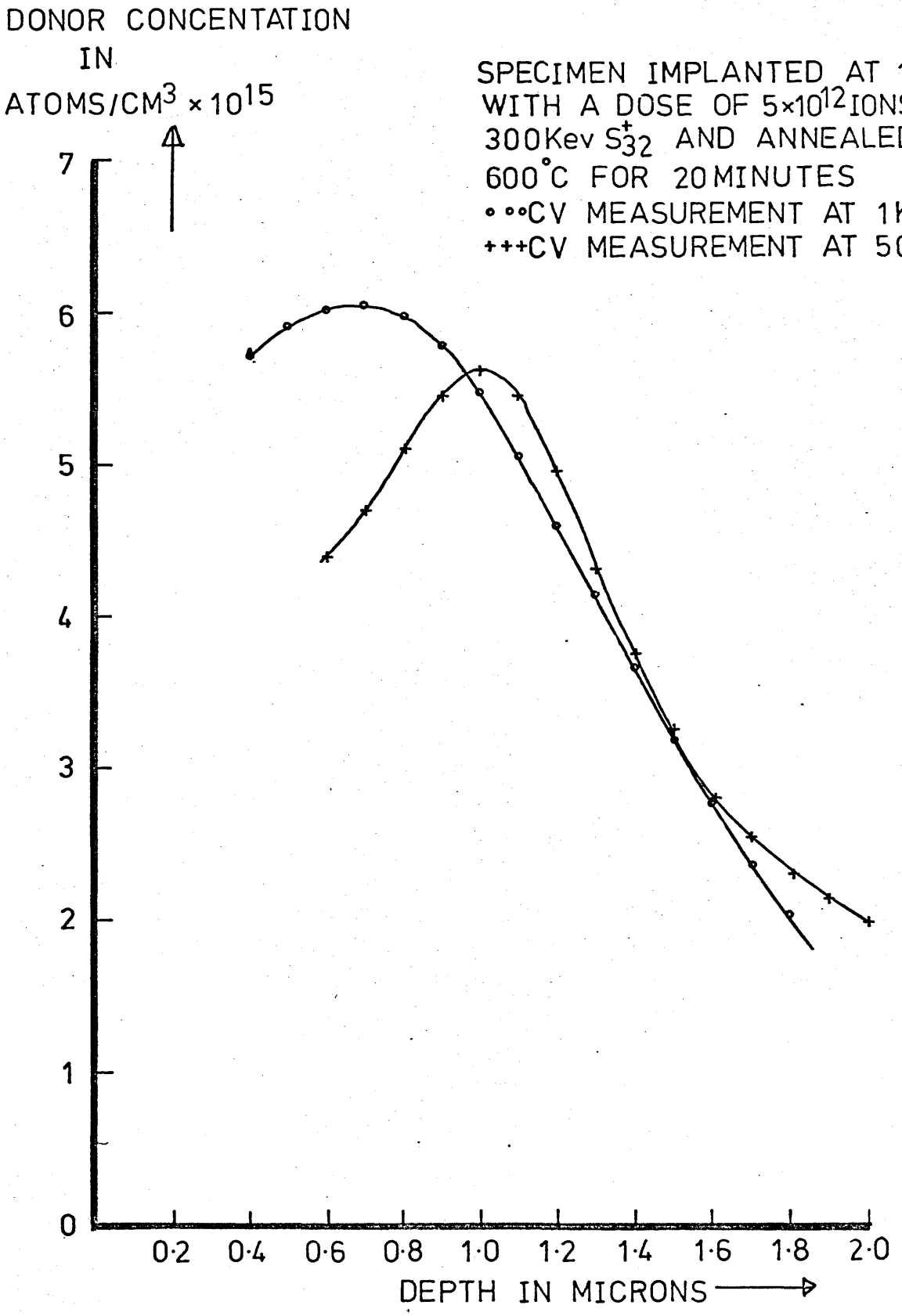


GRAPH 12 VARIATION OF CONCENTRATION PROFILE WITH FREQUENCY OF MEASUREMENT

## 4.4 Copeland Measurements

Copeland measurements were carried out on sulphur implanted epitaxial n on $n^+$ gallium arsenide to determine the electrical behaviour of the material under the following conditions:-

a) Variation with the temperature of the material during implantation (implant temperature).

b) Variation with subsequent anneal temperature.

c) Variation with ion implant energy.

d) Variation with the implanted dose of ions.

All measurements were carried out using 1.5 mm gold Schottky barriers on the implanted surface of the gallium arsenide. Results plotted on each graph were obtained using specimens from the same slice of epitaxial material. Using the Copeland equipment with an R.F. current of 200 microAmps and by varying the diode d.c. reverse bias, plots of net donor concentration versus depth from the surface of the material were obtained directly. The net donor concentration is plotted on a logarithmic scale.

Graphs 13 and 14 show the variation of net donor concentration versus depth for different implant temperatures (20°C, 100°C and 180°C). Tables VIa and VIb show the variation of carrier activity under the profile, peak carrier concentration and depth of peak concentration for different implant temperatures (20°C, 100°C and 180°C). The percentage carrier activity was calculated using equation (51).

Measurements were carried out for anneal temperatures up to and including 800°C. The specimens annealed at 800°C proved to form

leaky diodes so no useful results were obtained. Similarly in specimens which had not been annealed the diodes were leaky.

Graphs 15, 16, 17 and 18 show the variation of net donor concentration versus depth for different anneal temperatures. In the graphs 15, 16 and 17 specimens were annealed at 500°C, 600°C and 700°C for 20 minutes in a nitrogen atmosphere. In Graph 15 the specimens were implanted at room temperature; in Graph 16 the specimens were implanted at 100°C and in Graph 17 the specimens were implanted at 180°C. The other implantation conditions were identical in each of these cases. Graph 18 shows the variation after annealing at 500°C, 600°C and 650°C with the specimens implanted at 180°C.

Tables VIIa,b,c,d, and e show the variation of carrier activity under the profile, peak carrier concentration and depth of peak concentration for different anneal conditions.

Graph 19 shows the variation of net donor concentration versus depth for different implant energies, from 100 keV to 400 keV. Table VIII a and b shows the variation of carrier activity under the profile, peak carrier concentration and depth of peak concentration for different implant energies. Measurements were carried out for a range of implantation doses from $10^{12}$ions/cm$^2$ to $10^{15}$ions/cm$^2$. In specimens implanted with doses greater than $10^{14}$ions/cm$^2$, the measuring diodes proved to be leaky, such that no meaningful results were obtained. The results are plotted in Graphs 20, 21, 22, 23, 24, and 25 for different implantation conditions. Tables IX a,b,c,d and e show the variation of carrier activity under the profile, peak carrier concentration and depth of peak concentration for different implant doses.

In order to determine whether or not the deep donor concentration peak was due to channelling or diffusion the following experiment was carried out. Two similar specimens from the same slice were implanted under identical conditions, that is at room temperature with a dose of $10^{13}$ions/cm$^2$, 300 keV sulphur 32. The first specimen was annealed at 650°C for 20 minutes in a nitrogen atmosphere. 5000 Å was stripped from the implanted surface of the second specimen followed by annealing at 650°C for 20 minutes in a nitrogen atmosphere. The net carrier concentration versus depth for this experiment is shown in Graph 26.

All measurements carried out were on specimens implanted with sulphur 32. Graph 27 shows the variation of carrier activity with depth for specimens implanted with sulphur 32 and sulphur 34. Graph 28 shows the variation of donor concentration with depth for a specimen implanted at room temperature with a dose of $3 \times 10^{13}$ions/cm$^2$ of 300 keV protons and afterwards annealed at 650°C for 20 minutes in a nitrogen atmosphere.

SPECIMENS IMPLANTED WITH A DOSE OF $10^{12}$ IONS/CM$^2$ 300 Kev $S^+_{32}$ ANNEALED AT 650°C FOR 20 MINS IN A NITROGEN ATMOSPHERE
∘ ∘ ∘ IMPLANTED AT ROOM TEMP
× × × IMPLANTED AT 100°C
+ + + IMPLANTED AT 180°C
– – – UNIMPLANTED REFERENCE
IMPLANTED 7° OFF NORMAL

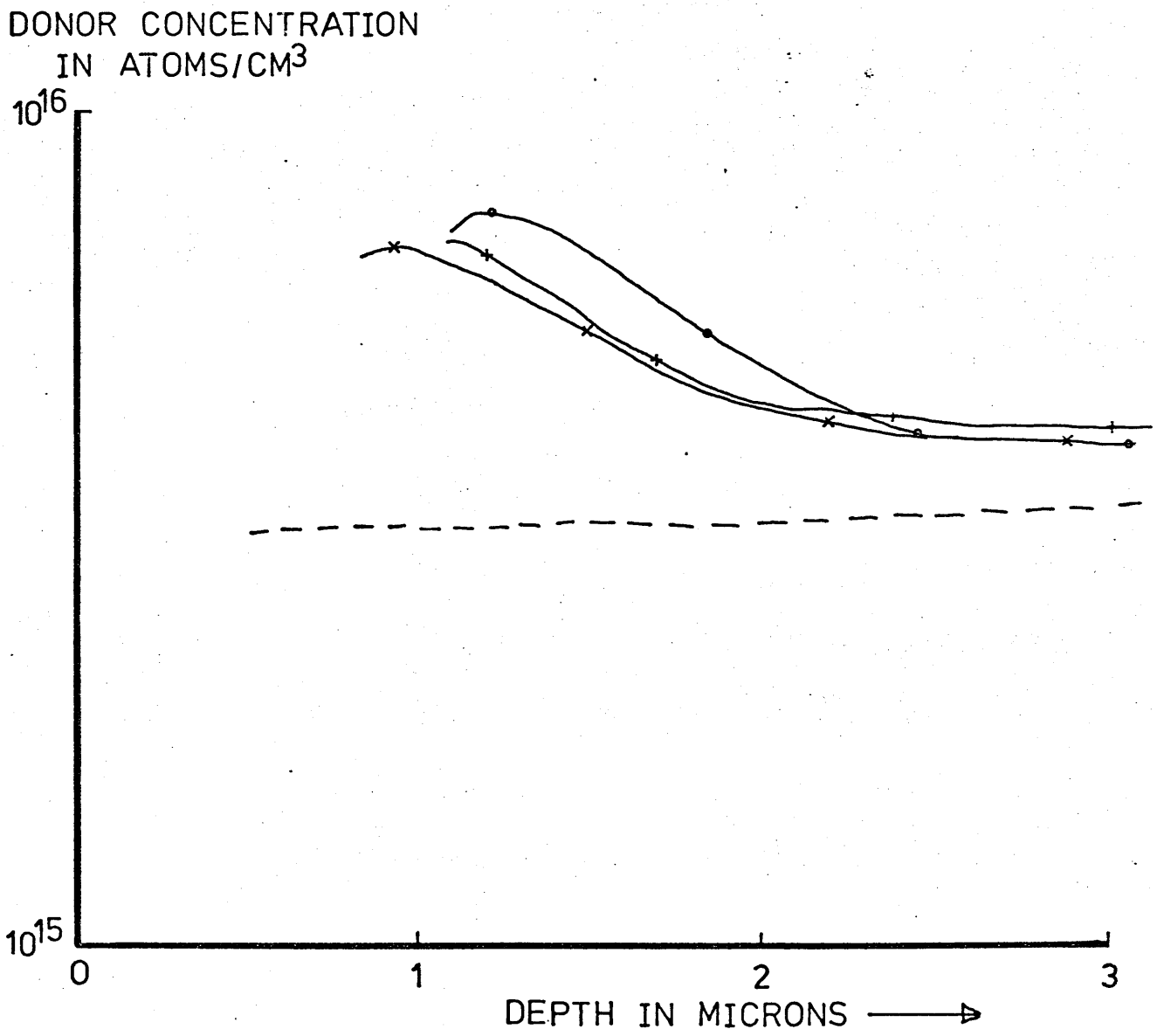


GRAPH 13 COPELAND MEASUREMENTS - VARIATION OF DONOR CONCENTRATION WITH IMPLANT TEMPERATURE

SPECIMENS IMPLANTED WITH A DOSE OF $5\times10^{12}$ IONS/CM$^2$ 400Kev $S^+_{32}$ ANNEALED AT 650°C FOR 20 MINUTES IN A NITROGEN ATMOSPHERE
ooo IMPLANTED AT ROOM TEMP
xxx IMPLANTED AT 100°C
+++ IMPLANTED AT 180°C
--- UNIMPLANTED REFERENCE
IMPLANTED 7° OFF NORMAL

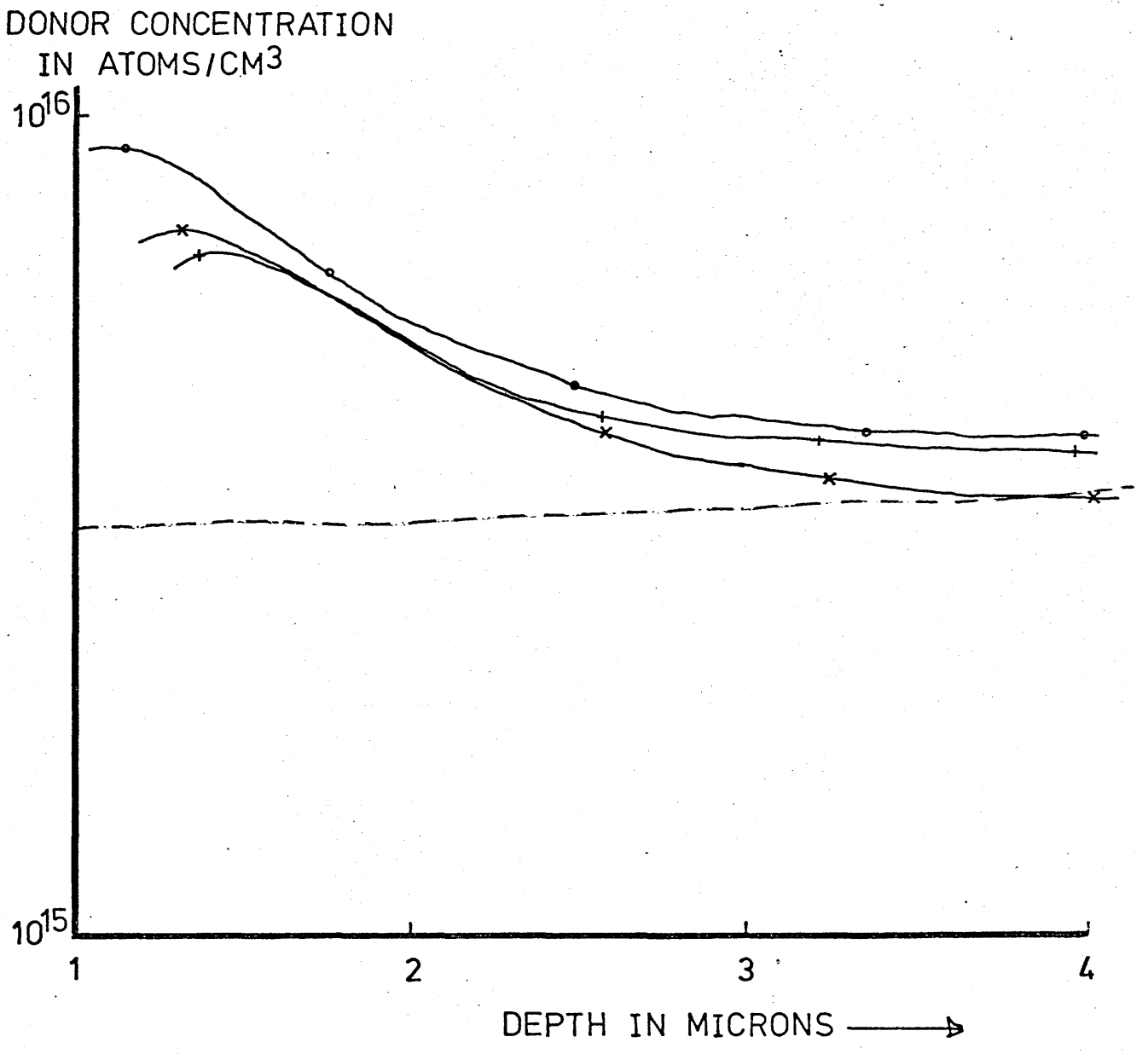


GRAPH 14 COPELAND MEASUREMENTS-VARIATION OF DONOR CONCENTRATION WITH IMPLANT TEMPERATURE

SPECIMENS IMPLANTED AT 20°C
WITH A DOSE OF $10^{13}$ IONS/CM$^2$ 300Kev
$S^+_{32}$ AND ANNEALED FOR 20MINUTES
IN A NITROGEN ATMOSPHERE
o o o ANNEALED AT 500°C
× × × ANNEALED AT 600°C
+ + + ANNEALED AT 700°C
--- UNIMPLANTED SPECIMEN

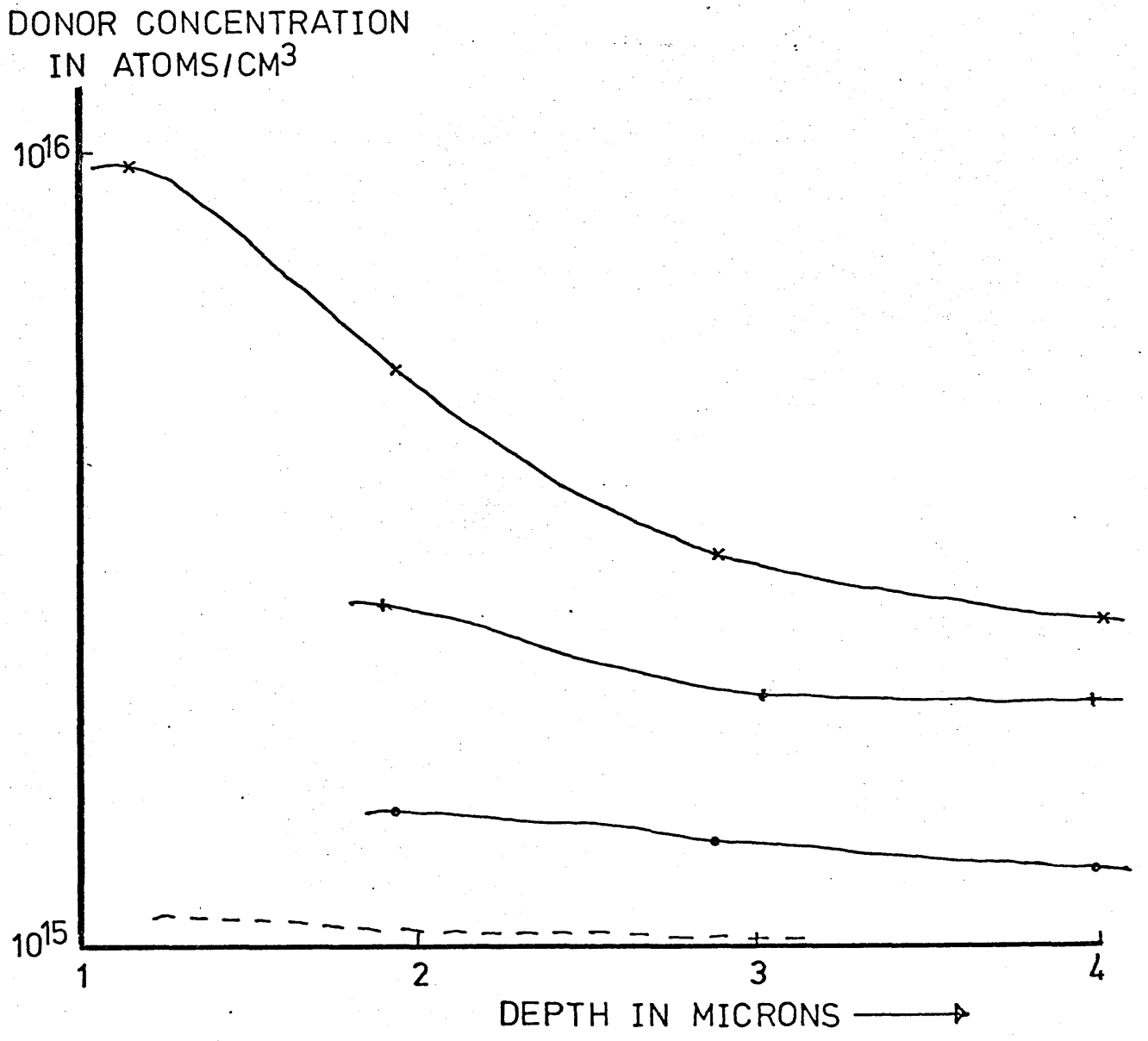


GRAPH 15 COPELAND MEASUREMENTS-VARIATION OF DONOR CONCENTRATION WITH ANNEAL TEMPERATURE

SPECIMENS IMPLANTED AT 100 C
WITH A DOSE OF $10^{13}$ IONS/CM$^2$ 300Kev
$S^+_{32}$ AND ANNEALED FOR 20MINUTES
IN A NITROGEN ATMOSPHERE
ooo ANNEALED AT 500°C
××× ANNEALED AT 600°C
+++ ANNEALED AT 700°C
IMPLANTED 7° OFF NORMAL

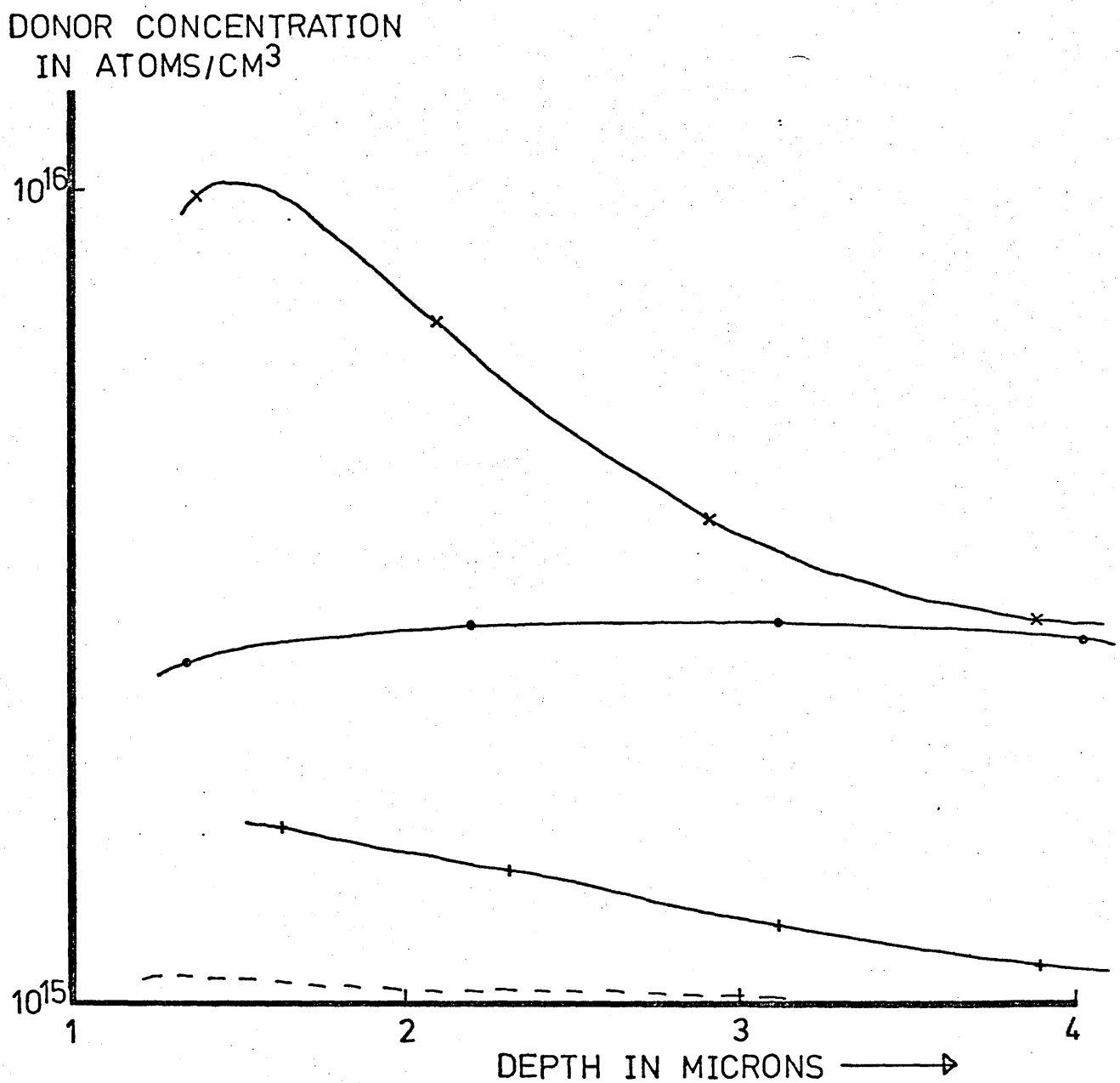


GRAPH 16 COPELAND MEASUREMENTS - VARIATION OF DONOR CONCENTRATION WITH ANNEAL TEMPERATURE

IMPLANTED 7° OFF NORMAL
SPECIMENS IMPLANTED AT 180°C
WITH A DOSE OF $10^{13}$ IONS/CM$^2$ 300Kev
$S^+_{32}$ AND ANNEALED FOR 20MINUTES
IN A NITROGEN ATMOSPHERE
°°°ANNEALED AT 500°C
×××ANNEALED AT 600°C
+++ANNEALED AT 700°C
---UNIMPLANTED REFERENCE

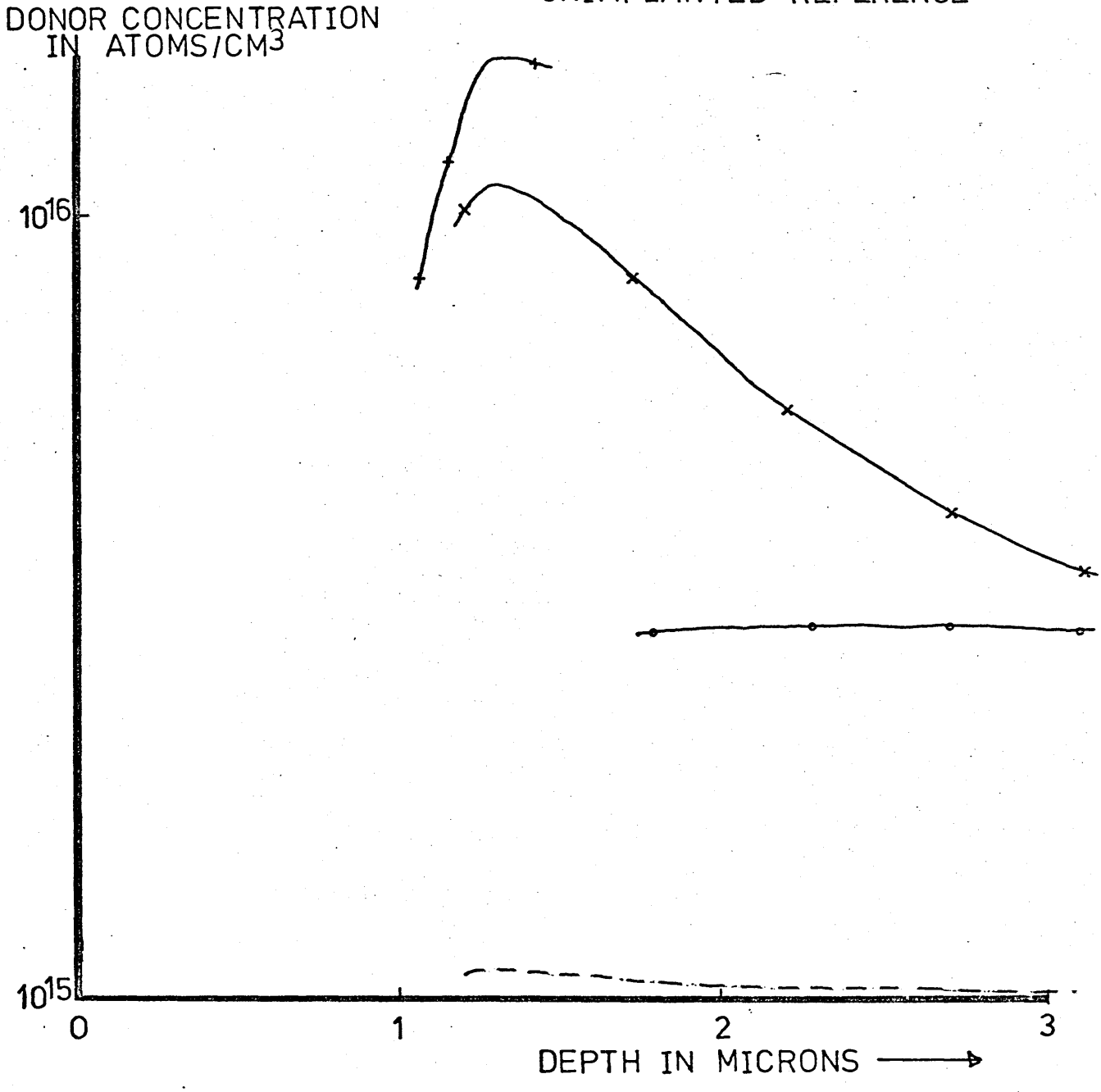


GRAPH 17 COPELAND MEASUREMENTS-VARIATION OF DONOR CONCENTRATION WITH ANNEAL TEMPERATURE

SPECIMENS IMPLANTED AT 180°C WITH A DOSE OF $5\times10^{12}$ IONS/CM$^2$ 300Kev $S^+_{32}$ AND ANNEALED FOR 20MINUTES IN A NITROGEN ATMOSPHERE

∘ ∘ ∘NO ANNEAL

× × ×ANNEALED AT 500°C

+ + + ANNEALED AT 600°C

⊗ ⊗ ⊗ANNEALED AT 650°C

– – –UNIMPLANTED REFERENCE

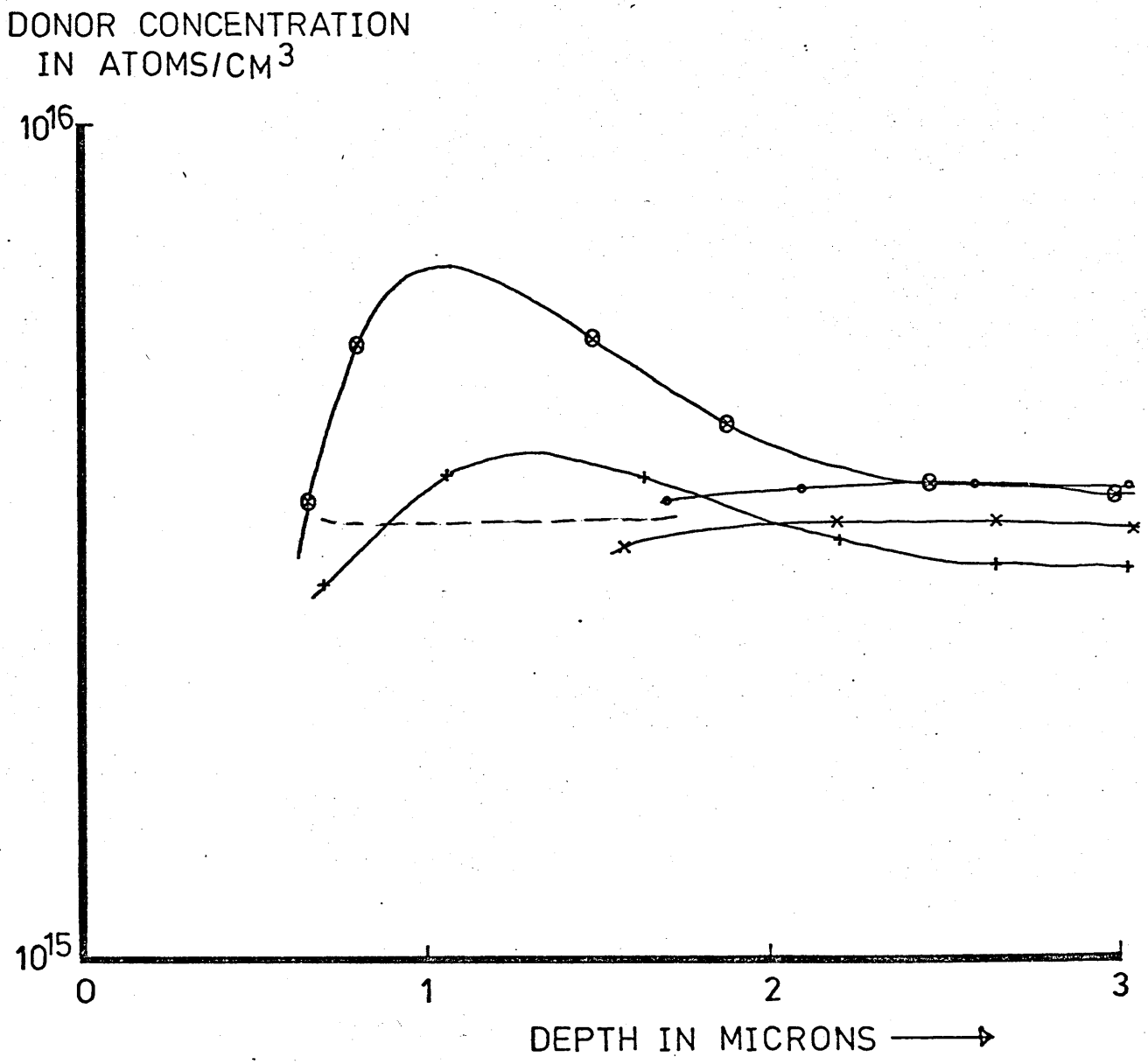


GRAPH 18 COPELAND MEASUREMENTS- VARIATION OF DONOR CONCENTRATION WITH ANNEAL TEMPERATURE

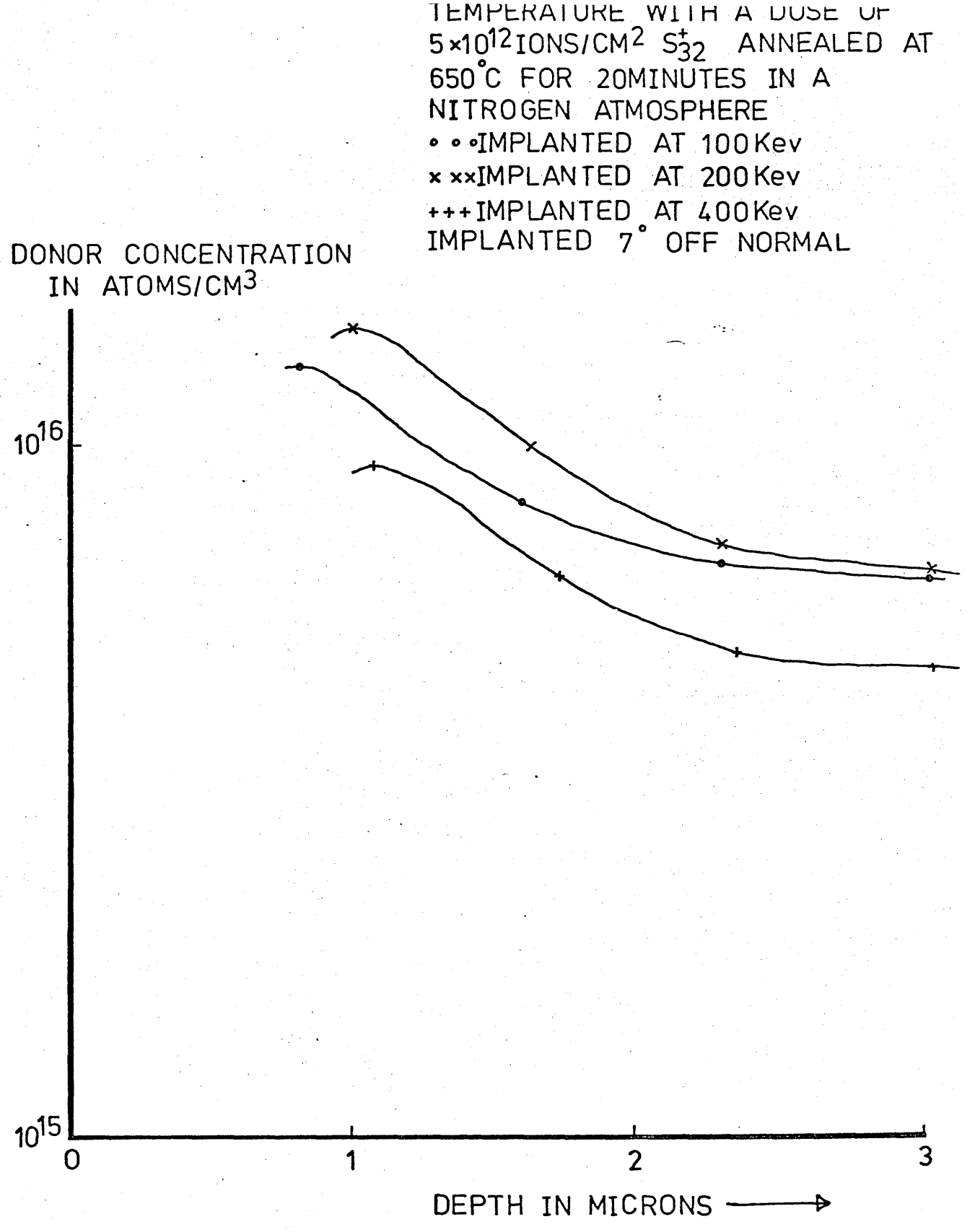


GRAPH 19 COPELAND MEASUREMENTS-VARIATION OF DONOR CONCENTRATION WITH IMPLANT ENERGY

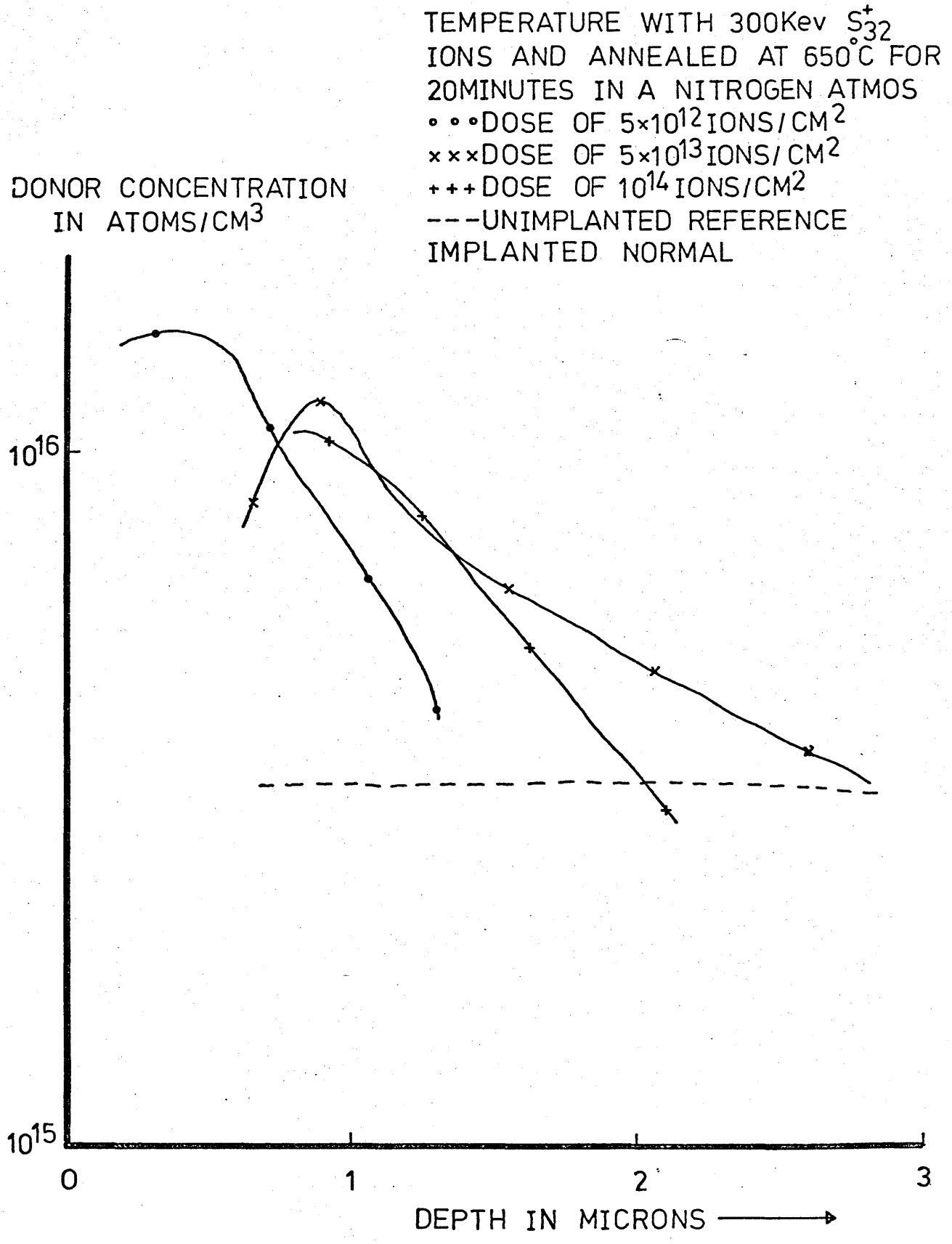


GRAPH 20 COPELAND MEASUREMENTS-VARIATION OF DONOR CONCENTRATION WITH IMPLANT DOSE

TEMPERATURE WITH 300Kev $S^{+}_{32}$ IONS AND ANNEALED AT 650°C FOR 20MINUTES IN AN ARSENIC ATMOSPHERE

∘ ∘ ∘DOSE OF $10^{12}$IONS/CM$^2$

× × ×DOSE OF $5\times10^{12}$IONS/CM$^2$

+ + + DOSE OF $10^{13}$IONS/CM$^2$

– – –UNIMPLANTED REFERENCE

IMPLANTED NORMAL

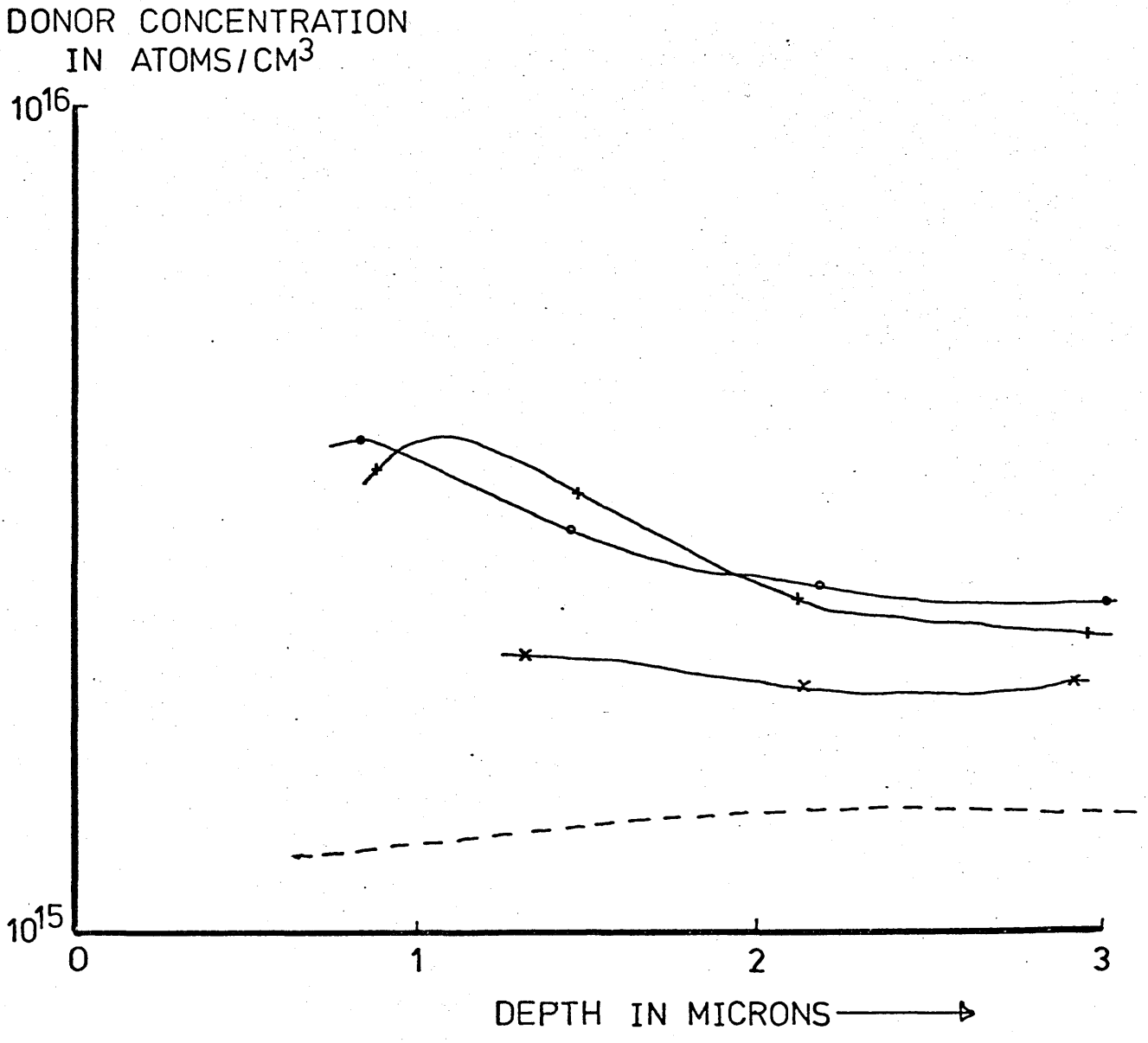


GRAPH 21 COPELAND MEASUREMENTS-VARIATION OF DONOR CONCENTRATION WITH IMPLANT DOSE

WITH 300Kev $S^{+}_{32}$ IONS AND
ANNEALED AT 650°C FOR 20MINS
IN A NITROGEN ATMOSPHERE
∘ ∘ ∘DOSE OF $10^{12}$IONS/CM$^2$
× × ×DOSE OF $10^{13}$IONS/CM$^2$
+ + +DOSE OF $10^{14}$IONS/CM$^2$
---UNIMPLANTED REFERENCE
IMPLANTED 7° OFF NORMAL

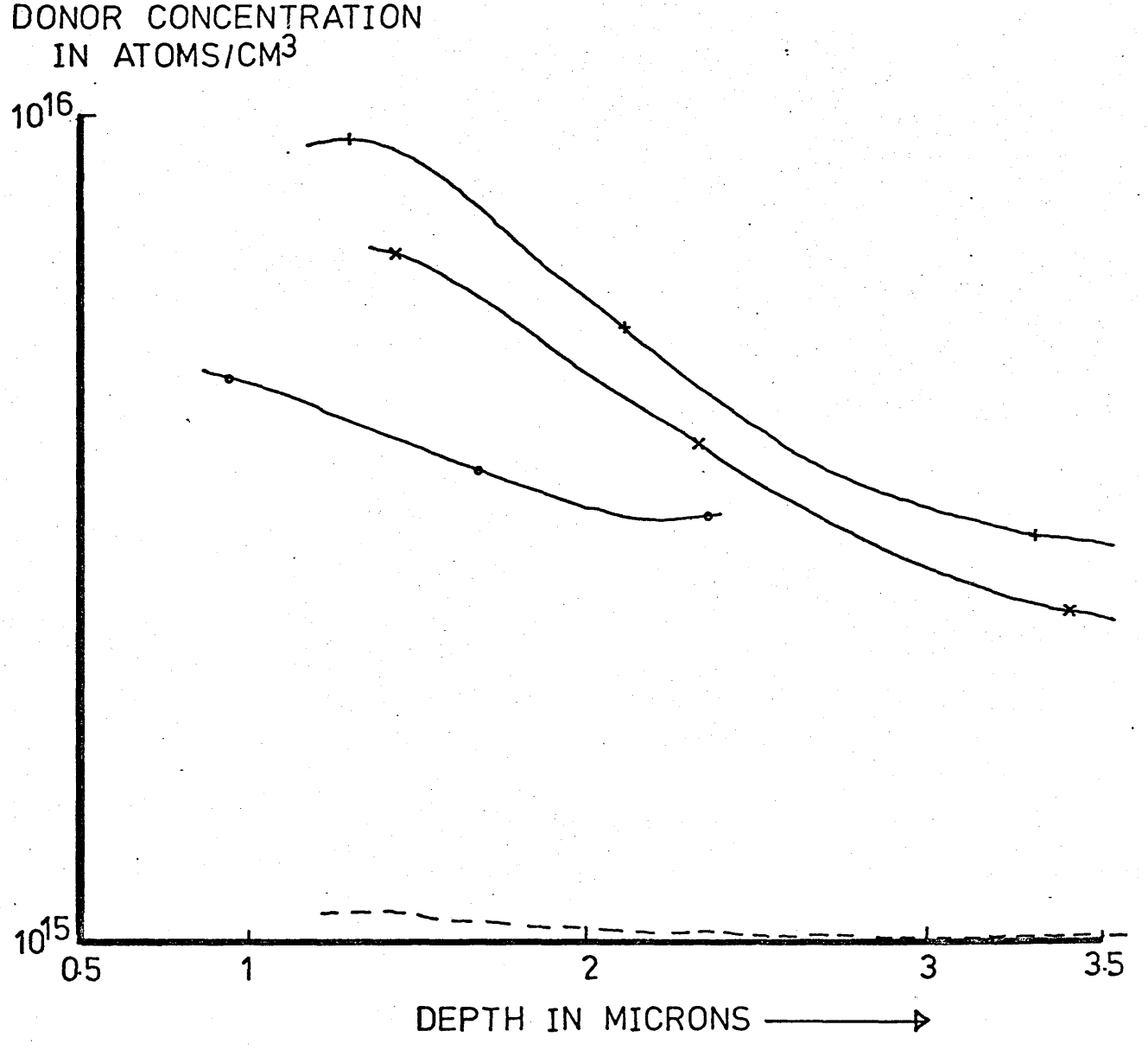


GRAPH 22 COPELAND MEASUREMENTS-VARIATION OF DONO
CONCENTRATION WITH IMPLANT DOSE

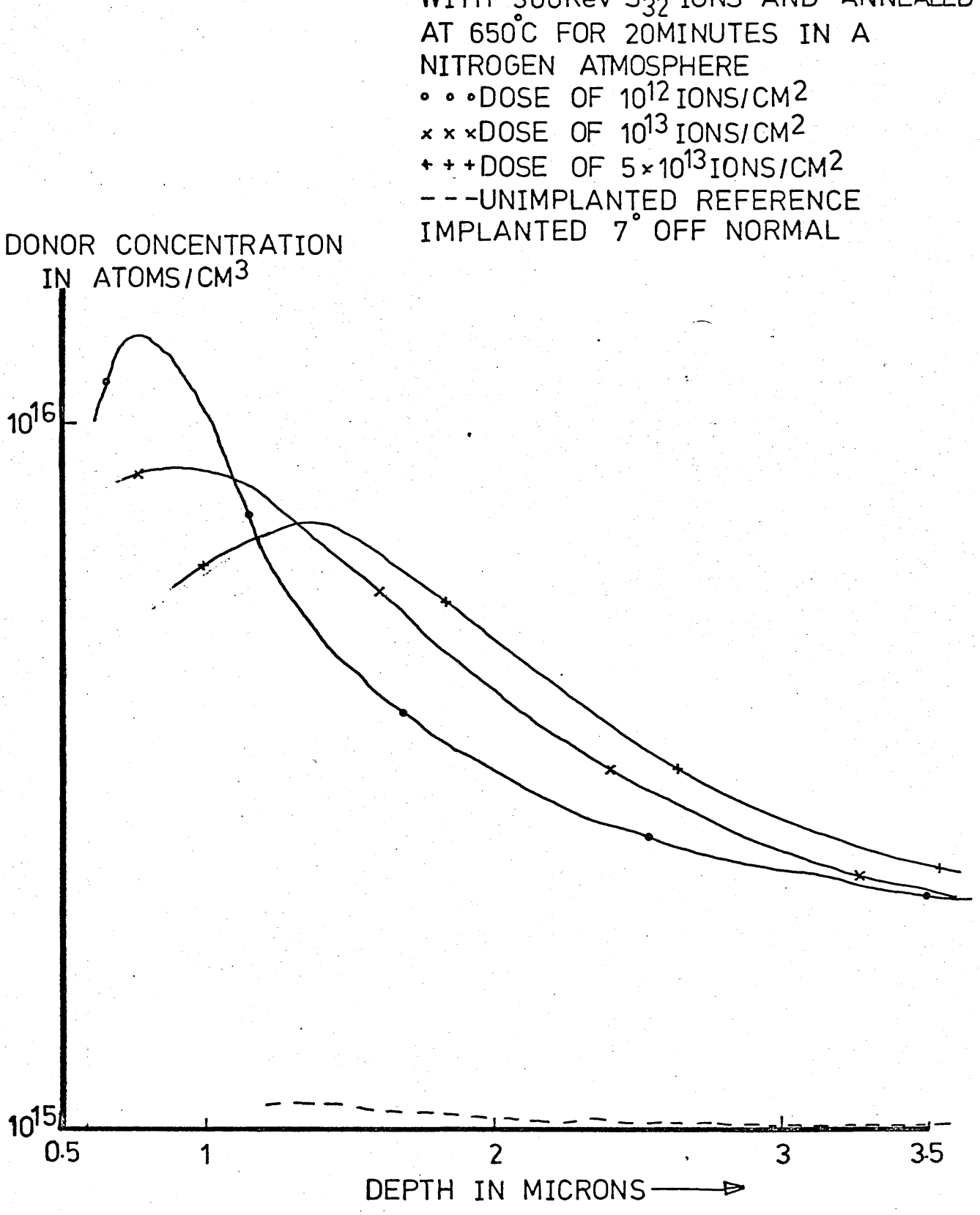


GRAPH 23 COPELAND MEASUREMENTS-VARIATION OF DONOR CONCENTRATION WITH IMPLANT DOSE

WITH 300 Kev $S^{+}_{32}$ IONS AND ANNEALED AT 650°C FOR 20 MINUTES IN A NITROGEN ATMOSPHERE
° ° ° DOSE OF $5 \times 10^{12}$ IONS/CM$^2$
× × × DOSE OF $10^{13}$ IONS/CM$^2$
+ + + DOSE OF $10^{14}$ IONS/CM$^2$
– – – UNIMPLANTED REFERENCE
IMPLANTED NORMAL

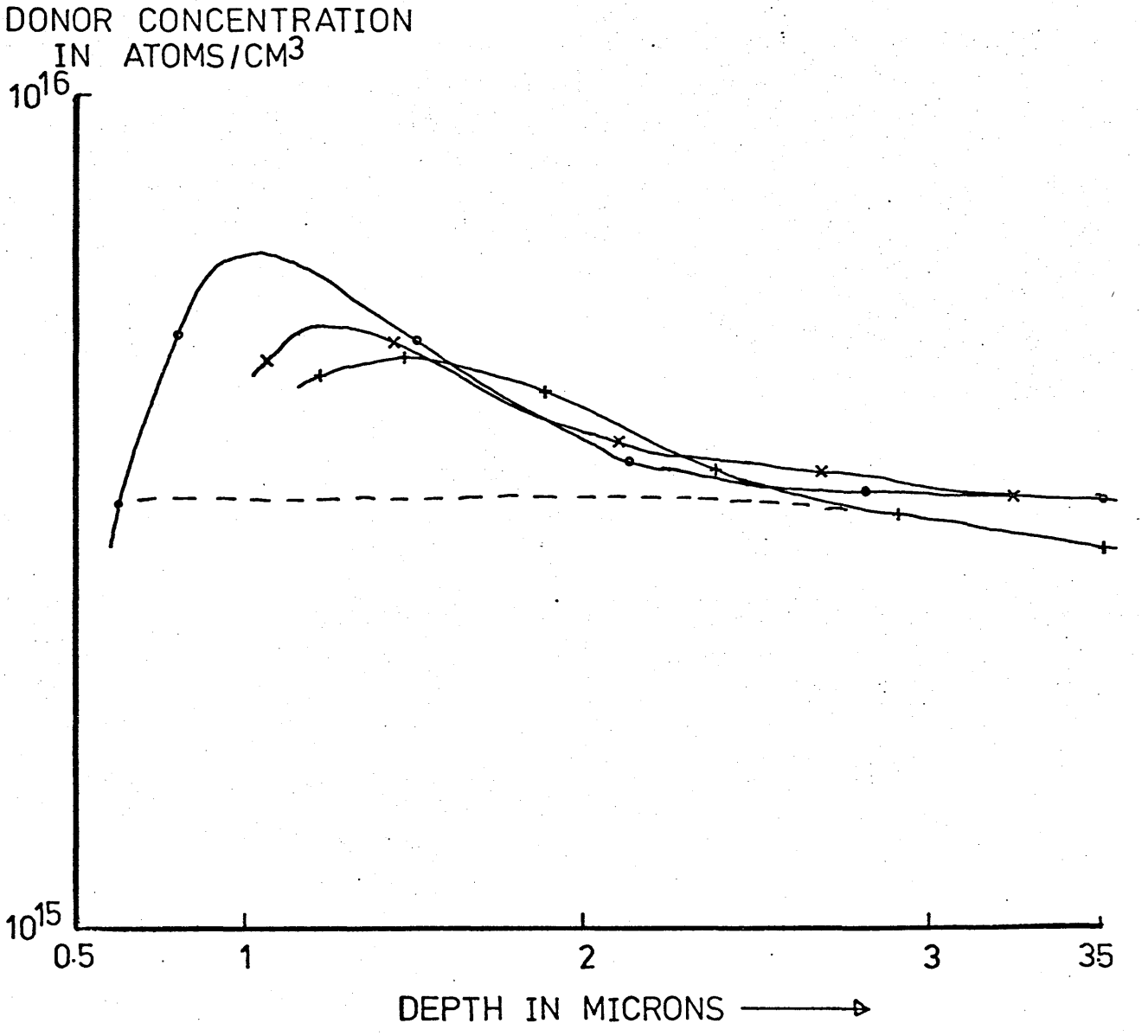


GRAPH 24 COPELAND MEASUREMENTS - VARIATION OF DONOR CONCENTRATION WITH IMPLANT DOSE

WITH 300Kev $S^{+}_{32}$ IONS AND
ANNEALED AT 650°C FOR 20MINS
IN A NITROGEN ATMOSPHERE
∘ ∘ ∘DOSE OF $10^{13}$IONS/CM$^2$
× × ×DOSE OF $10^{15}$IONS/CM$^2$
- - -UNIMPLANTED REFERENCE
IMPLANTED 7° OFF NORMAL

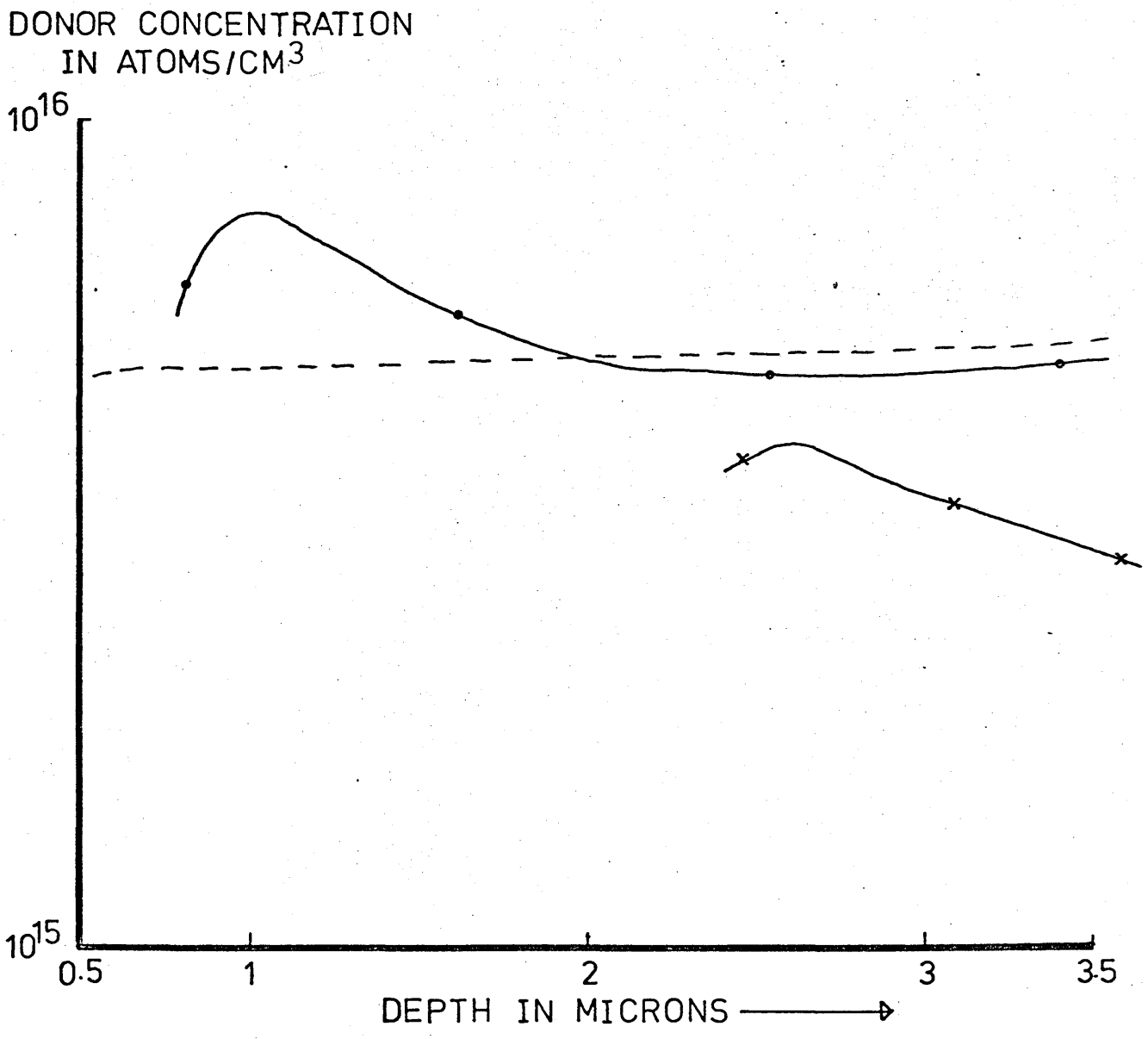


GRAPH 25 COPELAND MEASUREMENTS-VARIATION OF DONOR CONCENTRATION WITH IMPLANT DOSE

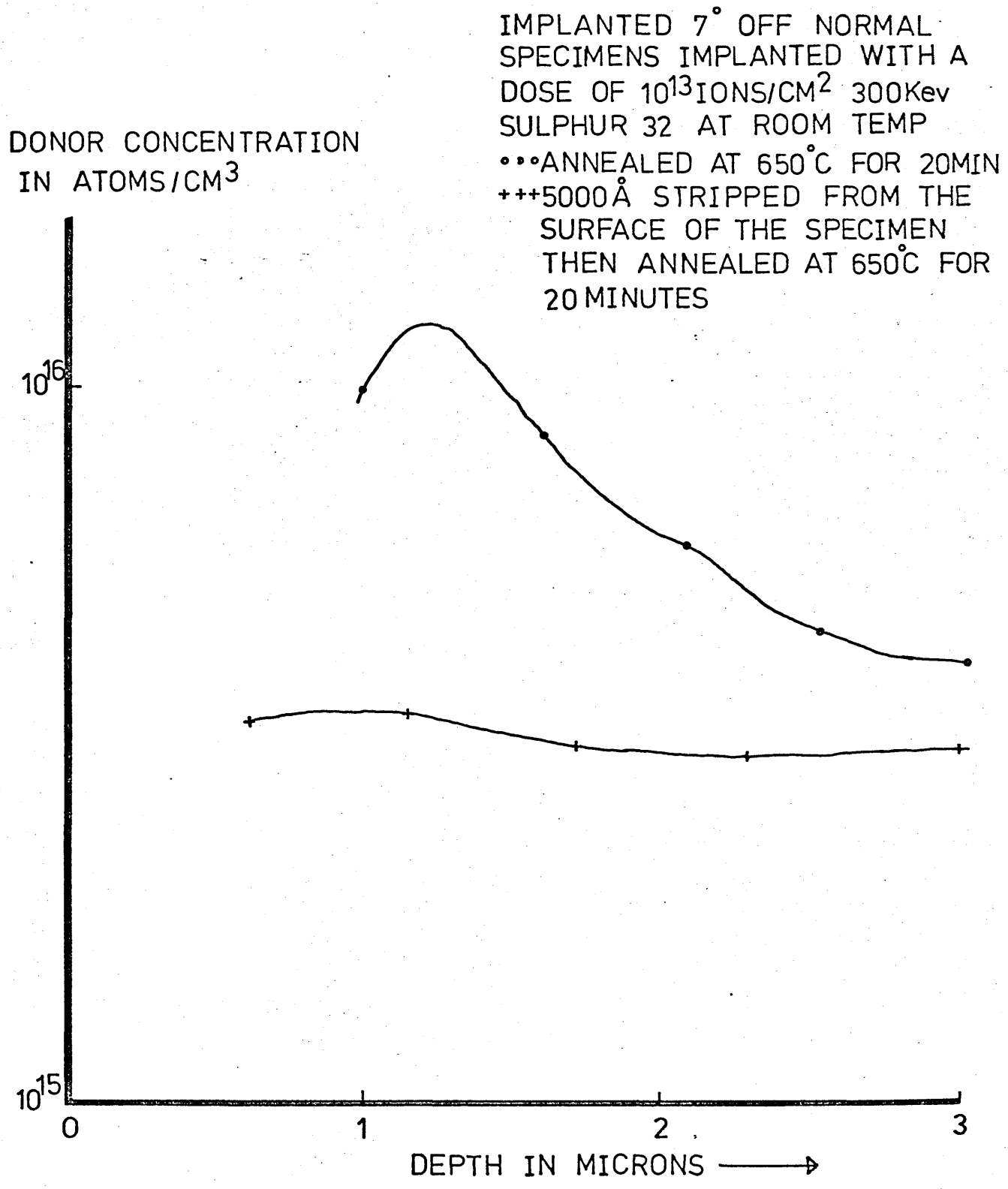


GRAPH 26 STRIPPING EXPERIMENT-COPELAND PROFILES OF TWO IDENTICALLY IMPLANTED SPECIMENS, ONE WITH 5000Å STRIPPED FROM THE SURFACE PRIOR TO ANNEALING

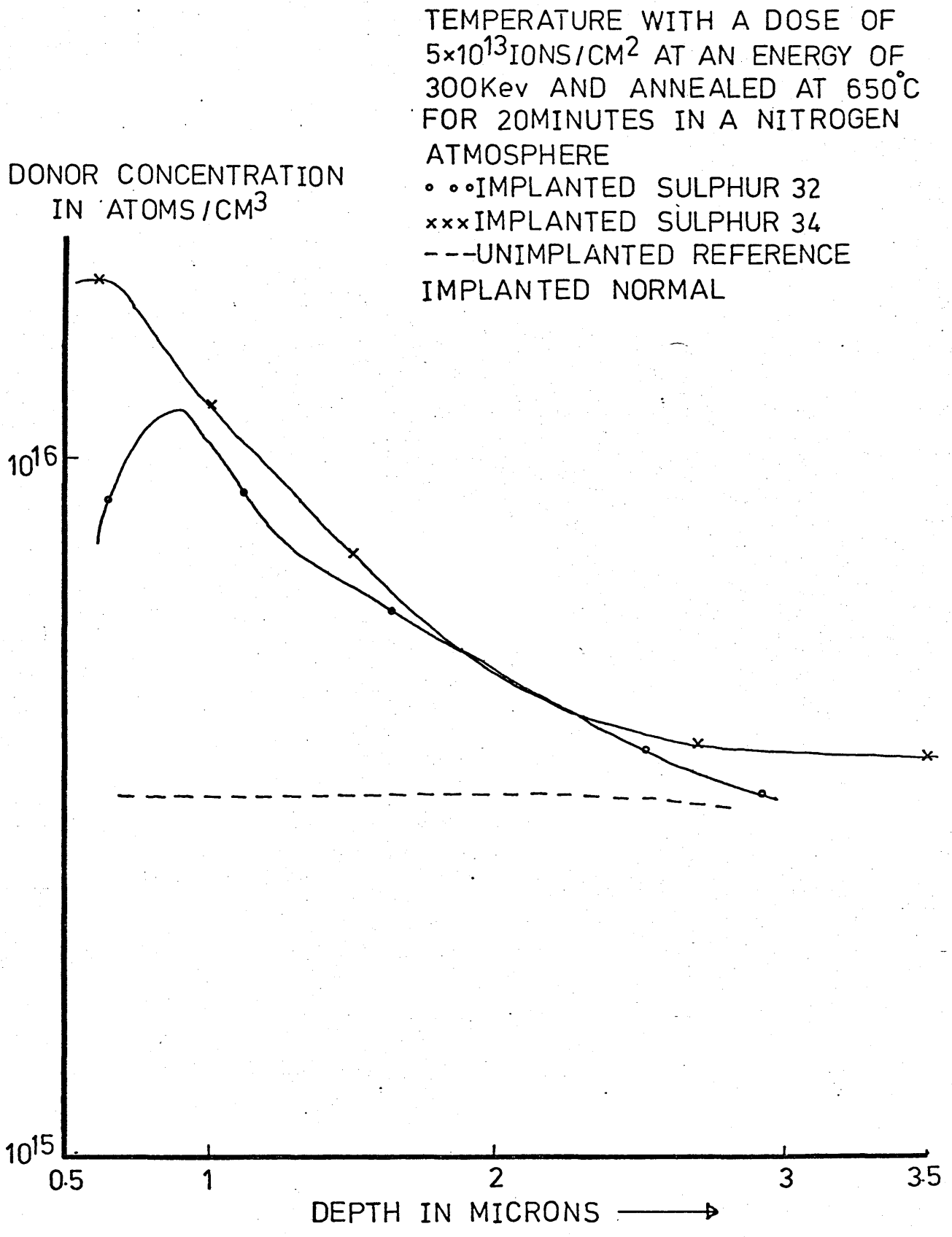


GRAPH 27 COPELAND MEASUREMENTS-VARIATION OF DONO CONCENTRATION WITH IMPLANT SPECIES

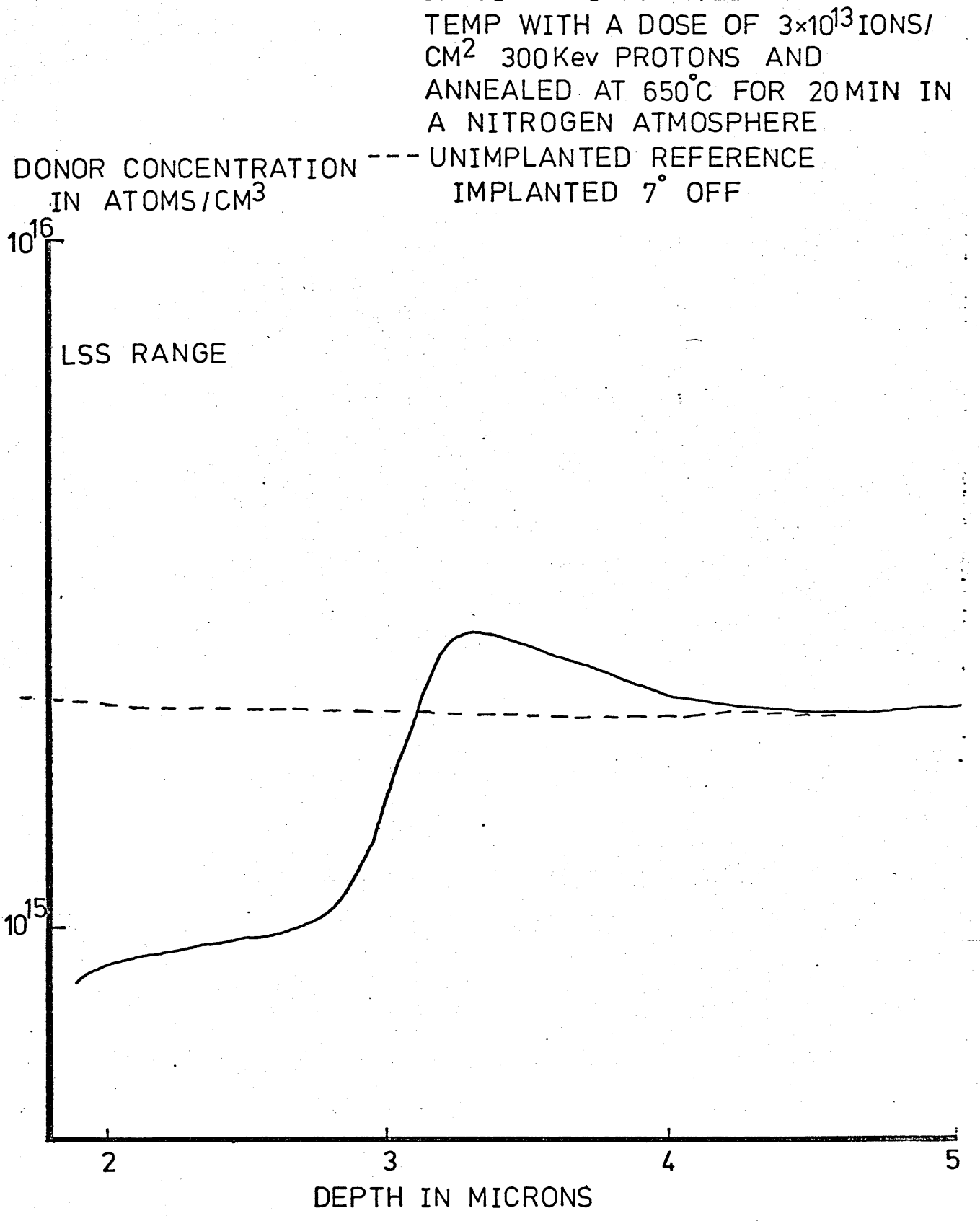


GRAPH 28 COPELAND MEASUREMENTS-VARIATION OF DONOR CONCENTRATION AFTER IMPLANTING WITH PROTONS

TABLE VI

VARIATION WITH IMPLANT TEMPERATURE

a) Specimens implanted with a dose of $10^{12}$ ions/cm$^2$ 300 keV $S_{32}$ ions and annealed at 650°C for 20 minutes in a nitrogen atmosphere.

| Implant Temperature | Peak Concentration in atoms/cm$^3$ | Peak Depth in microns | Percentage electrical activity |
|---|---|---|---|
| 20°C | $7.5 \times 10^{15}$ | 1.2 | 60.4 |
| 100°C | $6.9 \times 10^{15}$ | 0.95 | 53.8 |
| 180°C | $7.0 \times 10^{15}$ | > 1.1 | 53.2 |

b) Specimens implanted with a dose of $5 \times 10^{12}$ ions/cm$^2$ 400 keV $S_{32}$ ions and annealed at 650°C for 20 minutes in a nitrogen atmosphere.

| Implant Temperature | Peak Concentration in atoms/cm$^3$ | Peak Depth in microns | Percentage electrical activity |
|---|---|---|---|
| 20°C | $9.3 \times 10^{15}$ | 1.1 | 19.3 |
| 100°C | $7.3 \times 10^{15}$ | 1.3 | 12.0 |
| 180°C | $6.9 \times 10^{15}$ | 1.4 | 10.7 |

CARRIER ACTIVITY

% carrier activity = [(Average Concentration $N_{AV}$ under the profile - background concentration) $\times$ depth $\times 10^{-6}$]/ dose.cm$^{-2}$% ..... (51)

a) Specimens implanted at room temperature with a dose of $10^{13}$ ions/cm$^2$ 300 keV $S_{32}$ ions and annealed in a nitrogen atmosphere for 20 minutes.

| Anneal Temperature | Peak Concentration in atoms/cm$^3$ | Peak Depth in microns | Percentage electrical activity |
|---|---|---|---|
| 500°C | Max $1.45 \times 10^{15}$ | not measurable | 1.2 |
| 600°C | $9.0 \times 10^{15}$ | 1.1 | 13.1 |
| 700°C | Max $2.6 \times 10^{15}$ | at 1.8 | 3.7 |
| 800°C | Specimen leaky | | |

b) Specimens implanted at 100°C with a dose of $10^{13}$ ions/cm$^2$ 300 keV $S_{32}$ ions and annealed in a nitrogen atmosphere for 20 minutes.

| Anneal Temperature | Peak Concentration in atoms/cm$^3$ | Peak Depth in microns | Percentage electrical activity |
|---|---|---|---|
| 500°C | Max $1.65 \times 10^{15}$ | | 6.4 |
| 600°C | $1.21 \times 10^{16}$ | 1.5 | 17.8 |
| 700°C | Max $2.9 \times 10^{15}$ | | 1.2 |
| 800°C | Specimen leaky | | |

c) Specimens implanted at 180°C with a dose of $10^{13}$ ions/cm$^2$ 300 keV $S_{32}$ ions and annealed in a nitrogen atmosphere for 20 minutes.

| Anneal Temperature | Peak Concentration in atoms/cm$^3$ | Peak Depth in microns | Percentage electrical activity |
|---|---|---|---|
| 500°C | $2.9 \times 10^{15}$ | - | 6.8 |
| 600°C | $1.1 \times 10^{16}$ | 1.3 | 17.8 |
| 700°C | $1.6 \times 10^{16}$ | 1.3 | |
| 800°C | Specimen leaky | | |

d) Specimens implanted at 180°C with a dose of $5 \times 10^{12}$ ions/cm$^2$ 300 keV $S_{32}$ ions and annealed in a nitrogen atmosphere for 20 minutes.

| Anneal Temperature | Peak Concentration in atoms/cm$^3$ | Peak Depth in microns | Percentage electrical activity |
|---|---|---|---|
| 20°C | no activity | peak | 1.2 |
| 500°C | no activity | peak | 1.1 |
| 600°C | $4 \times 10^{15}$ | 1.3 | 0.6 |
| 650°C | $6.7 \times 10^{15}$ | 1.05 | 8.0 |

e) Specimens implanted at room temperature with a dose of $5 \times 10^{12}$ ions/cm$^2$ 300 keV $S_{32}$ ions and annealed in an arsenic atmosphere for 20 minutes.

| Anneal Temperature | Peak Concentration in atoms/cm$^3$ | Peak Depth in microns | Percentage electrical activity |
|---|---|---|---|
| 500°C | no activity peak curves lie above background at $2.4 \times 10^{15}$ atoms/cm$^3$ | | |
| 600°C | $6.9 \times 10^{15}$ | 1.1 | 5.0 |
| 650°C | $3.2 \times 10^{15}$ | 1.3 | 6.5 |

TABLE VIII

VARIATION WITH IMPLANT ENERGY

a) Specimens implanted at room temperature with a dose of $5 \times 10^{12}$ ions/cm$^2$ $S_{32}$ ions and annealed at 650°C for 20 minutes in a nitrogen atmosphere.

| Implant Energy | Peak Concentration in atoms/cm$^3$ | Peak Depth in microns | Percentage electrical activity |
|---|---|---|---|
| 100 keV | $1.3 \times 10^{16}$ | 0.8 | 33.4 |
| 200 keV | $1.47 \times 10^{16}$ | 1 | 40 |
| 400 keV | $9.3 \times 10^{15}$ | 1.05 | 19.8 |

b) Specimens implanted at room temperature with a dose of $5 \times 10^{12}$ ions/cm$^2$ $S_{32}$ ions and annealed at 650°C for 20 minutes in an arsenic atmosphere.

| Implant Energy | Peak Concentration in atoms/cm$^3$ | Peak Depth in microns | Percentage electrical activity |
|---|---|---|---|
| 200 keV | $9.3 \times 10^{15}$ | 0.8 | 8.5 |
| 300 keV | $3.2 \times 10^{15}$ | 1.3 | 6.5 |
| 400 keV | $6.6 \times 10^{15}$ | 1.6 | 3.1 |

TABLE IX

VARIATION WITH IMPLANT DOSE

a) Specimens implanted at room temperature with 300 keV $S_{32}$ ions and annealed at 650°C for 20 minutes in a nitrogen atmosphere.

| Implant Dose (ions/cm$^2$) | Peak Concentration in atoms/cm$^3$ | Peak Depth in microns | Percentage electrical activity |
|---|---|---|---|
| $5 \times 10^{12}$ | $1.5 \times 10^{16}$ | 0.4 | 15 |
| $5 \times 10^{13}$ | $1.2 \times 10^{16}$ | 0.88 | 1.4 |
| $10^{14}$ | $> 1.15 \times 10^{16}$ | $< 0.6$ | 0.6 |

b) Specimens implanted at room temperature with 300 keV $S_{32}$ ions and annealed at 650°C for 20 minutes in an arsenic atmosphere.

| Implant Dose (ions/cm$^2$) | Peak Concentration in atoms/cm$^3$ | Peak Depth in microns | Percentage electrical activity |
|---|---|---|---|
| $10^{12}$ | $7.5 \times 10^{15}$ | 0.8 | 26 |
| $5 \times 10^{12}$ | $3.2 \times 10^{15}$ | 1.3 | 6.5 |
| $10^{13}$ | $8.7 \times 10^{15}$ | 1.05 | 4.4 |

c) Specimens implanted at 100°C with 300 keV $S_{32}$ and annealed at 650°C for 20 minutes in a nitrogen atmosphere.

| Implant Dose (ions/cm$^2$) | Peak Concentration in atoms/cm$^3$ | Peak Depth in microns | Percentage electrical activity |
|---|---|---|---|
| $10^{12}$ | $5 \times 10^{15}$ | 0.65 | 69.2 |
| $10^{13}$ | $6.9 \times 10^{15}$ | 1.35 | 11.2 |
| $10^{14}$ | $9.4 \times 10^{15}$ | 1.3 | 1.5 |

d) Specimens implanted at 180°C with 300 keV $S_{32}$ ions and annealed at 650°C for 20 minutes in a nitrogen atmosphere.

| Implant Dose (ions/$cm^2$) | Peak Concentration in atoms/$cm^3$ | Peak Depth in microns | Percentage electrical activity |
|---|---|---|---|
| $10^{12}$ | $1.35 \times 10^{16}$ | 0.78 | 86 |
| $10^{13}$ | $8.8 \times 10^{15}$ | 0.92 | 9.1 |
| $5 \times 10^{13}$ | $7.3 \times 10^{15}$ | 1.4 | 1.4 |

e) Specimens implanted at 180°C with 300 keV $S_{32}$ ions and annealed at 650°C for 20 minutes in a nitrogen atmosphere.

| Implant Dose (ions/$cm^2$) | Peak Concentration in atoms/$cm^3$ | Peak Depth in microns | Percentage electrical activity |
|---|---|---|---|
| $5 \times 10^{12}$ | $6.5 \times 10^{15}$ | 1.02 | 6.3 |
| $10^{13}$ | $5.3 \times 10^{15}$ | 1.2 | 2.5 |
| $10^{14}$ | $5 \times 10^{15}$ | 1.5 | 0.05 |

## 4.5 Capacitance-Voltage Measurements

Capacitance-voltage measurements were carried out on sulphur implanted epitaxial n on $n^+$ gallium arsenide to determine the electrical behaviour of the material under the following conditions:-

a) variation with the implant temperature

b) variation with anneal temperature

c) variation with implant energy

d) variation with implant dose

Measurements were carried out on the same specimens used for the Copeland measurements. The capacitance against voltage of each specimen was measured at two frequencies, 1 kHz and 50 kHz. Using the equations in Section 2.4.1 the net carrier concentration versus depth was found for the specimen at these frequencies. The variation of net carrier concentration versus depth with the implantation temperatures of 20°C, 100°C and 180°C is shown in Graphs 29 and 30. The two graphs are plotted for different implant conditions. Tables X a and b show the variation of carrier activity for the different implant temperatures (20°C, 100°C and 180°C).

The variation of net carrier concentration versus depth with the anneal temperatures 500°C, 600°C and 650°C for 20 minutes are shown in Graphs 31 and 32. In the case of Graph 31 the specimens were annealed in an arsenic atmosphere and for Graph 32 in a nitrogen atmosphere. Tables XI a and b show the variation of carrier activity for the different anneal temperatures from room temperature to 650°C.

Graph 33 shows the variation of net carrier concentration versus depth with implant energies from 100 keV to 400 keV. Table XII

shows the variation of carrier activity for different implant energies from 100 keV to 400 keV.

The variation of net carrier concentration versus depth with the range of implant doses from $10^{12}$ions/cm$^2$ to $5 \times 10^{13}$ions/cm$^2$ are shown in Graphs 34, 35 and 36. Graph 34 shows results of specimens annealed in an arsenic atmosphere. Tables XIII a,b,c and d show the variation of carrier activity for a range of implant doses from $10^{12}$ions/cm$^2$ to $10^{14}$ions/cm$^2$. Graph 38 shows some typical ($1/C^2$) versus voltage curves for an implanted and unimplanted specimen. Graph 39 is again a ($1/C^2$) versus voltage curve, but in this case anomalous effects are occurring around zero bias.

Diode depletion width at zero bias versus net donor concentration were plotted for a gold-gallium arsenide Schottky diode in Graph 40 and the theoretical breakdown voltage of an abrupt junction versus concentration were plotted in Graph 41. Graph 42 shows the variation of donor concentration versus depth after implanting the specimen with a dose of $6 \times 10^{12}$ions/cm$^2$ of 120 keV argon at room temperature. The specimen was subsequently annealed at 500°C for one hour in a nitrogen atmosphere. The measurements were made at a frequency of 1 kHz.

The variation of the percentage electrical activity with implant temperature, energy and dose were plotted in Graphs 43 to 46.

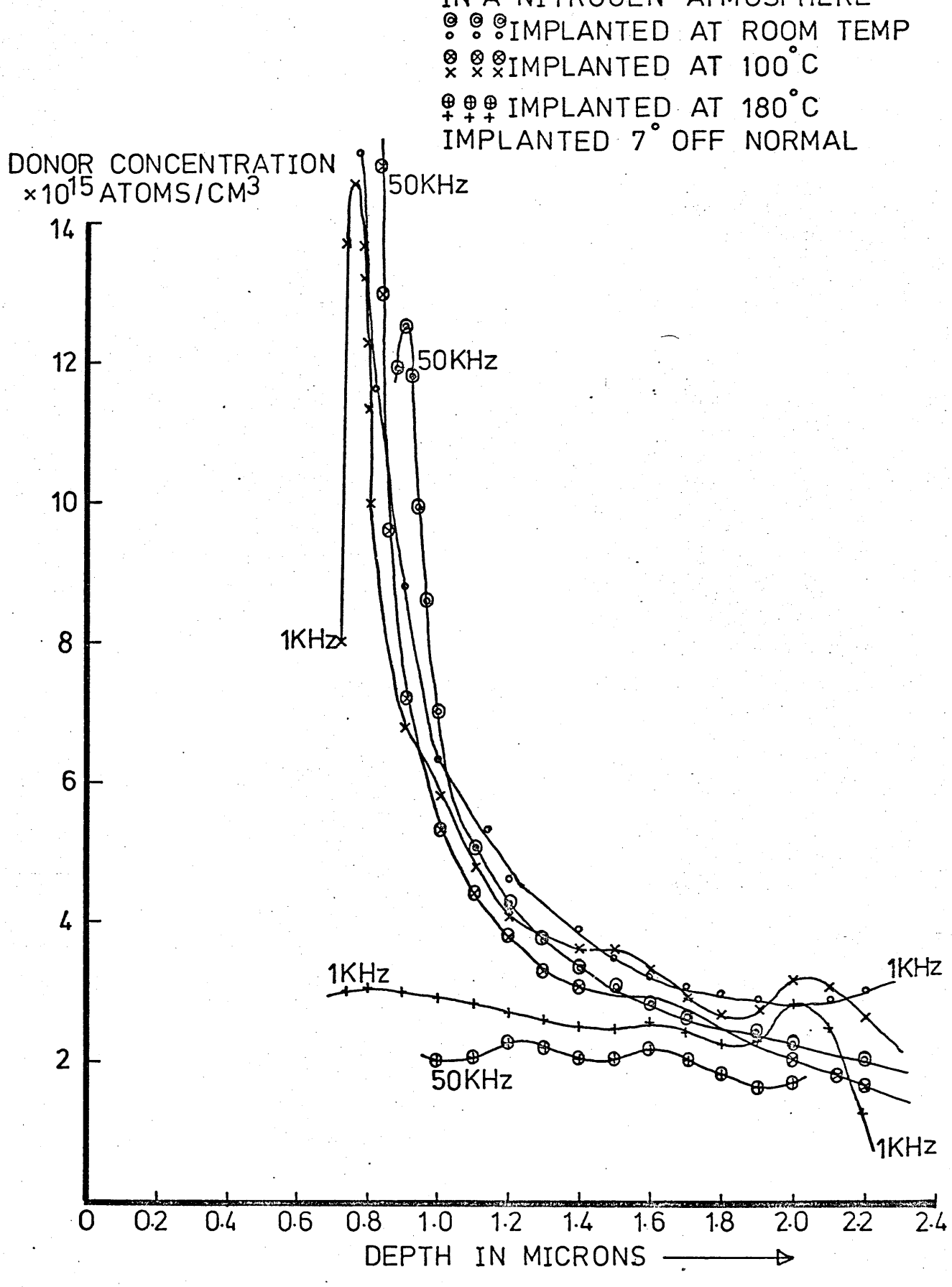


GRAPH 29 CV MEASUREMENTS - VARIATION OF DONOR CONCENTRATION WITH IMPLANT TEMPERATURE

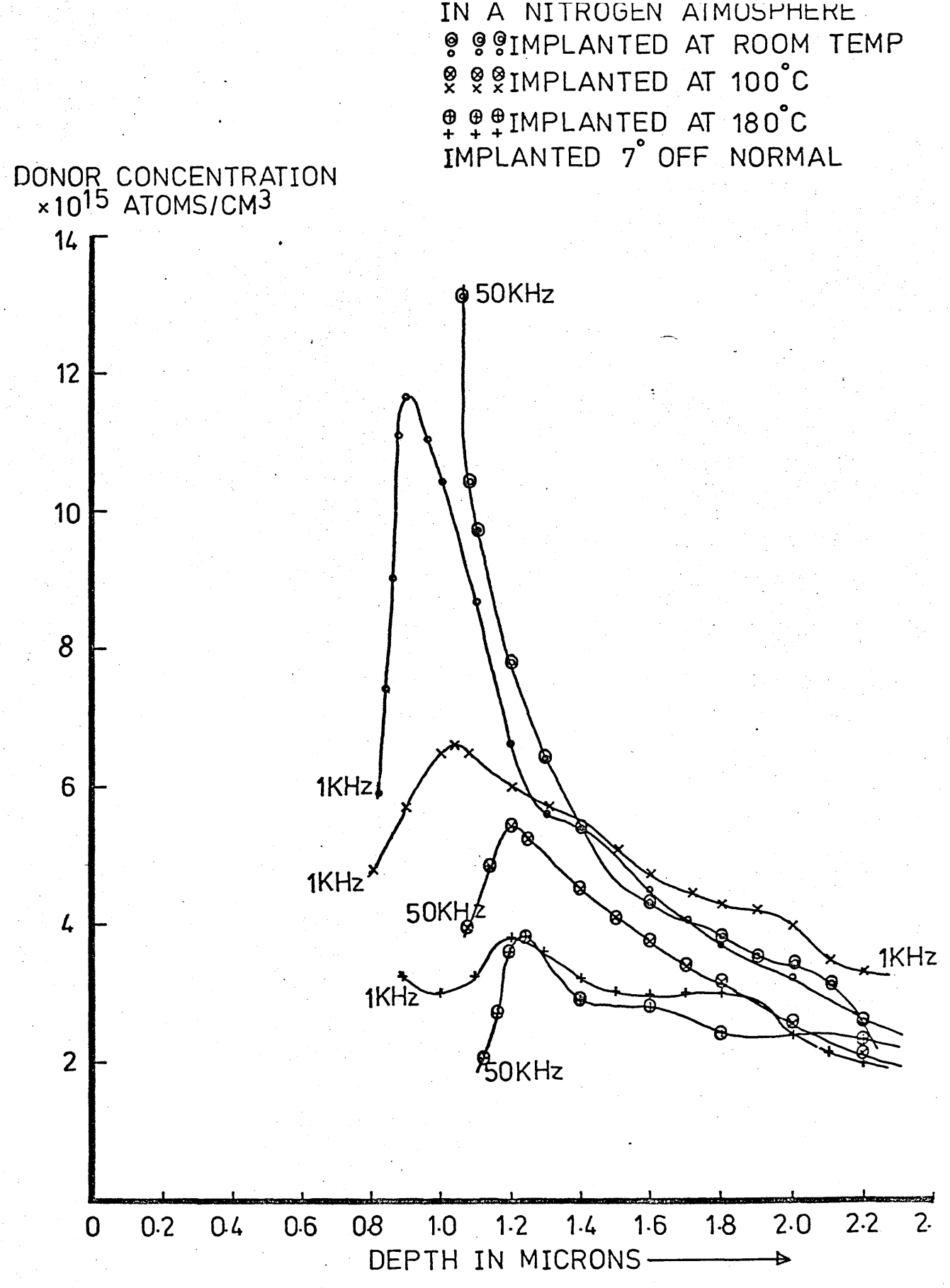


GRAPH 30 CV MEASUREMENTS - VARIATION OF DONOR CONCENTRATION WITH IMPLANT TEMPERATURE

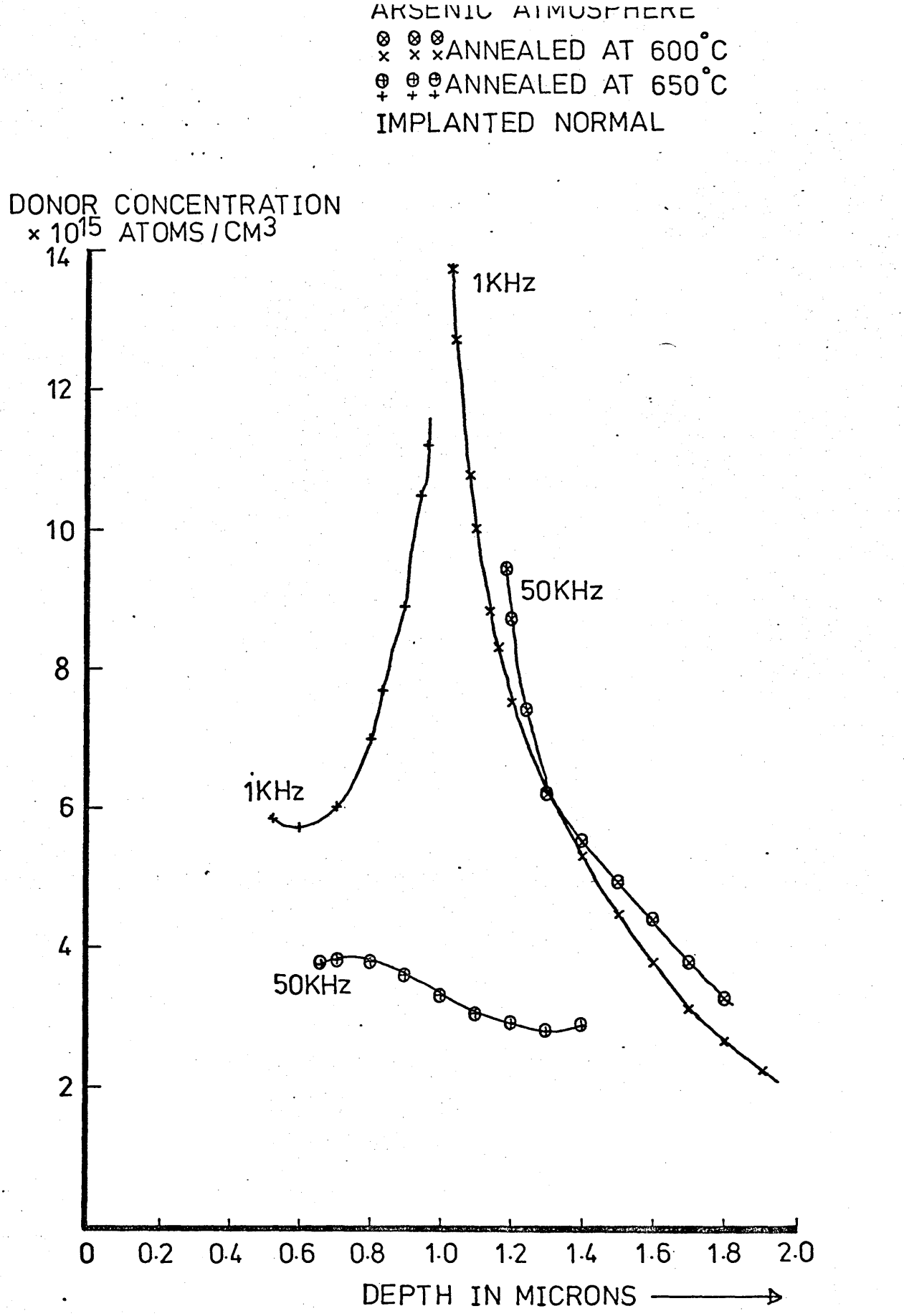


GRAPH 31 CV MEASUREMENTS - VARIATION OF DONOR CONCENTRATION WITH ANNEAL TEMPERATURE

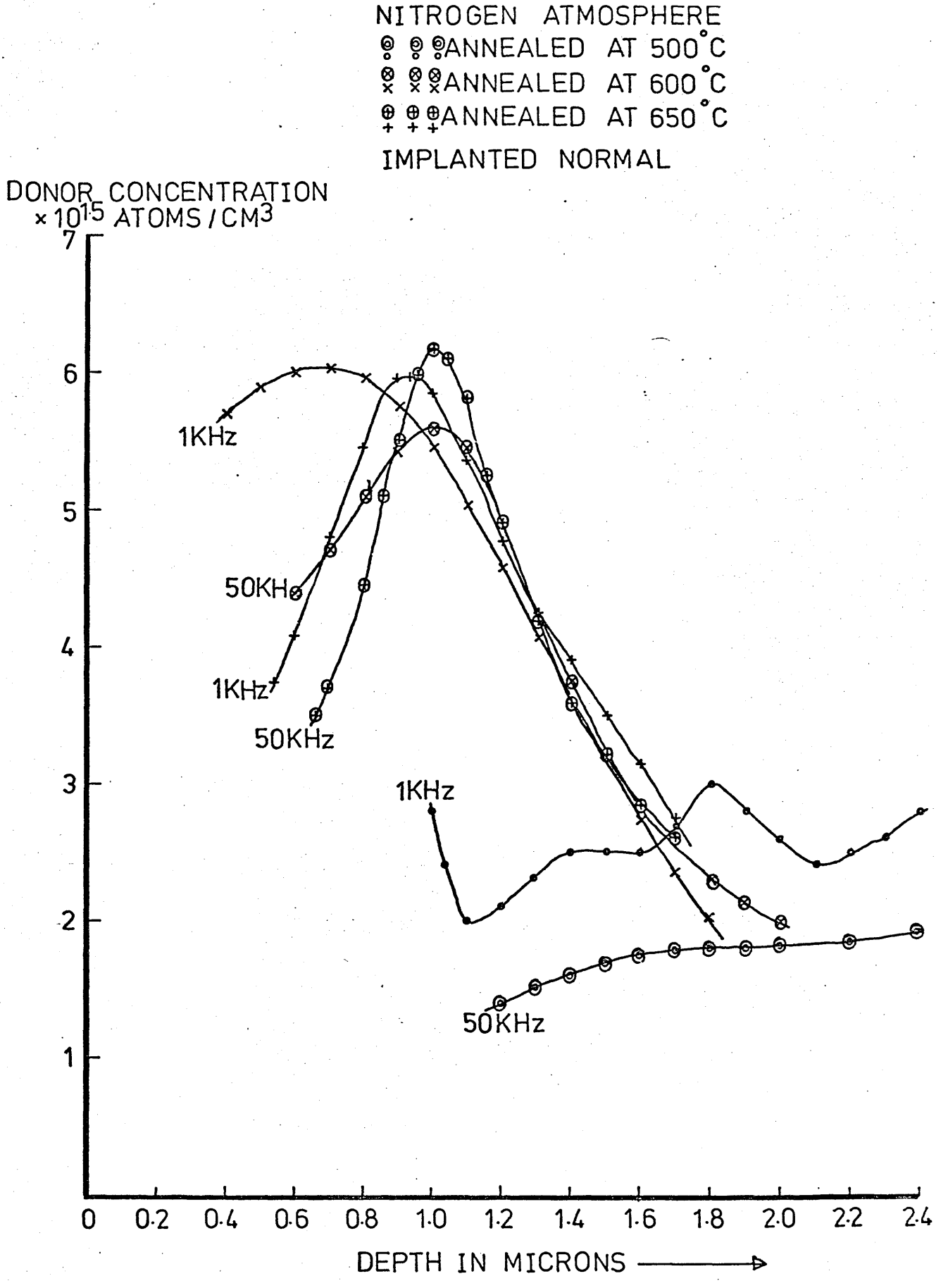


GRAPH 32 CV MEASUREMENTS - VARIATION OF DONOR CONCENTRATION WITH ANNEAL TEMPERATURE

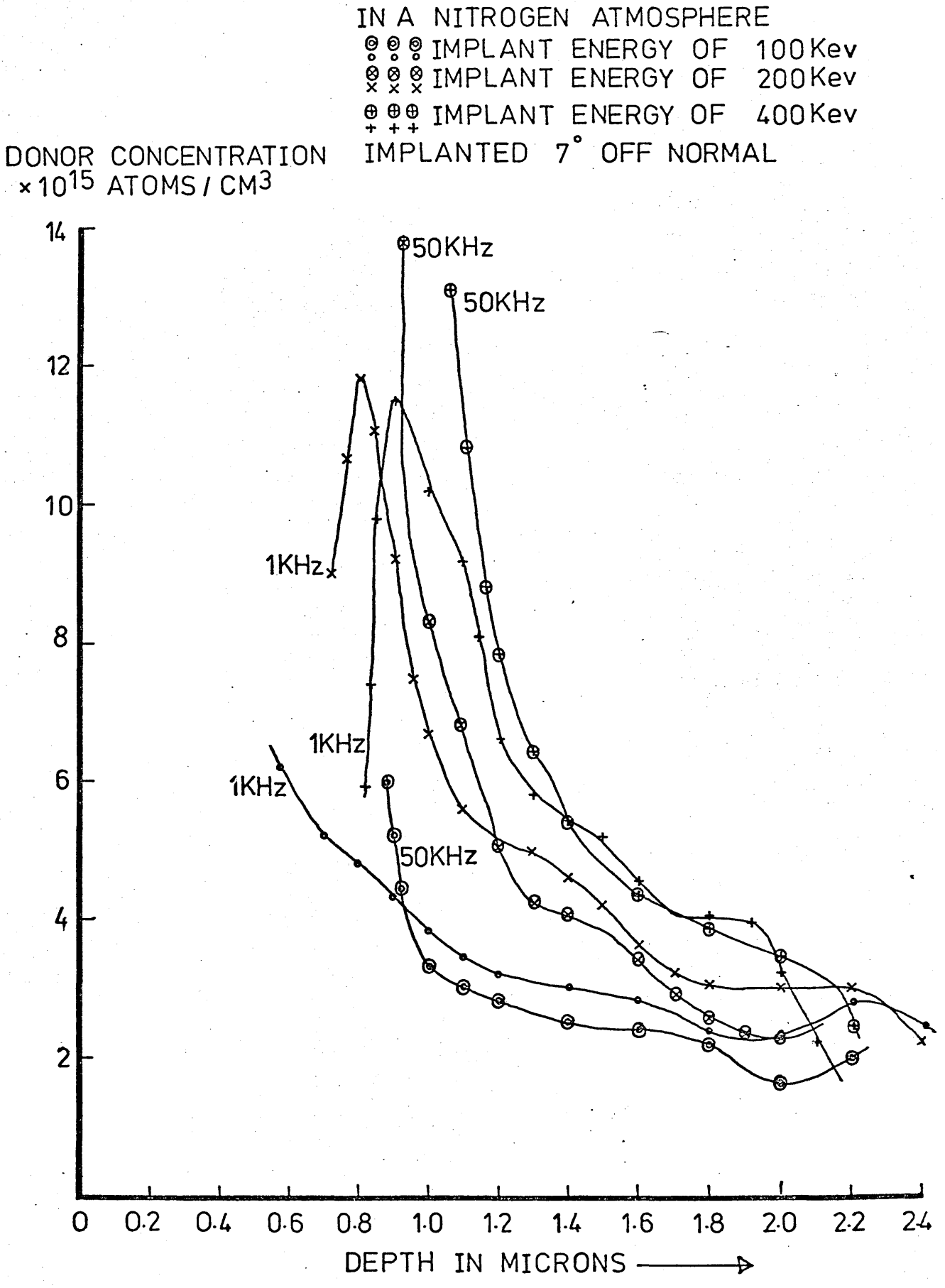


GRAPH 33 CV MEASUREMENTS - VARIATION OF DONOR CONCENTRATION WITH IMPLANT ENERGY

IN AN ARSENIC ATMOSPHERE

⊙ ⊙ ⊙ DOSE OF $10^{12}$ IONS / $CM^2$

⊕ ⊕ ⊕ DOSE OF $10^{13}$ IONS / $CM^2$

IMPLANTED NORMAL

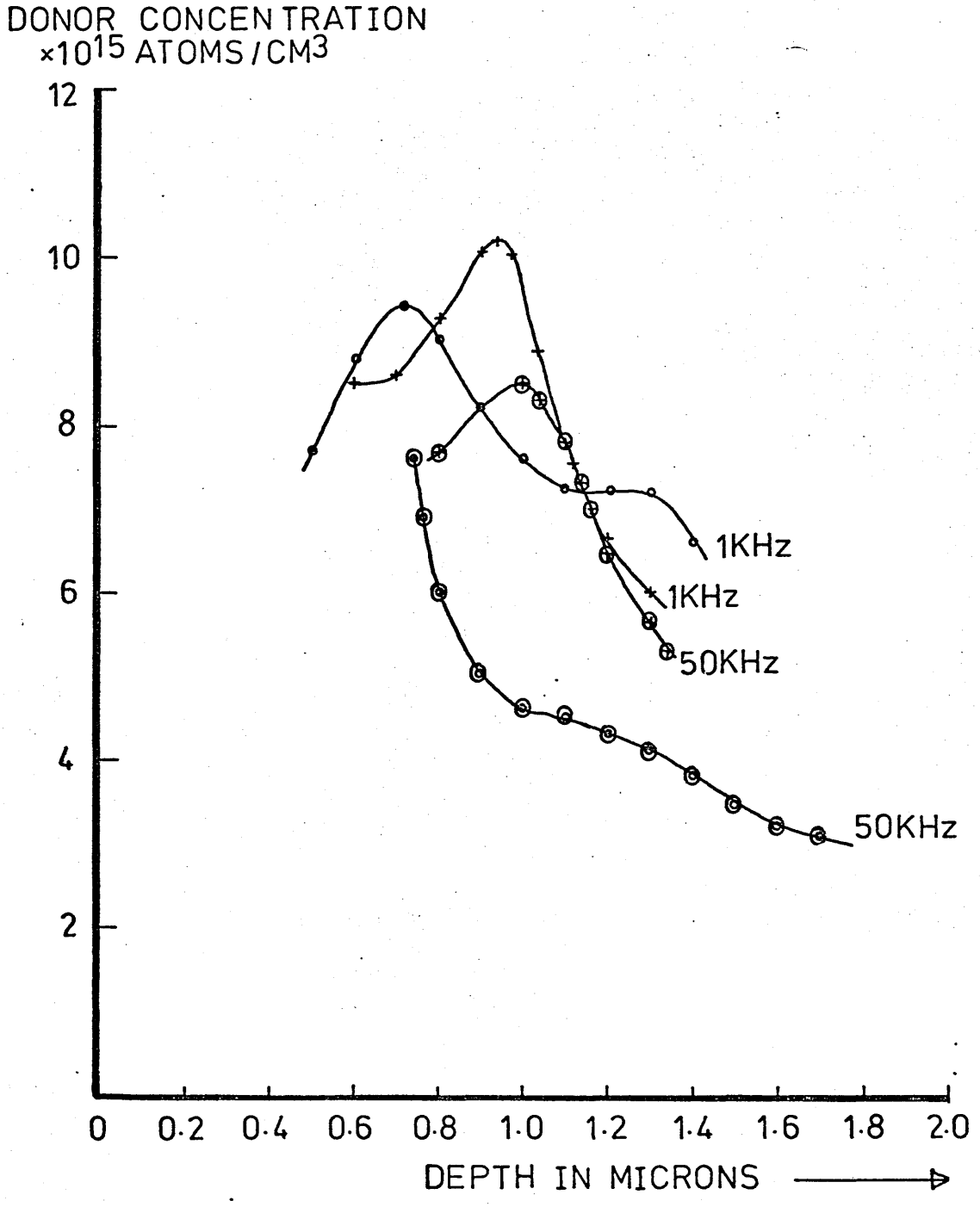


GRAPH 34 CV MEASUREMENTS - VARIATION OF DONOR CONCENTRATION WITH IMPLANTED DOSE

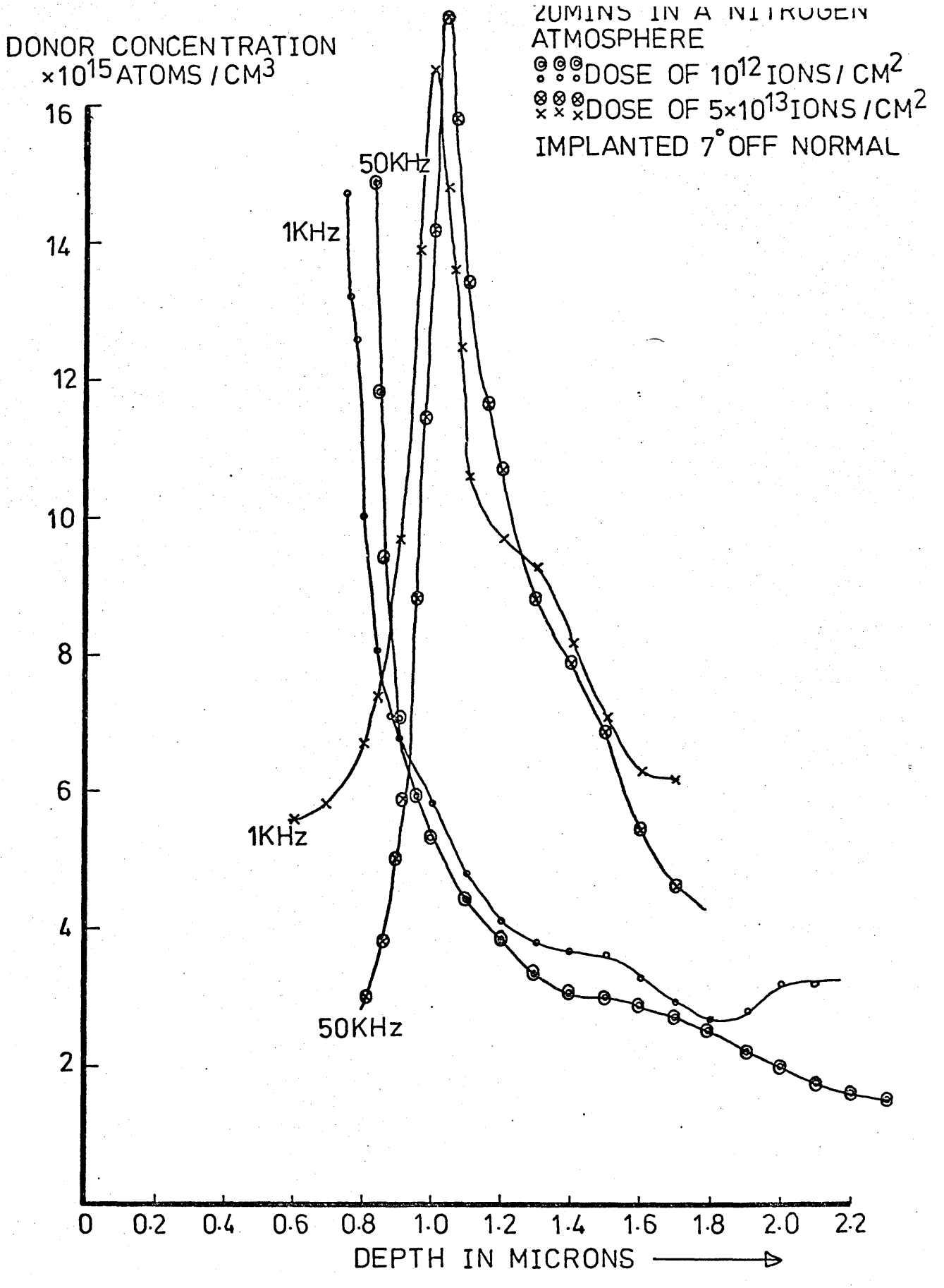


GRAPH 35 CV MEASUREMENTS - VARIATION OF DONOR CONCENTRATION WITH IMPLANT DOSE

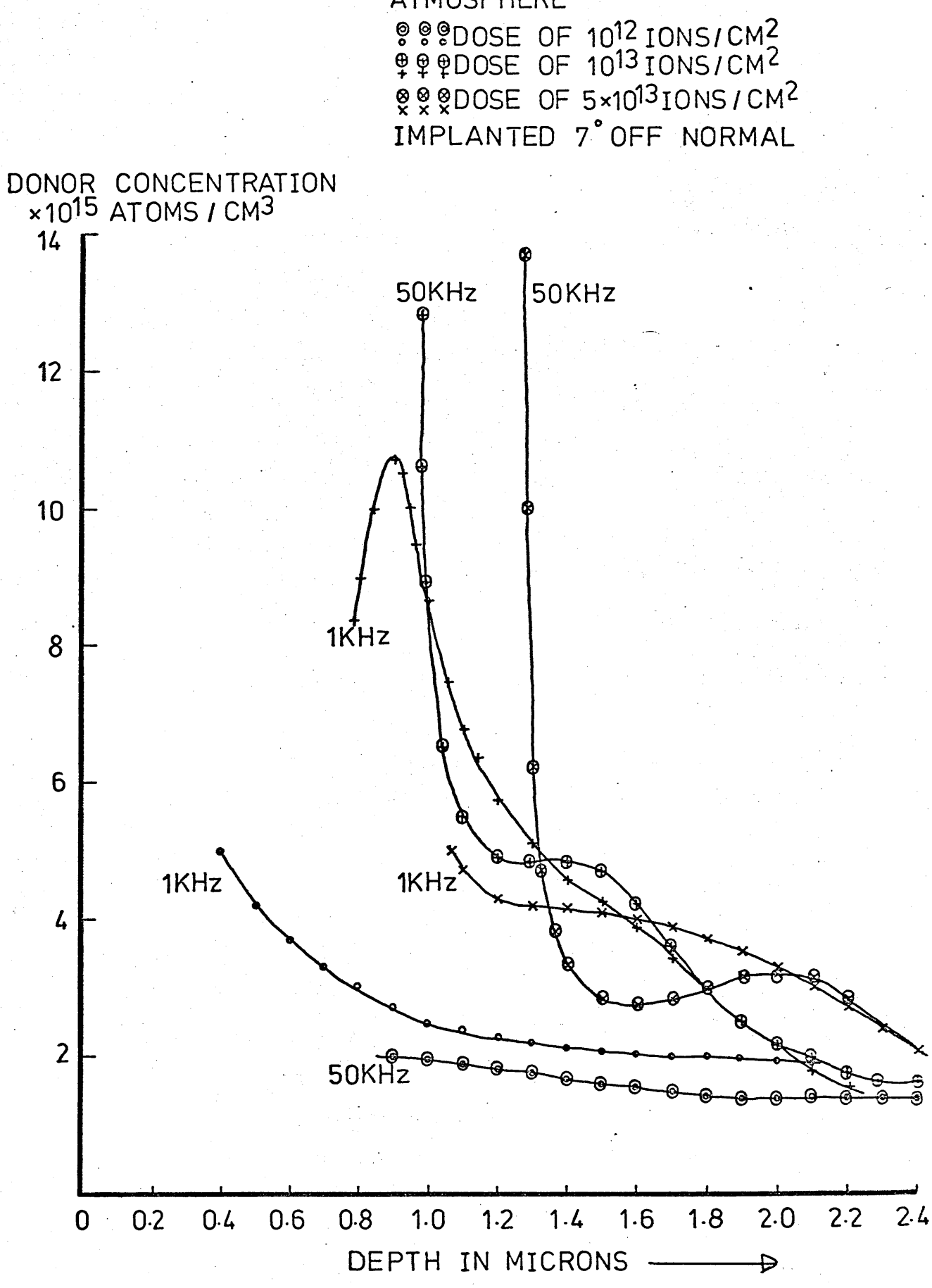


GRAPH 36 CV MEASUREMENTS-VARIATION OF DONOR CONCENTRATION WITH IMPLANT DOSE

SPECIMEN IMPLANTED AT ROOM TEMPERATURE WITH A DOSE OF $10^{12}$ IONS/CM$^2$ 300Kev $S^+_{32}$ IONS ANNEALED AT 650°C FOR 20MINS IN AN ARSENIC ATMOSPHERE. IMPLANTED NORMAL TO SPECIMEN

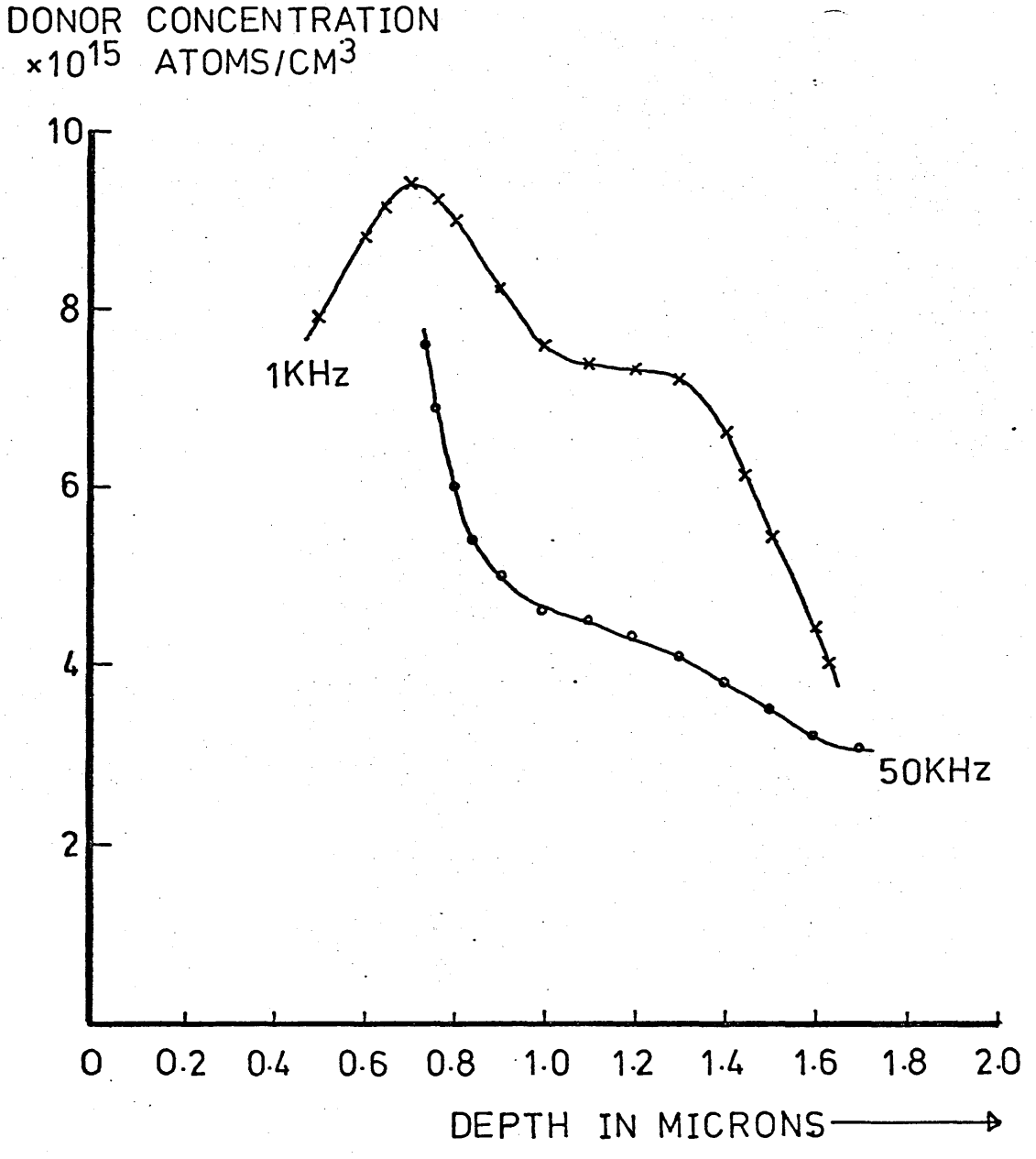


GRAPH 37 CV MEASUREMENTS - VARIATION OF DONOR CONCENTRATION WITH DEPTH

×××MEASURED AT 50KHz $N_D = 1.7 \times 10^{15}$ ATOMS/CM$^3$

+++SPECIMEN IMPLANTED AT ROOM TEMP
WITH A DOSE OF $10^{12}$ IONS/CM$^2$ 300Kev
$S^+_{32}$ ANNEALED 650°C FOR 20MINUTES
MEASURED AT 1KHz

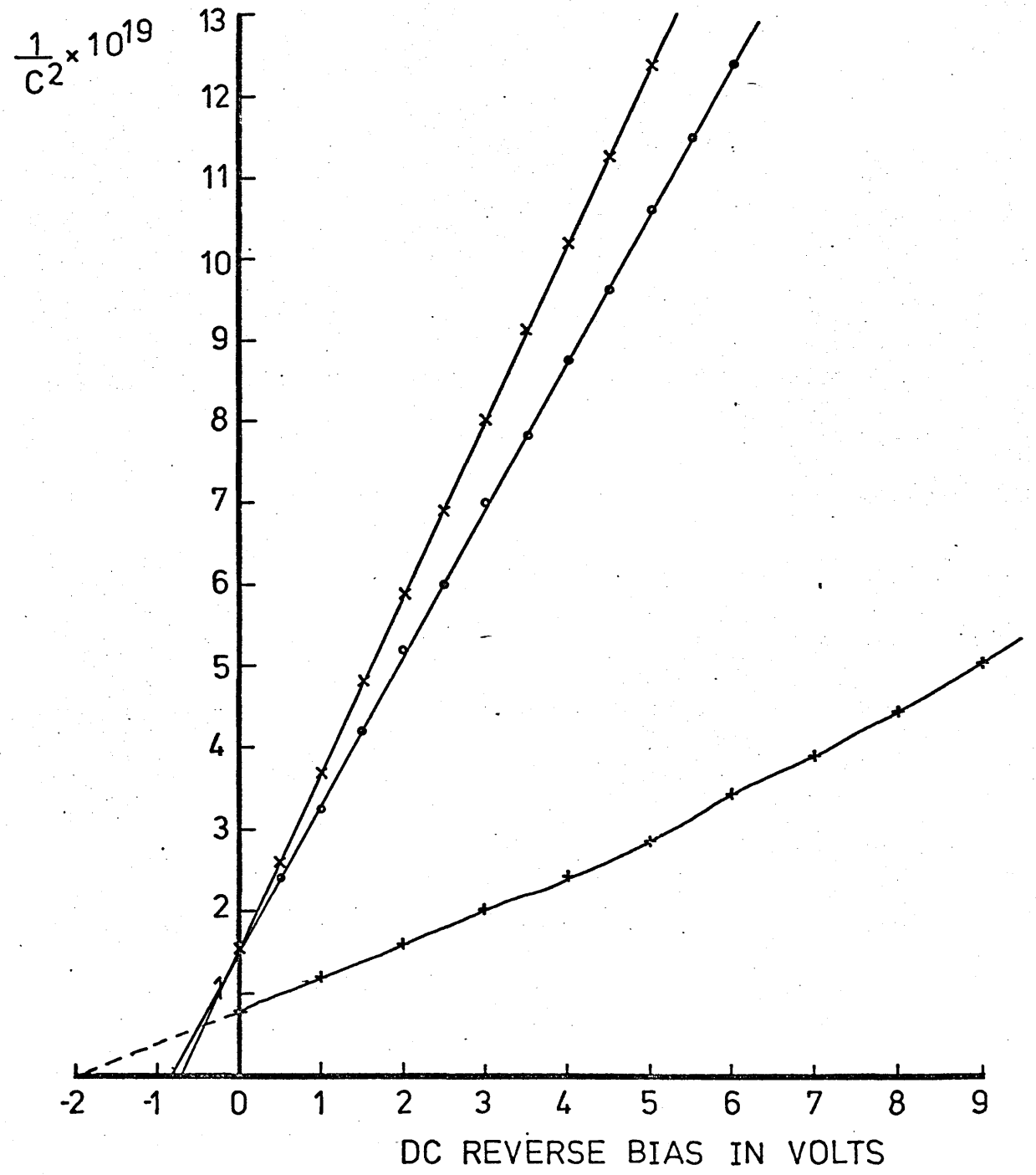


GRAPH 38 RECIPROCAL OF CAPACITANCE SQUARED $(1/C^2)$ VERSUS DC REVERSE BIAS

SPECIMEN IMPLANTED AT ROOM TEMP WITH A DOSE OF $6\times10^{13}$ IONS/CM$^2$ 100 Kev P IONS ANNEALED AT 500°C FOR 1 HOUR

ooo MEASURED AT 10KHz

××× MEASURED AT 1KHz

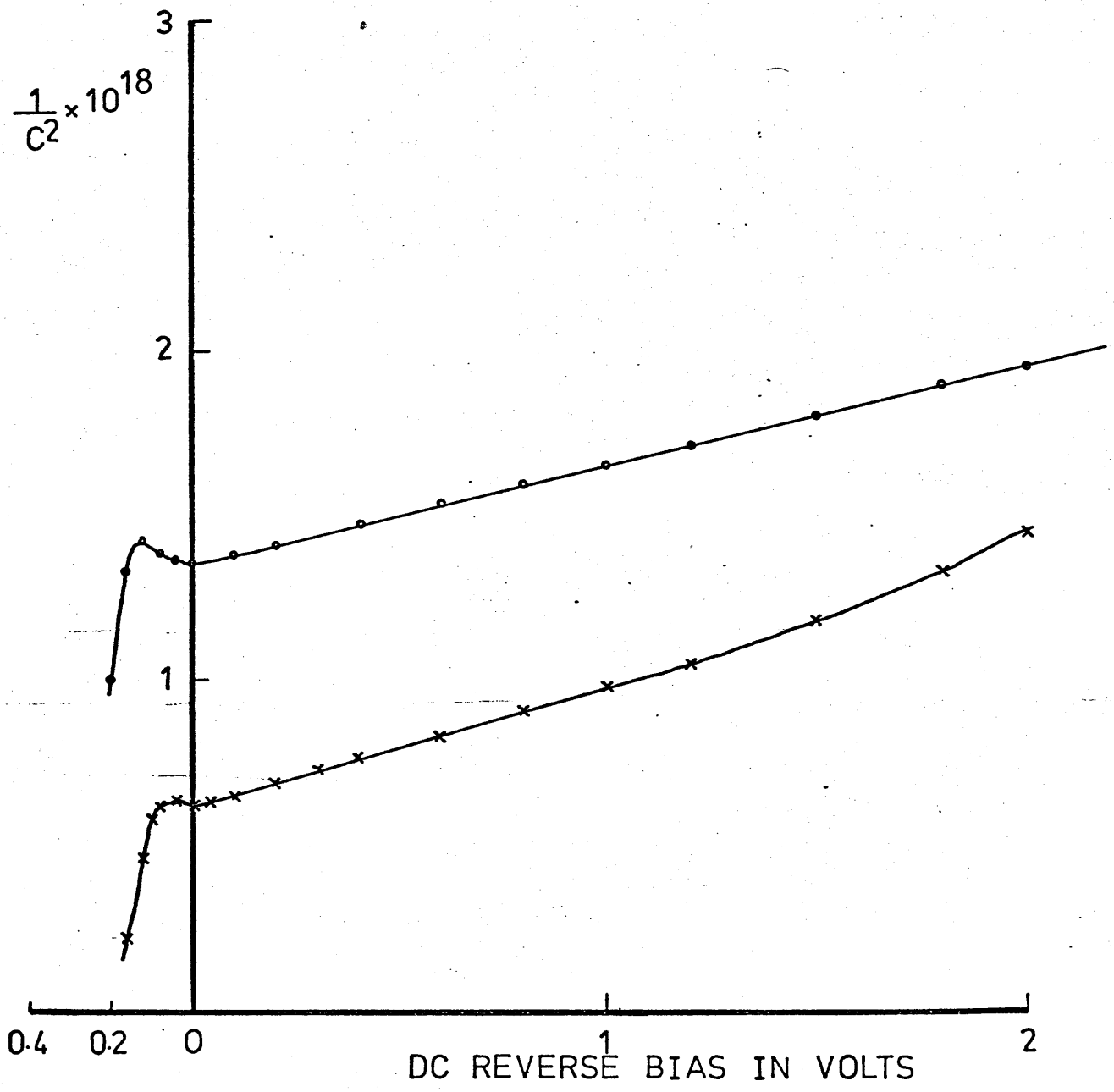


GRAPH 39 RECIPROCAL OF CAPACITANCE SQUARED ($1/C^2$) VERSUS DC REVERSE BIAS

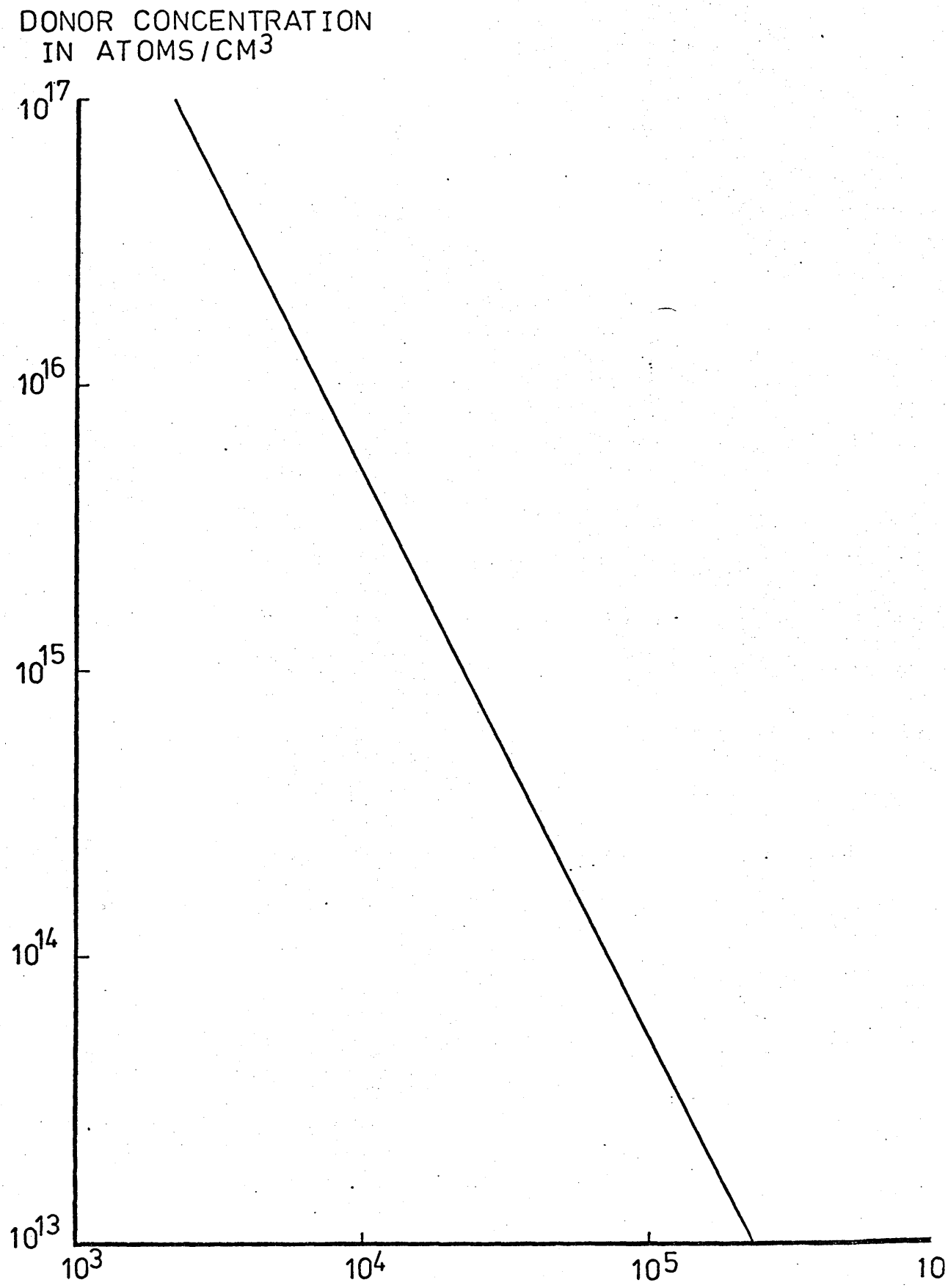


GRAPH 40 DIODE DEPLETION WIDTH AT ZERO BIAS VERSUS NET DONOR CONCENTRATION FOR GOLD ON GaAs SCHOTTKY DIODE

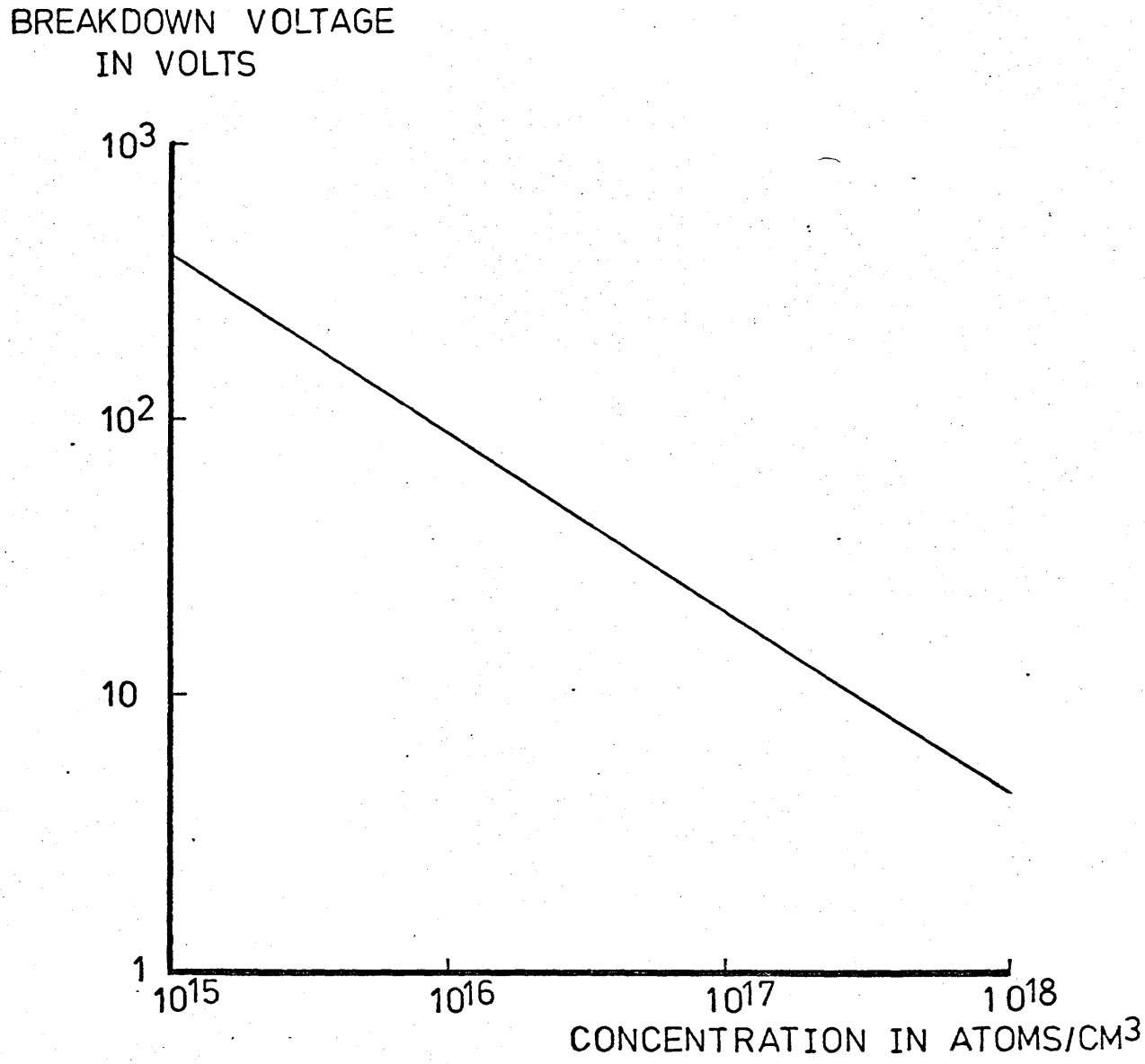


GRAPH 41 BREAKDOWN VOLTAGE OF AN ABRUPT JUNCTION VERSUS CONCENTRATION

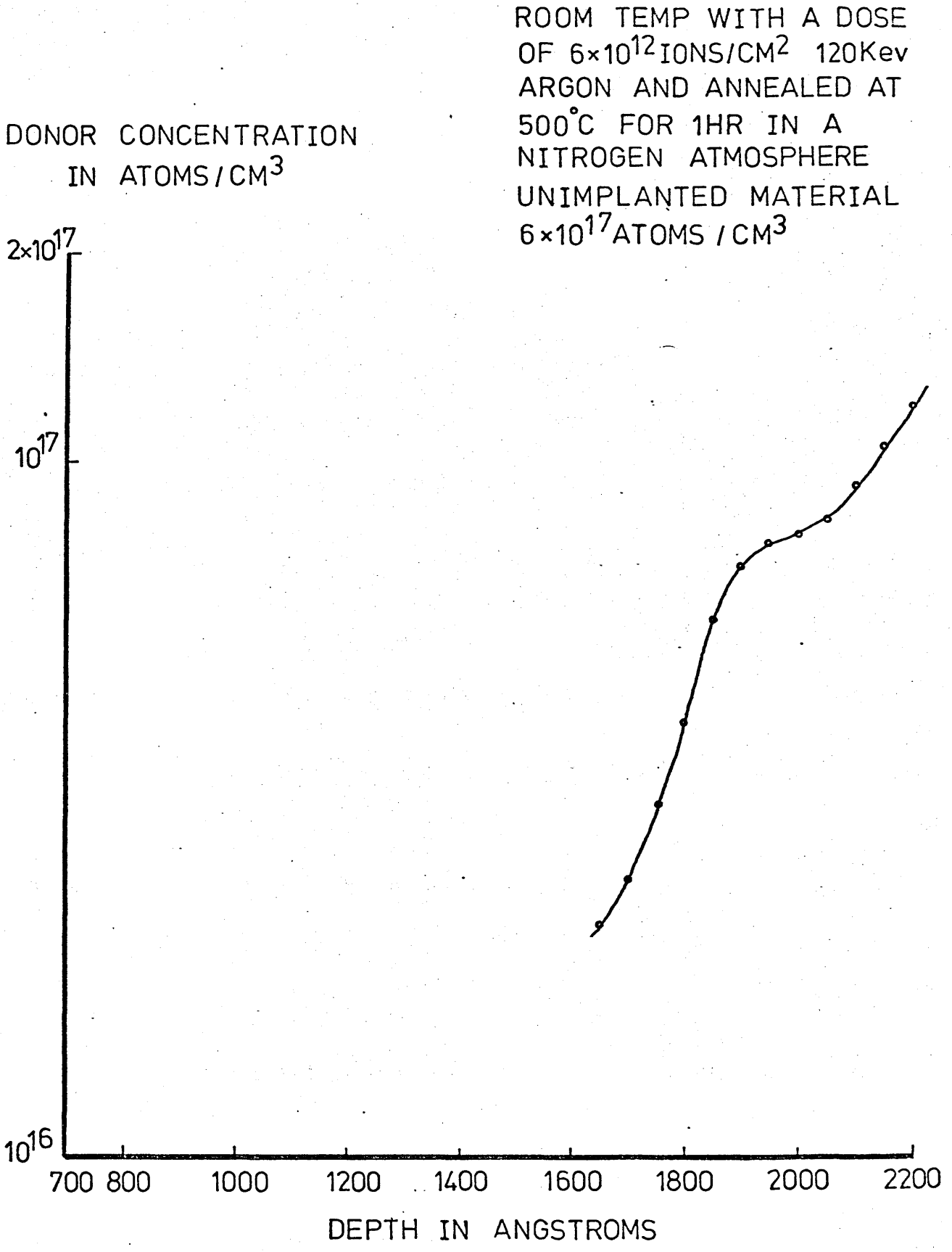


GRAPH 42 CV MEASUREMENTS - VARIATION OF DONOR CONCENTRATION AFTER IMPLANTING WITH ARGON

CARRIER ACTIVITY

% carrier activity = [(average concentration $N_{AV}$ - background concentration) $\times$ depth $\times 10^{-6}$]/Dose.$cm^{-2}$ ..... (51)

TABLE X

VARIATION OF CARRIER ACTIVITY WITH IMPLANT TEMPERATURE

a) Specimens implanted with a dose of $10^{12}$ions/$cm^2$ 300 keV $S_{32}$ ions annealed at 650°C for 20 minutes in a nitrogen atmosphere.

| Implant Temperature | % activity measured at 1 KHz | % activity measured at 50 KHz |
|---|---|---|
| room | 35.6 | 28 |
| 100°C | 32.5 | 29.8 |
| 180°C | 4.1 | 1.4 |

b) Specimens implanted with a dose of 5 $\times$ $10^{12}$ions/$cm^2$ 400 keV $S_{32}$ ions and annealed at 650°C for 20 minutes in a nitrogen atmosphere.

| Implant Temperature | % activity measured at 1 KHz | % activity measured at 50 KHz |
|---|---|---|
| room | 10.5 | 9.3 |
| 100°C | 8.9 | 6.8 |
| 180°C | 0.5 | - |

TABLE XI

VARIATION OF CARRIER ACTIVITY WITH ANNEAL TEMPERATURE

a) Specimens implanted at room temperature with a dose of $5 \times 10^{12}$ ions/cm$^2$ 300 keV $S_{32}$ ions and annealed for 20 minutes in an arsenic atmosphere.

| Anneal Temperature | % activity measured at 1 KHz | % activity measured at 50 KHz |
|---|---|---|
| 500°C | no measurable change | no measurable change |
| 600°C | 8.7 | 8.3 |
| 650°C | 12.1 | 3.5 |

b) Specimens implanted at 180°C with a dose of $5 \times 10^{12}$ ions/cm$^2$ 300 keV $S_{32}$ ions and annealed in a nitrogen atmosphere for 20 minutes.

| Anneal Temperature | % activity measured at 1 KHz | % activity measured at 50 KHz |
|---|---|---|
| room | - | - |
| 500°C | 1.7 | 0.6 |
| 600°C | 7.5 | 8.5 |
| 650°C | 6.8 | 7.9 |

TABLE XII

VARIATION OF CARRIER ACTIVITY WITH IMPLANT ENERGY

Specimens implanted at room temperature with a dose of $5 \times 10^{12}$ ions/cm$^2$ $S_{32}$ ions annealed at 650°C for 20 minutes in a nitrogen atmosphere.

| Implant Energy | % activity measured at 1 KHz | % activity measured at 50 KHz |
|---|---|---|
| 100 keV | 3.2 | 2.9 |
| 200 keV | 8.7 | 6.6 |
| 400 keV | 10.5 | 9.3 |

TABLE XIII

VARIATION OF CARRIER ACTIVITY WITH IMPLANT DOSE

a) Specimens implanted at room temperature with 300 keV $S_{32}$ ions and annealed at 650°C for 20 minutes in an arsenic atmosphere.

| Implant Dose | % activity measured at 1 KHz | % activity measured at 50 KHz |
|---|---|---|
| $10^{12}$ ions/cm$^2$ | 74 | 28.4 |
| $5 \times 10^{12}$ ions/cm$^2$ | 12.1 | 3.5 |
| $10^{13}$ ions/cm$^2$ | 8.1 | 7.5 |

b) Specimens implanted at 100°C with 300 keV $S_{32}$ ions and annealed at 650°C for 20 minutes in a nitrogen atmosphere.

| Implant Dose (ions/cm$^2$) | % activity measured at 1 KHz | % activity measured at 50 KHz |
|---|---|---|
| $10^{12}$ | 32.5 | 29.8 |
| $5 \times 10^{13}$ | 2.1 | 1.8 |

c) Specimens implanted at 100°C with 300 keV $S_{32}$ ions and annealed at 650°C for 20 minutes in a nitrogen atmosphere.

| Implant Dose (ions/cm$^2$) | % activity measured at 1 KHz | % activity measured at 50 KHz |
|---|---|---|
| $10^{12}$ | 87.6 | 23.1 |
| $10^{13}$ | 3.3 | 3.0 |
| $10^{14}$ | 0.5 | 0.8 |

d) Specimens implanted at 180°C with 300 keV $S_{32}$ ions and annealed at 650°C for 20 minutes in a nitrogen atmosphere.

| Implant Dose (ions/$cm^2$) | % activity measured at 1 KHz | % activity measured at 1 KHz |
|---|---|---|
| $10^{12}$ | 28.6 | 19.7 |
| $10^{13}$ | 6.1 | 5.4 |
| $5 \times 10^{13}$ | 0.9 | 0.8 |

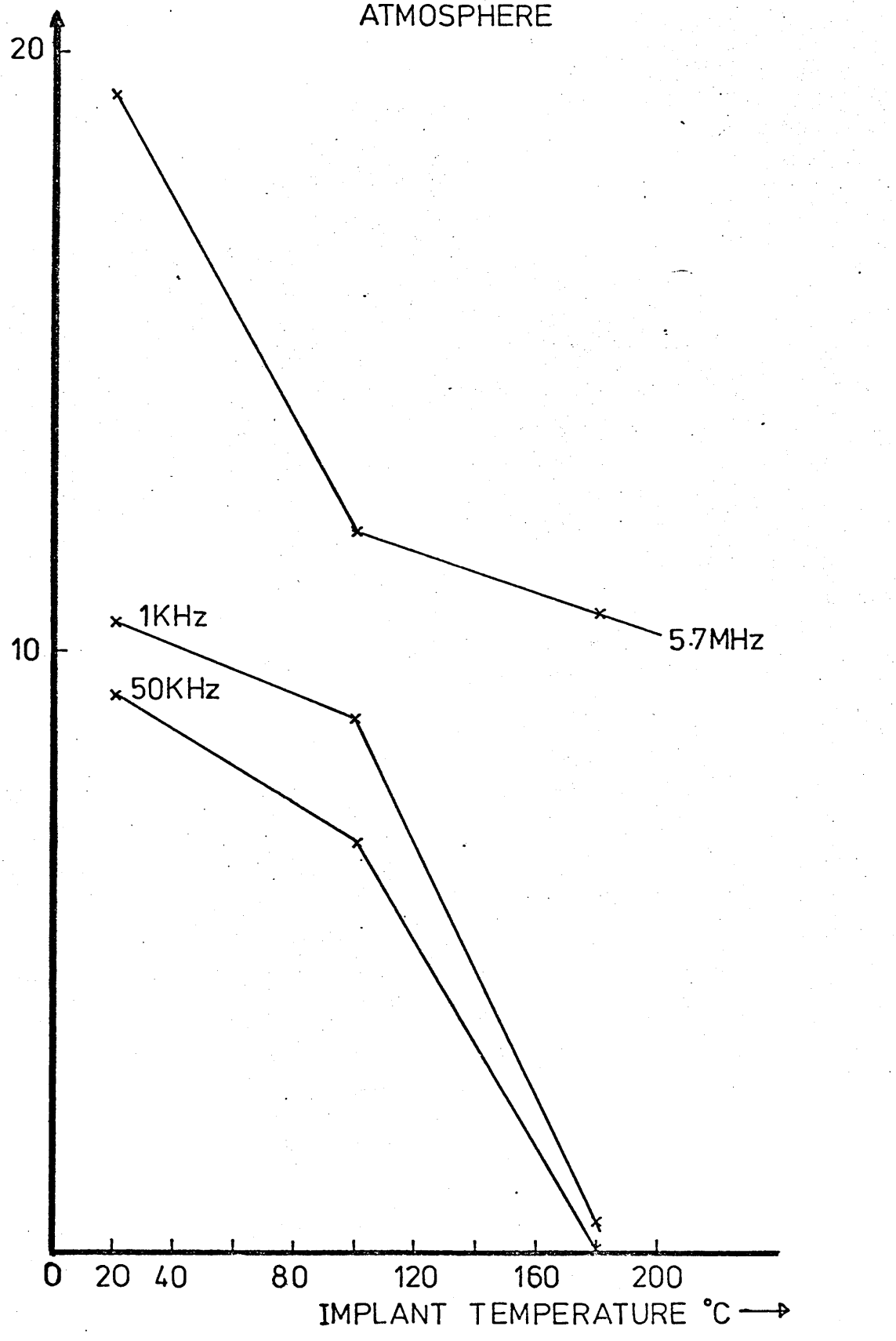


GRAPH 43 VARIATION OF PERCENTAGE ELECTRICAL ACTIVITY WITH IMPLANT TEMPERATURE

SPECIMEN IMPLANTED AT ROOM TEMPERATURE WITH A DOSE OF $5\times10^{12}$ IONS/CM$^2$ $S^+_{32}$ IONS AND ANNEALED AT 650°C FOR 20 MINS IN A NITROGEN ATMOSPHERE

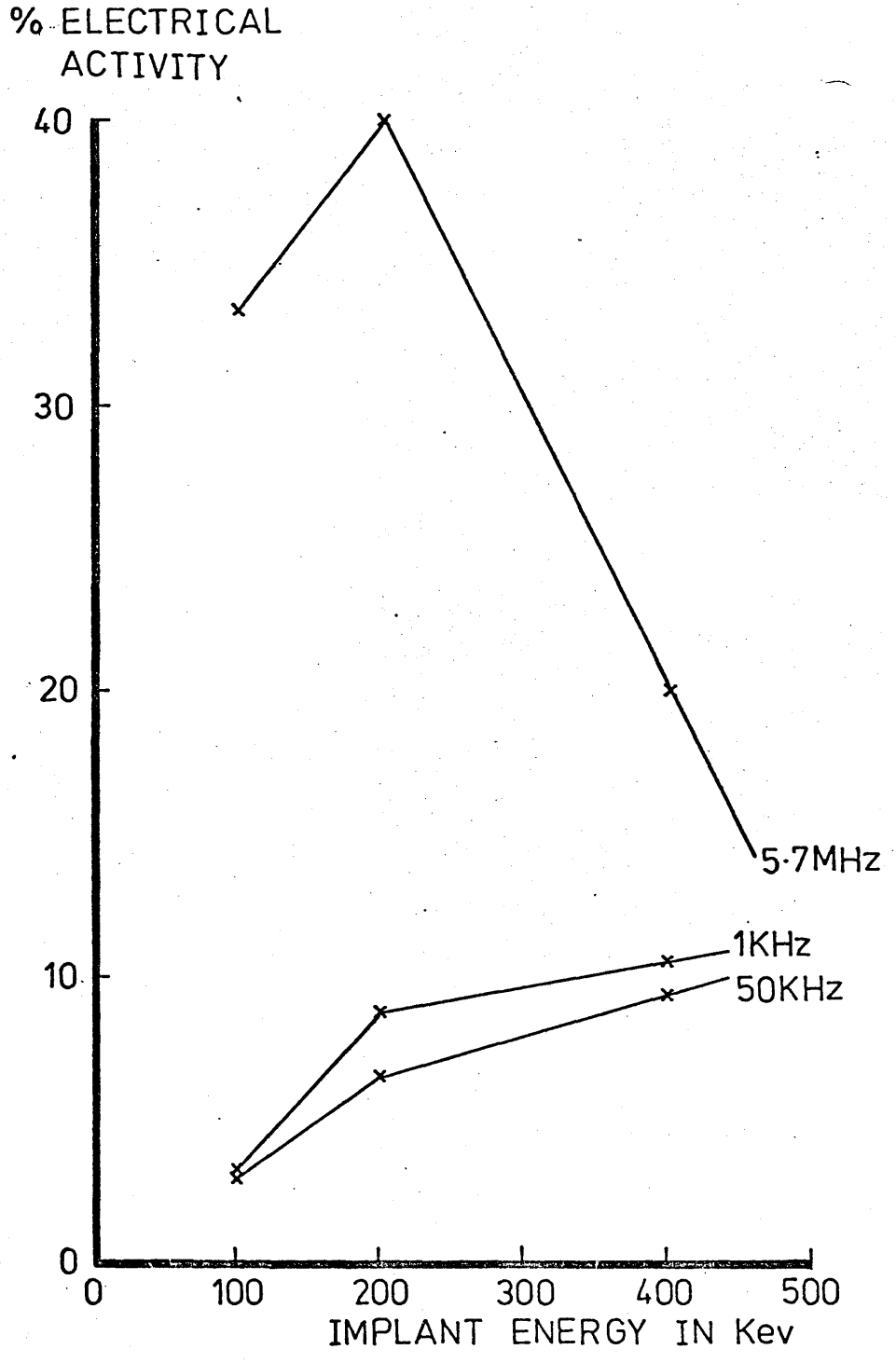


GRAPH 44 VARIATION OF PERCENTAGE ELECTRICAL ACTIVITY WITH IMPLANT ENERGY

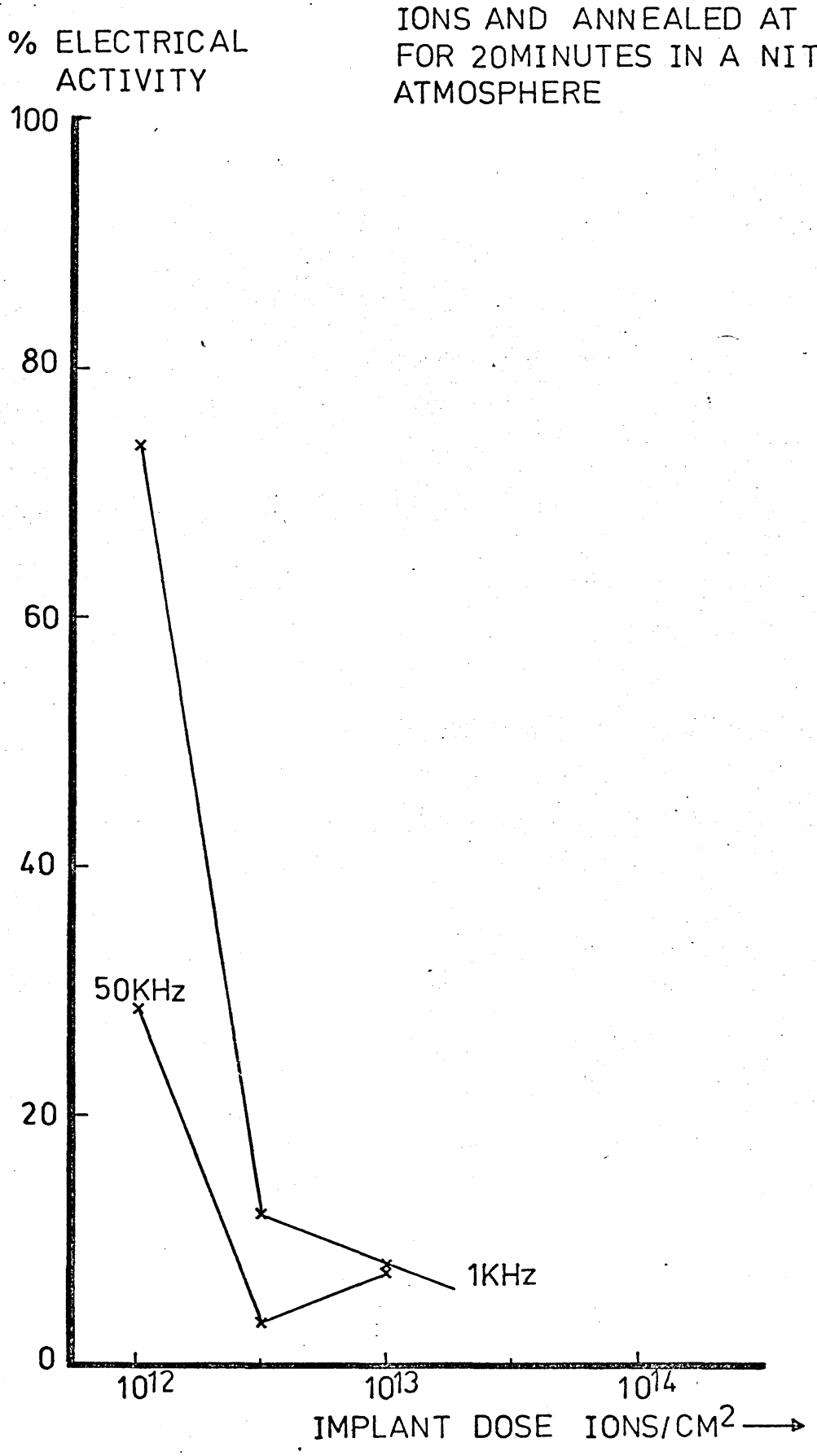


GRAPH 45 VARIATION OF PERCENTAGE ELECTRICAL ACTIVITY WITH IMPLANT DOSE

SPECIMEN IMPLANTED AT 180°C WITH 300Kev $S^{+}_{32}$ IONS AND ANNEALED AT 650°C FOR 20 MINUTES IN A NITROGEN ATMOSPHERE

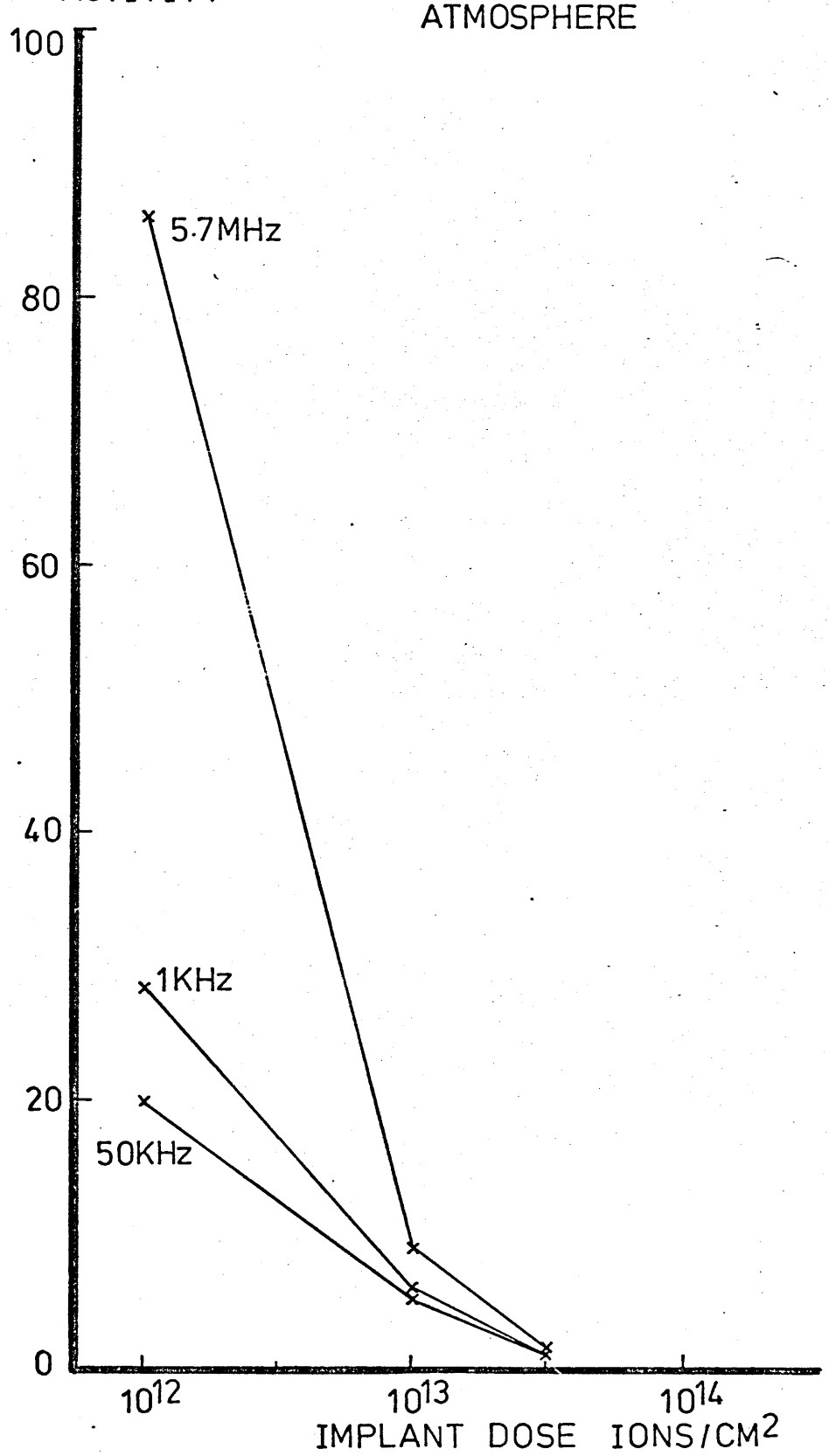


GRAPH 46 VARIATION OF PERCENTAGE ELECTRICAL ACTIVITY WITH IMPLANT DOSE

## 4.6 Hall Measurements

To substantiate results obtained from capacitance-voltage measurements, measurements were carried out on n-type epitaxial gallium arsenide using a different measurement technique. The Hall technique was chosen as being the most likely to yield useful information on the implanted specimens. Measurements were carried out at room temperature and at varying temperatures down to liquid nitrogen temperature.

Six specimens from a single slice of epitaxial n-type on semi-insulating gallium arsenide were implanted with sulphur 32 as follows:-

Specimen $S_{18}R_2C/1$

Implanted with the specimen at room temperature with an ion beam energy of 300 keV and a dose of $10^{13}$ions/cm$^2$.

Specimen $S_{18}R_2C/2$

Implanted with the specimen at 100°C with an ion beam energy of 300 keV and a dose of $10^{13}$ions/cm$^2$.

Specimen $S_{18}R_2C/3$

Implanted with the specimen at 180°C with an ion beam energy of 300 keV and a dose of $10^{12}$ions/cm$^2$.

Specimen $S_{18}R_2C/4$

Unimplanted reference specimen

Specimen $S_{18}R_2C/5$

Implanted with the specimen at 180°C with an ion beam energy of 300 keV and a dose of $10^{13}$ions/cm$^2$.

Specimen $S_{18}R_2C/6$

Implanted with the specimen at 180°C with an ion beam energy of 300 keV and a dose of $10^{14}$ions/cm$^2$.

All implanted specimens were implanted with the surface normal inclined 7° to the incident ion beam.

All specimens were annealed at 650°C for 20 minutes in an atmosphere of nitrogen.

### 4.6.1 Hall Measurements versus Temperature

Hall measurements were carried out on three specimens $S_{18}R_2C/1,2$ and 3, i.e. specimens implanted with 300 keV sulphur ions, one with an implant temperature of 180°C and dose of $10^{12}$ions/cm$^2$, one with an implant temperature of 100°C and a dose of $10^{13}$ions/cm$^2$, the third specimen being a room temperature specimen with a dose of $10^{13}$ions/cm$^2$. The specimens were cooled down to liquid nitrogen temperatures and Hall measurements taken as the specimens warmed up to room temperature. Using the equations in Section 2.6 the specimen resistivity, mobility and concentration were calculated. Graph 47 shows the resistivity plotted against 1000/Temperature. Graph 48 shows the mobility plotted against 1000/Temperature and Graph 49 shows mobility, resistivity and conductivity plotted against 1000/Temperature for the specimen implanted with a dose of $10^{12}$ions/cm$^2$.

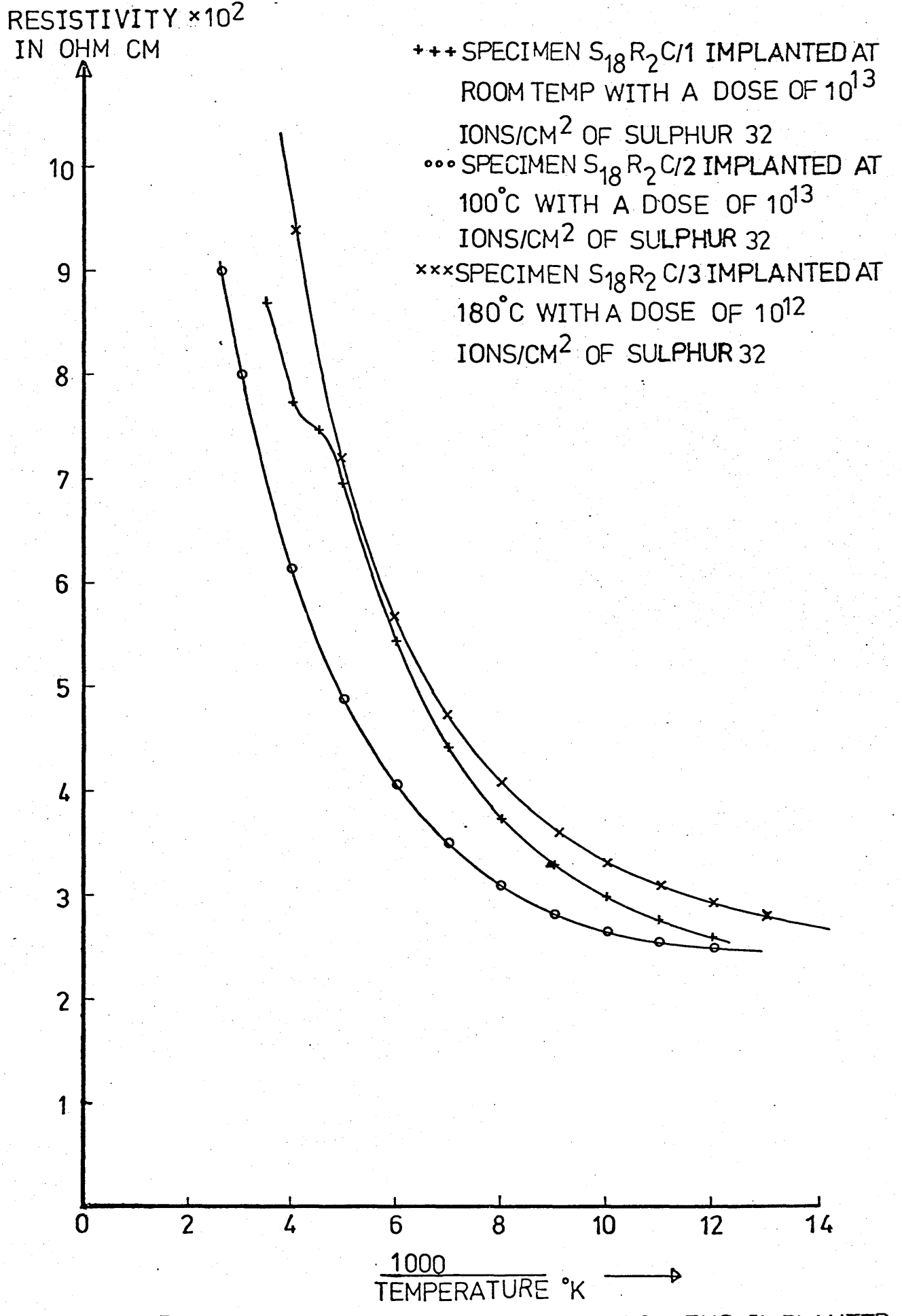


GRAPH47 RESISTIVITY Vs TEMPERATURE SPECIMENS IMPLANTED WITH AN ENERGY OF 300Kev AND ANNEALED AT 650 °C FOR 20 minutes

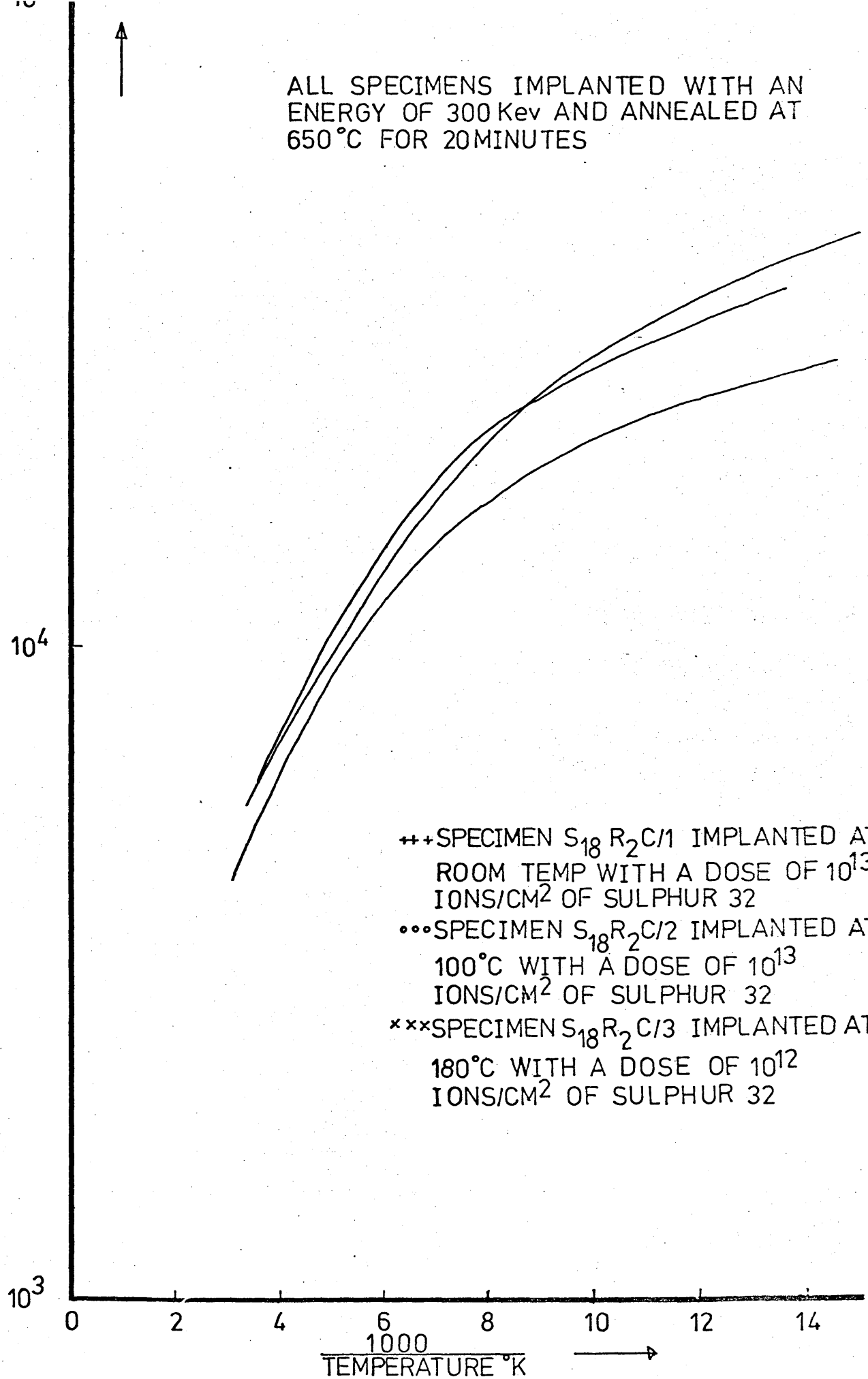


GRAPH 48 HALL MEASUREMENTS - VARIATION OF MOBILITY WITH TEMPERATURE

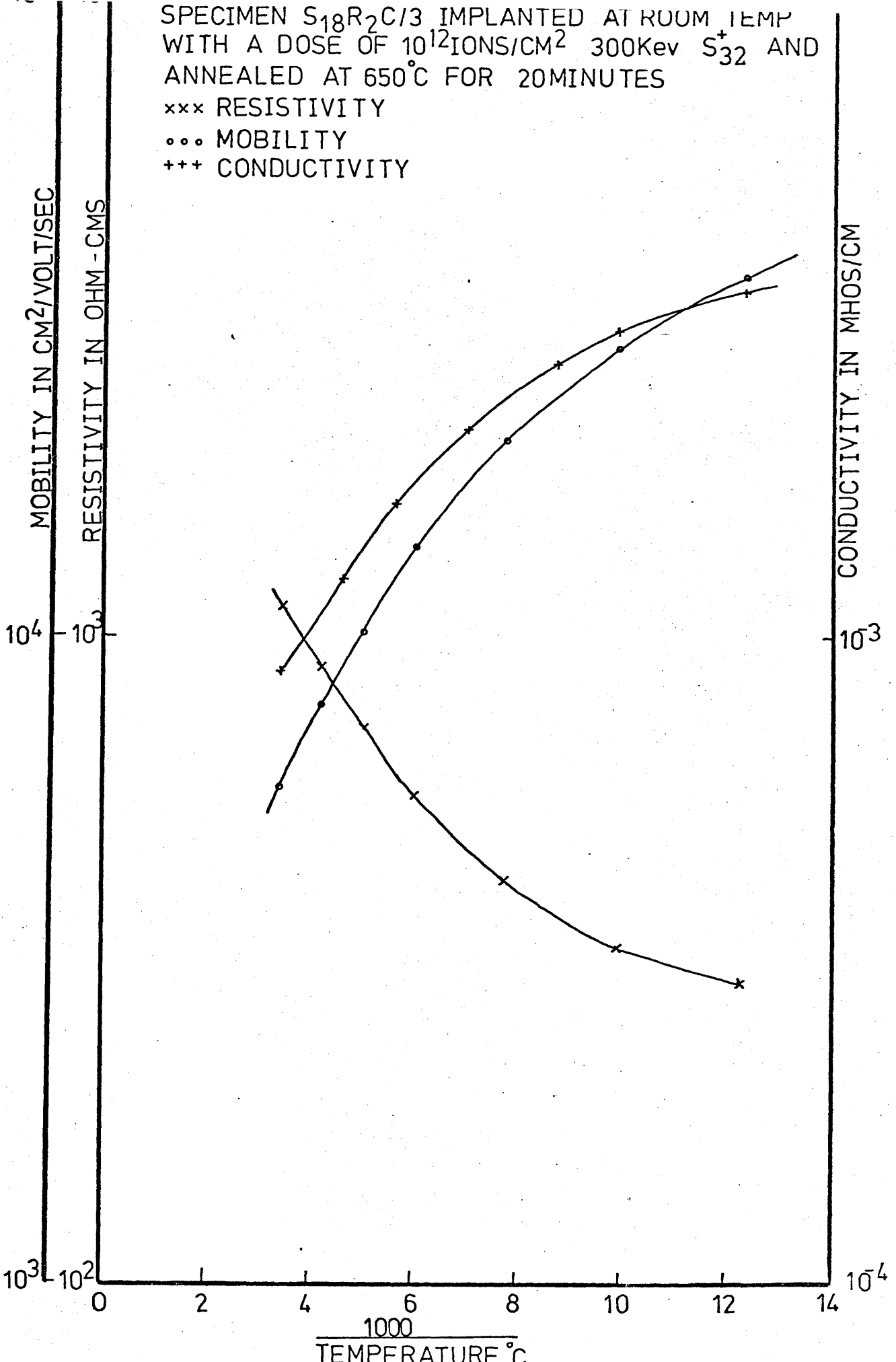


GRAPH 49 HALL MEASUREMENTS - MOBILITY, RESISTIVITY, AND CONDUCTIVITY VERSUS TEMPERATURE

### 4.6.2 Hall Measurements versus Depth

Hall measurements were carried out on all the specimens, with a series of readings being taken after removing successive layers from the surface of the specimen. Using the equations in Section 2.6 the specimen's sheet resistance, mobility and concentration versus depth from the surface of the specimen were calculated. Graphs 50 and 51 show the sheet resistance plotted against the depth from the surface of the specimen. Graph 52 shows the active donor concentration plotted against the depth from the surface of the specimen for different implant doses. Graph 53 shows the active donor concentration plotted against the depth from the surface of the specimen for different implant temperatures, the unimplanted specimen is plotted in Graph 54. Graphs 55 and 56 show the mobility plotted against the depth from the surface of the specimen.

From the graphs of donor concentration versus depth the average concentration was found and using equation (51) the percentage carrier activity under the profile found. The results of this are shows in Table XIV.

ALL SPECIMENS IMPLANTED WITH A DOSE OF $10^{13}$ IONS/CM$^2$ SULPHUR 32 AT AN ENERGY OF 300Kev AND ANNEALED AT 650°C FOR 20MINUTES

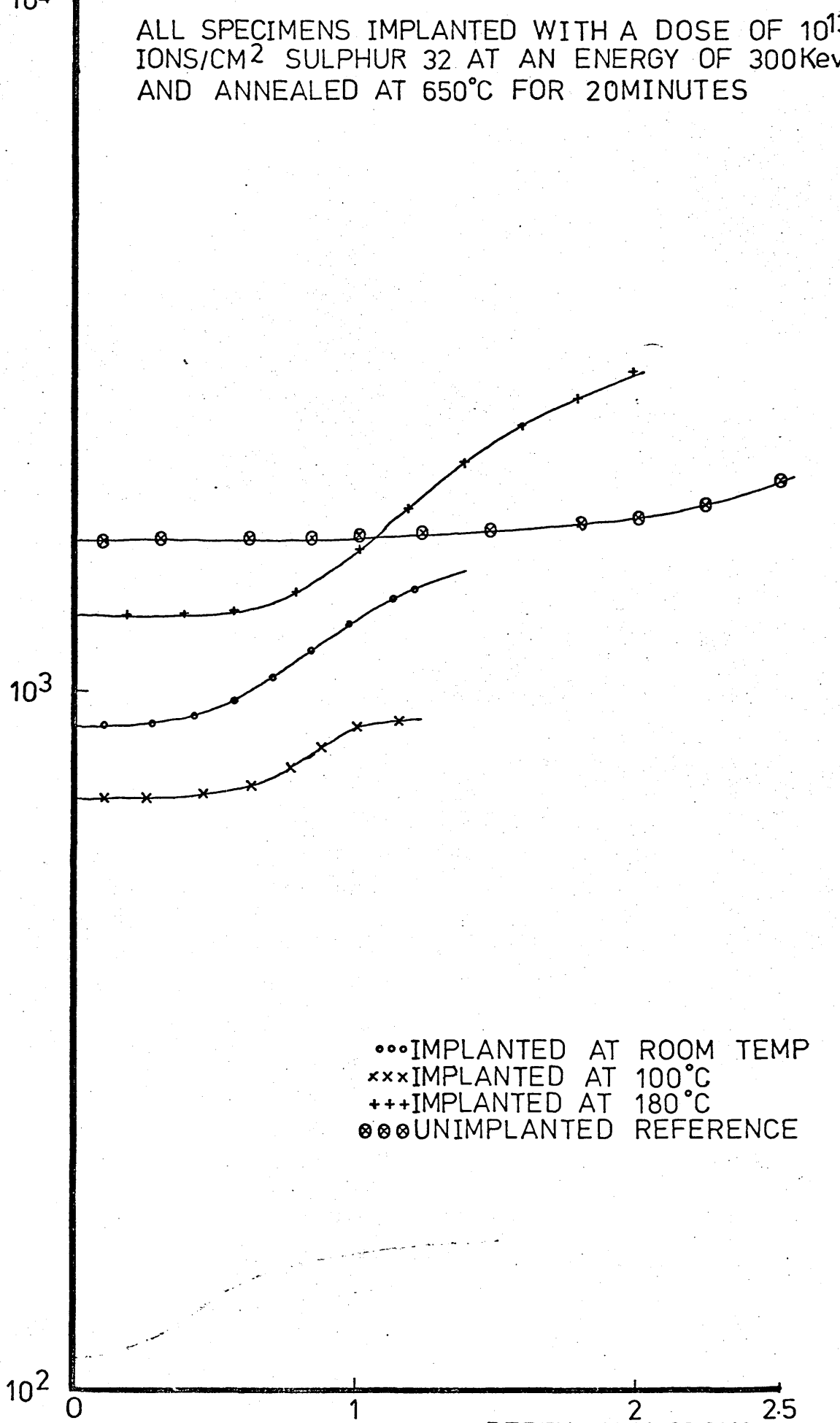


GRAPH 50 HALL MEASUREMENTS-VARIATION OF SHEET RESISTIVITY WITH IMPLANT TEMPERATURE

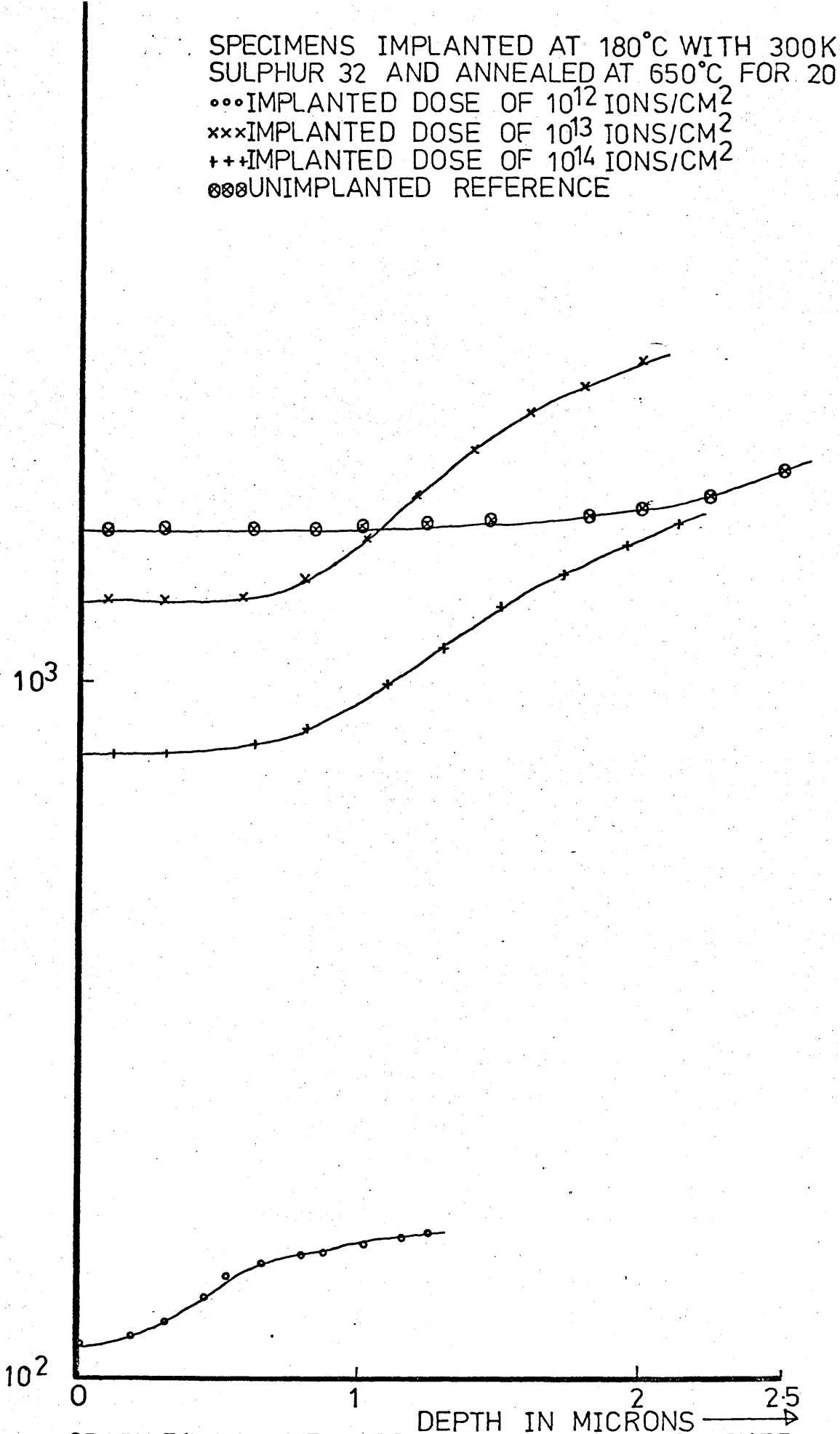


GRAPH 51 HALL MEASUREMENTS - VARIATION OF SHEET RESISTIVITY WITH ION DOSE

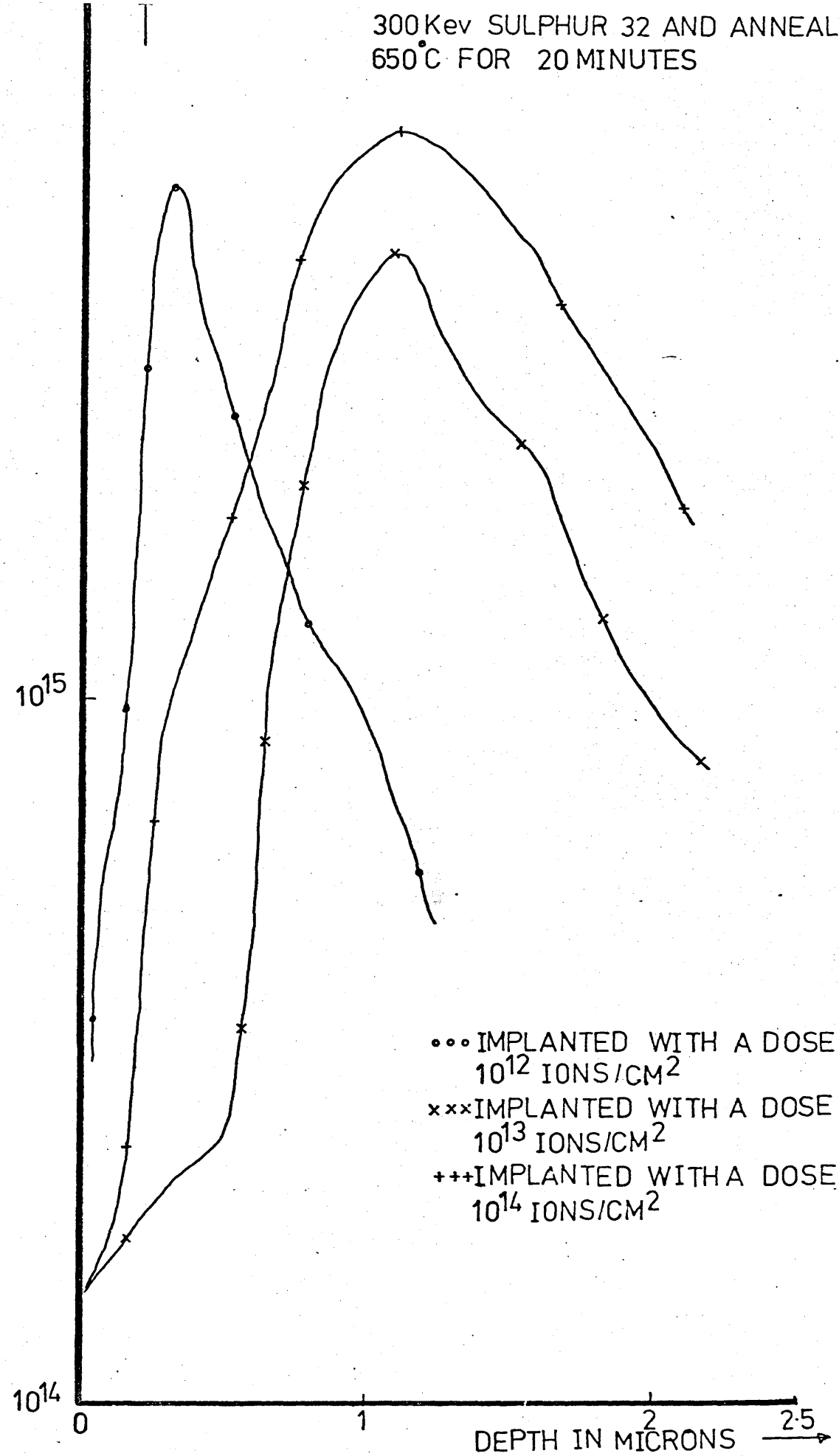


GRAPH 52 HALL MEASUREMENTS - VARIATION OF DONOR CONCENTRATION WITH ION DOSE

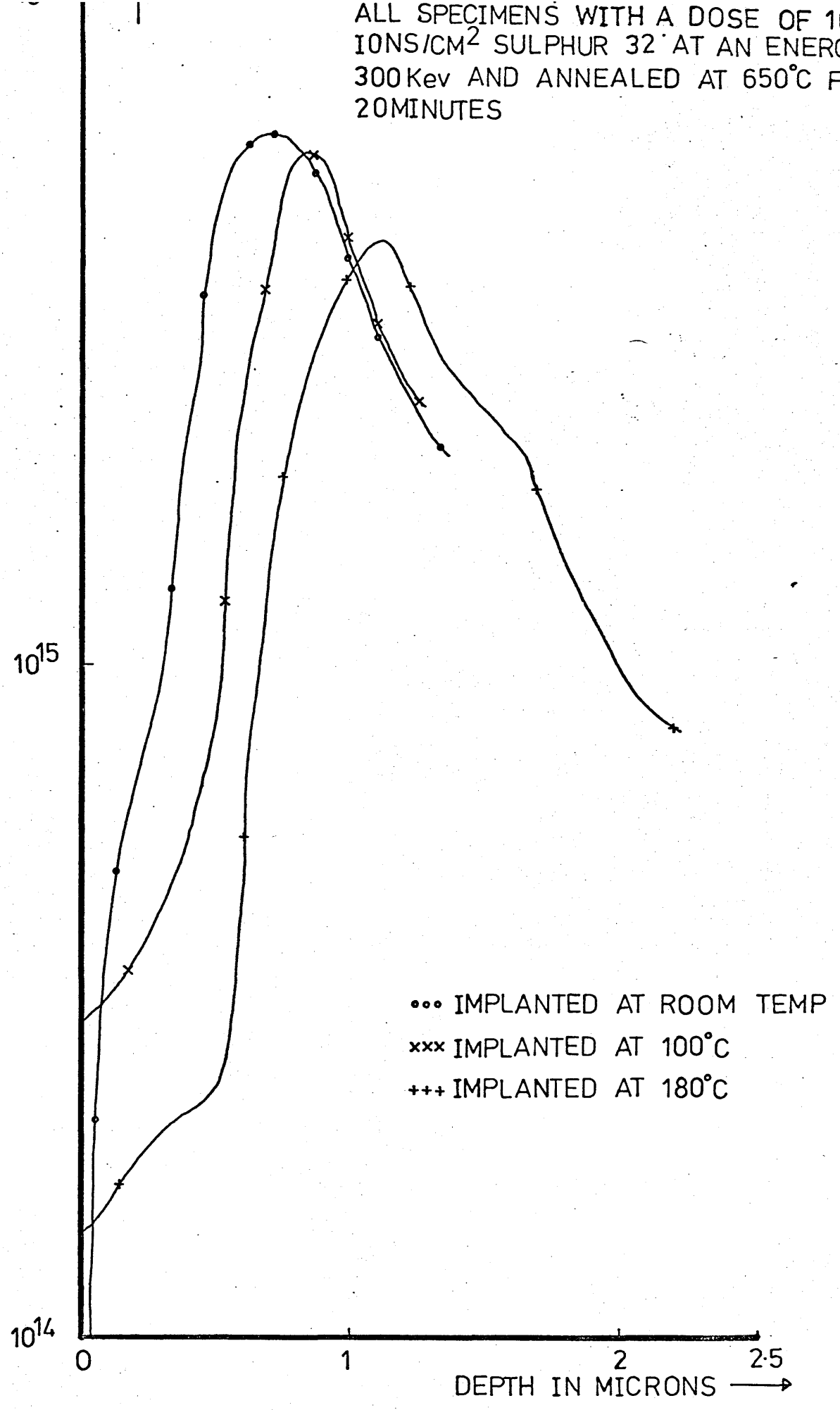


GRAPH 53 HALL MEASUREMENTS - VARIATION OF DONOR CONCENTRATION WITH IMPLANT TEMPERATURE

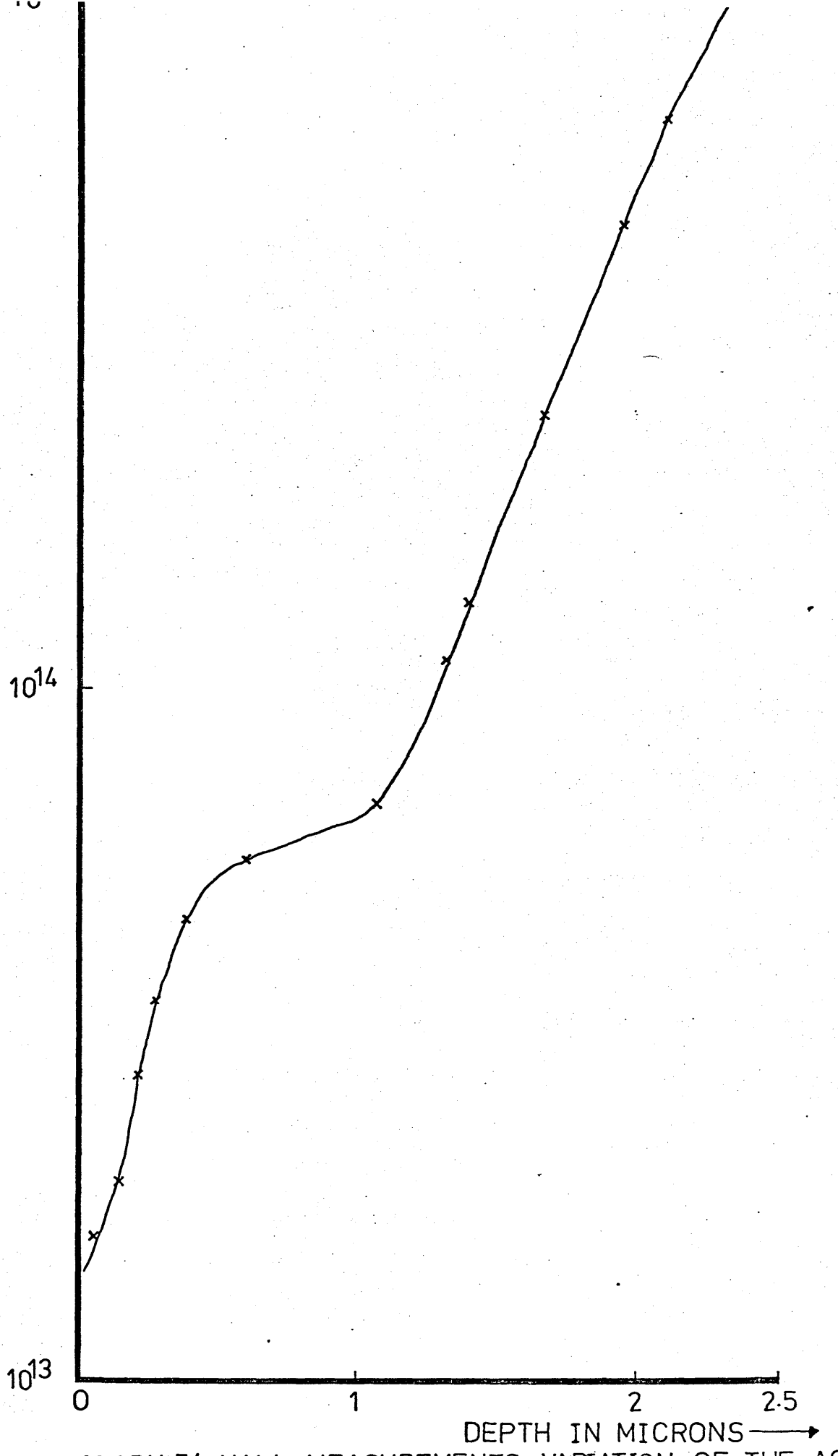


GRAPH 54 HALL MEASUREMENTS - VARIATION OF THE ACTIVE DONOR CONCENTRATION WITH DEPTH FOR THE

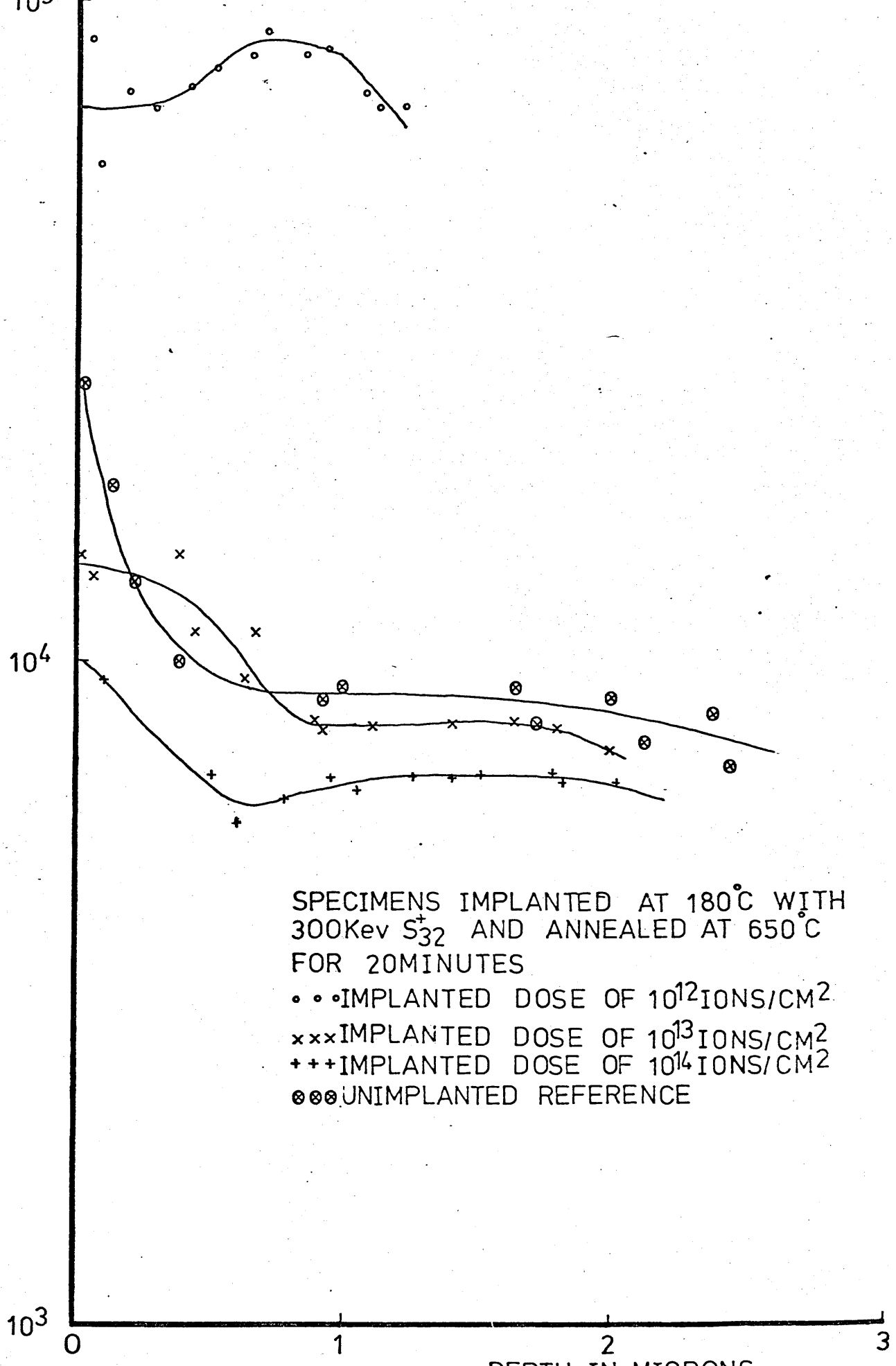


GRAPH 55 HALL MEASUREMENTS-VARIATION OF MOBILITY WITH ION DOSE

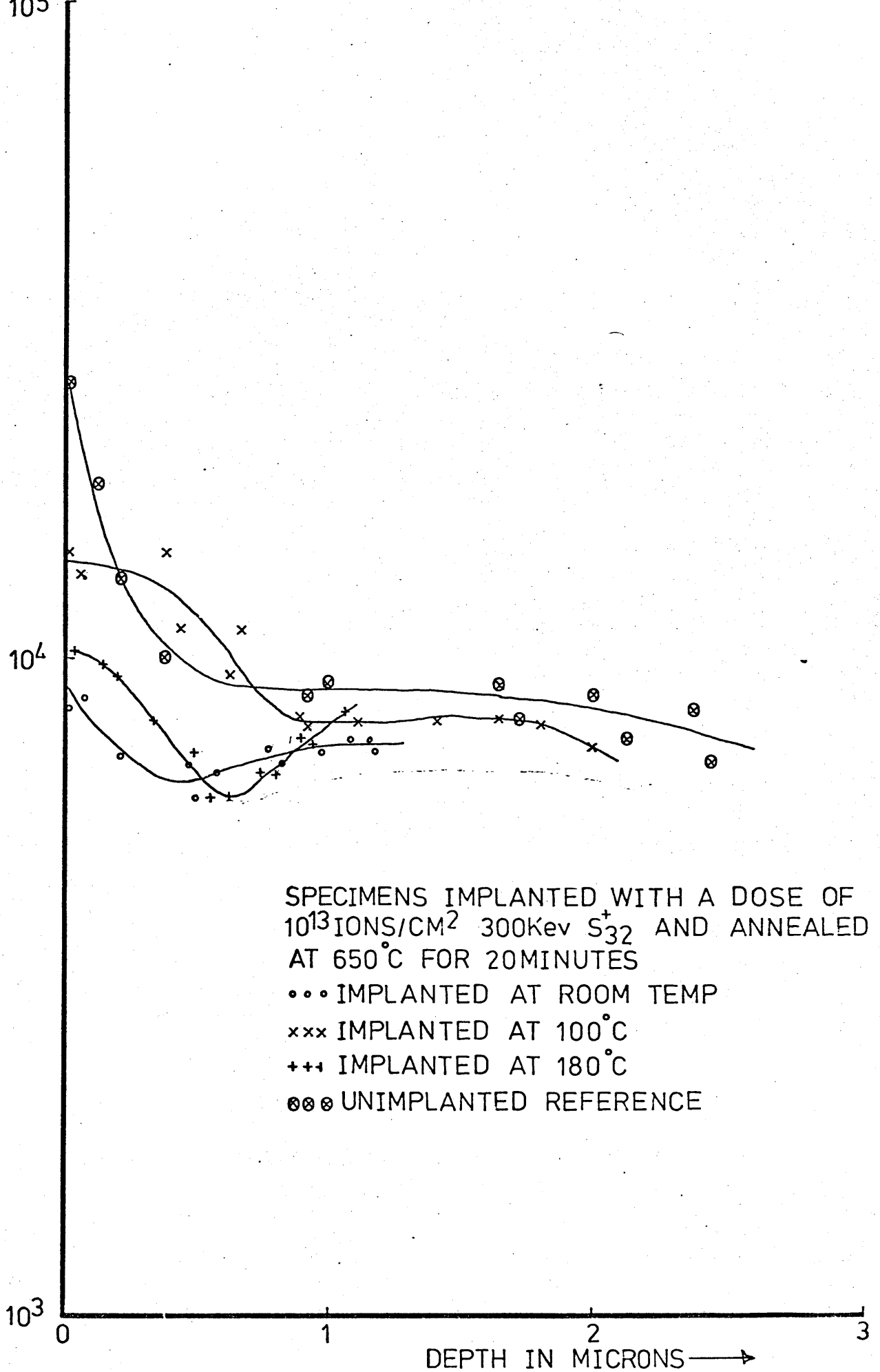


GRAPH 56 HALL MEASUREMENTS-VARIATION OF MOBILITY WITH IMPLANT TEMPERATURE

CARRIER ACTIVITY FROM HALL MEASUREMENTS

% Carrier Activity = Average Conc. Nav. (background conc.) × Depth (microns)
(underprofile) $\times 10^{-2}$/Dose($cm^{-2}$) ..... (51)

Background material = $3.005 \times 10^{14}$ atoms/$cm^3$.

| | % Carrier Activity (underprofile) |
|---|---|
| Dose (implants 180°C, annealed 650°C, 300 keV, $S^{+}_{32}$) | |
| $10^{14}$ ions/$cm^2$ | 0.62% |
| $10^{13}$ ions/$cm^2$ | 2.86% |
| $10^{12}$ ions/$cm^2$ | 17.0% |
| Implant Temperature ($10^{13}$ ions/$cm^2$, 300 keV, $S^{+}_{32}$) | |
| Room Temperature | 3.9% |
| 100°C | 2.9% |
| 180°C | 2.86% |

## 4.7 Thermal Probe Measurements

Thermal probe measurements indicated that after room temperature ion implantation, the surface of the n-type specimens had turned to p-type. This was noted for phosphorous implants with doses of $5 \times 10^{13}$ions/cm$^2$ and $5 \times 10^{14}$ions/cm$^2$ into $6 \times 10^{17}$atoms/cm$^3$ n-type gallium arsenide. To find if the p-type layer was due to the chemical effect of phosphorous ions or due to mechanical damage during bombardment, argon was implanted into material of the same concentration with doses of $5 \times 10^{11}$, $5 \times 10^{12}$ and $5 \times 10^{13}$ions/cm$^2$. The thermal probe results from the specimens implanted with doses of $5 \times 10^{12}$ions/cm$^2$ and $5 \times 10^{13}$ions/cm$^2$ indicated the formation of a p-type surface layer, with the higher dose appearing to be more p-type than the lower dose specimen. The specimen with a dose of $5 \times 10^{11}$ions/cm$^2$ still had an n-type surface, although the indication was that the surface was not as n-type as the original material.

Annealing of specimens at temperatures of 400°C or 500°C for 15 minutes appeared to have a small effect in reducing the p-type layer. With all the specimens the p-type layer appeared to disappear after annealing at 500°C for one hour or 600°C for 15 minutes.

## 5.0 DISCUSSION

For convenience the discussion chapter has been broken down into 5 main sections, namely:-

1) Thermal probe measurements
2) Current-Voltage characteristics
3) Capacitance-Voltage measurements
4) Profile measurements
5) Hall measurements

With some early phosphorus and argon implanted specimens thermal probe measurements were carried out to determine the specimen surface type, i.e. n or p-type, after implanting and annealing. No actual results have been included in the Results section since little information can be obtained from these measurements. However, a summary of these results is given in Section 4.7.

In the case of 2), 3) and 4) specimens were prepared for capacitance-voltage and Copeland measurements and in addition current-voltage measurements were carried out on the same specimens.

A series of Hall measurements were carried out to substantiate the results obtained from the capacitance-voltage and Copeland measurements. It is perhaps worth noting here that in Section 4.1 are included the Copeland calibration curves i.e. graphs 1, 2 and 3. All of these calibration curves are linear, although for graph 2 the logarithmic d.c. output of the 11.4 MHz amplifier channel is only approximately linear over one decade. Care therefore has to be taken to ensure that any concentration measurements fall within this decade.

## 5.1 Thermal Probe Measurements

When carrying out capacitance-voltage or Copeland measurements using a surface metal barrier diode on n-type material, it is important to ensure that after implantation and subsequent annealing the surface of the material is still n-type. If this were not the case, there would be uncertainty in knowing if the depth measured was the true depth from the surface or the depletion width, from the p-type layer to the n-type background material. Furthermore, the new junction formed would not necessarily be an abrupt junction, introducing more error into the technique. The thermal probe measurements did show that immediately after implanting an n-type specimen with a heavy ion e.g. argon or phosphorus, the surface of the material had become p-type. This occurred with doses as low as $5 \times 10^{12}$ions/cm$^2$ of argon, whereas implanting with a dose of $5 \times 10^{11}$ions/cm$^2$ of argon the surface still remained n-type. It was found that where a surface p-type layer existed this could be removed by annealing at 500°C for one hour, or at 600°C for 15 minutes.

The conclusion which can be drawn from this work is that immediately after implanting an n-type gallium arsenide specimen at room temperature with a dose greater than $5 \times 10^{11}$ions/cm$^2$ of a heavy ion, such as argon, the surface of the crystal has suffered severe structural damage. The acceptor centres produced by this structural damage are sufficient to compensate the donor centres at the surface and leave an excess of acceptor centres. Thus the surface of the material is turned to p-type. Subsequent annealing causes re-ordering of the crystal structure and a reduction in the number of acceptor centres. However, this reduction was not found to be sufficient to return to an n-type surface until the specimen had been annealed at 500°C for one hour, or 600°C for 15 minutes.

The abruptness of the surface barrier diode can be assessed using current-voltage measurements. This technique was adopted for the sulphur implanted specimens in preference to the thermal probe method, because of possible surface damage, produced by the method. Furthermore, the thermal probe technique was only useful in indicating the presence of an n or p-type surface layer.

## 5.2 Current-Voltage Characteristics

Current-forward bias voltage characteristics taken on a metal semiconductor diode can in principle yield useful imformation about the mobility of carriers, their lifetime, barrier height and the quality of the barrier. In practice however, it was found difficult to obtain these values, except the quality of the barrier. The factor n in equation (6) determines the "quality" of the barrier i.e. how abrupt it is. For an ideal Schottky barrier n=1, but in practice however, it is never unity. Variations from the ideal case occur due to an interfacial layer between metal and semiconductor, image force lowering of the potential barrier, and the influence of surface states. Two typical current density J-forward bias voltage V curves are shown in Graph 4, one of an implanted specimen and another of an unimplanted reference sample. Consider the unimplanted specimen, three regions can be identified. The centre portion of the curve is a straight line and follows a $J \propto \exp. eV/nKT$ law, conduction is by drift and diffusion. The factor n is determined from the slope of the line and in this case was found to be $n = 1.03$, which indicates a near ideal characteristic. For high values of current and applied forward bias, current limiting occurs due to the bulk resistance of the specimen. For low values of applied bias the -1 term in equation (2) becomes significant causing a reduction in the current as the bias decreases.

In the case of the implanted sample, a further region can be identified. At a value of about 100 mV applied voltage a flattening occurs in the characteristic. This is a region where recombination currents predominate over the diffusion current. The effect of implanting ions into the specimen has been to produce damage and disorder in the crystal lattice, which has given rise to recombination centres in the forbidden region of the band gap.

The value of n obtained from the diffusion portion of the curve in this case was found to be 1.28. In a lot of cases, it is difficult to assess the n value. If sufficient damage is introduced into the crystal then the centre portion of the curve is missing and the current is further limited by the additional ohmic resistance due to damage, see Graphs 7 and 8. In Graph 8 the effects of the deliberate introduction of damage upon the forward I-V characteristic is illustrated. Curve A shows an unimplanted reference specimen, having an n value of 1.02, that is a Schottky diode with near ideal characteristics. A similar specimen was implanted at room temperature with a dose of $3 \times 10^{12}$ ions/cm$^2$, 300 keV protons. The specimen was not annealed, so that any effect is due purely to the damage introduced by the protons losing energy in the structure.

Since the value of n is in part a measure of the abruptness, it gives an indication of the validity of concentration-depth profiles taken from capacitance-voltage measurements on Schottky diodes. This is due to the analysis of capacitance-voltage data to obtain concentration-depth profiles and depends upon the diode having an abrupt junction. Any deviation will lead to errors in the final profile.

The effects of dose, energy and anneal temperature upon the forward current-voltage characteristics can be seen in Graphs 5, 6 and 7.

Tables V lists the variation of n with dose, energy, anneal and implant temperature for sulphur implanted gallium arsenide specimens.

The following trends were noted:-

1) Effects of Dose: as dose increases, the n value increases.

2) Effect of Energy: as energy increases, the n value increases.

3) Effect of Implant Temperature: as temperature increases, the n value decreases.

4) Effect of Anneal: as dose and incident beam energy increase more damage will be created in the crystal causing a possible increase in surface states or the production of an interfacial layer, so increasing the n value. Annealing however, decreases the n value until 650°C, after this temperature a significant increase in n occurs.

Consider Graph 4, the value of n obtained from the diffusion portion of the curve was 1.28 indicating that the diode is not ideal and that one or more of the effects mentioned earlier is causing a deviation from ideality. For the diffusion region of the J-V characteristics using equation (5) the mobility of electrons ($\mu_n$) can be calculated knowing the barrier height $V_d$ of the diode from capacitance measurements. Alternatively, knowing the mobility the barrier height $V_d$ can be calculated. For the two diodes in Graph 4 the barrier heights were assessed from the ($1/C^2$) versus voltage curves in Graph 38, and the electron mobilities calculated. For the case of the implanted specimen, because the curve ($1/C^2$) versus voltage is not a straight line, accurate assessment of the barrier height is not possible from the technique, and a barrier height the same as the unimplanted specimen of 0.8 Volts was assumed. From this a $\mu_n$ of 6640 $cm^2$/Volt-sec. was obtained for the unimplanted

specimen and a $\mu_n$ of 1940 $cm^2$/Volt-sec for the implanted specimen, indicating a decrease in the net electron mobility in the implanted region of the diode. Due to the exponential term of $\phi_{Bn}$ in equation (5), from which the mobility is calculated, a small variation in the barrier height causes a large change in the value of mobility. Using the capacitance-voltage technique, accurate assessment of the barrier height is only possible for unimplanted specimens. The barrier height cannot be measured using the measuring equipment in section 3.3.2, to better than 0.05 Volts. The technique can, therefore, only be used to give an indication of the net mobility. In the technique, the permittivity, $\varepsilon$, and the density of states, $N_c$, have to be assumed to be constant and the net donor density, $N_D$, used.

Consider the recombination region of the J-V characteristic in Graph 4. From equations (7) and (9) for recombination it can be seen that from the slope of the curve the factor, $\beta$, can be calculated and from the extrapolated intercept with the current density axis an indication of the barrier height or electron lifetime, $\tau$, can be found. From the J-V characteristic of the implanted specimen, a value of $\beta$ was found to be $\beta = 4.83$, it would normally be expected to have a value of 2. Deviation occurring from the normal behaviour due to surface states or an interfacial layer introduced by the implantation of ions creating damage in the structure. Substituting a value of $V_d = 0.8$ Volts as used previously, gave a value for the electron lifetime of $2.3 \times 10^{-10}$ sec. This is a net value for the electron lifetime in a wafer of material the thickness of the depletion width at zero bias. The technique is sensitive to changes in barrier height, but not quite so sensitive as when measuring mobility. It makes accurate assessment of electron lifetimes difficult, but for damaged material they are always very small.

## 5.3 Capacitance-Voltage Measurements

### 5.3.1 Limitations in the Capacitance-Voltage Technique

The two most obvious limitations to the capacitance-voltage method of doping concentration measurements are the minimum depth resolution due to zero bias depletion width and the maximum depth due to diode breakdown.

In equation (13) it can be seen that for a surface barrier diode at zero bias there is a minimum depth to which measurements can be made. This minimum depth is determined by the net average donor concentration within the depletion region. Graph 40 shows the effect of donor concentration on the minimum depletion width; for uniformly doped material, as the concentration increases the depletion width decreases. The result is that to measure the concentration of the surface barrier near to the surface, the net average donor concentration has to be high.

Sze and Gibbons[88] showed that the avalanche breakdown voltage of an abrupt and linear graded p-n junction is proportional to the net average doping concentration, see Graph 41 for a one-sided abrupt junction at 300°K. However, breakdown voltages may be lowered by microplasma effects, surface leakage and field concentration at the edges of the junctions. The technique is further limited by the net concentration of donor atoms due to degeneracy of the material at high donor concentrations. Degeneracy occurs at room temperature for Gallium Arsenide at about $10^{18}$atoms/cm$^3$.

Initially measurements were carried out on material with an initial donor concentration of $6 \times 10^{17}$atoms/cm$^3$. This material was chosen to see as much of the front edge of the implanted donor peak

as possible. Difficulties occurred; surface barriers were difficult to form and breakdown occurred at very low voltages (1 or 2 Volts typically). To try to extend the range of measurements the surface barrier diodes were forward biassed and strange results were obtained (see Graph 39). It is not clear why the peak around zero bias occurred. It may be due to a resonance effect in the measuring equipment or due to the effect of surface states. Around zero bias the effect of surface states becomes increasingly significant, such that a true representation of the profile will not be obtained near the zero bias and into forward bias. Initially these results were thought to indicate an insulating layer being formed on the surface of the material. However, using MIS theory still does not explain the results obtained.

Due to the difficulties with these initial measurements the technique was given a closer investigation. For forward bias the $(1/C^2)$ versus voltage characteristics deviated from the linear relationship expected. It was discovered that the deviation was due primarily to the magnitude of the capacitance bridge modulating voltage. This caused the diode current to increase drastically when measurements were carried out with low forward bias. The solution was to reduce the modulating voltage, and not to take measurements near the zero bias point or in forward bias. In order to determine what information could be derived from the measurements, theoretical capacitance-voltage curves were calculated for a given background donor concentration and for a range of implanted doses for a given impurity atom. The calculations assumed that the profile followed a Gaussian distribution and that 100% of the ions had become active. To speed up the calculations a computer program was developed. The results from these calculations make it possible to design the experiment to fit the results required. They showed that for optimum

results the starting material should be between $10^{15}$ and $10^{16}$atoms/cm$^3$ for the experiments envisaged i.e. when implanting with a donor atom.

The results from the capacitance-voltage measurements are given in Section 4.5 and the concentration profiles are discussed further in Section 5.4 along with profiles obtained using the Copeland technique.

### 5.3.2 Capacitance-Voltage against Frequency

As stated previously in Section 2.4.2 when one or more energy level is present in the band-gap, especially deep levels, variation of the diode capacitance will occur with the measurement frequency. Consider a metal-semiconductor barrier with one shallow donor level in the semiconductor, which is completely ionised at room temperature. As the measurement signal frequency is varied there will be no change in the measured capacitance. If however, a deep donor or acceptor level is present, as the modulating frequency is varied, at some frequency this level will respond and there will be a change in capacitance[68,89] (see Section 2.4.2). This argument will apply to any other donor or acceptor level which is not ionised at room temperature. Three typical capacitance-frequency curves are shown in Graphs 9, 10 and 11 for three sulphur implanted n on $n^+$ epitaxial specimens. Different curves have been plotted on these graphs for a range of constant reverse bias voltages. Measurements were taken over a frequency range 500 Hz to 100 kHz, these limits being set by the measuring system.

In Graph 9, for the unimplanted specimen the capacitance is fairly constant over the frequency range with no bias and with 1 Volt reverse bias, indicating the presence of only ionised energy levels. If

the implanted specimen is now considered, this was implanted at room temperature with a dose of $10^{14}$ions/cm$^2$ 300 keV sulphur ions and then annealed at 650°C for 20 minutes in a nitrogen atmosphere. With no reverse bias the graph shows a large change in capacitance from 500 Hz to 100 kHz, that is the capacitance decreasing with frequency and starting to level off. This would indicate the possibility of a two level system, probably one deep donor level and one shallow donor level, although more than two levels could be present. If it had been possible to increase and decrease the range of measuring frequencies it would have been expected that the capacitance would level off. The measurements taken with a reverse bias of 2 Volts show a less marked change in capacitance, indicating that deeper in the specimen the concentration of deep levels is decreasing. This is consistent with the damage and impurity atom distribution peaking and then decreasing, not necessarily together. By depleting beyond the peaks, it would be expected that the concentrations could decrease. This is shown more clearly in Graph 10. The specimen was implanted at room temperature with a dose of $10^{13}$ions/cm$^2$ 300 keV sulphur ions and annealed at 650°C for 20 minutes. In this case a range of measurements were taken from zero bias to 8 Volts reverse bias. As the bias increases, the curves gradually approach those of the unimplanted specimen. The depths examined at zero bias fall within the implanted region. As the reverse bias is increased the depletion region increases in width and passes through the implanted region. The capacitance-frequency curves in this case, tend to the original background frequency. Due to the limited frequency range of measurements it is not possible to extract values for the level response time, the deep level concentration, $N_D$, and the deep energy level. The unimplanted specimen in this case shows an increase in capacitance at the low

frequency, indicating the presence of a deep donor level.

Graph 11 shows the capacitance-frequency curves of a specimen implanted at room temperature with a dose of $5 \times 10^{12}$ions/cm$^2$ 300 keV sulphur annealed at 600°C for 20 minutes. The curves follow a similar pattern to those described previously, but the situation is more complicated because the unimplanted specimen shows a rapid change in capacitance at low frequencies, indicating the presence of a deep donor level in the unimplanted specimen.

Graph 12 shows the effect of frequency upon the donor concentration-depth profile of a specimen implanted at 180°C with a dose of $5 \times 10^{12}$ions/cm$^2$ 300 keV sulphur annealed at 600°C for 20 minutes and measured using the capacitance-voltage technique. The profile measured at 1 kHz shows a broader peak with a higher concentration and nearer to the surface than that measured at 50 kHz. If only shallow energy levels were present it would be expected that the curves would coincide. However this graph indicates the presence of a deep donor peak nearer to the surface than the shallow donor i.e. if the 50 kHz curve is considered to be predominantly due to a shallow level or levels. The tails of the two curves coincide approximately.

This variation of capacitance with frequency means that care must be exercised in the choice of frequency at which capacitance-voltage measurements are carried out. If the concentration of only shallow levels is required, then a sufficiently high measuring frequency must be chosen to ensure that only these levels respond to this signal. As can be seen from the graphs presented, in some cases, even at 100 kHz, some error could occur in the true concentration of the shallow levels. For the Copeland equipment a frequency of 5.7 MHz was chosen to ensure that only shallow level concentrations were measured.

For this very reason the Copeland method becomes useful in

ion implantation studies to distinguish between the shallow chemical doping levels and the deeper levels introduced by structural damage. Energy levels produced by crystal structural damage will be at deeper energy levels than those obtained from the chemical doping by sulphur. Sulphur, in fact, produces a shallow donor level at 0.007 eV from the conduction band[71]. The energy level produced by sulphur in gallium arsenide was measured using thermal stimulated currents[90] as 0.006 eV[91]. The results obtained using the manual capacitance-voltage technique will be effected by deep levels in the band-gap due to damage or chemical impurities (see Table II for a list of possible chemical impurities). Therefore by carrying out manual low frequency and Copeland measurements on an implanted specimen, it is possible to distinguish between a shallow chemical doping concentration profile and a structural damage concentration profile.

In the discussion so far, on the capacitance-frequency curves, the presence of deep levels has been noted in the implanted specimens which do not appear to be present in the unimplanted specimens. The introduction of these deep levels must be due to the implantation process and subsequent annealing.

## 5.4 Profile Measurements

Results from the Copeland measurements and capacitance-voltage measurements are given in Sections 4.4 and 4.5 respectively. No results have been included for bulk gallium arsenide specimens. These measurements proved to be unsuccessful, because of the poor quality of the metal-semiconductor barriers i.e. they were leaky, with low breakdown voltages and in some cases produced ohmic contacts.

Results are limited to implant doses of sulphur 32 between $10^{12}$ions/cm$^2$ and $10^{14}$ions/cm$^2$. The lower figure being the lowest

practicable implant dose and the upper figure the limiting dose at which successful diodes could be made. Above $10^{14}$ions/cm$^2$ the Schottky diodes prepared proved to be very leaky. For a similar reason the highest feasible anneal temperature was found to be 700°C.

The following general trends were noted in the Copeland results given in Sections 4.4:-

1) Effect of Implant Temperature

As the implant temperature increased from room temperature to 180°C the percentage electrical activity decreased and the depth of the peak increased with its concentration decreasing. Some leveling off in the percentage activity and peak concentration occurred between 100°C and 180°C.

2) Effect of Anneal Temperature

As the anneal temperature increased the percentage electrical activity increased up to 600°C, then decreased as temperature increased for specimens annealed in a nitrogen atmosphere. For specimens annealed in an arsenic atmosphere the percentage electrical activity increased up to 650°C then decreased. In all cases no appreciable activity was noted at, or below, an anneal temperature of 500°C. The peak concentration depth increased up to a temperature between 600°C and 700°C. The concentration reached a maximum at a temperature between 600°C and 700°C. For specimens implanted at 180°C the peak concentration occurred between 650°C and 700°C, whereas for specimens implanted at room temperature and 100°C the peak concentration occurred at 600°C.

3) Effect of Energy

As the implant energy was increased the percentage electrical activity increased to 200 keV, then decreased; the depth of the concentration peak increased and the maximum concentration occurred at 200 keV.

4) Effect of Dose

As the implant dose increased the percentage electrical activity decreased, the depth of the concentration peak increased and the concentration peak decreased. In all cases the depth of the concentration peak was observed to be two or three times that predicted from Lindhard[70] Range Theory. The specimens exhibited super-tails, sometimes extending 3 or 4 microns from the surface of the specimen. The maximum peak concentration observed was $1.7 \times 10^{16}$ atoms/cm$^3$ and a range of carrier activities, from zero to 86% was observed.

The following general trends were noted in the manual capacitance-voltage results given in Section 4.5:-

1) Effect of Implant Temperature measured at 50 kHz

As the implant temperature increased from room temperature to 180°C, the percentage electrical activity decreased.

Effect of Implant Temperature measured at 1 KHz

As the implant temperature increased from room temperature to 180°C, the percentage electrical activity decreased.

2) Effect of Anneal Temperature measured at 50 kHz

As the anneal temperature increased from room temperature to 650°C, the percentage electrical activity increased from 500°C to a

peak at 600°C and then decreased to 650°C.

Effect of Anneal Temperature measured at 1 kHz

As the anneal temperature increases from room temperature to 650°C, the percentage electrical activity increased from 500°C to a peak at 600°C for the 180°C implanted specimen, or increased to 650°C for the room temperature implanted specimen.

3) Effect of Implant Energy measured at 50 kHz

As the energy increased from 100 keV to 400 keV the percentage electrical activity increased.

Effect of Implant Energy measured at 1 kHz

As the energy increased the percentage electrical activity increased.

4) Effect of Implant Dose measured at 50 kHz

As the dose increased the percentage electrical activity decreased.

Effect of Implant Dose measured at 1 kHz

As the dose increased the percentage electrical activity decreased.

In Section 4.4 the carrier activities under the profile curves are expressed as a percentage of the total dose. The percentage carrier activity was found from the Copeland results by extracting the area under the curve, thus obtaining the average carrier concentration and then applying the equation (51). These results will be subject to error since the carrier profile cannot be displayed fully. It will

indicate however the trends in the implantation process. In some instances abnormally high values of percentage carrier activity were obtained e.g. Table VIIIa with the corresponding Graph 19. Here the tail of the profile does not appear to return to the background concentration, this is most likely to be due to the original material not being homogeneous. The variation in background concentration would lead to the high value of percentage carrier activity obtained. This is highlighted when comparison is made of these results with the analogous manual capacitance-voltage results given in Table XII. The Copeland results percentage carrier activity being very much higher than those obtained from the capacitance-voltage results. From the manual capacitance-voltage measurements the measured capacitance gives the total charge in the diode depletion region. Therefore by taking the capacitance measurement at the largest value of reverse bias, the average concentration from the surface to the depth can be found. Using this value in equation (51) will yield a less erroneous result than that obtained from Copeland measurements. For these reasons care has to be taken when comparing the percentage electrical carrier activity results obtained from Copeland and capacitance-voltage measurements.

A more detailed discussion of these results will follow.

### 5.4.1 Variation of the Concentration Profile with Implant Temperature

The variation of the concentration profile with implant temperature is shown in graphs 13, 14, 29 and 30. In graphs 13 and 29 the specimens were implanted with a dose of $10^{12}$ions/cm$^2$ sulphur 32 ions at an energy of 300 keV and then annealed in a nitrogen atmosphere at 650°C for 20 minutes. Three implant temperatures were employed for the experiment, namely room temperature, 100°C and 180°C.

From the Copeland measurements in graph 13 and Table VIa as the implant temperature increases from room temperature to 180°C the percentage electrical carrier activity decreases, the peak concentration decreases and remains approximately constant and the peak depth decreases to 100°C then increases to 180°C. The tails of the profiles extend deep into the material to approximately 2 microns depth i.e. to about twice the depth of the peak. The tails do not return to the background material, as previously described this will give erroneously high values for the electrical activity. From the C-V measurements in graph 29 and Table Xa as the implant temperature increases from room temperature to 180°C, the percentage electrical activity decreases when measured at 1 KHz and at 50 KHz increases slightly to 100°C, then decreases significantly at 180°C. A comparison of the percentage electrical activities measured at 1 KHz and 50 KHz shows a decrease from 1 KHz to 50 KHz, the difference decreasing as the implant temperature increases to 180°C. The higher values of percentage activity at 1 KHz probably being due to deep levels from damage in the crystal structure, the damage appearing to decrease at 100°C and 180°C. The concentration peak appears to be shallower at 1 KHz than 50 KHz, indicating a damage peak closer to the surface of the specimen than the impurity peak.

A slightly different behaviour was noted for the specimens implanted with a dose of $5 \times 10^{12}$ ions/cm$^2$ sulphur 32 ions at an energy of 400 keV and then annealed in a nitrogen atmosphere at 650°C for 20 minutes. These results are shown in graphs 14 and 30. From the Copeland measurements in graph 14 and Table VIb as the implant temperature increases from room temperature to 180°C the percentage electrical activity decreases and the peak depth increases. The tails of the profiles extend deep into the material up to approximately 3

microns i.e. to about twice the depth of the peak. From the C-V measurements in graph 30 and Table Xb as the implant temperature increases from room temperature to 180°C the percentage electrical activity decreases when measured at 1 KHz and 50 KHz. From a comparison of the percentage electrical activity measured at 1 KHz and 50 KHz, at room temperature and 100°C the concentration peak is nearer the surface at 1 KHz than 50 KHz.

It would be expected that as the implant temperature increased a reduction in the specimen damage would occur, with an increase in the chemical doping. This was not found to be the case. A comparison of the results obtained at 5.7 MHz, 50 KHz and 1 KHz is given in graph 43. From the Copeland results the chemically active donor concentration decreases with increasing implant temperature and tends to level off between 100°C and 180°C. This could be due to one of the following reasons:-

i) As the implant temperature increases there is a decrease in impurity atoms on substitutional sites.

ii) The active chemical donors are being compensated by a shallow acceptor level. The concentration of the acceptors increasing with implant temperature.

iii) Electrically inactive vacancy-chemical donor complexes are forming as the implant temperature increases.

Consider (i), for sulphur atoms to be electrically active they must be on substitutional lattice sites i.e. either on gallium or arsenic sites. If immediately after implantation a large number of impurities are on substitutional sites, for them to be inactive they

must be transferred to interstices. Zelevinskaya and Kachurin[73] postulated that Group VI atoms initially occupy gallium vacancies and are transferred to interstices by heating the material to between 600°C and 700°C. It may be possible that during implantation the transfer to interstitial sites occurs at much lower temperatures, the higher temperature (180°C) aiding the process more than the lower temperature of 100°C. This could be analogous to the self-annealing of damage during implantations at elevated temperatures, which has been observed[92,93] to occur at much lower temperatures than otherwise would be expected. This reduction in structural damage due to self-annealing during implantation leads to another possible explanation.

As the implant temperature increases, a decrease in structural damage will occur, with the decrease tending to level off. A corresponding reduction will occur in the number of vacancies for occupation by the chemical dopant. The net result being a reduction in electrical donor activity with increasing implant temperature.

The presence of shallow acceptor levels in (ii) is considered more fully in Section 5.4.5. It appears unlikely that the reduction in donor activity was due to the presence of shallow acceptor levels.

The formation of electrically inactive vacancy-chemical donor complexes in (iii) also is considered in more detail in Section 5.4.5. The formation of such complexes as a direct result of self-annealing is possible, this leading to a reduction in the concentration of electrically active shallow donors. The number of complexes increasing with implant temperature and the number tending to level off as the temperature increases. This levelling off with increasing implant temperature being due to the levelling off of reduction in the structural damage. This damage will not be completely eliminated because of the

formation of complexes in the structure.

From the manual capacitance-voltage measurements at 50 KHz, as the implant temperature increases the percentage electrical activity decreases i.e. the chemical doping, plus some deep levels due to structural damage, decreased. At any implant temperature there was a reduction in the percentage electrical activity measured at 50 KHz to the obtained by Copeland measurements. This reduction in percentage electrical activity was due to the shallow chemical donor levels being compensated by an acceptor level, or levels, deeper in the band-gap, which respond to the 50 KHz measuring frequency. These deeper acceptor levels are a result of the structural damage. As the implant temperature increased the difference between the percentage electrical activity at 5.7 MHz and 50 KHz decreased, indicating a reduction in the concentration of acceptor levels and hence a reduction in structural damage. However between 100°C and 180°C this difference increased indicating an increase in structural damage.

From the manual capacitance-voltage measurements at 1 KHz, as the implant temperature increased the percentage electrical activity decreased being fairly level between room temperature and 100°C and decreasing rapidly from 100°C to 180°C i.e. chemical doping plus some deep levels due to structural damage. Comparing the percentage electrical activities measured at 50 KHz and 1 KHz at any particular implant temperature, there was an increase at 1 KHz. This increase in percentage electrical activity at 1 KHz indicates that as well as the shallow chemical donor level, a deep acceptor level and a deep donor level are responding to the measuring frequency. This deep donor level being due to the structural damage.

As the implant temperature increases the peak depth increases;

this could be due to the movement of donors by diffusion during implantation, the higher the temperature the greater the diffusion. This diffusion could be enhanced by the presence of crystal damage. The question of whether or not the deep profiles were due to diffusion or channelling is discussed further in Section 5.4.3. The slightly differing behaviour at the two implant conditions was probably a result of the crystal damage.

### 5.4.2 Variation of the Concentration Profile with Anneal Temperature

To determine the effects of anneal temeprature, a series of specimens were implanted at 180°C with a dose of $5 \times 10^{12}$ ions/cm$^2$ sulphur 32 ions at an energy of 300 keV. The specimens' surfaces were passivated with silicon dioxide and annealed in a nitrogen atmosphere for a fixed period of 20 minutes. The specimens were annealed at 500°C, 600°C and 650°C, a further specimen was not annealed. The results of this experiment are shown in graphs 18 and 32, and Tables VIId and XIb. In graph 18 with no anneal and with an anneal temperature of 500°C there was only a slight increase in carrier activity with no sign of a concentration peak. At 600°C a peak appeared in the profile and at 650°C the peak concentration has increased still further. These results are summarised in Table VIId. At 600°C an apparent decrease in percentage electrical activity occurred this was due to the profile tail falling below the background concentration. This is probably not a real result but due to the inhomogeneity of the material again. Another effect can be noted and that is a decrease in the depth of the peak after annealing at 650°C.

As the anneal temperature increases a reduction in the crystal damage will occur i.e. a recrystallisation of the damaged material will

occur from the interface with the damaged material. An increase in the number of impurity atoms on substitutional lattice sites would be expected also. The results of the manual capacitance-voltage measurements for these specimens are plotted in graph 32 and Table XIb. After annealing at 500°C no apparent peak donor concentration occurred and only a small percentage carrier activity was observed (of the order of 1%). The profile at 1 KHz has a higher average donor concentration than at 50 KHz, indicating a large amount of damage in the specimen. At 600°C a large donor concentration peak was observed, at 1 KHz this peak was broad and nearer the surface of the material than that at 50 KHz. This points to the presence of a possible damage peak nearer the surface of the material than the impurity concentration peak. After annealing at 650°C the broad peak at 1 KHz and 600°C had disappeared and the 1 KHz peak lay much closer to the 50 KHz concentration peak. However, the 1 KHz concentration peak was still nearer to the surface of the material. After annealing at 650°C a significant reduction in the specimen damage appears to have occurred.

Consider the results in Table XIb for the variation of percentage donor activity with anneal temperature at 50 KHz:-

1) After no anneal and annealing at 500°C there was only a slight increase in the specimen donor activity.

2) After annealing at 600°C the percentage activity was 8.5%; annealing at 650°C the activity appeared to decrease to 7.9%. For the specimen in Table XIa a more significant drop to 3.5% after annealing at 650°C was noted.

V.M. Zelevinskaya and Kachurin[73] noticed a similar occurrence for 30 keV sulphur into gallium arsenide. They postulated the following:-

a) Assume Group VI atoms implanted into gallium arsenide initially occupy gallium vacancies and are transferred to arsenic vacancies only after heating at 700°C. Assume too that the Group VI atoms occupying vacancies are donors, whereas those occupying interstices are acceptors.

b) Annealing at 500°C to 600°C destroys the deep compensating centres generated by ion bombardment and the Group VI atoms, occupying gallium vacancies, are responsible for the weak n-type conductivity.

c) At 600°C to 700°C the impurity atoms are transferred to interstices and the electron density decreases.

d) Above 700°C the impurities begin to occupy arsenic vacancies and the doped layers acquire properties typical of heavily doped n-type gallium arsenide.

The series of specimens implanted with a dose of $10^{13}$ ions/cm$^2$ sulphur 32 ions at an energy of 300 keV and annealed in a nitrogen atmosphere for 20 minutes, substantiated this theory. Three series were in fact implanted at room temperature, 100°C and 180°C and the specimens were annealed at 500°C, 600°C 700°C and 800°C. These results are plotted in graphs 15, 16 and 17 and summarised in Tables VIIa, b and c. With all specimens a peak occurred in the percentage electrical activity at 600°C followed by a subsequent decrease at 700°C. All specimens annealed at 800°C proved to form leaky Schottky diodes so that no meaningful results were obtained. These results follow the pattern of Zelevinskaya's and Kachurin's postulate.

To compare annealing techniques another series of specimens were implanted at room temperature with a dose of $5 \times 10^{12}$ ions/cm$^2$ sulphur

32 ions with an energy of 300 keV. Afterwards the specimens were annealed in an arsenic atmosphere for 20 minutes, these anneals being carried out using two furnaces and the specimens contained in an evacuated quartz phial. The anneals were carried out at the Mullard Research Laboratory, Redhill. The results are summarised in Table VIIe and some variation can be seen in the observed behaviour when compared with the specimens in Table VIId annealed in a nitrogen atmosphere. The pattern does follow, however, the other specimens, again annealed in a nitrogen atmosphere, in Table VIIa. The percentage electrical activity increases to an anneal temperature of 650°C, with the peak concentration reaching a maximum at 600°C then decreasing to 650°C.

### 5.4.3 Variation of the Concentration Profile with Implant Energy

Graphs 19 and 33 and Tables VIIIa, b and XII show the variation of concentration profile with implant energy. From Lindhard[70], as the energy of the incident beam increased the peak concentrations occurred deeper in the material and also decreased in value, with a general broadening of the peak. The range of sulphur and the projected standard deviation from Lindhard is given in Table IV for several different energies up to 400 keV. It can be seen that the depth of the peak increased with energy and the peak concentration was smaller, but was significantly deeper than predicted in Table IV. The tail of the profile also extended to a greater depth into the material. This is in agreement with work published by Sansbury and Gibbons[72].

From Table VIIIa for a specimen implanted at room temperature with a dose of $5 \times 10^{12}$ ions/cm$^2$ sulphur 32 ions and annealed at 650°C for 20 minutes in a nitrogen atmosphere, it can be seen that as the

energy increased the peak depth increased, the peak concentration increased to 200 keV and then decreased to 400 keV, and the percentage electrical activity increased to 200 keV, then decreased to 400 keV, with an overall decrease to 400 keV.

The results given in Table VIIIb are from specimens implanted under the same conditions as those described for Table VIIIa, but annealed at 650°C for 20 minutes in an arsenic atmosphere. As the energy increased the peak depth increased, the percentage electrical activity decreased and the peak concentration decreased to 300 keV then increased to 400 keV with an overall decrease. The pattern was broadly similar to that in Table VIIIa, although for those specimens annealed in an arsenic atmosphere the peak concentration achieved was lower, the percentage electrical activity was lower and the peak was deeper in the material.

Considering the manual capacitance-voltage measurements at 1 KHz and 50 KHz plotted in graph 33 and the results in Table XII, as the implant energy increased the peak depth increased and the percentage electrical activity increased. A comparison of the variation of percentage electrical activity with implant energy is plotted in graph 44 for the measuring frequencies of 5.7 MHz, 50 KHz and 1 KHz. At the 1 KHz and 50 KHz measuring frequencies the percentage electrical activity increased with increasing energy. This was caused by the presence of a deep donor level. The electrical activity at 50 KHz was always less than that at 5.7 MHz, indicating the presence of a deep acceptor level compensating the shallow chemical donor at 50 KHz. At 5.7 MHz as the implant energy increased the percentage electrical activity increased to a peak at 200 keV then decreased to 400 keV. The difference between the activities at 5.7 MHz and 50 KHz also peaked at 200 keV. For this to occur the chemical

doping concentration must peak at 200 keV and also the concentration of deep acceptors must peak at the same energy. Both must then decrease with increasing energy.

During implantation as the ion enters the crystal it will lose energy to the crystal, slow down and eventually come to rest within the crystal. The process of slowing down, loss of energy, will result in disruption and damage to the crystal structure. As the incident ion energy increases so must the structural damage increase. Immediately after implantation it would be expected from Lindhard (Table IV) that as the energy increases the distribution of implanted atoms will move into the material, the height of the peak concentration will decrease and the distribution broaden. Similarly this would be expected for the damage distribution, although the damage peak will be at a shallower depth than the impurity peak. During subsequent heat treatment a reduction in the damage peak will occur and the impurity peak will move deeper into the material due to diffusion. A similar behaviour was noted for increasing dose in Section 5.4.4. The reduction in chemical doping was probably caused by the increase in electrically inactive gallium-donor complexes. A further pointer to suggesting that the number of electrically inactive complexes have increased at 400 keV is that the concentration of deep acceptors has decreased. This relationship between the deep acceptor and the reduction in chemical doping suggests that the deep acceptor level was due to gallium vacancies and the reduction in chemical doping due to the formation of electrically inactive gallium-donor complexes.

Considering the behaviour for implant energies up to 200 keV, as the energy increased the chemical doping concentration increased and the deep acceptor concentration increased. The increase in the

deep acceptor concentration was a direct result of the increase in damage, this is in contrast to the behaviour above 200 keV. The increase in the chemical doping concentration was due to one of two factors, either more impurities were moving to substitutional lattice sites or not so many electrically inactive complexes were being formed. Both of these could be occurring at the same time. The reason for this change in behaviour at 200 keV is not fully understood although it would appear to be connected with the crystal damage and the possible formation of electrically inactive complexes.

In all cases donor concentration profiles much deeper than predicted by Lindhard[70] were obtained. The specimens exhibited super-tails, sometimes extending 3 or 4 microns from the surface of the specimen. Two possible explanations for the deep profile are that channelling of implanted ions has occurred or that sulphur has diffused deeper into the material during annealing. Sansbury and Gibbons[72] showed that the deep profile was due to diffusion and not channelling. It might be, perhaps, damage enhanced diffusion, i.e. damage centres in the semiconductor produce an enhancement in the diffusion rate by the motion of the impurity atoms from damage centre to damage centre. The results indicated that the damage centres themselves moved deeper into the semiconductor. To determine whether or not the deep profile was due to channelling or diffusion the following experiments were carried out:-

a) The specimen was turned sufficiently off any major channelling direction to minimise the channelling effect.

b) The specimen was implanted with sulphur and then the theoretical depth of the profile was removed by etching prior to annealing. If the deep profile was due to

channelling the removal of the surface layer would have made no difference to the unimplanted profile, although it would appear to be shallower. If it was due to diffusion during annealing, all the sulphur ions would have been removed and no increase in electrical activity would result.

For case (a) specimens were implanted normal to their surfaces and also turned 7° off the normal to the surface to minimise channelling, in both cases deep profiles were obtained. In one instance, see graph 37, a classical channelled profile was obtained at 1 KHz. However, this was not the case at 50 KHz and the peak concentration was still much deeper than Lindhard predicts.

For case (b) two specimens from adjacent positions on a slice of epitaxial material were implanted under identical conditions at room temperature with a dose of $10^{13}$ ions/cm$^2$ sulphur 32 ions with an energy of 300 keV. One specimen was annealed at 650°C for 20 minutes in a nitrogen atmosphere, the second specimen had 5000 Å stripped from its surface and then was annealed at 650°C for 20 minutes in a nitrogen atmosphere. The results from this experiment are shown in graph 26, no increase in electrical activity occurred after stripping. The experiment was repeated, but unfortunately yielded no useful results from the stripped specimen due to the Schottky diode being leaky. Although the above experiment has not been corroborated, the indications are that the deep profile was due to damage-enhanced diffusion.

### 5.4.4 Variation of the Concentration Profile with Implant Dose

The Copeland results for the variation of the concentration profile with implant dose are given in graphs 20, 21, 22, 23, 24 and 25 and also summarised in Table IX. It can be seen from these results that as the implant dose increased the percentage electrical activity

decreased. For the low dose implants ($10^{12}$ions/cm$^2$), percentage electrical activities as high as 86% were obtained and falling to less than 1% for the higher dose implants. There was some doubt about the reliability of the high values of percentage electrical activity in Table IXb, c and d. These correspond to graphs 21, 22 and 23 and it can be seen that the tails of the profiles do not return to the unimplanted material. A possible shift in background due to inhomogeneity in the material would lead to high values of percentage electrical activity. Implants were carried out with a dose of $10^{15}$ions/cm$^2$ but because of leaky diodes no reliable results were obtained.

As the implanted dose increased by two orders of magnitude only comparatively small changes occurred in the peak concentration. The highest value of peak concentration obtained being $1.5 \times 10^{16}$atoms/cm$^3$ in these results. Some increases and decreases occurred in the peak concentrations obtained.

Consider the capacitance-voltage measurement results given in graphs 34, 35 and 36 and the percentage electrical activities in Table XIII. For the measurements at 50 KHz and 1 KHz the percentage electrical activity decreased with increasing implant dose. The percentage electrical activities measured at 1 KHz were greater than those measured at 50 KHz with the difference decreasing as the dose increased. Consider Table XIIIa for an implant dose of $10^{12}$ions/cm$^2$ at 1 KHz the percentage electrical activity was calculated to be 74% and at 50 KHz to be 28%. For a dose of $5 \times 10^{12}$ions/cm$^2$ at 1 KHz the percentage electrical activity was now 12% and at 50 KHz to be 3.5%. These results are plotted in graph 45.

For the specimens in graph 34 implanted at room temperature

the peak at 1 KHz appears to have a higher net donor concentration than at 50 KHz indicating a larger number of donor type damage centres at a slightly greater depth. Again in graphs 35 and 36 the peak at 1 KHz is shallower than at 50 KHz.

Summarising, the effects of implant dose on the electrically active donor concentration were as follows:-

a) The depth of the donor concentration peak increased with increasing dose.

b) From the Copeland measurements the maximum chemical doping concentration was $1.5 \times 10^{16}$atoms/cm$^3$.

c) From the manual capacitance-voltage measurements at 1 KHz the maximum donor concentration was $1.7 \times 10^{16}$atoms/cm$^3$.

d) The percentage electrical activity decreased with increasing dose at all measuring frequencies.

Consider the percentage electrical activities plotted for the specimens implanted at 180°C in graph 46. At all measuring frequencies (d) above applies, also at any particular implant dose the percentage electrical activity decreases from being measured at 5.7 MHz to 50 KHz. The percentage electrical activity increases from being measured at 50 KHz to 1 KHz. The decrease in percentage electrical activity from 5.7 MHz to 50 KHz being due to deep acceptor levels produced by the structural damage compensating the shallow chemical donor level. Thereby the net donor concentration at 50 KHz is effectively reduced. The increase in percentage electrical activity from 50 KHz to 1 KHz was due to a deep donor level responding to the measuring frequency of 1 KHz, but not at 50 KHz. This indicates that the deep donor

level is at a deeper energy level than the deep acceptor level.

The decrease in the percentage electrical activity due to chemical doping as indicated by the Copeland measurements with increasing implant dose could be due to three factors:-

i) A decrease in the number of impurity atoms on substitutional lattice sites.

ii) An increase in the number of shallow acceptor levels compensating the shallow donor concentration.

iii) The formation of electrically inactive vacancy-impurity complexes.

In the case of (ii) we have assumed that the only levels responding to the 5.7 MHz measuring frequency are the shallow donor levels due to chemical doping. Shallow acceptor levels have been observed by C.S. Fuller et al.[94] at 0.1 eV from the valence band and which they attributed to clusters of gallium vacancies. They did however observe also that these clusters dissociate within the temperature range 500°C to 700°C to form stable donor-vacancy complexes. In our case the specimens have been annealed at 650°C so that any clusters present should have dissociated to form stable donor-vacancy complexes. These gallium vacancy-donor complexes may be similar to those described in Section 5.4.5 and may be electrically inactive. If this were the case then (ii) above would seem unlikely, but (iii) above becomes possible.

Consider (i) and (iii), why should the number of impurity atoms on substitutional sites decrease with increasing dose? In fact the number of impurity atoms on substitutional sites is not decreasing, but remaining approximately constant. If the net chemical

donor concentration remains nearly constant as the dose increases, then from equation (51) the percentage electrical activity will decrease. The question to be answered should now be, why does the net chemical donor concentration remain constant with increasing implant dose? As the implant dose increases there will be an increase in the structural damage and damage peak. Associated with this increase in damage, the number of gallium and arsenic vacancies will increase. Heat treatment of the specimens at 650°C will reduce the structural damage substantially, and hence the number of gallium and arsenic vacancies. Heat treatment however will increase the number of chemical complexes, so that the number of electrically inactive gallium-donor complexes will increase. The greater the initial damage the more of these electrically inactive gallium-donor complexes likely. Zelevinskaya and Kachurin postulated[73] that after annealing the material between 600°C and 700°C, impurity atoms are transferred to interstices and that by annealing at 500°C to 600°C the deep compensating centres generated by ion bombardment are reduced. The overriding effect of these two processes being that the net impurity donor concentration remains approximately constant. Sansbury and Gibbons[72] have also observed that the peak donor concentration obtained for 70 keV sulphur implanted gallium arsenide was almost independent of implant dose. They observed that after implanting with a range of doses from $10^{13}$ to $10^{16}$ions/cm$^2$ a peak donor concentration of $2 \times 10^{17}$atoms/cm$^3$ was obtained.

The depth of the donor concentration peak increased with increasing dose. The deep profiles seem most likely to be caused by diffusion during heat treatment, this is discussed further in Section 5.4.3. Considering the material prior to annealing after implantation,

the damage peak will occur around the Lindhard range. The damage consisting of gallium and arsenic vacancies and complexes. As the specimen is annealed there will be a movement of impurity atoms into the material by diffusion, possibly the diffusion velocity enhanced by the damage to the crystal structure. As the dose increases the damage peak will increase and the number of centres available for damage enhanced diffusion will increase prior to annealing. The larger the damage peak the longer the heat treatment required at a particular temperature, in order to minimise the damage. The higher the dose therefore, the longer the time required to minimise the damage and the higher the diffusion velocity. The higher the dose, the deeper the donor concentration peak. If the enhancement of diffusion is due to damage centres, it would be expected that the effects of the damage extend deep into the material. The results show, in fact, that the effects of the damage extend deep into the material.

From a comparison of the percentage electrical activities at 50 KHz and 1 KHz the results indicate the presence of a deep donor level. From an examination of Table II, oxygen and selenium are the two most likely impurity atoms producing a deep donor level. Of the two, oxygen would appear to be the most likely with an energy level of 0.63 eV from the valence band. There were two possible sources for this oxygen:-

i) In diffusion of oxygen from the silicon dioxide encapsulation of the specimen during heat treatment.

ii) Oxygen present in the ion beam during implantation of the material.

In the case of the specimens annealed in an atmosphere of arsenic,

the results indicated the presence of a deep donor level. The specimens were annealed without the presence of silicon dioxide encapsulation. This eliminates (i) but not (ii), every effort was made to reduce the oxygen content of the ion beam, but it is not certain that no oxygen was present in the beam. The concentration peak at 1 KHz was shallower than at 50 KHz, indicating a slower diffusion velocity for the deep donor. Another possibility not considered so far, is that the deep donor level could be caused by the arsenic vacancy. It seems uncertain whether or not the arsenic vacancy forms a deep donor or acceptor level.

### 5.4.5 Variation of the Concentration Profile with Damage

Energetic ions implanted into a crystal structure produce lattice damage around the track of the ion within the crystal. At low implant ion doses, the damage forms within isolated regions in the crystal, as the dose increases the damage regions overlap to form an amorphous region within the surface layers of the crystal. Whitton and Carter[95] have observed the onset of the crystal damage to be $5 \times 10^{13}$ ions/cm$^2$ for 40 keV sulphur ions in gallium arsenide. They have also shown that for a dose of $3 \times 10^{12}$ ions/cm$^2$ of 40 keV krypton ions the crystal damage can be minimised if the crystal is held at 100°C during implantation.

Two effects which have been observed by other workers and which can be produced by crystal structural damage are the gallium and arsenic vacancies. The gallium vacancy produces an acceptor level at 0.1 eV[96] but has been observed by other workers to produce an acceptor level at 0.2 eV from the valence band[106,97]. In the case of the arsenic vacancy, it appears to be unresolved as to whether or not a donor or acceptor level is produced.

The situation becomes more complicated when annealing is carried out on the specimens. Heat treatment itself can produce acceptor levels in sufficient numbers to convert n-type gallium arsenide to p-type. M. Toyama and H.I. Koma[98] attributed this acceptor level to gallium vacancies with activation energies of 0.13 eV and 0.25 eV from the valence band. C.S. Fuller et al[94] observed an acceptor level at 0.1 eV which they attributed to clusters of gallium vacancies. These clusters dissociating at temperatures in the range 500°C to 700°C to form stable donor-vacancy complexes. Annealing of implanted gallium arsenide can produce gallium and arsenic vacancies as well as chemical complexes within the crystal structure, further complicating analysis.

Graphs 28 and 42 show the effects of crystal damage produced by implanting gallium arsenide with inert ions i.e. ions which do not react chemically with the material. The results shown in graph 28 are from a specimen implanted at room temperature with a dose of $3 \times 10^{13}$ ions/cm$^2$, 300 keV protons and annealed at 650°C for 20 minutes in a nitrogen atmosphere. The donor concentration can be seen to reach a minimum at around the LSS range and below the background material concentration. The profile reaches a maximum above the background material at 3.3 microns and then returns to the background material at 4.5 microns. At approximately the LSS range the effect of the damage is predominantly acceptor-like i.e. a reduction from the background doping occurred. Between 3.1 microns and 4.5 microns the net effect is an increase in the background donor level. In this instance the specimen was measured using the Copeland technique at a frequency of 5.7 MHz, so that only shallow levels would respond to the measuring frequency. With only shallow levels responding, the decrease in donor concentration at the LSS

range must be due to one of three possibilities:-

a) The shallow background donor levels are being compensated by shallow acceptor levels produced by the damage and subsequent annealing.

b) Within this region chemical impurities are leaving substitutional sites and going interstitial.

c) Possibly electrically active chemical dopant species are forming into inactive chemical-damage complexes as a result of the subsequent annealing and damage centres present.

As stated previously, shallow acceptor levels at 0.1 eV from the valence band have been observed by C.S. Fuller et al[94], which they attributed to clusters of gallium vacancies and which dissociated within the temperature range 500°C to 700°C to form stable donor-vacancy complexes. In our case the specimen was annealed at 650°C so that it seems unlikely that a shallow acceptor was present, due to the clusters of gallium vacancies. There is no other evidence to suggest the presence of a shallow acceptor. Eliminating (a) leaves (b) and (c) as possible explanations for the decrease in donor activity. It is difficult to differentiate between (b) and (c), however some pointers may be obtained from several authors, who have noted that impurities can enter the lattice as electrically inactive gallium-vacancy-donor complexes. L.J. Vieland and I. Kudmen[99] and R.W. Fane[100] postulate that at concentrations greater than $4 \times 10^{17}$atoms/cm$^3$ selenium could enter the lattice as an electrically inactive gallium vacancy-selenium complex. They noted that as a result, the electron concentration did not equal the impurity concentration at concentrations greater than $4 \times 10^{17}$atoms/cm$^3$. V.I. Fistful[101] and A.B.Y. Young and

G.L. Pearson[102] have observed a similar behaviour for tellurium and sulphur in gallium arsenide. When V.D. Okenev et al[103] irradiated gallium arsenide, a reduction in carrier concentration was noted. He attributed this reduction to the formation of a complicated defect associated with gallium vacancies, probably a $Ga_2.VGa.Te_3$ complex. It would appear from the above discussion that the most probable cause for the decrease in donor concentration is (c).

The minima in the donor concentration was approximately at the LSS range, it would be expected that if the damage peak occurred at the LSS range the gallium vacancy-donor complexes would be greatest also, resulting in the minima.

Graph 42 shows a specimen that was implanted at room temperature with a dose of $6 \times 10^{12}$ions/cm$^2$, 120 keV argon ions and annealed at 500°C for one hour in a nitrogen atmosphere. In this case a heavier ion than previously was used, the range of the ion was much less and also the resultant damage to the structure was greater. For this reason, a higher background concentration material was used for this experiment i.e. with a donor concentration of $6 \times 10^{17}$atoms/cm$^3$. The specimen was measured using manual capacitance-voltage measurements at a frequency of 1 KHz. Again the effect of implanting the specimen with an electrically inactive ion was to produce a decrease in the donor concentration, which can be attributed to electrically inactive gallium vacancy-donor complexes. Since the measurements were carried out at 1 KHz then the reduction in donor concentration could be due to the formation of deep acceptor levels. This graph shows the tail of the profile returning to the background concentration, deeper in the material. At 120 keV the LSS range of argon in gallium arsenide was 814 Å and the minimum in the concentration would appear to be tending towards this

range, suggesting a damage peak at or around the LSS range. The peak in the donor concentration is a significant feature of Graph 28 . The peak appears at a depth of 3.3 microns, almost double the Lindhard range and was probably due to the diffusion of chemical impurities during annealing into the material. These chemical impurities finishing up on substitutional lattice sites and producing shallow donor centres.

Summarising, the main effect of implanting n-type gallium arsenide with an electrically inactive ion followed by heat treatment, was a reduction in donor level near the surface of the specimen. The minima in the donor concentration occurring at or around the LSS range with the damage peak occurring also at this depth. It is thought that this reduction was due to the formation of electrically inactive gallium vacancy-donor complexes. The formation of the complex being a direct result of the structural radiation damage and subsequent heat treatment.

## 5.5 Hall Measurements

Hall measurements were made on sulphur 32 implanted epitaxial n-type on semi-insulating gallium arsenide, supplied by the Mullard Research Laboratory. The n region was orientated (100) and had a nominal concentration of $5 \times 10^{15}$atoms/cm$^3$. The measurements were carried out to substantiate the results obtained from Copeland and manual capacitance-voltage measurements. Information was also obtained on the behaviour of the concentration profile near the surface of the specimen and the conduction processes and mobility of the carriers.

The technique was subject to errors from the stripping thickness

measurements, variations in ambient temperature, contacts, measurement of the specimen current and the measurement of the small changes in voltage (see Section 2.6). The most significant error being due to the measurement of small changes in the stripping thickness.

The trends in the results due to variations in the implant dose and temperature are given in Tables XIV and XV.

### 5.5.1 Variation of Concentration Profile with Implant Temperature

As the implant temperature increased for a constant dose of $10^{13}$ ions/cm$^2$ of 300 keV sulphur 32 ions, the peak depth of the concentration profile increased and the height of the profile peak decreased. The annealing temperature and the duration of anneal remaining constant at 650°C for 20 minutes throughout the experiment. As the implant temperature increased the activity at the front edge of the distribution decreased; that is, there was a shift of the donor concentration distribution into the specimen, away from the surface of the specimen. For the room temperature and 100°C implants, the shift was slight, but was much greater between 100°C and 180°C. This shift was probably due to the movement of donors by diffusion during implantation into the material, the higher the temperature the higher the diffusion. Deep concentration profiles were obtained although there was no clear evidence of profile supertails because of the limited depth range of the measurements.

There was a slight decrease in percentage electrical activity from the room temperature to 100°C implant which then remained approximately constant from 100°C to 180°C. This result and those above are consistent with the behaviour observed and discussed in Section 5.4.1 for the Copeland and manual capacitance-voltage measurements.

From Graph 50 a decrease in sheet resistivity can be observed from a room temperature to 100°C implant followed by an increase at 180°C. As the implant temperature increases from room temperature to 100°C a reduction in crystal damage will occur due to self-annealing. This self-annealing during implantation has been observed[92] to occur at substantially lower temperatures than with normal annealing after implantation. This suggests that there was a reduction in crystal damage up to 100°C with a corresponding increase in mobility and donor concentration. The increase in sheet resistivity from 100°C to 180°C could be due to a decrease in donor concentration (as observed) and also due to a decrease in carrier mobility.

The variation of carrier mobility with implant temperature was plotted in Graph 56. The mobility increased from a room temperature implant to 100°C then decreased to 180°C. The mobility after implanting at 100°C was very similar to the unimplanted specimen; very high mobilities were obtained to several microns into the material in both implanted and unimplanted specimens. Wolfe, Stoffron and Spears[104] have observed anomolously high mobilities of the order of 15200 $cm^2$/V-sec in high purity gallium arsenide at room temperature. They considered that conducting inhomogeneities in a Hall sample can result in calculated mobilities which are too high, by as much as several orders of magnitude. They concluded that precipitates (probably gallium precipitates) are the main inhomogeneity observed in gallium arsenide specimens with anomolously high measured mobilities. The decrease in mobility going into the specimen from its surface could indicate a decrease in the number of conducting inhomogeneities (gallium precipitates) into the material. It is perhaps significant that the high mobilities were also observed in the unimplanted specimen. This specimen has undergone heat treatment, so that the high mobilities may have been a result of this

heat treatment. The formation of gallium precipitates near to the surface would suggest the loss of arsenic from the surface of the material i.e. to leave an excess of gallium such that precipitation can occur. From Graph 54 for the unimplanted specimen it can be seen that near the surface of the material there was a lack of donor activity after heat treatment and may be due to the loss of arsenic from the surface of the material. This is of course assuming a compensating action from the arsenic vacancy.

### 5.5.2 Variation of Concentration Profile with Implant Dose

From Graph 52 as the implant dose increased from $10^{12}$ions/cm$^2$ to $10^{13}$ions/cm$^2$, the concentration peak decreased and the whole profile shifted into the material i.e. the depth from the surface of the peak concentration increased. The decrease in peak concentration was small. As the peak concentration increased from $10^{13}$ions/cm$^2$ to $10^{14}$ions/cm$^2$ the concentration peak increased, the depth of the peak remained approximately the same and a broadening of the concentration profile occurred at $10^{14}$ions/cm$^2$. The variation of the peak concentration with dose was slight and a peak concentration of $6.5 \times 10^{15}$atoms/cm$^3$ was obtained. The variation of percentage electrical activity with dose is given in Table XIV. The percentage electrical activity decreased with increasing dose, the largest value obtained was 17% for a dose of $10^{12}$ions/cm$^2$. The trends in these measurements are consistent with those obtained from Copeland and manual capacitance-voltage measurements and give substantiation to these measurements.

The variation of sheet resistivity with implant ion dose was plotted in Graph 51. The resistivity increased from $10^{12}$ions/cm$^2$ to $10^{13}$ions/cm$^2$ then decreased slightly at $10^{14}$ions/cm$^2$. As the dose increased

it would be expected that the crystal damage would also increase, tending to level off above some value of dose. After annealing a similar pattern should still occur with the damage. Damage will increase the specimen's sheet resistivity, hence from the foregoing argument, as the dose increased it would be expected that the sheet resistivity would increase and tend to level off for higher doses. The sheet resistivity was observed to increase up to $10^{13}$ions/cm$^2$ and then decrease slightly. This is of course a simplified explanation and takes no account of the carrier mobility. The decrease in sheet resistivity above $10^{13}$ions/cm$^2$ may have been due to a decrease in carrier mobility. From Graph 55 it can be seen that the carrier mobility decreased with increasing implant dose. Very high carrier mobilities were observed for the specimen implanted with $10^{12}$ions/cm$^2$, much greater than the unimplanted specimen, and as described in Section 5.5.1 were thought to be due to gallium precipitates. The specimens implanted with doses of $10^{13}$ions/cm$^2$ and $10^{14}$ions/cm$^2$ follow a similar pattern of mobility to the unimplanted specimen. For these two doses either the number of gallium precipitates has decreased or their effect is being masked by the overall structural damage.

### 5.5.3 Hall Measurements versus Temperature

Hall measurements were carried out on three of the specimens down to liquid nitrogen temperature, see Graph 47. As the temperature fell to liquid nitrogen the sheet resistivity ($\rho$) decreased, indicating that carrier freeze out was not occurring. As the specimens were cooled the Fermi level moved towards the conduction band. If it passed through any donor level, such that they were below the Fermi level, those levels are said to be frozen i.e. they cannot contribute to the conduction processes. In Graph 47 this was not occurring and as the temperature fell, so the resistivity also fell. Also from Graph 49 as the temperature decreased the

mobility increased, being almost a mirror image of the sheet resistivity ($\rho$). The curve for the 300 keV $S^{+}_{32}$ $10^{13}$ions/cm$^2$ room temperature implant exhibited a flattening of the characteristics, which could be due to carrier freeze out.

The slope of the Arrhenius plot can be used to give the carrier activation energy. Since carrier freeze out was not occurring it was not possible to calculate the carrier activation energy from the Arrhenius plot.

In a perfect periodic lattice in which no vibrations take place, no scattering of charge carriers should occur. In practice, departures from perfect periodicity give rise to various scattering mechanisms. The scattering mechanisms can be classified as those due to lattice imperfections i.e. due to the presence of ionized and non-ionized impurities. In a real crystal, several scattering mechanisms occur simultaneously; their contribution to the total scattering varying strongly with temperature and impurity concentration. Usually (except in intrinsic semiconductors) two scattering mechanisms are dominant. These are:-

a) Scattering by impurities and by acoustical phonons, as observed in covalent semiconductors, such as silicon and germanium.

b) Scattering by impurities and by optical phonons, as observed in group III-V compound semiconductors.

For acoustical phonon (lattice) scattering the mobility is proportional to $m_{*}^{-5/2}\ T^{-3/2}$ and the resistivity is proportional to $T^{3/2}$.

For ionized impurity scattering the mobility is proportional to $m_{*}^{-1/2}\ T^{3/2}$ and the resistivity is proportional to $T^{-3/2}$. Scattering can

occur due to non-ionized impurity atoms, but is only of secondary importance since mobile carriers would have to approach extremely closely to the core of a neutral atom in order to be scattered by it. In ionic (polar) crystals, scattering depends mainly on lattice vibrations in which negative and positive ions move in opposite directions i.e. on optical vibrational modes (optical phonons). In a semiconductor with high dislocation density, which may be the case with an ion implanted specimen, the contribution by dislocation scattering to the carrier mobility may not be negligible. With dislocation scattering the carrier mobility is proportional to temperature and inversely proportional to the dislocation density. From this latter mechanism, for an implanted specimen, as the dose increases it would be expected that the dislocation density will increase and the mobility decrease. The overall effect on the mobility and resistivity will be a combination of these scattering mechanisms.

For the room temperature implanted specimen the mobility was found to be proportional to $T^{-1.57}$ and the resistivity proportional to $T^{1.02}$. For the specimen implanted at 100°C the mobility was found to be proportional to $T^{-1.36}$ and the resistivity proportional to $T^{0.9}$. For the specimen implanted at 180°C the mobility was found to be proportional to $T^{-1.45}$ and the resistivity proportional to $T^{1.13}$.

From the previous argument, the predominant scattering mechanism was due to lattice vibrations and consequently optical-phonon scattering.

## 6.0 CONCLUSIONS

The following conclusions were drawn from the experimental results obtained during the work on this thesis:-

1) Current-voltage measurements were found to be a useful tool for assessing the quality of the Schottky barrier diode (i.e. its abruptness). For implanted specimens, the assessment of carrier mobility and lifetime, using the technique, was difficult without an accurate value for the junction barrier height. However it did give an indication of net carrier mobility and lifetime.

2) Three techniques were employed to obtain carrier concentration versus depth profiles. The techniques were:- capacitance-voltage measurement , Copeland and Hall measurements.

Capacitance-voltage measurements were a useful, if slow, method of obtaining active carrier concentration profiles. However, the responding energy levels were critically dependent upon the measuring frequency, and this had to be chosen carefully to ensure that the carriers at the energy level of interest contributed to the depletion capacitance. This capacitance-frequency variation must be considered in any energy level/concentration evaluation. It should be possible, by completing capacitance-voltage measurements at different frequencies, to obtain the values of the different energy levels in the material, but highly sensitive measurements over a very wide frequency range would be necessary.

The Copeland measurements offer a fast, direct method for obtaining active carrier concentration profiles. Due to the high frequencies used by this technique, only shallow energy levels will respond to the measuring frequency. The practical ranges of implant

dose and anneal temperature for capacitance-voltage and Copeland measurements were found to be $10^{12}$ions/cm$^2$ to $10^{14}$ions/cm$^2$, and room temperature to 700°C respectively.

Hall measurements proved to be a slow, tedious technique; however, a lot of information was obtained from them, especially near the surface of the specimen. It is possible to use a wider range of implant dose and anneal temperature with this technique, than with the other techniques described above.

3) In all cases, the active carrier concentration versus depth profiles of sulphur 32 in gallium arsenide produced peak concentrations at depths in excess of the Lindhard (LSS) range, i.e. two or three times the LSS range. The specimens exhibited super-tails, extending in some cases, 3 or 4 microns from the surface of the specimen. These deep concentration profiles could be due to channelling or diffusion, but the evidence points towards them being due to diffusion, or possibly diffusion enhanced by damage centres.

4) The concentration-depth profiles were dominated by the effects of crystal damage, produced by the implantation process. The effect of crystal damage was to produce deep acceptor levels and a deep donor level. It is considered that the deep acceptor level, or levels, was due to gallium and arsenic vacancies. It is not certain whether or not the deep donor level was due to arsenic vacancies or to substitutional oxygen. The oxygen was probably present in the implanted ion beam.

5) The damage peak, as expected, was nearer the surface than the impurity peak. From the damage study, the peak occurred at the Lindhard (LSS) range. From proton bombardment, after annealing the minima in the donor concentration occurred at the LSS range,

however a donor peak occurred deeper in the material. The minima in the impurity donor concentration was considered to be due to the formation of electrically inactive gallium vacancy-impurity donor complexes. These complexes did not diffuse into the material during heat treatment. The donor peak deeper in the material being due to the diffusion of impurity donor centres into the material during heat treatment.

The electrical behaviour of the material under different implant conditions i.e. implant temperature, dose and energy can be explained using the concept of an electrically inactive gallium vacancy-donor complex being present after annealing at 650°C.

6) The optimum implant temperature, for the highest peak donor concentration and percentage electrical activity, was at room temperature.

7) No appreciable electrical activity occurred for anneal temperatures below 500°C.

8) The optimum anneal temperatures for the highest peak donor concentration and percentage electrical activity was between 600°C and 700°C, probably 650°C.

9) The annealing results followed Zelevinskaya and Kachurin's postulate[73].

10) A saturation of the peak impurity concentration occurred with increasing dose and the maximum active impurity concentration obtained was $1.6 \times 10^{16}$ atoms/cm$^3$. This was considered to be due to the formation of electrically inactive gallium vacancy-impurity donor complexes.

11) A range of percentage electrical activities were obtained from zero to 86%, with an optimum dose of $10^{12}$ions/cm$^2$ for the highest peak concentrations.

12) The trends in the results obtained by Hall measurements substantiated those obtained by Copeland and manual capacitance-voltage measurements.

13) Anomolously high values for carrier mobility were obtained using Hall measurements. It was considered that these were due to conducting inhomogeneities and probably gallium precipitates.

14) From Hall measurements the predominant carrier scattering mechanism was optical-phonon scattering.

## 7.0 RECENTLY PUBLISHED DEVELOPMENTS

### 7.1 General

The experimental work contained within this thesis was carried out during the period October 1969 to October 1973. Subsequent improvements in encapsulation techniques, outlined in Section 7.2, have produced higher peak doping concentrations and efficiencies than those observed here, this being a result of the higher anneal temperatures possible i.e. up to 1000°C with a silicon nitride encapsulant. The reported electrical activity of sulphur, even for low doses, has ranged from 10% to 100%. The maximum carrier concentration reported for high doses has been typically $\leq 10^{18}cm^{-3}$.

Diffusion seems to be more pronounced for implanted sulphur than for silicon, selenium or tellurium. Diffusion of the implanted sulphur deeper into the substrate is usually significant[107][108], but is consistent with reported diffusion coefficients[109]. For low dose ($7 \times 10^{12}cm^{-2}$) 100 keV sulphur implants Eisen[108] observed little difference between implants performed at room temperature and at 350°C. This insensitivity to implant temperature was probably associated with a low defect density being present even after implantation at room temperature. Eisen[110] has shown that for a room temperature implant, considerable lattice disorder is introduced into the crystal by a high dose implant. Stolte[111] has reported that the doping efficiency of the implanted and annealed layers increases with implant temperature reaching 85% for moderate dose implants of sulphur at 500°C followed by a 900°C anneal, using a silicon nitride protective layer. He also found significant variations in the carrier mobility of the implanted and

annealed layers with the properties of the substrate material. In addition to this effect he found that there was a conversion process at elevated anneal temperatures (700°C - 900°C), which rendered chromium-doped semi-insulating gallium arsenide more conductive.

Work by Fujimoto[112] has indicated that the electrical activity is also dependent upon implant energy.

Using implanted radioactive tracer sulphur ions and a sputtered silicon nitride encapsulating layer, substantial out-diffusion of sulphur has been found during annealing[113]. The amount of out-diffusion was dependent upon the depth of the implanted sulphur. A large percentage of the out-diffused sulphur was found in a surface layer, which could be removed by hydrochloric acid, implying that there may be an interfacial native oxide. The encapsulant, the method of deposition and the predisposition surface treatment may, therefore, be a critical factor in controlling the out-diffusion of implanted sulphur. It has also been reported that the number of residual deep levels in sulphur-implanted gallium arsenide depends on the temperature of implant and the encapsulant used for annealing[114].

## 7.2 Encapsulation

For the work reported in this thesis, specimens were annealed using pyrolytic silicon dioxide encapsulation. Using this technique measurements were found to be limited to anneal temperatures of up to 700°C. Gyulai[115] shows that when silicon dioxide was used to encapsulate gallium arsenide, significant out-diffusion of gallium occurred at 750°C. It is postulated that gallium vacancies are created, which can form complexes with group VI donors. The accumulation of gallium upon the outer surface of the silicon dioxide encapsulating layer has

been confirmed[116]. Silicon nitride, $Si_3N_4$, encapsulating layers are proving to be superior to silicon dioxide encapsulants. Higher electrical activities have been achieved in implanted specimens after annealing at 750°C, if encapsulated in silicon nitride rather than silicon dioxide[117]. Various methods are available for the deposition of silicon nitride layers, i.e. sputtering, r.f. plasma deposition and pyrolysis have all been used but the quality of layers has been found to vary from laboratory to laboratory for any particular technique. Donnelly and co-workers[118] have shown that samples of n-type gallium arsenide with donor concentrations greater than $10^{16}cm^{-3}$ could be coated with silicon nitride and subsequently annealed at temperatures up to 1000°C with unchanged properties. However, when the same process was carried out on the lightly doped epitaxial layers ($3 \times 10^{15}cm^{-3}$) needed for low frequency IMPATT diodes, erratic changes in their properties occurred. By modifying the method of deposition of the silicon nitride[119] these changes were reduced to unmeasureable levels. Using silicon nitride encapsulants, gallium arsenide has been annealed at temperatures up to 950°C, and electrical activities as high as 100% have been observed.

Aluminium nitride has been used successfully[120] as an encapsulant. Using a sputtered deposition of aluminium nitride on specimens implanted with $3 \times 10^{14}ions/cm^2$ of tellurium at 220 keV and annealed at 900°C, they recorded a peak electrical activity of $8 \times 10^{18}carriers/cm^3$, which is significantly higher than that measured in silicon nitride encapsulated specimens. However this is not true in all cases and low dose ($10^{13}cm^{-2}$) sulphur implanted specimens show higher activity when encapsulated with sputtered silicon nitride. In attempting to obtain more reproducible results Sealy and Surridge[121] have used evaporated aluminium films and thermally grown native oxides

plus aluminium. The aluminium is deposited at room temperature and has been found to be a reliable encapsulant up to 700° to 750°C. At higher temperatures they have found significant aluminium diffusion.

## 7.3 Applications

Sulphur implantations have been used to make ohmic contacts to Gunn diodes[122]. Shallow (< 1 μm) n-type doping profiles with a peak concentration of $8 \times 10^{17} cm^{-3}$ were obtained from 116 keV, $2.3 \times 10^{13}$ ions/$cm^2$ sulphur implanted into vapour phase epitaxial gallium arsenide and afterwards annealed at 800°C for 20 minutes using a 2000 Å pyrolytic silicon dioxide encapsulating layer. Sulphur implants have also been used to produce n-type layers in chromium-doped gallium arsenide for planar-Gunn-digital devices[123]. In this case a dose of $5 \times 10^{12}$ ions/$cm^2$ 200 keV sulphur ions was implanted through a 5000 Å silicon dioxide layer on the semi-insulating gallium arsenide substrate. The silicon dioxide layer was removed after implanting the sulphur and a further 3000 Å of silicon dioxide deposited onto the specimen, followed by an anneal at 800°C for 20 minutes in a hydrogen atmosphere. They have reported doping efficiencies as high as 90% with an average carrier concentration of $4 \times 10^{16} cm^{-3}$.

Three possible ways of using ion implantation in the fabrication of gallium arsenide MOSFETs are given below:-

1) Ion implantation is used for the source and drain regions in epitaxial material. The highly doped source and drain regions should reduce contact resistance and the gate-source charging time. In this case the thin epitaxial layer for the channel must still be grown with excellent control.

2) The n-epilayer is eliminated and the channel, source and drain are all implanted in a buffer layer.

3) The need for any epitaxy is removed by implanting the channel, source and drain directly into bulk grown semi-insulating gallium arsenide. Little work has been carried out on the source and drain implants, most of the effort has been directed towards implanting the channel directly into chromium-doped substrates. Both sulphur[124,125] and selenium[126] have been used for this purpose.

A 10 GHz Hi-Lo IMPATT device with 25.6% efficiency and a 1.7 W output has been reported where the Hi region was obtained by sulphur implantation[127]. The highly doped n-region was produced by implanting doses of sulphur ions from 0.2 to 1 × $10^{13}$ions/$cm^2$ at room temperature with energies between 30 and 300 keV. After implantation the wafer was encapsulated with pyrolytic silicon dioxide and annealed at 800°C for 20 minutes. The implanted layer had an electrical carrier concentration of 2 × $10^{17}cm^{-3}$ with the mobility as high as 3000 $cm^2$/V.sec. However, some spreading of the sulphur profile was observed. A d.c. to r.f. conversion efficiency of 37% combined with an output power of 3.4 W at 3.3 GHz has been obtained from a Schottky barrier gallium arsenide IMPATT diode having a Lo-Hi-Lo profile[128]. The donor spike or clump was produced by implanting silicon into an epitaxial layer with an n-type concentration of 1.65 × $10^{15}cm^{-3}$. Sulphur implants were found not to produce a profile with a sufficiently defined clump necessary for the Lo-Hi-Lo structure. The specimens were protected during and after implantation with pyrolytic silicon nitride, annealing being carried out at 850°C for 15 minutes.

FETs with ion implanted channels using sulphur and selenium, have been fabricated with device parameters comparable to the best epitaxially grown devices. Similarly Read-type IMPATT diodes in which the 'Hi' region has been made by the implantation of sulphur or silicon, are as good as the best devices employing epitaxial growth. The major advantages of better uniformity, better stability and higher yield have been demonstrated for these ion implanted devices.

## 8.0 REFERENCES


1. Carter, et al., J. Mat. Sci., 4, 208-217 (1969).
2. McCargo, Davies and Brown, Can. J. Phys., 41, 1231 (1963).
3. Davies, et al., Can. J. Phys., 42, 1070 (1964).
4. Dearnaley, et al., Can. J. Phys., 46, 587 (1968).
5. Tannenbaum, Solid State Electronics, 2, 123 (1961).
6. Davies, et al., Can. J. Chem., 38, 1526 (1960).
7. Whitton and Davies, Electrochem. Soc., III, 1347 (1964).
8. Whitton, J.L., J. Appl. Phys., 36, 3917 (1965).
9. Whitton, J.L., Can. J. Phys., 45, 1947 (1967).
10. Lutz, H. and Sizmann, R., Phys. Letters, 5, 113 (1963).
11. Lutz, H., et al., Nucl. Instr. Methods, 38, 241 (1965).
12. Anderson, T. and Sorenson, G., Can. J. Phys., 46, 483 (1968).
13. Klein, Felder et al., Can. J. Phys., 46, 597 (1968).
14. Fuller and Ditzenberg, J. Appl. Phys., 27, 544 (1956).
15. Inskeep, Rev. Sci. Instr., 34, 310 (1963).
16. Bond and Smits, Bell Syst. Tech. J., 35, 1209 (1956).
17. Valdes, L.B., Proc. I.R.E., 42, 420 (1954).
18. Smits, F.M., Bell Syst. Tech. J., 37, 711 (1958).
19. Evans, R.A. and Donovan, R.P., Solid State Electr., 10, 155 (1967).
20. Nicholas, K.H., Solid State Electr., 9, 35 (1966).
21. Beckenstoss, G., Bell Syst. Tech. J., 37, 669 (1958).
22. Eriksson, L., et al., J. App. Phys., 40, 842 (1969).
23. Davies, J.A., et al., Can J. Phys., 45, 4053 (1967).
24. Mayer, J.W., et al., Can. J. Phys., 46, 663 (1968).
25. Mead, C.A., Solid State Electr., 9, 1023 (1966).
26. Leenov, D. and Stewart, R.G., Proc. I.E.E.E., 56, 2095 (1968).
27. Baxandal, P.J., et al., J. Phys. E. Sci. Instr., 4, 213 (1971).

28. Califan, F.P. and Luciano, A., Rev. Sci. Instr., 41, 865 (1970).

29. Sze, S.M., Physics of Semiconductor Devices, Wiley (1969).

30. Schottky, W., Z. Physik, 118, 539 (1942).

31. Schibli, E., Solid State Electr., 13, 392-394 (1970).

32. Reutlinger, G.W., et al., Solid State Electr., 12, 31 (1969).

33. Copeland, J.A., I.E.E.E. Trans. Electron Devices ED-16, 448 (1969).

34. Meyer, N.I. and Guldbrandsen, T., Proc. I.E.E.E., 51, 1631 (1963).

35. Spiwock, R., I.E.E.E. Trans. Instr. and Meas. IM-18, No. 3 (1969).

36. Roberts, G.I. and Crowell, C.R., J. Appl. Phys., 41, 1767 (1970).

37. Sze, S.M. and Irvin, J.C., Solid State Electr., II, 599 (1968).

38. Gunn, J.B., Solid State Comm., I, 88 (1963).

39. Gunn, J.B., I.B.M. J. Res. Dev., 8, 141 (1964).

40. Hutson, A.R., et al., Phys. Rev. Letters, 14, 639 (1965).

41. Allen, et al., App. Phys. Letters, 7, 78 (1965).

42. Ridley, B.K. and Watkins, T.B., Proc. Phys. Soc. (Lond), 78, 293 (1961).

43. Hilsum, C., Proc. I.R.E., 50, 185 (1962).

44. Hall, R.N., et al., Phys. Rev. Letters, 9, 366 (1962).

45. Nathan, M.I., et al., App. Phys. Letters, 1, 62 (1962).

46. Quist, T.M., et al., App. Phys. Letters, 1, 91 (1962).

47. Schawlow, A.L. and Towner, C.H., Phys. Rev., 95, 282 (1954).

48. Fox, A.G. and Li, T., Bell Syst. Tech. J., 40, 433 (1963).

49. Braun, Ann. Physik Chem., 153, 556 (1874).

50. Wilson, Proc. Royal Soc., A133, 458 (1931).

51. Schottky, W., Naturwiss, 26, 843 (1938).

52. Mott, Proc. Camb. Phil. Soc., 34, 568 (1938).

53. Mead, Solid State Electr., 9, 1023 (1966).

54. Shockley, W., Bell Syst. Tech. J., 28, 435 (1949).

55. Hall, R.N. and Dunlap, W.C., Phys. Rev., 80, 467 (1950).

56. Teal, G.K., et al., Phys. Rev., 81, 637 (1951).

57. Pfann, W.G., Trans. A.I.M.E., 194, 747 (1952).

58. Tannenbaum, M. and Thomas, D.E., Bell Syst. Tech. J., 35, 1 (1956).

59. Lee, C.A., Bell Syst. Tech. J., 35, 23 (1956).

60. Frosch, C.J. and Denck, L., J. Electrochem. Soc., 104, 547 (1957).

61. Theurer, H.C., et al., Proc. I.R.E., 48, 1642 (1960).

62. Hoerni, J.A., I.R.E. Electron Devices Meeting, Washington D.C. (1960).

63. Lepselter, M.P., Bell Syst. Tech. J., 45, 233 (1966).

64. Shockley, W., U.S. Patent 2787564 (1954).

65. Gibbons, J.F., Proc. I.E.E.E., 56, 295 (1968).

66. Fuller, C.F. and Wolfstern, K.B., J. Phys. Chem. Solids, 27, 1889 (1966).

67. Bardeen, J. and Brattain, W., Phys. Rev., 74, 230 (1948).

68. Schibli, E. and Milnes, A.G., Solid State Electr., 11, 323-334 (1968).

69. Glover, G.H., I.E.E.E. Trans. Electron Devices, ED-19, No. 2, 138 (1972).

70. Lindhard, et al., Mat. Fys. Med. Det. Kongal. Dariske Vid Selskals, 33, 14 (1963).

71. Hutson, A.R., et al., Phys. Rev., 155, 786 (1967).

72. Sansbury and Gibbons, Rad. Effects, 6, 269 (1970).

73. Zelevinskaya, V.M. and Kachurin, G.A., Sov. Phys. Semi., 5, 1455 (1972).

74. Hesse, K. and Strack, H., Solid State Electr., 15, 767-774 (1972).

75. Roderick, E.H., J. Phys. D; App. Phys., 3, 1153 (1970).

76. Crowell, C.R. and Sze, S.M., Solid State Electr., 9, 1035 (1966).

77. Hildebrand and Gold, R.C.A. Rev., June (1970).

78. Amron, I., J. Electrochem. Soc., 5, 3 (1967).

79. Thomas, C.O., et al., J. Electrochem. Soc., 109 1055 (1962).

80. Chang, Y.F., Solid State Electr., 10, 281 (1967).

81. Amron, I., Electrochemical Tech., 2, 327 (1964).

82. Zaininger, K.H. and Heiman, F.P., Solid State Tech. (May, June 1970).

83. Shockley and Read, Phys. Rev., 87, 835 (1952).

84. Sah and Reddi, I.E.E.E. Trans. Electron Devices, ED-11, 345 (1964).

85. Van der Pauw, Philips Research Report, 13, 1 (1958).

86. Smith, B.L., Solid State Electr., 11, 502 (1968).

87. Bleicher, M. and Longe, E., Solid State Electr., 16, 375 (1973).

88. Sze, S.M. and Gibbons, G., App. Phys. Letters, 8, 111 (1966).

89. Roberts and Crowell, J. App. Phys., 41, 1767 (1970).

90. Schade H. and Herrick, D., Solid St. Electronics, 12, 857 (1969).

91. Private Communication with D.J. Titley, University of Surrey.

92. Mazey and Nelson, Rad. Effects, 1, 229 (1969).

93. Whitton, J.L. and Bellovance, G.R., Rad. Effects, 9, 127 (1971).

94. Fuller, C.S., et al., J. App. Phys., 38, 4339 (1967).

95. Whitton and Carter, International Conference on Atomic Collision Phenomena in Solids, Brighton, Sept. 1969, Published by North Holland.

96. Fuller, C.S., et al., Appl. Phys. Letters, 4, 48 (1964).

97. Bube, R.H. and MacDonald, H.E., Phys. Rev., 128, 2071 (1962).

98. Toyama, M. and Koma, H.I., Jap. J. App. Phys., 9, 376 (1970).

99. Vieland, L.J. and Kiedmen, I., J. Phys. Chem. Solids, 24, 437 (1963).

100. Fane, R.W., Solid State Electr., 6, 383 (1963).

101. Fistful, V.I., Heavily Doped Semiconductors, Plenum Press.

102. Young, A.B.Y. and Pearson, G.L., J. Phys. Chem. Solids, (GB), 31, 512 (1970).

103. Okenev, V.D., et al., Sov. Phys. Semicond., 4, 80 (1970).

104. Wolfe, Stoffron and Spears, J. App. Phys., 44, 732-4 (1973).

105. Wronski, C.R., J. App. Phys., 41, 3805 (1970).

106. Bube, R.H., Blanc, J. and Weisberg, L.R., Phys. Rev. Lett., 9, 252 (1962).

107. Mizutani, T. and Kurumada, D., Electron. Lett., 11, 639 (1975).

108. Eisen, F.H., et al., Application of Ion Beams to Materials, Inst. Phys. Conf. Ser. 28, 44 (1976).

109. Matino, H., Solid St. Electron., 17, 35 (1974).

110. Eisen, F.H., Osaka Conference, Aug. 1974.

111. Stolte, C.A., Tech. Dig. Int. Elect. Dev. Mtg., New York, IEEE, P. 585.

112. Fujimoto, M., et al., Ion Implantation in Semiconductors and Other Semiconductors, ed. F. Chernow, (New York Plenum).

113. Eisen, F.H. and Welch, B.M., Ion Implantation in Semiconductors and Other Semiconductors, ed. B. Crowder, (New York Plenum).

114. Yokoyama, N., et al., App. Phys. Lett., 24, 405 (1976).

115. Gyulai, et al., App. Phys. Lett., 17 332 (1970).

116. Bell, E.C., et al., Rad. Effects, 22 253 (1974).

117. Harris, J.S., et al., App. Phys. Lett., 21, 601 (1972).

118. Donnelly, J.P., et al., App. Phys. Lett., 27, 41 (1973).

119. Donnelly, J.P., et al., App. Phys. Lett., 29, No. 2 (1976).

120. Poshley, R.D. and Walch, B.M., Solid St. Electron., 18, 977 (1975).

121. Sealy B.J. and Surridge R.K., Thin Solid Films, 26, L19 (1975).

122. Lee, D.H., Berenz, J.J. and Bernick, R.L., Electron. Lett., 11, 99 (1975).

123. Mizutani, T. and Kurumada, K., Electronics Lett., 11, 639 (1975).

124. Hunsperger, R.G. and Hirsch, N., Solid St. Electron., 18, 349 (1975).

125. Higgins, J.A., et al., Electron. Lett., 12, 18 (1976).

126. Higgins, J.A., et al., North American Gallium Arsenide Symposium, (1976).

127. Berenz, J.J., et al., Electronics Lett., 10, 157 (1974).

128. Bozler, C.C., et al., App. Phys. Lett., 29 No. 2 (1976).